SOL·GEL PRODUCTION

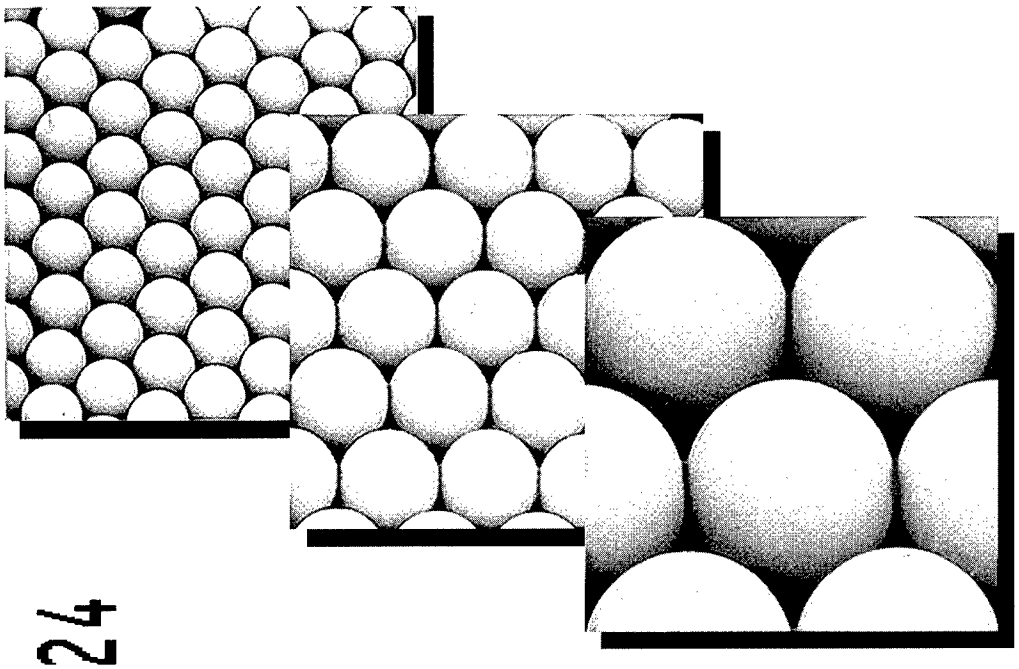

Editor:

Helmut Schmidt

ttp TRANS TECH PUBLICATIONS

Key Engineering Materials

ISSN 1013-9826

Specializing in the Field of Basic and Applied Aspects of Advanced Ceramic Materials and Composites

Internet:

The table of contents of each volume is freely available on the Internet through Trans Tech Publications' Preview Service (preview@ttp.ch) as well as on the World Wide Web at http://www.ttp.ch/perdcs/kem.htm.

Subscription Information:

Key Engineering Materials is published in 16 volumes per year. In 1998, volumes 137-152 are scheduled to be published. The subscription rate is CHF 98.75 per volume or CHF 1580.00 per year.

Trans Tech Publications Ltd
Brandrain 6 • CH-8707 Uetikon-Zuerich • Switzerland
Fax +41 (1) 922 10 33 • e-mail: ttp@ttp.ch
http://www.ttp.ch

REPORT DOCUMENTATION PAGE

Form Approved
OMB No. 0704-0188

1. AGENCY USE ONLY *(Leave blank)*	2. REPORT DATE	3. REPORT TYPE AND DATES COVERED
	1998	Conference Proceedings 24 - 25 May 1993

4. TITLE AND SUBTITLE
Sol-Gel Production

5. FUNDING NUMBERS
N00014-93-J-9046

6. AUTHOR(S)
Helmut Schmidt

7. PERFORMING ORGANIZATION NAME(S) AND ADDRESS(ES)
Institut fur Neue Materialien Im Stadtwald Gebaude
43 6600 Saarbrucken
Germany

8. PERFORMING ORGANIZATION REPORT NUMBER

9. SPONSORING/MONITORING AGENCY NAME(S) AND ADDRESS(ES)
Technical Director
Office of Naval Research International Field Office
PSC 802 Box 39
FPO AE 09499-0700

10. SPONSORING/MONITORING AGENCY REPORT NUMBER

11. SUPPLEMENTARY NOTES

12a. DISTRIBUTION AVAILABILITY STATEMENT
Approved for public release, distribution is unlimited

12b. DISTRIBUTION CODE

13. ABSTRACT *(Maximum 200 words)*
Compilation of abstracts collected for the conference entitled "Sol-Gel Production" held in Germany, 24 - 25 May 1993.

14. SUBJECT TERMS
ceramics, alumina, Sol-Gel, oxide, optical fiber, hard coatings, silicon

15. NUMBER OF PAGES

16. PRICE CODE

17. SECURITY CLASSIFICATION OF REPORT	18. SECURITY CLASSIFICATION OF THIS PAGE	19. SECURITY CLASSIFICATION OF ABSTRACT	20. LIMITATION OF ABSTRACT

Sol-Gel Production

Proceedings of the First International Conference on Application and Commercialization of Sol-Gel Processing, Saarbrücken, Germany

Editor:

Helmut Schmidt

TRANS TECH PUBLICATIONS LTD
Switzerland • Germany • UK • USA

Table of Contents

Key Engineering Materials Vol. 150 (1998) pp. 1-6

Sol-Gel Production of Silica Microparticles

T. Adachi, J. Kawashima, M. Shoshi, M. Matsubara,
K. Sakai and T. Nakasone

UBE-NITTO KASEI Co., Ltd, 2-2-1 Yabutanishi, Gifu 500, Japan

Keywords: Monodispersed, Silica, Microparticle, Coefficient of Variation, Spacer Particle, Liquid Crystal Display (LCD)

Abstract

The monodispersed silica particles of diameters in the range of 0.2–8.0 μm were produced by the sol–gel method. The silica particles were prepared by the building–up process, in which the seed silica particles dispersed in the ammonia–water–alcohol solution were grown to larger particles by adding dropwisely tetraethoxysilane in the solution. The typical coefficient of variation of the diameter of the particles was less than 1.5% in the diameter range of 1.5–8.0 μm. These particles are applied as spacers for controlling the thickness of a liquid crystal layer between two glass substrates in the liquid crystal display panel.

1. Introduction

Monodispersed silica microparticles are attracting much attention in the field of electronics, because of the low thermal expansivity and high mechanical stability. We are producing a family of micron size monodispersed silica microparticles, which are named HIPRESICA. HIPRESICA particles are characterized by the completely spherical shape, extremely narrow particles size ditribution and high purity. HIPRESICA particles are synthesized from a silicon alkoxide solution by the sol–gel method. The avarage particle size of HIPRESICA can be controlled in the range from 0.2 to 8.0 μm.

2. Preparation of monodispersed silica microparticles

2.1. Procedure of preparation

Silica particles of submicron size are synthesized by Stöber process [1]. Tetraethoxysilane (TEOS), alcohol, water and ammonia are mixed at once in the reaction vessel. The particles of micron size are synthesized by "bulding–up" process, in which the seed silica particles dispersed in the solution of water, alcohol and ammonia are grown to larger particles by adding TEOS dropwisely in the solution [2]. A typical procedure of preparing monodispersed silica particles is shown in Fig. 1. As a hydrolysis–polycondensation reaction proceeds, hydrolyzed products are deposited on the surface of the seed particles, so that the seed particles grow to larger particles. After adding TEOS, the solution is aged for a few hours under stirring, and is converted to the dispersion of silica in water by evaporating alcohol and ammonia from the

solution. Then the silica dispersion is freeze-dried in order to avoid the aggregation of silica particles. The dry gel particles are heated at a given temperature below 1000 °C.

2.2. Control of particle size

The size of the resulting particles is controlled by the size and amount of seed particles and amount of TEOS which is calculated from the difference between the volume of the aimed size of particles and the seed particles. The as-prepared particles have a large amount of silanol groups and a small amount of organic residue, such as adsorbed alcohol or unreacted ethoxy groups. On heating the gel particles at higher temepratures, these organic residues are burned out and silanol groups are converted to H_2O, so that the particles are accompanied with a small shrinkage. Consequently, the aimed size of resultant silica particle must be controlled in expectation of the srinkage on heating. The SEM pictures of typical sizes of HIRESICA are shown in Fig. 2.

3. Application of HIPRESICA as spacers for LCD devices

3.1. Spacer of LCD

The most useful application of monodispersed silica particles of micron size is the spacer of liquid crystal display devices (LCDs). Fig. 3 shows the cross-section of a liquid crystal cell. The spacer particles are employed to control the distance between two glass substrates with depositted indium-tin oxide (ITO) electrode films. The procedure of assembling a liquid crystal cell is shown in Fig. 4. The spacers dispersed in the mixed solvent of water and alcohol are sprayed on the glass substrate during evaporation of the solvent. The epoxy resin sealant are spread on the surroundings of the other glass substrate by printing. The epoxy resin printed substrate is put upon the substrate which holds spacers and pressed as it is

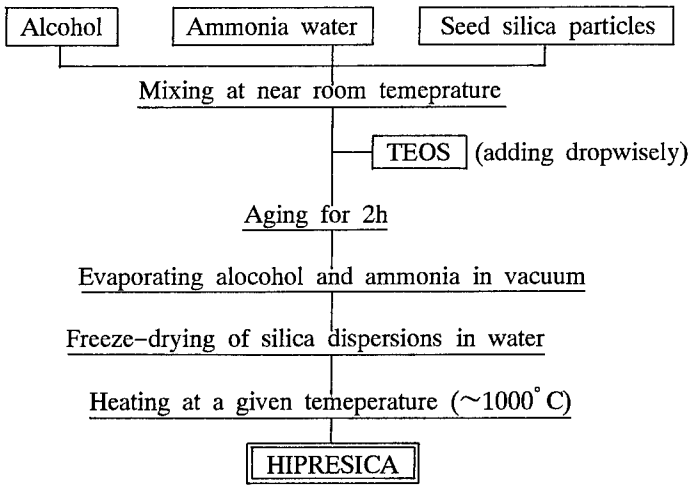

Fig. 1 A typical procedure of preparing monodispesed silica particles.

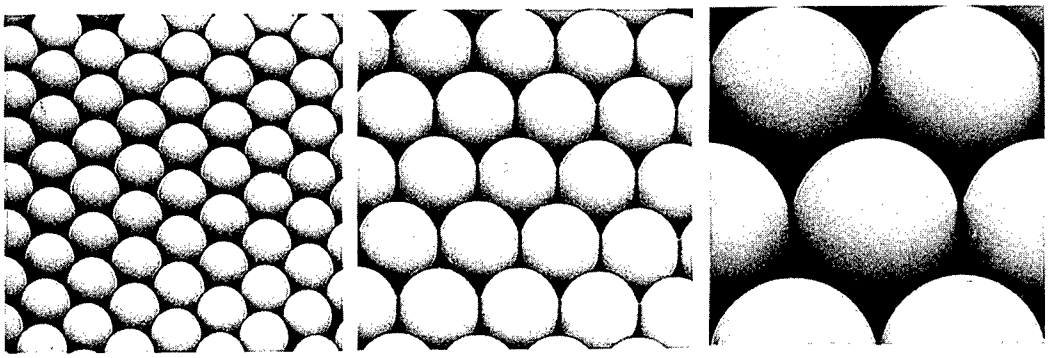

Fig. 2 SEM photographs of HIPRESICA.

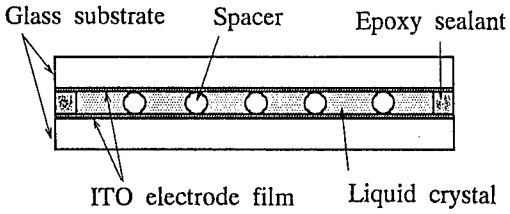

Fig. 3 The cross section of a LCD panel.

heated. This procedure is used for curing the epoxy resin sealant and making the distance of two substrates uniform. At this pressing procedure, the undulation of the glass substrate can be removed. Finally, a liquid crystal is poured from the gate into the cell which has been vaccum-treated beforehand and then the gate is sealed.

3.2. Characterization of HIPRESICA as LCDs spacers

3.2.1. Comparison with other spacer materials

Chopped glass fibers and organic polymer particles are used as the spacer for twisted nematic (TN) LCDs which are used in clocks or calculators. Fiber spacers and organic polymer spacers are shown in Fig. 5. Recently, a super-twisted nematic (STN) type of LCDs have been developed in response to a market demand for higher resolution displays, such as personal computers or word processors. To achieve very high uniformity of the thickness of a liquid crystal layer required for STN LCDs, the higher uniformity is required for the size of the spacer particles. The deviation of the thickness of a STN liquid crystal layer must be suppressed to less than 0.1 μm. The narrow particle size distribution of HIPRESICA can meet the requirement.

3.2.2. Particle size distribution of HIPRESICA

The standard deviation of the particle size distribution of HIPRESICA is less than that of polymer spacer particles which are synthesized by a radical polymerization of styrene(St)-

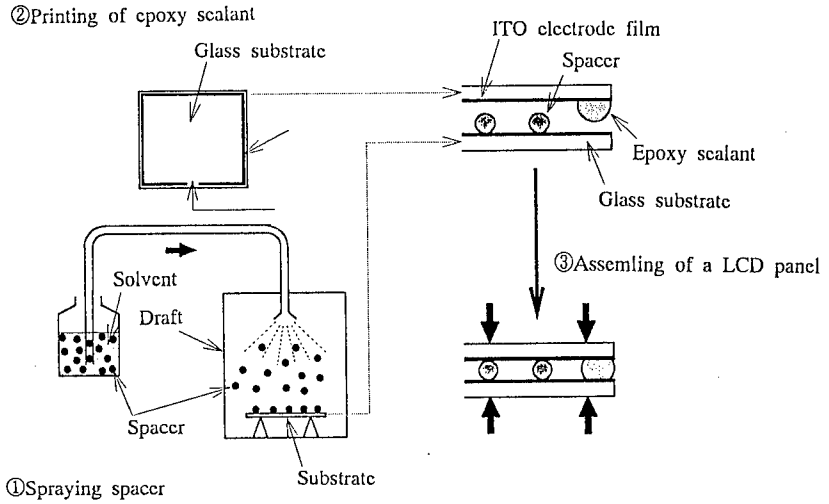

Fig. 4 The procedure of assembling a LCD panel.

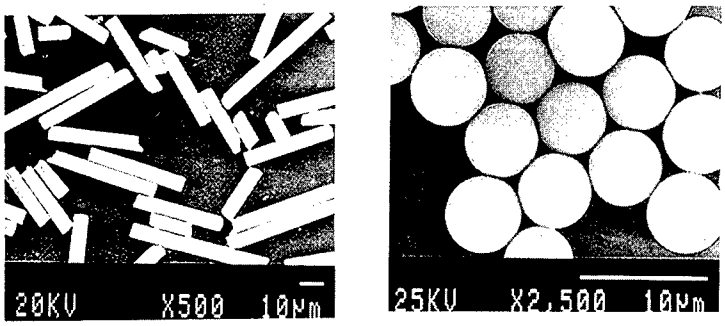

Fiber spacers St-DVB polymer spacers

Fig. 5 SEM photographs of glass fiber spacers and St-DVB polymer spacers

divinylbenzene (DVB) monomers using a molecular diffusion method [3]. The typical particle size distribution of HIPRESICA and St-DVB polymer spacers are shown in Fig. 6. The typical coefficient of variation (C.V.) of HIPRESICA is about one third of that of St-DVB polymer spacers. Although the mechanism of generating the monosized silica particles is not elucidated, the resulting particles of the aimed size can be prepared with the accuracy of $\pm 0.1\,\mu$m by districtly controlling the preparation condition.

3.2.3. Other properties of HIPRESICA

Crystal form, specific gravity, refractive index and specific surface area of HIPRESICA are

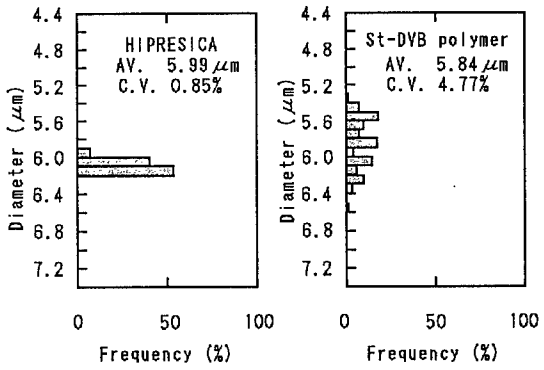

Fig. 6 Particle size distribution of HIPRESICA and St-DVB polymer spacers

Table 1 Properties of HIPRESICA

Item	Measurement method	Measured value
Crystal form	X-ray diffraction	Amorphous*1
Specific gravity	Specific gravity bottle	1.8-2.2
Refractive index	Refractmetry	1.35-1.45
Specific surface area	BET method	≒ 3 m^2g^{-1}*2

*1 after heating at 1000°C
*2 measured with 1.0 μm particles

listed in Table 1. The specific gravity and refractive index of the as-dried silica particles (gel particles) are 1.8 and 1.35, respectively, and the specific surface of the gel particles is about two times larger than the theoretical value of a sphere, it is assumed that microscopic voids or silanol groups remain in the gel particles. When the gel particles are heated at 1000 °C, the specific gravity and the refractive index of the particles are equal to those of fused silica. The linear shrinkage of the diameter of gel particles with heating at 1000°C is about 10%. The amounts of metallic impurities in HIPRESICA particles measured by inductively coupled plasma spectrometry (ICP) or atomic absorption spectrometry are shown in Table 2. Most of metallic impurities in HIPRESICA particles are less than 3 ppm, and radioactive elements, such as uranium and thorium, are less than 0.1 ppb. A liquid crystal is easily decomposed by alkaline ions, especially Na^+. The high purity of HIPRESICA is succeeded in the purity as the material directly contacted with a liquid crystal.

The load-displacement curves of 6.0 μm of HIPRESICA and a St-DVB polymer spacer are shown in Fig. 7. As the polymer spacer is easily deformed with a small load compared with HIPRESICA, it is difficult to adjust the thickness of a liquid crystal layer at the pressing process.

4. Conclusions

Silica microparticles named HIPRESICA are highly monosized in the diameter range of 1.5-8.0 μm.

Table 2 Metallic impurities in HIPRESICA particles

Element	Measurement method	Measured value
Na	Atomic absorption spectrometry	<2 ppm
K	Atomic absorption spectrometry	<2 ppm
Ca	ICP	<3 ppm
Fe	ICP	<2 ppm
U	ICP mass	<0.1 ppb
Th	ICP mass	<0.1 ppb

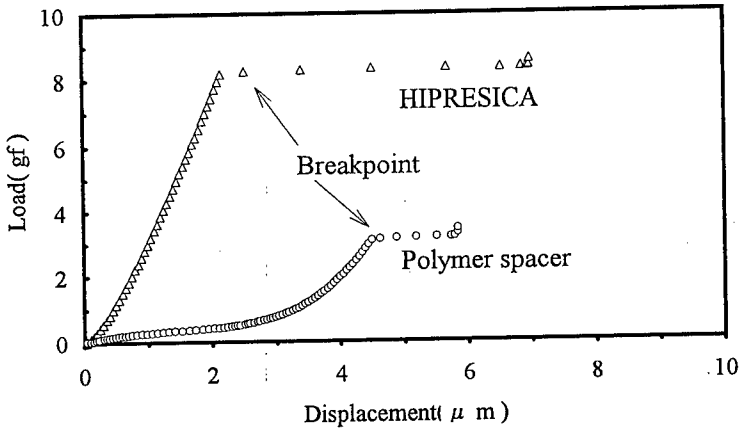

Fig. 7 Load-displacement curces of HIPRESICA and a St-DVB polymer spacer. The loading speed is 0.27 gf/sec.

A typical coefficient of variation of particle size is less than 1.5%. The most useful application of HIPRESICA is the spacer for a LCD panel.

Acknowledgements
The authors thank Prof. Sumio Sakka of Kyoto University for the kind assistance in preparation of the manuscript of the paper.

References

[1] W. Stöber, A. Fink and E. Bohn, *J. Colloid Interface Sci.*, **26**, 62 (1968)
[2] K. Nakanishi and Y. Takamiya, *J. Ceram Soc. Japan*, **96**, 719 (1988)
[3] G.W. Poehleim, R.H. Ottewill and J.W. Goodwin, Ed., "Science and Technology of Polymer Colloids", Martius Nijihoff Publishers, New York (1983)

Key Engineering Materials Vol. 150 (1998) pp. 7-14

Synthesis of Zircon-Based Ceramic Pigments via Sol-Gel Methods

C.C. Agrafiotis and C.J. Stournaras

Cereco S.A., P.O. Box 146, GR-34100 Chalkida, Greece

Keywords: Sol-Gel, Zircon, Vanadium, Praseodymium, Ceramic Pigments

Abstract: The inherent advantages of the Sol-Gel method are explored in the synthesis of zircon-based ceramic pigments. Zircon - Vannadium blue and Praseodymium - yellow powders were produced from the respective alkoxides and compared versus conventional ceramic pigments with respect to firing conditions for zircon - phase formation and colour development. The effects of mineralizers, aging time, and pigmenting substance on the phase composition and on the colour of the products were studied. It is shown that under appropriate conditions zircon - based pigments comparable to the commercial ones can be synthesized.

1. Introduction: Zircon - based ceramic pigments possess the two most important properties of any ceramic pigment: superior resistance to dissolution and tinctorial strength (1). They are traditionally produced by firing the precursor oxide powders (ZrO_2, SiO_2) together with the oxide of the pigmenting ion (V_2O_5, Pr_6O_{11}, Fe_2O_3, Cr_2O_3) at relatively high temperatures for extended periods of time. Additives (called mineralizers) which are alkali fluorides or chlorides, are necessary in small quantities in order to facilitate the completeness of reaction and the incorporation of the pigmenting ion into the zircon host lattice. The focus is on three particular pigments: Zircon - Vannadium blue, Zircon - Praseodymium yellow and Zircon - Iron pink, since from these three, one can achieve the whole palette of colours, with appropriate mixing.
Thus it is expected that the inherent advantages of the sol-gel synthesis route (i.e. very high homogeneity and very small particle size of the powders synthesized), would enable the production of ceramic pigments that can either develop the desired colour at much lower firing temperatures and/or produce pigments of better quality.
There are two routes via which one can synthesize these powders by sol-gel. In the first (Colloidal Gel) the precursor materials are colloids or salts, which are dissolved in acid - containing water. The addition of alkalis (e.g. NH_4OH) to the colloidal solution causes gelation. Alternatively, one can start from alkoxides as precursor materials (Polymeric Gel). These are dissolved in alcohol medium containing the amount of water necessary for hydrolysis and an acid catalyzer. The gelation occurs via a hydrolysis - condensation mechanism. From that point on, the procedure is common for both methods: the gels are dried, calcined at intermediate temperatures for the removal of organics and water, mixed of necessary with the mineralizers and then fired at the

temperature appropriate for colour development.

Only recently though, attention has been paid to the synthesis of zircon - based ceramic pigments by sol-gel methods. In a series of publications (2-5) Monros et al. have studied the synthesis of V-blue pigments both by polymeric and colloidal routes. They established that upon heating from the gel, metastable tetragonal zirconia is first formed, then transition to monoclinic occurs and immediately after the zircon phase is formed. They also studied the effects of different organic precursors for ZrO_2 and optimized the hydrolysis conditions for the polymeric gel route. Oheim et al (6), have studied the synthesis of Pr-yellow pigments from polymeric gels, with respect to the effect of the addition of various mineralizers and seeding agents. The emphasis of the present work is also on the polymeric synthesis route, following the guidelines suggested in (2-5).

2. Experimental: As precursor materials for the oxides of Si and Zr TEOS (Merck Chemicals) and Zr-n-propoxide (Alfa Chemicals) were employed for the polymeric gel route, whereas Colloidal Silica (Degussa, Aerosil 200) and $ZrOCl_2*4H_2O$(Alfa) were respectively selected for the colloidal route. For the substances containing the pigmenting ion $VOCl_3$, NH_4VO_3, $VO(C_5H_7)_2$ and $PrCl_3*6H_2O$ (all from Alfa) were used. For the case of polymeric gel, the hydrolysis procedure proposed in (5) was followed. TEOS was prehydrolyzed in absolute ethanol at 70°C for 2 hours. The solution was allowed to cool at room temperature before Zr-n-propoxide was added. After 24 hours of co-hydrolysis, the remaining water necessary for condensation was added and the gels so formed were allowed to age at room temperature for various periods of time. On the other hand, for the colloidal gel route, the zirconium salt was dissolved in water, the salt containing the pigmenting ion in acid-containing water, and the two solutions were added to a solution of colloidal silica at 70°C under vigorous stirring. Gelation in this case was achieved by dropwise addition of ammonia solution.
As suggested in (4) and (5), V-Zircon pigments corresponding to the following stoichiometries were synthesized:

$$(ZrO_2)_{0.90}(SiO_2)_{1.00}(V_2O_5)_{0.05}$$

$$(ZrO_2)_{0.96}(SiO_2)_{1.00}(V_2O_5)_{0.02}$$

whereas for the Pr-Zircon case a composition of:

$$(ZrO_2)_{0.99}(SiO_2)_{1.00}(Pr_6O_{11})_{0.01}$$

was tested, which is similar to that of commercial pigments.

3. Results - Discussion:

i) Polymeric Gel:

The processing steps were similar for the case of V- and Pr-doped samples. The gels were dried first at 80°C and then at 120°C for the removal of alcohol and water. The products consisted of soft particulates agglomerated for both V and Pr. These particulates had to be grinded in order to obtain fine powders, which were subsequently calcined at temperatures between 650-1250°C for 12 hours. In all the experiments on the Vannadium-Zircon system $VOCl_3$ was used as the V-containing compound, unless otherwise stated.
After calcination at 650°C the products are still amorphous. The first

crystalline phase to appear upon heating is metastable tetragonal ZrO_2 at 750-800°C depending on the vannadium content of the samples. Immediately after the temperature where the transformation of tetragonal to monoclinic zirconia takes place, the zircon phase appears as well, its proportion being increased with an increase of the firing temperature.

Two typical DTA and TGA runs are shown in Fig.1. The difference between the two samples is that sample 1 was gellified by adding the amount of water required for condensation to the solution, whereas sample 2 was allowed to gellify slowly by absorbing moisture from the atmosphere. Both samples exhibit a weight loss of about 20 wt% at temperatures 550-750°C which is due to the loss of solvent and organics (first endothermic and first exothermic peaks). They also exhibit a further weight loss of 3-5% in the range 750-900°C accompanied by exothermic transfornations which are attributed to the crystallization of zirconia from the amorphous phase and further transformation to zircon.

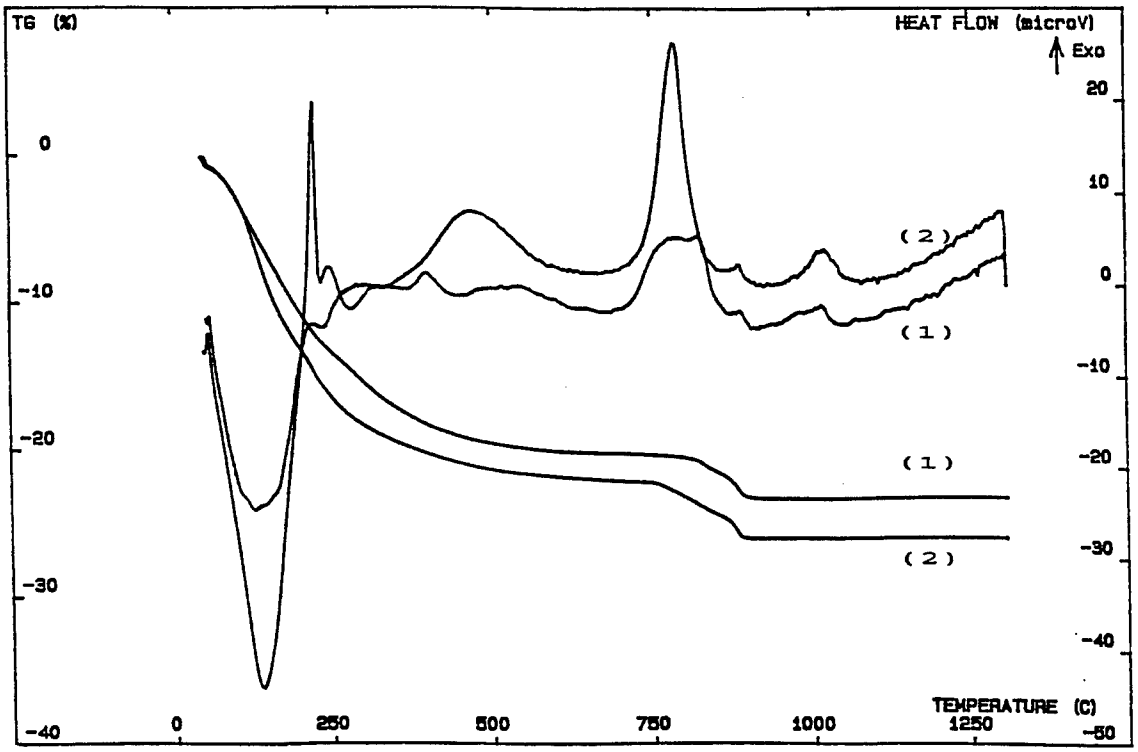

Fig.1: TGA and DTA curves for zircon- V samples.
1: Instant gelation, 2: Slow gelation.

Effect of Mineralizers: It is suggested (3) that with low vannadium contents (0.02) and at high firing temperatures (1200°C) the turquoise-blue colour is stabilized without the addition of any mineralizers. However, in our case, when the sol-gel powders were fired without mineralizers, it was impossible to obtain a colour similar to the commercial one, even at high firing temperatures. V-doped zircon changes from yellow at 700°C to soft green at 800°C and to dark green at 1200°C, whereas Pr-doped powder develops a light yellow colour at 1200°C. In comparison, conventionally made pigments develop the

commercial turquoise-blue and sun-yellow colours at 850 and 1200°C respectively. Therefore, the addition of mineralizers was judged necessary. NaF was selected and mixed with pre-calcined powders in a proportion of 0.2 moles of NaF per 1 mole of zircon.

For the Zircon-V case the addition of NaF shifts the colour of the samples towards turquoise-blue and simultaneously favors the crystallization of more phases at lower temperatures. Thus, at 800°C, the transformation of tetragonal to monoclinic zirconia has proceeded and silica together with zircon also appear. At higher firing temperature (900°C) the relative amounts of tetragonal and monoclinic zirconia disappear in favor of zircon. These results are summarized in Table 1.

Effect of the amount of V: For the same firing temperature an increase of the amount of V facilitates the transformation of tetragonal and monoclinic zirconia to zircon. This effect is shown also in Table 1 where the two stoichiometries with respect to V_2O_5, 0.02 and 0.05 moles are compared. At 800°C for the case of 0.05, the transformation of tetragonal to monoclinic zirconia is almost completed and the amount of zircon is drastically increased. Silicon oxide is also transformed to cristobalite. In general, the transformation of silicon oxide to cristobalite or the crystallization of cristobalite directly from the amorphous phase are favored by an increase of the quantity of vannadium (7). Even at higher firing temperatures where the content of phases other than zircon progressively diminishes, their relative amount remains higher for the case of less vannadium (0.02).

Temp. (°C)	Sample Pure (0.02)	Sample (0.02)+NaF	Sample (0.05)+NaF
650	Amorphous	Amorphous	Amorphous
800	T(w)	T(vs)M(vs)Z(m)S(m)	T(vw)M(vs)Z(s)C(m)
900	T(s)Z(vs)M(w)	T(w)M(w)Z(vs)C(tr)	M(tr)Z(vs)C(tr)
1000		M(tr)Z(vs)C(tr)	M(t)Z(vs)C(tr)

Table 1: Effect of mineralizer and quantity of Vannadium on Phase composition.
T: tetragonal zirconia, M: monoclinic zirconia, Z: zircon, S: silicon oxide, C: cristobalite
tr: traces, w: weak, m: medium, s: strong, vs: very strong
($VOCl_3$ as V-containing compound, samples not aged at all)

Effect of aging time: A comparison among three samples (aged for 7, 2 days and not aged at all) is shown in Fig.2. Aging seems to play an important effect on the composition of the final product. In the not aged sample, the prevailing phase after firing at 850°C is monoclinic zirconia, with tetragonal still present, whereas longer aging times favor a more complete development of the zircon phase during the firing step.

Efeect of V-containing compound: Having established the necessity of mineralizers and the stoichiometry of 0.05 moles of V_2O_5 as the optimum one, experiments were carried out with various V-containing compounds as precursor materials. In addition to $VOCl_3$, NH_4VO_3 and a Vannadium

alkoxide $VO(C_5H_7)_2$, (denoted as V-OR) were tested.
Comparative results for firing temperatures of 800°C are shown in Fig.3. It seems that the change on the pigmenting compound does not have a major effect on the final product. At both firing temperatures, products from different V-containing compounds look very similar to one another, with the product from $VOCl_3$ appearing slightly better, following by the product from V-OR.

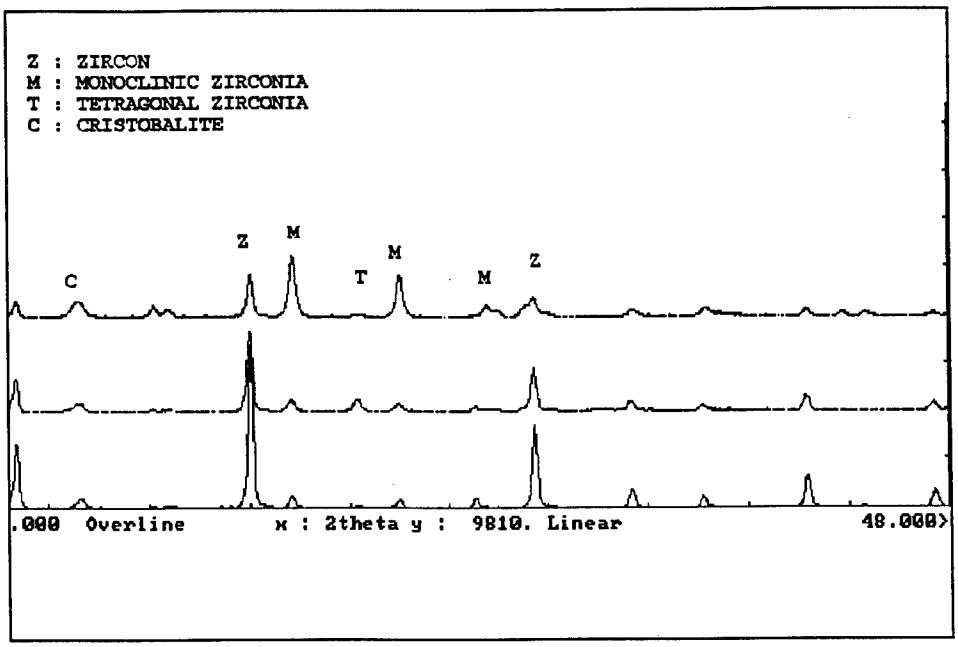

Fig.2: Effect of aging time on phase composition. Top curve: not aged sample, middle curve: 2 days, lower curve: 7 days.

The colour of all aged samples, fired at 800°C is turquoise-blue similar to that of the conventionally-made powders. A comparison with respect to phase composition between sol-gel made and conventionally made powder is shown in Fig.4

Similar results were obtained for the case of Pr. Addition of NaF was necessary in order to turn the color from pale-yellow to sun-yellow at 1200°C but only at 1250°C the color was as strong as the conventional one.

For the case of Pr, $MgCl_2$ was used alternatively as a mineralizer (6), which has the additional advantage of being soluble in ethanol, and thus it can be added directly to the sol itself rather than mixed with the dried gel. It occured that $MgCl_2$ improved slightly the phase composition compared to NaF, leaving only traces of tetragonal and monoclinic zirconia in the fired sample. However, this was not accompanied by an improvement on the colour of the powder, but on the contrary, powders doped with $MgCl_2$ developed a much softer yellow colour, dissimilar to both the conventional and the NaF-doped sol-gel ones. This phenomenon was also observed by Oheim et al.(6), who also point out the necessity of mineralizer addition and of the high firing temperatures required for colour development for the Pr-Zircon system.

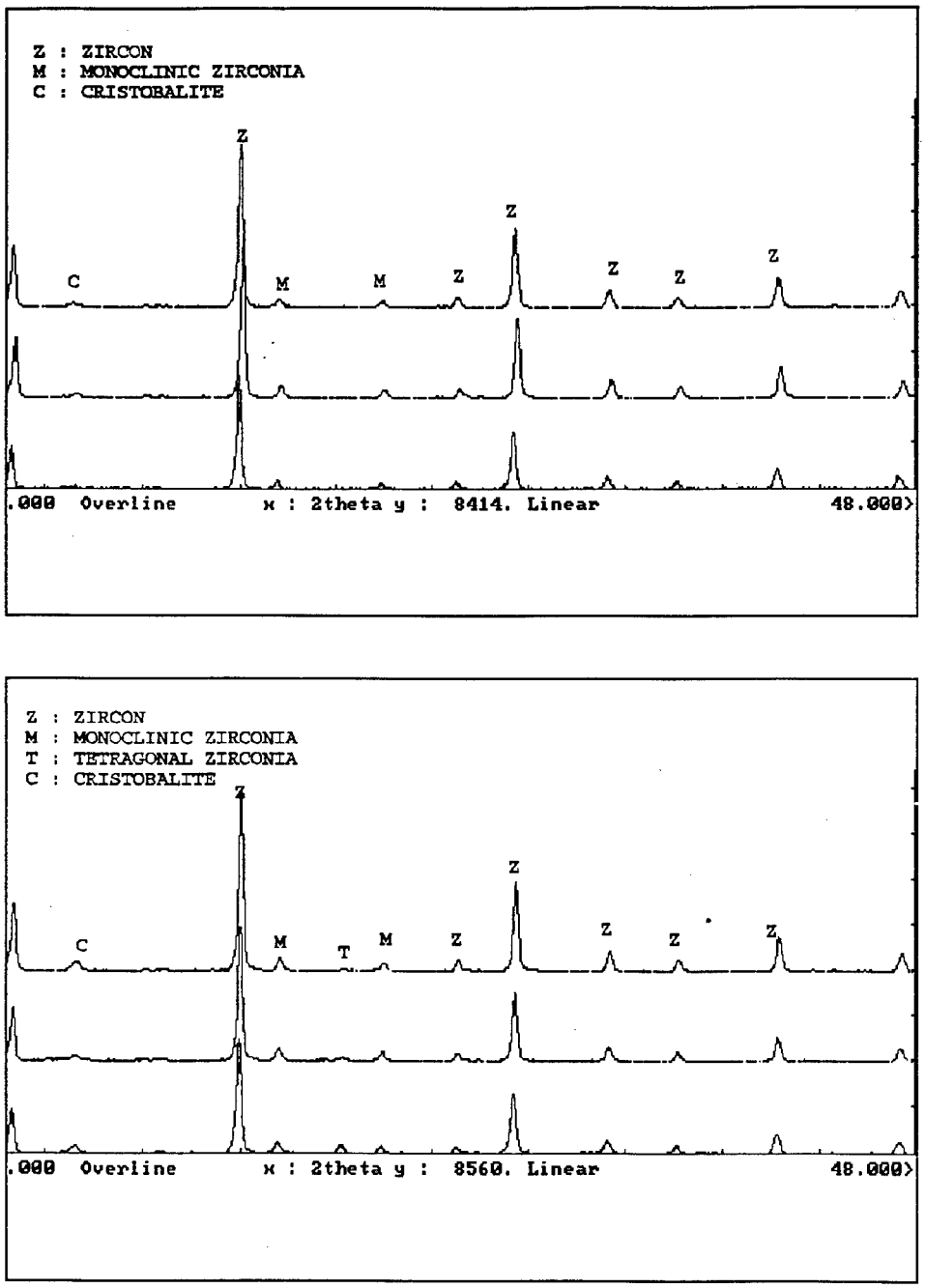

Fig.3: Effect of V-containing compound on phase composition for the Zircon-V system.
Upper graph: 850°C, lower graph: 800°C. Upper curves $VOCl_3$, middle curves VOR, lower curves NH_4VO_3.

ii) Colloidal Gel:

The Colloidal route has the advantage of much cheaper precursor materials since alcohol and alkoxides are replaced by water and salts, respectively. Preliminary experiments on the Pr-zircon system were performed and pigments with the same stoichiometry as in the polymeric gel case were synthesized. NaF was used as a mineralizer, dissolved in the aqueous colloidal solution of the precursor powders. When fired at 1200°C the colloidal powder developed a much stronger sun-yellow colour than the corresponding polymeric one, very much comparable to that of the conventional. However, the phases of both tetragonal and monoclinic zirconia still exist on the product, indicating that there is still room for the optimization of synthesis. Further experiments with both V and Pr systems are under way in order to explore the potential advantages of the colloidal method and complete a detailed comparison between these two routes.

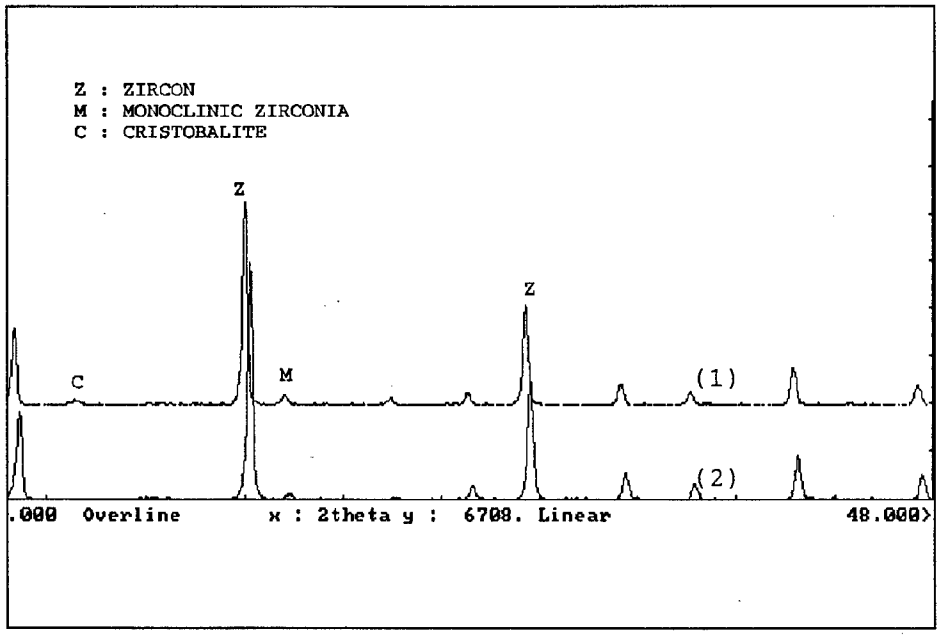

Fig. 4: Comparison between sol-gel made (1) and (2) Zircon -V blue pigment. Firing temperature 850°C.

4. Conclusions: In summary, with respect to colour development, the combination of mineralizer, appropriate aging time and any of the three tested V-containing compounds, produces a powder with turquoise-blue colour, similar to that of the conventionally made powder, at temperatures around 800-850°C. These preliminary experiments are promising and indicate that a combination of both lower firing temperatures and better pigment quality is possible. The colloidal route can render the sol-gel process economically more attractive, but it seems that the major edge of the sol-gel technology lies on the superior quality of the pigments produced. The sol-gel made pigments are currently tested versus conventional ones upon commercial tiles with respect to colour stability and tinctorial strength in order to evaluate their performance under industrial conditions.

5. References:

1. R.A.Eppler, Cer.Bull. 56, 213, (1977)
2. G.Monros, J.Carda, P.Escribano and J.Alarcon, J.Mat.Sci.Lett.9, 184, (1990)
3. G.Monros, J.Carda, M.A.Tena, P.Escribano, V.Cantavella and J.Alarcon, Mat.Res.Bull.27, 753, (1992)
4. G.Monros, J.Carda, M.A.Tena, P.Escribano and J.Alarcon, J.Mat.Sci.27, 351, (1992)
5. G.Monros, J.Carda, M.A.Tena, P.Escribano, M.Sales and J.Alarcon, J.Non-Cryst.Solids 148, 588, (1992)
6. R.Oheim, H.Paulus and C.Russel, J.Mat.Sci.Lett. 10, 1171, (1991)
7. G.Monros, J.Carda, M.A.Tena, P.Escribano and J.Alarcon, J.Mat.Sci. Lett. 9, 484, (1990)

Key Engineering Materials Vol. 150 (1998) pp. 15-20

Sol-Gel Ceramic Pigments

A. Atkinson[1], J. Doorbar[2], D.L. Segal[1] and P.J. White[3]

[1] AEA Technology, Materials Chemistry, 429 Harwell, Didcot, Oxfordshire, OX11 ORA, UK

[2] H & R Johnson Tiles Ltd., Tunstall, Stoke-on-Trent, Staffordshire, ST6 4JX, UK

[3] Portmeirion Potteries Ltd., Stoke-on-Trent, Staffordshire, ST4 7QQ, UK

Keywords: Sol-Gel, Ceramic Pigments, Decorations

Abstract

Aqueous sol-gel processing has been used to prepare a range of ceramic pigment compositions. The synthesis of pink and yellow-green pigments is described in detail and the application of sol-gel pigments to ceramic ware is outlined. Potential advantages of sol-gel syntheses over conventional ceramic pigments are highlighted.

Introduction

Ceramic pigments are doped multicomponent oxides, for example Cr-doped calcium zirconate, a yellow/green ceramic. Conventional ceramic pigments are made by solid-state reaction between powders [1]. The fired cake is ground, refired and reground to give a pigment powder. High temperatures are frequently required for these solid-state reactions, thus greater than 1573K for chrome-alumina pinks [1]. However this conventional process for pigment synthesis has several disadvantages. Firstly high reaction temperatures are energy intensive and thus increase the production costs. In addition the size distribution of the powder which affects colour intensity and chemical homogeneity which affects colour quality are difficult to control. Finally grinding for particle size reduction introduces chemical contamination that also affects colour quality. Sol-gel processing is under intense worldwide investigation [2-4], particularly for synthesis of advanced ceramics, but has received much less attention for application in conventional ceramics such as tableware and tiles. However sporadic references have been published on the preparation of ceramic pigments by sol-gel processing, for example the uvarovite pigment Victoria Green [5] by reaction of tetraethoxysilane with metal nitrates and chlorides. Vanadium-zircon blue [6] has been made from a range of precursors suitable for sol-gel processing of metal-organic compounds and sol-gel processing of oxide dispersions, thus zirconium propoxide and fumed silica, while a praseodymium-zircon yellow was obtained [7] from a doped tetraethoxysilane solution.

The main objective of the present study is to exploit the inherent advantages of the sol-gel process [8]. Advantages of sol-gel processing over conventional solid state reactions are improved chemical homogeneity due to mixing at the colloidal level, lower reaction temperatures, versatility due to handling liquid feeds, avoidance of dusts produced on mixing powders and the ability to produce powders with good flow properties. As an aqueous-based process, scale-up avoids handling of organic solvents. A secondary objective is to evaluate the pigments in decorations on ceramic ware.

Experimental

Sol-gel synthesis of pigments

Sol-gel preparations are illustrated by the synthesis of pink and yellow/green pigments. Flow sheets for the preparation of these ceramics are shown in Fig. 1 and Fig. 2.

Sol preparation

In a representative synthesis of the pink pigment (Fig. 1) 13.7 g of zinc nitrate (Fluka) and 4.87 g of chromic nitrate were dissolved in 13.0 cm^3 of a sol, aluminium chlorohydrate (Albright and Wilson). 0.35 g of boric acid (Unichem) dissolved in 30 cm^3 of H_2O were added to form a doped sol with a total oxide concentration of 200 g dm^{-3} and composition 40.5 w/o Al_2O_3; 3.5 w/o B_2O_3; 37.4 w/o ZnO; 18.6 w/o Cr_2O_3.

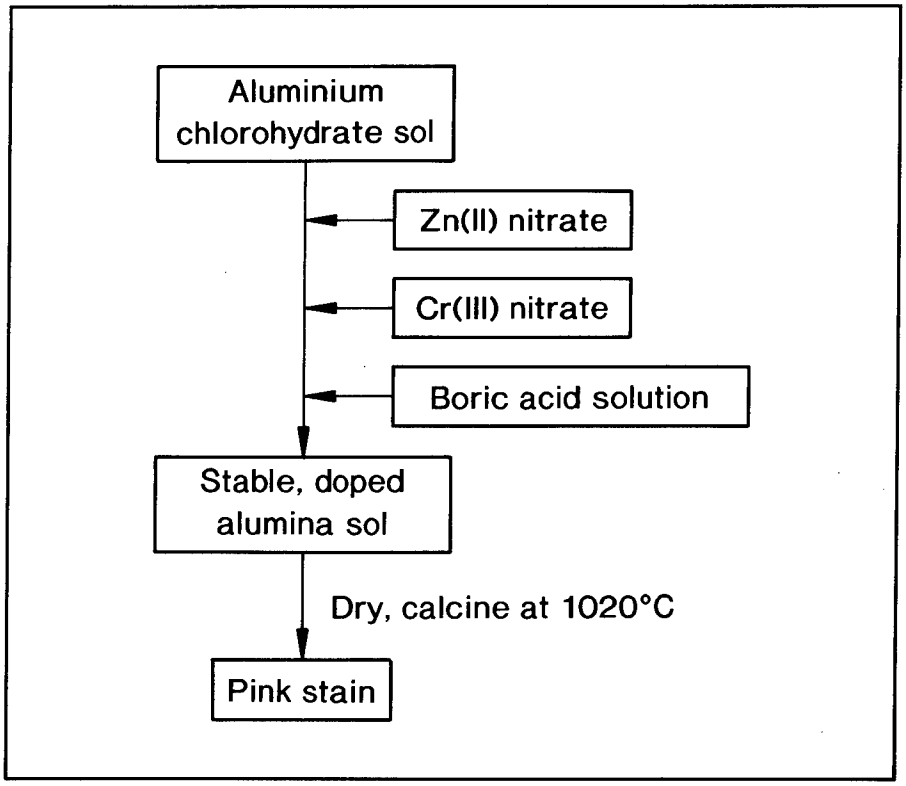

Fig 1. Preparation of a sol-gel pigment

In a representative preparation of a Cr-doped $CaZrO_3$ pigment (Fig. 2) zirconia sol containing 500 g dm^{-3} of oxide was prepared by addition of zirconium carbonate (Magnesium Elektron) to nitric acid [9]. 131.7 g of calcium nitrate (Johnson Matthey) were dissolved in H_2O and added to 137.4 cm^3 of the zirconia sol so that the doped sol had a calcium zirconate composition and total oxide concentration of 154 g dm^{-3}. An aliquot of doped sol containing 10 g of oxide was added to chromia sol whose preparation is described in [10] to give a chromia content of 5 w/o.

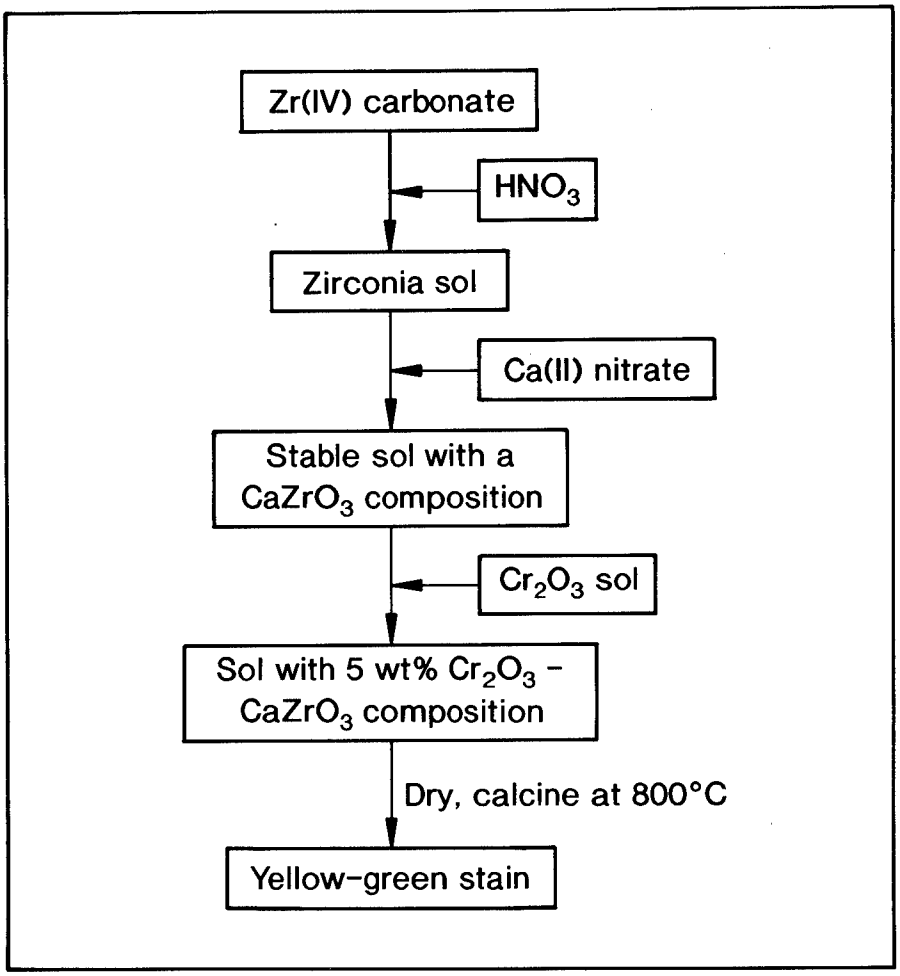

Fig 2. Preparation of a sol-gel pigment

Conversion of sols to pigments and decoration

Doped sols were converted to pigments and decorations by several methods. For example free-flowing pigment powders were obtained from sols (Fig. 3) while sol-gel materials could be converted into decorations as illustrated in Fig. 4; further details on the development of these decorations will be described separately.

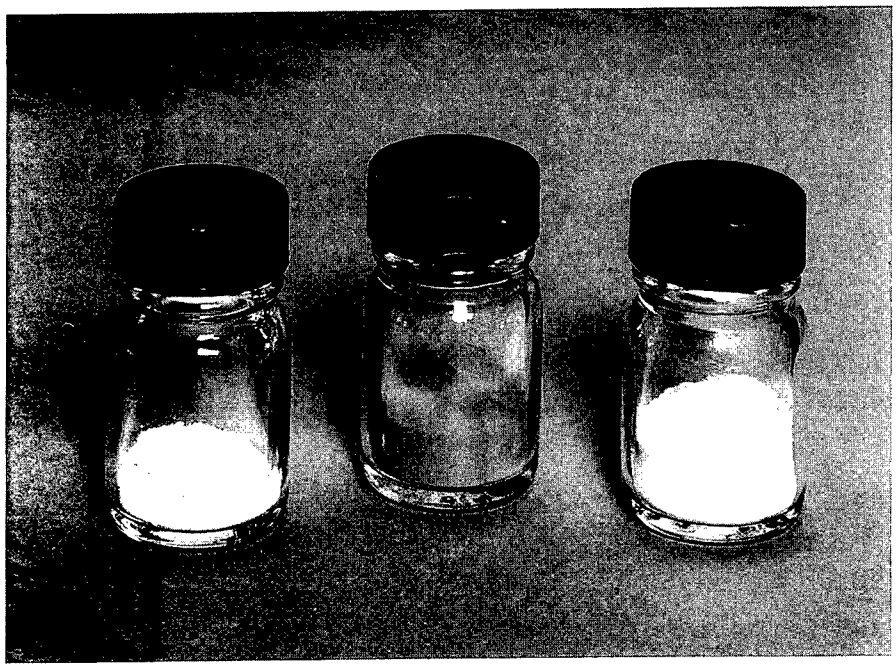

Fig 3. Sol-gel ceramic pigments

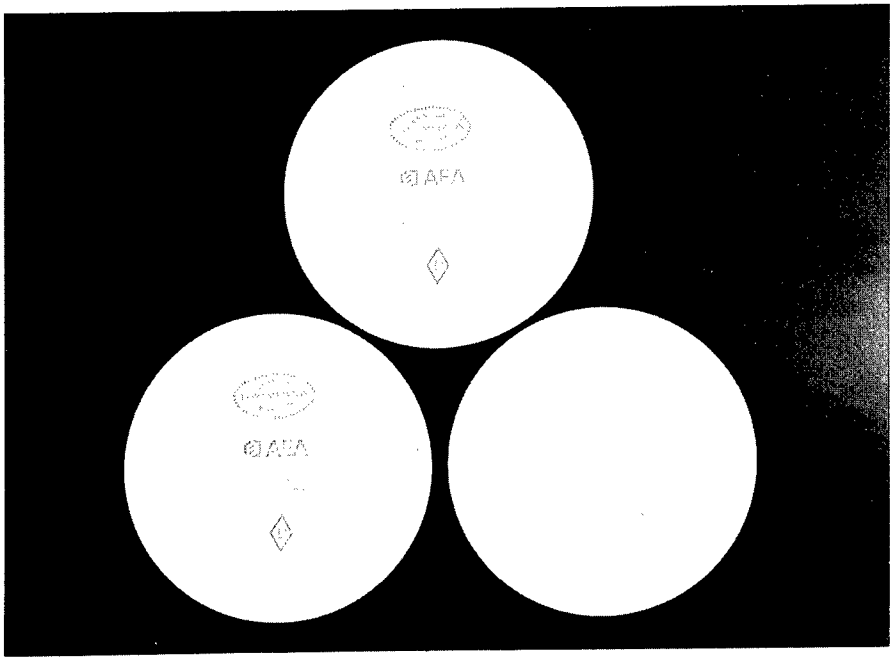

Fig 4. Ceramic decorations from sol-gel materials

Advantages of sol-gel syntheses

This study showed that aqueous sol-gel processing routes to ceramic pigments produced cleaner colours that have a firing tolerance over a wide temperature range. Powders derived from sols have good rheological properties, particularly advantageous when they are converted to decorations and the absence of organic solvents in this processing route will facilitate the scale-up of the sol-gel process to the manufacturing stage.

References

[1] C.G. Harman and C.W. Parmelee, Ceramic Glazes, 3rd edition, Cahners Books (1973).
[2] G. Pouskouleli and T. A. Wheat, Canad. Ceram. Quart. 25 (May 1990).
[3] C.J. Brinker and G.W. Scherer, Sol-Gel Science. The Physics and Chemistry of Sol-Gel Processing, Academic Press (1990).
[4] D.L.Segal, Chemical Synthesis of Advanced Ceramic Materials, Cambridge University Press (1989).
[5] J. Carda, G. Monros, P. Escribano, M.J. Orts and J. Alarcon, Bol. Soc. Esp. Ceram. Vidrio. **28**, 15 (1989).
[6] G. Monros, J. Carda, M.A. Tena, P. Escribano and J. Alarcon, J. Mater. Sci., **27**, 351 (1992).
[7] R. Oheim, H. Paulus and C. Russel, J. Mater. Sci. Lett. **10**, 1171 (1991).
[8] A. Atkinson and D.L. Segal, in Ceramic Technology International 1993, edited by I. Birkby, Sterling Publications, 187 (1992).
[9] J.L. Woodhead, United Kingdom Patent 1,181,794 (1970).
[10] United Kingdom Patent 2059933A.

Acknowledgments

This research and development was carried out with partial financial support from the UK LINK Nanotechnology Programme. We thank Mrs R E Evans and Mr R M Guppy (AEA Technology), Ms A Allen (Portmeirion Potteries Ltd), and Mr M Thompson (H & R Johnson Tiles Ltd) for their contribution to this programme.

Key Engineering Materials Vol. 150 (1998) pp. 21-32

Characterization of Oxide Layers Deposited by Sol-Gel

K. Bange

Schott Glaswerke, R & D, Otto-Schott-Str. 2, D-55127 Mainz, Germany

Keywords: SiO_2, TiO_2, Oxide Films, Sol-Gel, Thin-Film Analysis, Composition, Density, Stress

ABSTRACT

Some representative characteristics of oxide films produced by sol-gel are briefly described, and several relevant methods of thin-film analysis to determine these quantities are indicated. The most powerful information of the analytical techniques is given, and some typical problems that may occur by the analysis of oxide thin films are discussed. With a few selected results, the meaningfulness is demonstrated for some modern methods.

1. INTRODUCTION

Modern thin-film technology gains an increasing relevance in material and product development and occupies more and more key positions in that field. In particular, thin oxide layers play a dominant role in the improvement of chemical and physical properties of glass surfaces, because they contain the important characteristics of glass as, for instance the transparency in the visible spectrum, or the electrical insulation. Various deposition techniques can be applied for the production of oxide layers on glass, but the large-scale production [1,2,3].

A broad spectrum of analytical tools is available, principally for sufficient characterization of thin films, but the unusual characteristics of oxide layers are a challenge for the methods of thin-film analysis, because special problems arise from the application on oxides. Besides the well-known traditional techniques, e. g. optical spectroscopy, various analytical techniques exist which give microscopical information on thin films and interfaces. Especially the fast development in the filed of surface analysis in the last decade allows for a powerful description of technical thin films today. Since these types of methods in general work with electrons, ions and photons, various problems can be generated by the analysis of oxidic thin films.

In this short report some characteristic quantities of oxide layers are described, some relevant analytical methods are briefly mentioned, and some problems by the analysis of oxide layers are reported. By various examples, an approach is illustrated how analysis can be used in an efficient way in service labs.

2. ANALYSIS OF OXIDE LAYERS

It is well known that properties of films are influenced by the deposition parameters and conditions. Variations are possible, for example, in the refractive index, the adhesion, the colour, the films thickness, etc. To produce layers in an efficient way, it is necessary to know the relevant size in the deposition process that influences a certain film property. They are for films produced by sol-gel, the composition of solution, the substrate temperature, the interaction during the film formation with the substrate and with the surrounding atmosphere.

Macroscopic as well as microscopic films properties are necessary for a sufficient description of oxide layers, e. g. refractive index, absorption, film thickness, adhesion, stress, density, scattering, hardness as macroscopic quantities, and composition of elements, chemical binding state of elements, stoichiometry, topography, roughness of the surface, formation of interfaces, crystalline or amorphous, and also the structure of the crystal at microscopic sizes.

Various analytical methods are available to obtain such types of information. Generally, they use as a probe photons, electrons and ions, but also forces, e. g. in atomic force microscopy (AFM) [4]. The different probes interact with the certain volume of the samples and create emitting photons, electrons or ions, which are detected. The acronyms for some methods are given in Tab. 1. Photons are used as probe in optical spectroscopy [5] to determine the transmittance (T), the reflectance ®, and the absorptance (A), in total integrated scattering (TIS), in angle resolved scattering (ARS) [6], in x-ray reflectivity spectroscopy (XRS) [7], in x-ray diffraction (XRD) [5], Raman spectroscopy [5], and spectroscopy for chemical analysis (ESCA) [8]. Electrons are the probe in transmission electron microscopy (TEM), energy dispersive x-ray analysis (EDX), electron diffraction (ED) [5], and Auger electron spectroscopy (AES) [8]. Ions are applied as primary particles in secondary ion mass spectroscopy (SIMS), ion beam spectra chemical analysis (IBSCA) [5], nuclear reaction analysis (NRA), and Rutherford backscattering spectroscopy (RBS) [5]. More details on these methods are given in the quoted references.

The requirements on the methods for thin-film analysis are fairly high for a sufficient characterization of thin oxide layers. It is desired that they detect, a large range of elements with a low detection limit, that they possess a high lateral resolution and a low information depth. Additionally, they should give information on the state of oxidation and the binding state of elements, work non-destructively and quantitatively. Each of the methods has its special advantage. With the high degree of complexity of oxidic sol-gel layers, a multi-method approach is necessary for a powerful description of the layers.

Additional problems arise from the application of the thin-film analysis on non-ideal samples, so, for instance, on oxidic layers. While an ideal object for the methods of thin-film analysis is electrically conductive, possesses a smooth and plain surface in a sufficiently large dimension and consists of one homogeneous phase, oxide layers produced by sol-gel exhibit nearly opposite properties. So, for example, oxide layers are described in solid state physics in general as a perfect insulator with an occupied valence band and the empty conduction band. The band gap is, in general, some electron volts broad, whereby the films are transparent in the visible spectrum of light. As mentioned before, thin-film analysis uses as a probe (primary beam) charged particles. But also the secondary beam can consist of charged species. Both can induce charging effects on non-conductive surfaces. An emitting photo electron or Auger electron in the electron spectroscopical methods (ESCA) may create a positive centre which cannot be neutralized, since non-conductive materials have not enough delocalized electrons in the conduction band. This creates a positive outer potential near the surface, which retards electron emission. These effects are to be recognized in the electron spectrum by positive shift, which often leads to misinterpretations of electron spectroscopic data where this shift in the binding energy scale of ESCA spectra is often understood as additional oxidation state.

Many other artifacts are possible in the analysis of thin oxide films. Ionized gases are usually used for the removal of material in element-depth profiling, as well as in the preparation of speciments for TEM investigations. Typically, argon is applied in an energy range from 1 - 10 keV for sputtering. During sputtering, very different effects occur, for instance, backscattering, trapping, reemission, emission of electrons, and photons, but also changes

in the surface structure and topography. Additional problems are created by the sputtering of multicomponent systems. For oxidic materials, changes in the stoichiometry in the surface region are reported, which are in general explained by the difference in the mass of the elements and the surface energy between elements. These effects, known as „preterential sputtering", are very pronounced in oxide layers with heavy metal elements, like Ta_2O_5 and WO_3 [9].

Table 1: Analysis oriented towards problems

Film properties	Methods
microscopic	
• composition	SIMS, IBSCA, RBS, NRA, ESCA, AES
• state of oxidation	ESCA
• structure of crystals	XRD, ED, Raman
• roughness of surfaces	AFM, TEM, XRS
• formation of interfaces	TEM, XRS
macroscopic	
• density	XRS, RBS
• stress	bending
• adhesion	micro intender
• optical quantities (n, k)	T, R, A
• scattering	TIS, ARS
• hardness	milling, etc.
• thickness	R, T, A, TEM, XRS, stylus

3. ANALYSIS ORIENTED TOWARD PROBLEMS ON THIN FILMS

Thin-film analysis can give support in trouble shooting, in the development of thin films, for the optimisation of processes, and also for control of production. For this type of work, a special approach is necessary, especially because the instruments used are in general fairly expensive, and the degree of complexity in the analysis of oxidic thin film is very high and, therefore time-consuming. Only the investigation of well-defined problems and samples allows, in that way, an efficient application of the techniques. A selection of samples of significance is the starting-point of a successful analysis. Also a critical assessment of the available method and of their potentials, in connection to the working hypothesis and the problems to be investigated is the basis, i. e. the selection of the most powerful instrument referred to problem that has to be studied is one of the key questions which has to be solved. This approach has to be typical in industrial service labs. To illustrate this approach, Tab. 1 summarizes some typical film properties and connects these with methods which give the desired information. Obviously, different methods can be applied to obtain a certain topic. So, for example, the film composition can be analysed by SIMS, IBSCA, RBS, NRA, ESCA,, AES, etc. Each method has its merits but also its shortcomings. Both should be known to select the appropriate methods for a special problem to be investigated. This will be demonstrated in the following by few selected examples.

3.1 COMPOSITION

The physical and chemical properties of thin oxide films produced by sol-gel are strongly influenced by the deposition parameters and conditions used. Thereby, the film composition possesses a strong influence. Beside the expected components, such as oxygen and metal, technical oxide films contain various other elements. In part, these are due to doping materials, to create special film properties, but also undesired components can be found in the film. As illustrated in Tab. 1, various methods can be applied to study the film composition.

The film composition can change also during testing procedures or application. For that type of investigation, methods are necessary which have to detect smallest variations, i. e. they must be very sensitive. For such type of studies, the combination of SIMS and IBSCA is an appropriate tool, because it allows the detection of9 low concentrations of elements, and also small changes. Such effects are illustrated in Fig. 1. NaI depth profiles are shown for SiO_2 layers deposited on soda-lime glass. Two different sample treatments are depicted. One was heated to 500 °C for 1 h, the other was boiled in H_2O for 48 h. A comparison with the as-deposited data exhibits that the temperature treatment leads to a diffusion of sodium into the SiO_2 layer. A different behaviour is to be observed after the boiling procedure. The sodium is leached out of the glass interface, diffused through the SiO_2 film, and can be analysed in the adjoining water. The data shown demonstrate that, for qualitative detection of elements IBSCA, is a very sensitive method.

Only few methods are available that allow a quantitative analysis of element composition in thin films. Usually, a combination of different methods is necessary to obtain a full quantitative data set. Especially the hydrogen content is difficult to determine quantitatively in thin films. But this quantity possesses a strong influence on certain film properties, especially for optically active layers [10], and is, for other materials a good indicator for several film characteristics. With some experimental care, a quantitative measure of additionally hydrogen depth profiling. Some results are depicted in Fig. 2 for TiO_2 films on soda-lime glass. The depth profiles are given for materials heated to different temperatures. The higher amount of hydrogen at the films surface (at 6.4 MeV) indicates water adsorption at the interface air/film. The film/glass interface is located at an energy of 6.55 MeV. For a film heated up to 170 °C, a H/Ti ratio of approximately 0.5 is analysed. With increasing temperatures, the amount of hydrogen decreases. In-situ NRA measurement as a function of the temperature T, exhibits two regions for hydrogen desorption. One is for $T < 200$ °C where a continuous H decrease is observed, the second one is for $T > 300$ °C [11].

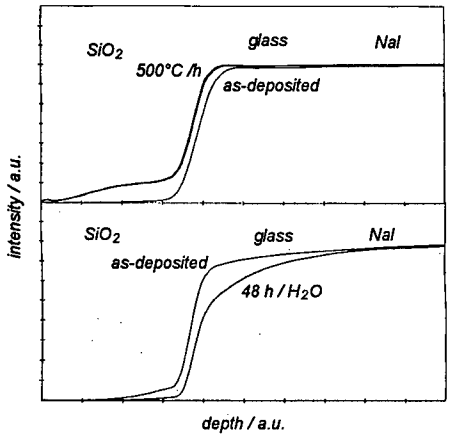

Fig. 1: IBSCA depth profile of the NaI line from SiO_2 films on soda-lime glass.

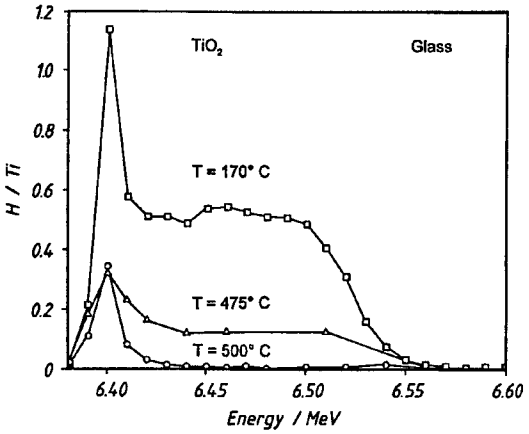

Fig. 2: Hydrogen depth profile of TiO_2 layer on glass. The film is heated to different temperatures.

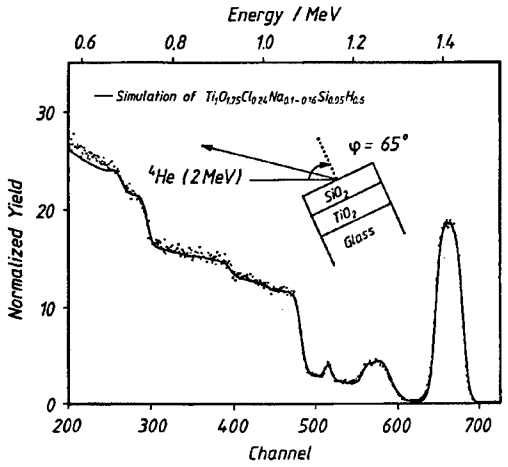

Fig. 3: RBS spectra of a TiO_2 film on soda-lime glass. The layer contains different impurities.

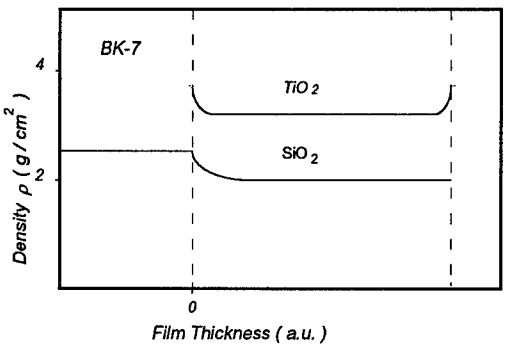

Fig. 4: Density versus film thickness of SiO_2 and TiO_2 films on BK-7 glass.

For an exact quantitative analysis of the other elements, especially the heavier ones, RBS is an excellent tool. The non-destructive techniques allow an exact determination of the oxygen/metal ratio, but also the analysis of the other elements. One example is depicted in Fig. 3 for a titanium dioxide film on soda-lime glass. Beside Ti and O, also Na and Cl are analysed in the film. The doping material SiO_2 is diffused during the annealing procedure on top of the film surface. Wile Cl can be explained as a residue of the sol-gel solution, Na is diffused from the glass substrate in the film. The shown result is fairly typical for TiO_2 sol-gel layers deposited n soda-lime glass without a SiO_2 blocking barrier. Only the exact quantities vary.

Some data of a full quantitative analysis of TiO_2 films deposited by different techniques are given in Tab. 2 for comparison. Beside the films produced by dip coating (DC) and spin coating (SC), also the compositions are given for films produced by physical vapour deposition method (PVD). It is obvious that the layers deposited by reactive evaporation (RE), ion assisted deposition (IAD), sputtering (SP), and ion plating (IP) contain different impurities that can be related to the deposition technique. While the undesired elements in the sol-gel process are due to solution or diffusion products from the glass, in the PVD techniques the impurities can be referred also to the special deposition conditions, so, for example, argon which is a gas in the sputtering process, or carbon and molybdenum which are crucible materials.

Table 2: Composition of TiO_2

Sol-Gel:	DC:	$TiO_{1.9}\ Cl_{0.08}\ Ca_{0.01}\ H_{0.04}$
	SC:	$TiO_{1.75}\ Cl_{0.24}\ Na_{0.1}\ H_{0.6}$
PVD:	RE:	$TiO_{2.08}\ C_{0.25}\ H_{0.1}\ Si_{0.03}$
	IAD:	$TiO_{2.04}\ C_{0.1}\ H_{0.25}$
	SP:	$TiO_{2.04}\ Ar_{0.05}\ H_{0.05}\ Ta_{0.003}$
	IP:	$TiO_{1.99}\ H_{0.01}\ Mo_{0.002}$

3.2 DENSITY

It is generally accepted today that most of the deposition techniques create films with densities which strongly deviate from the respective bulk densities. Especially, problems arise in films with a reduced density when they are used at temperatures where water desorption and adsorption can occur [12]. This mechanism can lead to the destruction of films [5].

There are a number of techniques available for estimating the density of thin films.

- The refractive index n for visible light is a reasonable indicator of the film density in porosity, undoped material. For instance, in TiO_2 films prepared by different deposition conditions resulting in different densities, the index n varies by as much as 0.4 [13].
- The hydrogen content determined by NRA or the infrared absorption of the OH groups is an indirect and qualitative indicator for the film density. The hydrogen concentration is strongly linked with n [14,15].
- A relatively good value for the film density can be calculated from the mass of the film monitored by an oscillating quartz and the film thickness measured independently.
- The film density can be determined quantitatively by RBS, provided the precise stoichiometry (also hydrogen content) and the film thickness are known [16].
- The film density can be determined with great precision by means of x-ray reflectivity spectroscopy [7, 17]. Additionally, the film thickness and the interface roughnesses can be deduced from the experimental data [17].

Table 3: Density ρ (g/cm^3) roughness σ (nm) and thickness δ (nm) of SiO_2 and TiO_2 film deposited by dip coating (DC), ion plating (IP) and reactive evaporation (RE)

sample	substrate		intermediate layer			main layer			surface layer		
	ρ [g/cm^3]	σ [nm]	ρ [g/cm^3]	δ [nm]	σ [nm]	ρ [g/cm^3]	δ [nm]	σ [nm]	ρ [g/cm^3]	δ [nm]	σ [nm]
SiO_2/DC/BK-7	2,49	1,8	2.33	3,4	2,0	2,12	16,3	2,0	2,01	76,4	0,33
TiO_2/DC/BK-7	2,49	1,06	3,69	3,7	2,8	3.23	71,3	2,22	3,74	3,7	0,68
TiO_2/IP/BK-7	2,49	0,99				3,93	92,7	0	3,79	3,6	0,87
TiO_2/RE/BK-7	2,49	0,42	3,82	4,4	0	3,57	110,8	2,24			

Some results of SiO_2 and TiO_2 films deposited by dip coating (DC) on BK-7 are summarized in Tab. 3. For comparison, also the quantities are depicted for TiO_2 films deposited by two PVD methods [17]. It can be recognized that the films produced by DC exhibit an increased density in the vicinity of the glass/film interface, in a thickness range of 3 - 4 nm. While for SiO_2, the density further decreases in direction of the film surface and finally remains constant, for TiO_2 films the density increased in the surface region. This behavior is illustrated in the schematic representation in Fig. 4. By comparison of DC densities with data of PVD films [17], it can be concluded that density inhomogeneities in oxidic thin films are fairly general phenomena. Also in

the glass/film interface region for RE film, or in the surface region for IP films, changes in the densities can be recognized.

3.3 STRESS

More and more sophisticated products are based on multi-layer systems or on thick-film techniques. For the sol-gel dip-coating procedure, this is demonstrated in this conference for multi-layer interference filters [18]. For the increased complexity of such type of coatings on glasses, a detailed knowledge of the mechanical properties of the single film is necessary. The basic properties of the single films are important, to guarantee the functionality of the final product. So, for example, the stress of the films, in connection with the adhesion of the materials, should be below a certain limit to avoid cracking or detachment of coatings causing a catastrophic failure of coated systems. Additionally it is necessary to understand how the intrinsic stress of the films may be influenced.

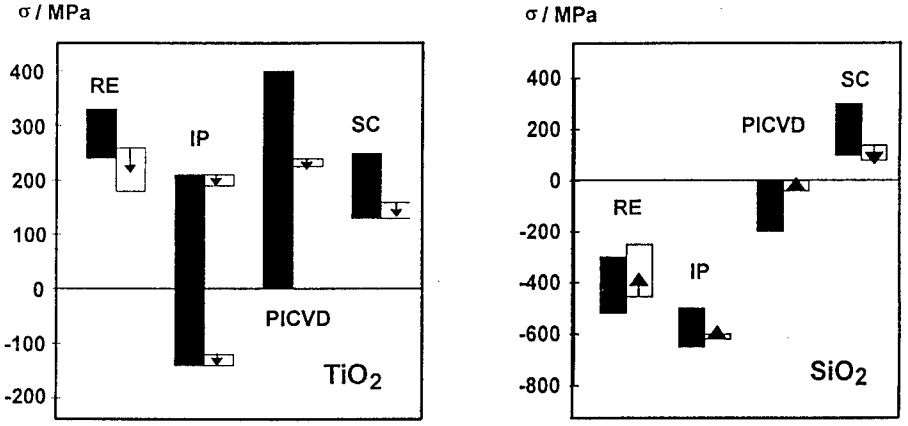

Fig. 5: Range of variation in stress in TiO_2 and SiO_2 films produced by different parameters (black bars) and different techniques. The range of stress relaxation is depicted also (open bars).

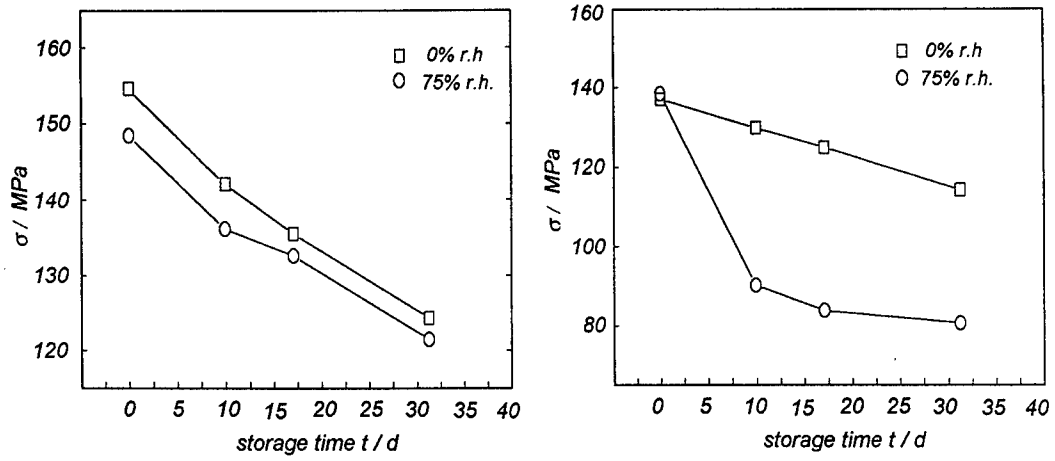

Fig. 6: Variation in stress in TiO_2 and SiO_2 films deposited by spin coating, as a function of time stored in different reactive humidity (r. h.).

Various methods are reported to determine the stress in films. Some are very useful for very thick films, while others can be applied on crystalline materials [19]. Also, with the bending-beam method, i. e. the deflection of the free end of a one-side clamped substrate strip, or the central deflection of a two-sided clamped strip, the stress can be measured. But since in practice the two-dimensional deformation of the substrate is the important quantity, this effect is analysed. The surface topography of the samples is investigated by using of a ZYGO Mark IV interferometric system. The interference fringes pattern are analysed by an imaging processing algorithm, and the corresponding information of the surface curvature is transferred to a PC system. The surface profile of the specimen is obtained before and after coating, or the treatment procedures. The differences of th4se data sets result in a spherical, shaped structure, superposed to the substrate topography, due to the influence of the stress component of the film. The radius of the curvature of this sphere is determined by means of a fitting routine, and the film stress can be calculated when the elastic constants (Young's modulus and Poissons's ratio) of the substrates are known. With the used experimental set-up, stress of less than 10 MPa for a 100 nm thick film can be analysed, which is an adequate precision for thin-oxide layers [20].

Some typical results for stress in TiO_2 and SiO_2 films with a thickness of approximately 100 nm are depicted in Fig. 5. The black bars represent the variation in stress obtained by differences in the deposition parameters of the respective technique. The films produced by spin coating (SC) exhibit a weak tensile stress of the order of 200 MPa. Similar to the RE films, which were also deposited at higher temperature, they show no strong dependence on the production parameters. For TiO_2 films, deposited by ion plating (IP) and plasma impulse chemical vapour deposition (PICVD), large differences are observed in the stress with respect to the used coating conditions [20].

Results on relaxation of film stress with time after production are also depicted in Fig. 5. Typical stress relaxation data for each deposition process are indicated by the open bars. The direction of stress relaxation is given by the arrows. It is obvious that the film deposited by SC possessed a tendency to decrease in stress after the deposition.

The changes in stress as a function of the time are different for SC SiO_2 and TiO_2 films. This is illustrated in Fig. 6. While for TiO_2 films the relaxation effect is independent of the relative humidity of the surrounding atmosphere of the film, SiO_2 layers exhibit a strong dependence on the relative humidity. A large decrease in the tensile stress of SiO_2 (60 MPa) is observed at a relative humidity of 75 %, while in dry air the changes are only approximately 20 MPa. In the crystalline TiO_2 film, the relaxation effect is not as large as in SiO_2.

The trends for stress relaxation in oxidic thin films can be summarized as follows: Sress relaxation is influenced by the relative humidity in SiO_2, but not for TiO_2 films. For films with a high density (IP, PICVD), the effect is less pronounced. Crystalline materials exhibit smaller changes in stress than amorphous materials (at the same film density). Porous and amorphous materials exhibit a large relaxation effect.

4. SUMMARY

The few selected examples demonstrate that, in thin-film analysis, no universal method exists for the determination of all the quantities necessary to describe oxidic thin films. For sufficient characterization of thin oxide films, methods are necessary which give complementary information. An exact knowledge of the power of the different methods is necessary for their efficient use when approaching problem solving in thin-film development and production.

5. REFERENCES

1. H. Schröder, Phys. Thin Films 5, 87 (1969)

2. H. Dislich, Glastech. Ber. 579, 228 (1984)

3. E. Hußmann, this proceeding

4. E. Meyer, Progress Surf. Sci. 41, 3 (1992)

5. K. Bange et al., „Stabilization of Oxidic Thin Films", BMFT final report (13N 5476) (1991)

6. J. M. Bennett, L. Mattsson, „Surface Roughness and Scattering", Am. Optical Soc. Washington D. C. (1989)

7. B. Lengeler, Adv. X-ray Anal. 35, 127 (1992)

8. H: W. Werner, R. P. H. Garten, Rep. Prog. Phys. 47, 221 (1984)

9. K. Bange, O. Becker, „Schichtkunde: Schnittstelle zwischen Verfahren und Anwendung", VDI Verlag, Düsseldorf, 86 (1991)

10. K. Bange, T. Gambke, Adv. Mat. 1, 10 (1990)

11. M. Laube, C. Ottermann, W. Wagner, H. Niederwald, F. Rauch, K. Bange, Glastech. Ber., submitted

12. K. Gürtler, K. Bange, W. Wagner, F. Rauch, H. Hantsche, Thin Solid Films 175, 185 (1989)

13. K. Bange, C. Ottermann, O. Anderson, U. Jeschkowski, M. Laube, R. Feile, Thin Solid Films 197, 279 (1991)

14. F. Rauch, W. Wagner, K. Bange, Nucl. Instr. Meth. Phys. Res. B 42, 263 (1989)

15. C. Ottermann, K. Bange, W. Wagner, M. Laube, F. Rauch, Surf. Interf. Anal. 19, 435 (1992)

16. B. P. Hichwa, G. Caskey, Surf. Coat. Technol., 33, 393 (1987)

17. M. Hüppauff, K. Bange, B. Lengeler, Thin Solid Films 230, 191 (1993)

18. N. Arfsten, this proceeding

19. H. K. Pulker, „Coatings on Glass", Elsevier, Amsterdam (1984)

20. C. Ottermann, J. Otto, U. Jeschkowski, O. Anderson, M. Hemin, K. Bange, Proc. MRS, in press

Key Engineering Materials Vol. 150 (1998) pp. 33-40

Mechanical Precision in Sol-Gel Manufacturing of 3-D Components

L. Costa

GDE, Via Rivoltana 13, I-20090 Segrate (MI) Italy

Keywords: Sol-Gel, Net-Shape, Manufacturing, Near Net-Shape, Silica, Silica Glass, Monolithic, Amorphous, Hypercritical, Densification, Miniaturisation, New Material, New Processes, Resonator, Gyroscope

ABSTRACT: capability for precision-manufacturing in ultra-pure silica glass by sol-gel moulding is demonstrated. The products, three dimensional, ideally isotropic, might be manufactured on any geometry compatible with state of the art moulding. Net-Shape Manufacturing to an Accuracy of 50μm is feasible now.

INTRODUCTION: the Enichem/GDE sol-gel moulding technology is a proprietary technology based on patents and "Know-how" for the synthesis, moulding and eventual densification of materials and manufacts of silica and/or other metal oxides. The "Synthesis" comprehends all the processes for the formulation and preparation of special colloidal dispersions (sols) composed of hydrolized metal alkoxides and/or other chemical precursors and of granular metal oxide materials of proper morphological characteristics. It also includes the proper conditioning of such sols for controlled polycondensation. "Moulding" is the process for fabrication of monolithic, amorphous aerogels in silica and/or other metal oxides. Such aerogels are characterised as: three-dimensional, free of intrinsic dimensional limitations, ideally isotropic and free of structural defects. They can be manufactured on any geometry compatible with the state of the art of moulding. "Densification" comprehends the process or series of processes for the conversion of amorphous, monolithic aerogels consistent with Enichem standards into glasses of corresponding composition. The "Densification" process operates exclusively on isotropic materials producing an ideally linear contraction in all directions resulting in a miniaturised "Dense" copy of the aerogel. Since the contraction factor of densification is predictable, the result is the fabrication of glass products in NET or NEAR NET SHAPE [1...5].

OBJECTIVES OF THIS WORK: as the title of this paper states, it is typical application of this technology the precision manufacturing of relatively large, 3-D components, specifically amorphous, monolithic components. The activity of GDE in this field may be illustrated with the example of the amorphous silica resonator, known also as the "WINE GLASS RESONATOR", a vital component of the HRG (Hemispherical Resonator Gyroscope) system. An overview of the device as published by Delco on Design News is given FIG. 1.

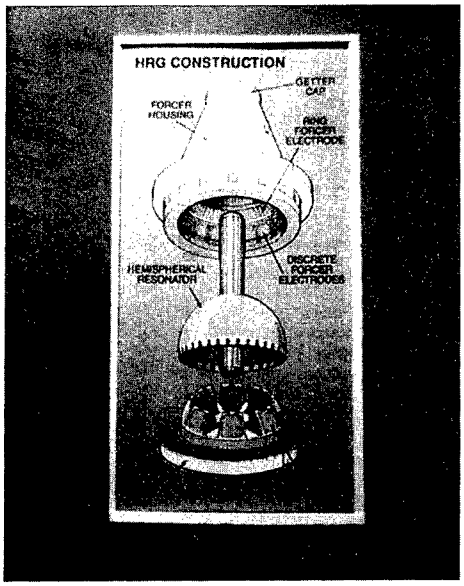

Fig. 1 Hemispherical Resonator Gyroscope (After Design News)

The Hemispherical Resonator Gyroscope is composed of three parts made of silica glass; the resonator is the central one. High purity is required to match the specified physical properties of the device. For more details on the HRG system the reader is referred to the original publication [6].
The dimensional specifications, as one can expect, are particularly demanding for the resonator for which all diameters, radii of curvature and thicknesses are critical. All critical dimensions have tolerances in the order of micrometers. Although at the time the manufacturing of such pieces by conventional sol-gel processes was considered beyond the state of the art of the technology, the challange to Near-Net Shape Manufacturing of the resonator was picked up by the GDE with "ad hoc" processes and succesfully brought to a technical accomplishment.

EXPERIMENTAL

Figure 2 shows results of the three typical manufacturing steps: the gel phase of the product, immerged in liquid inside a beaker, the aerogel phase that maintains the exact dimensions of the gel and the dense phase rappresented by the silica glass product of similar morphology, but reduced dimensions.

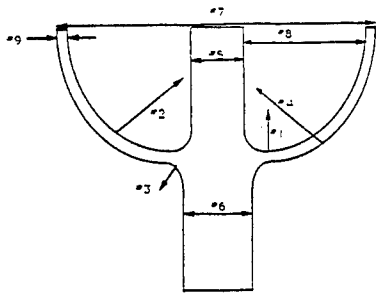

Fig. 2 The 3 manufacturing phases of Sol-Gel moulding

Several series of silica glass resonators were made for the purpose of verifying the degree of dimensional control exercized on the product by the process. Pertinent data are given in tables 1 to 4.

Fig. 3 illustrates on a schematic drawing the dimensions that were measured on a series of seven prototypes. The determinations were made by an indipendent, well qualified laboratory in the U.S. acceptable to both GDE and perspective buyer. Only deviations from the specified dimensions will be shown on these tables: real dimensions remain sensitive information.

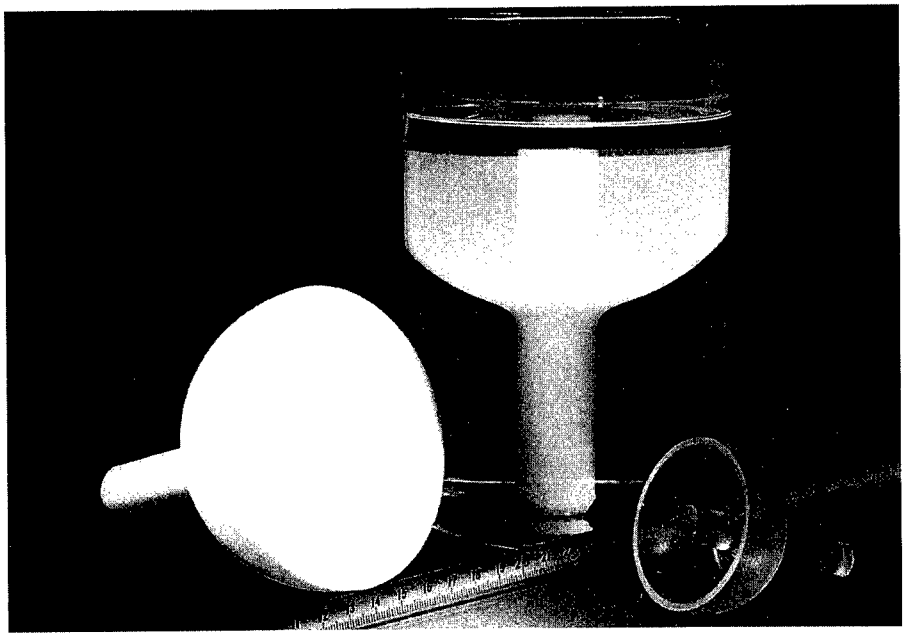

Fig. 3 Dimesion compared on resonator

Table 1 summarizes the results of a reproducibility test. The seven prototypes reported on this table were realized with laboratory procedures. A preliminary moulding was used on the assumption that for a reproducibility test moulding specifications are not required several sets of measurements were made and statistically treated.

REPRODUCIBILITY TEST

N	DESCRIPTOR	STAND DEV.	LARG DEV.
1	Radius of curvature at bottom of cup	1,233%	3,176%
2	Inner radius of cup	0,531%	1,558%
3	Outer radius at bottom of cup	0,773%	1,850%
4	Outer radius of cup	0,680%	1,929%
5	Diameter at top of stem	0,569%	1,438%
6	Diameter at bottom of stem	0,237%	0,675%
7	Diameter at top of cup	0,125%	0,333%
8	Distance from stem to cup	0,480%	1,323%
9	Thickness of cup	1,450%	4,712%

Table 1

The data of Table 1 show standard deviation generally within 1% of the specified dimension.

Table 2 summarizes the results of an Accurancy Test run on 6 samples still manufactured with the same laboratory procedures, but with a new moulding within specifications; only one set of original measurments was available. The data are given as percent deviations from the specified Near-Net Shape dimensions.

ACCURANCY TEST
(moulding at specifications)

N.	Descriptor	20 (%)	21 (%)	22 (%)	23A (%)	23B (%)	23C (%)
2	Inner radius of cup	0,996	0,111	1,881	1,291	1,955	1,328
3	Outer radius at bottom of cup	0,927	-0,137	1,853	1,579	1,990	2,162
4	Outer radius of cup	-2,452	-2,277	0,350	0,000	-1,401	-2,452
6	Diameter bottom stem	-0,867	-1,530	0,396	0,203	0.074	0.240
7	Outer diameter of cup	-0,446	-0,807	0,944	0,923	0.738	0,789
10	Inner diameter of cup	-0,411	-0,658	1,399	1,481	1,399	1,481

Table 2

From the data of Table 2 one can verify an Accurancy in average slightly worst than 1%. Samples 23A, 23B and 23C were made with an improved procedure and on that ground they constitute a subset to be analyzed separatly.
Table 3 provides the Precision Test for the samples of Table 2.

PRECISION TEST
(Moulding at specifications)

N.	DESCRIPTOR	STAND. DEV.	MAX DEV.
2	Inner radius of cup	0,666%	1,136%
3	Outer radius at bottom of cup	1,862%	3,051%
4	Outer radius of cup	0,849%	1,505%
6	Diameter bottom cup	1,006%	1,420%
7	Outer diameter cup	0,489%	1,154%
10	Inner diameter cup	0,203%	1,176%

Table 3

Percent deviations from the mean are given for the entire set of 6 semples. The subset of the last 3 samples: 23A, 23B and 23C is treated in Table 4: only maximum deviations are listed due to the limited number of samples.

PRECISION FOR SUBSET 23 ONLY

N.	DESCRIPTOR	STAND. DEV.	MAX DEV.
2	Inner radius of cup		0,280%
3	Outer radius at bottom of cup		1,295%
4	Outer radius of cup		0,327%
6	Diameter bottom cup		0,057%
7	Outer diameter cup		0,105%
10	Inner diameter cup		0,098%

Table 4

One can observe that for the same samples the values of precision of Table 3 are improved but still comparable to those of the accuracy of Table 2. By comparing, instead, the subset of Table 4 with the entire set of Table 3 one can verify a substantially superior precision for the limited subset (samples 23A, 23B, 23C). Such precision, even if determined from maximum deviation data, corresponds in the worst case to a maximum of 90μm and to only 7μm in the best case.

SUMMARY

We have illustrated, with the example of the H.R.G., the feasibility under proper conditions of fabrication in N.N.S. of objects of critical morphology with accurancy and precision within 50μm.
Activity in GDE covers the fields of duplication of optical surfaces, generation of lens profiles as by specifications, fabrication in net shape of objects within 50μm dimensional specifications.

An overview of that work might be perceived from the series of figs 4...7.
Fig. 4 rappresents one hemisphere in silica glass and two meniscuses with optical surfaces produced by sol-gel moulding.

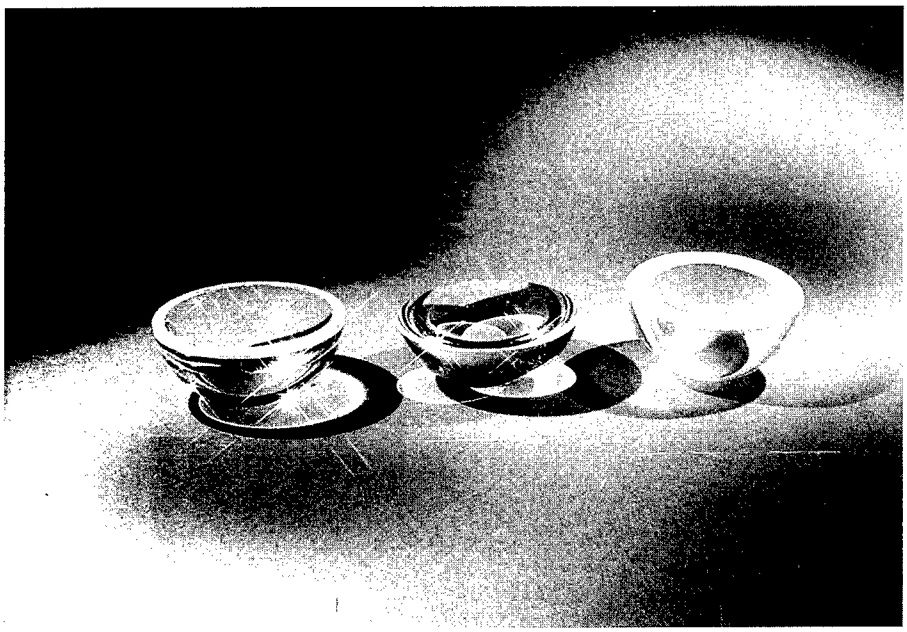

Optical finish directly by solgel - moulding

Fig. 5 rappresents an aerogel of aspherical profile compared to the theorical profile generated from the equation of the asphere (external dark locus).

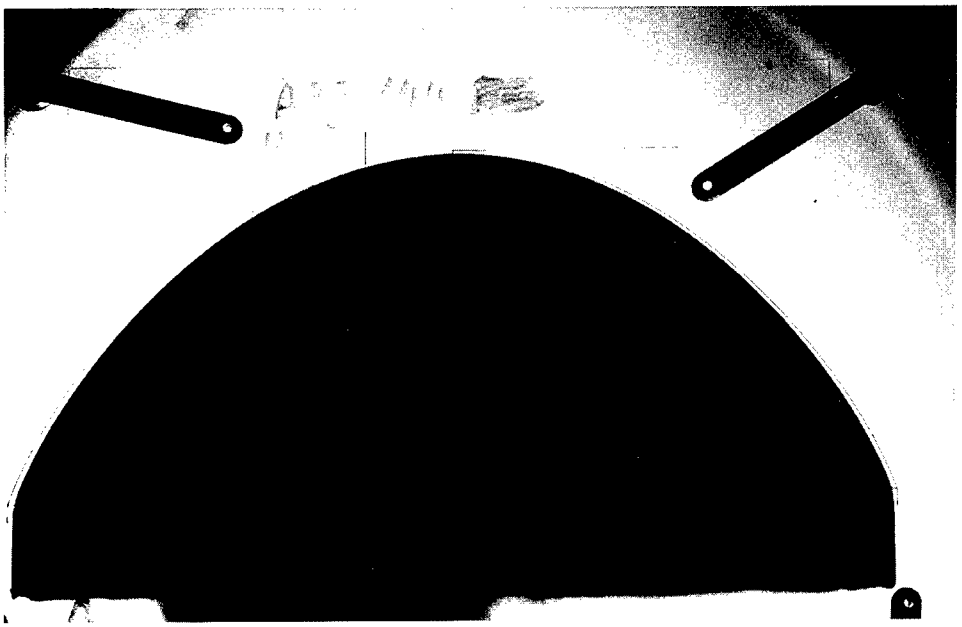

Fig. 5 Aspherical profile on aerogel

Fig. 6 rappresents a 15,7 mm silica glass lens obtained from sol-gel moulding and subsequent densification. The aspherical profile of the lens is compared to the theorical profile generated from the equation of the asphere (external dark locus).

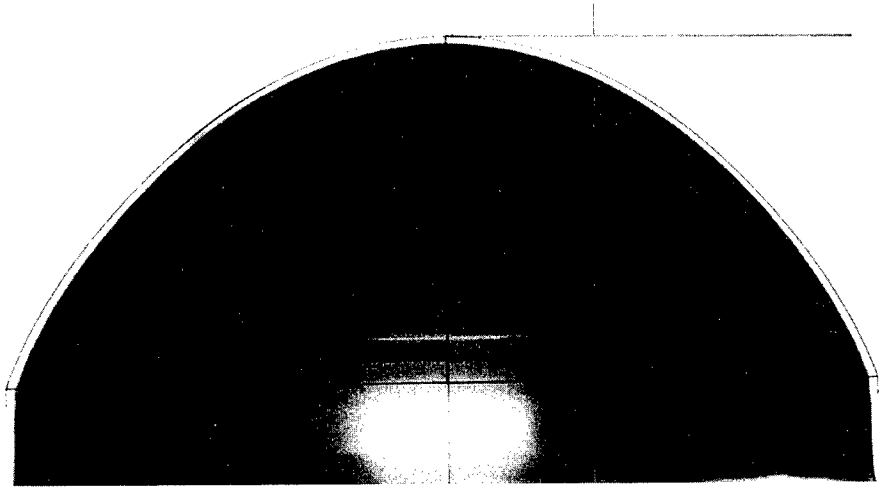

Fig. 6 Aspherical profile on silica glass

Fig. 7 rappresents an aerogel before densification. Compared to the theorical profile generated from the equation of the asphere. The aerogel was produced by a distinct process of that of fig. 5.

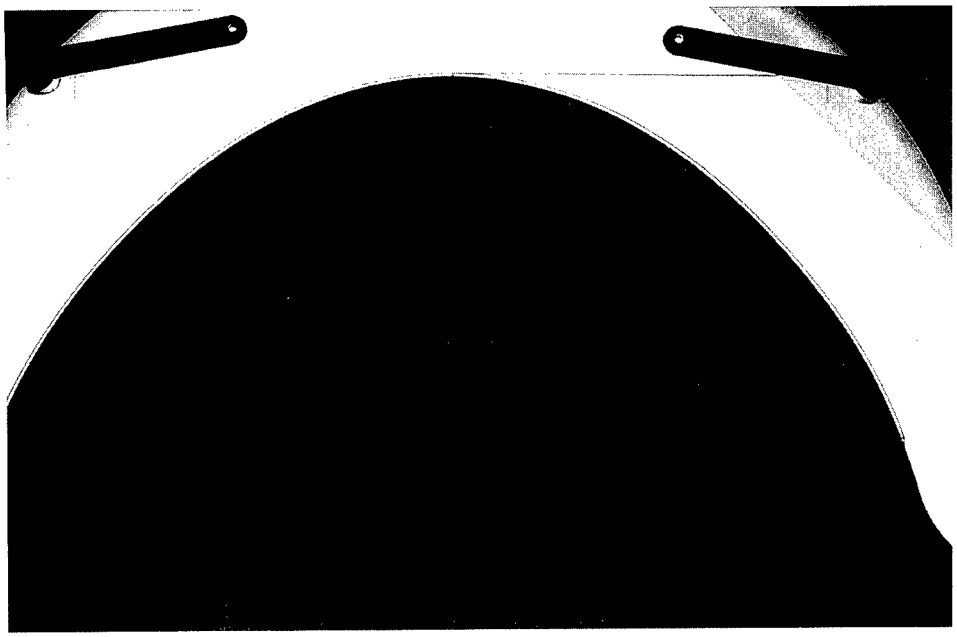

Fig. 7 Aspherical profile on aerogel

In the pictures of figs 4...7 the external dark locus was shifted by a small distance from the Net-Shape product to facilitate evaluation by the observer. No optical finish was privided to the internal mould surface. (Lead marks might be observed on the dense product of fig. 6).

From the data shown on these three fig.s an accuracy of better than one part in tenthousand might be demonstrated. In the case of these lenses it corresponds to +/- 1,5μm. This is not the limit in accuracy that the process can provide: it is the sensitivity limit of the testing ability inside GDE.
The real limit has to be determined by optical methods as soon as optical surfaces will be a standard feature on aspherical lenses by sol-gel moulding.

CONCLUSION

We are convinced that the sol-gel technology is ready now for entering the large and articulate market of chemical fabrication with dimensional specifications in the order of those offered by mechanical fabrication. The economic implications in the market of high-temp. high hardness manufacts is very attractive.

REFERENCES

1. Italian Patent Application N. 2996 Feb. 10.1989;
"Process for preparing monoliths of aerogels of metal oxides".

2. Italian Patent Application N. 2925 feb. 10.1989;
"Glass-like monoliths constituted by silicon oxide and titanium oxide and process to prepare them".

3. Italian Patent Applicasion N. MI 92A 001824 July.28.1992;
"Method for the preparation of gels containing boron".

4. Italian Patent Application N. MI 91A 00986 Apr.10.1991.
"Process for the preparation of monolithic gels having mullitic composition".

5. Italian Patent Application N. MI 92A 002038;
"Process for the preparation of optical components and devices in Net-shape or in Near-Net shape and products obtained".

6. M.A. Gottschalk, Design News, 135 (1992).

Key Engineering Materials Vol. 150 (1998) pp. 41-48

On the Thermal and Photochemical Stabilities of Photochromic Spirooxazine Dyes Encapsulated in Ormocer Matrices Derived by Sol-Gel Processing

L. Hou[1,2], B. Hoffmann[2], M. Mennig[2] and H. Schmidt[2]

[1] Shanghai Institute for Optics and Fine Mechanics, Academia Sinica, Shanghai, P.R.China

[2] Institut für Neue Materialien, Universitätscampus, Gebäude 43, Im Stadtwald, D-66123 Saarbrücken, Germany

Keywords: Spirooxazine-Ormocer, Sol-Gel Processing, Photochromism, Thermal and Photochemical Stabilities

Spiroindolinonaphthoxazine (abbreviated as SO), a most promising class of photochromic dyes due to their better photochromic response to UV irradiation (e.g. sunlight), higher fading rate of the coloured form and higher photofatigue resistance, is incorporated into Ormocer matrices synthesized by the sol-gel route aiming to achieve some application prospects. As for all technical applications the stability of the materials as a function of time and/or under certain harsh circumstances must be considered and improved if necessary. In the present work the thermal and photochemical stabilities of our photochromic SO-Ormocer gels and coatings are investigated by room temperature (RT) holding, heat treatment and UV irradiation experiments and compared with the SO-PMMA coatings. It is shown by our results that both the thermal and photochemical stabilities of our SO-Ormocer coatings are similar to those of the SO-PMMA coatings. Considering that both the photochromic response and the fading rate of our SO-Ormocer coatings are much better than those of the SO-PMMA coatings, it is reasonable to conclude that the overall performance of our SO-Ormocer coatings is acceptable for certain application purposes.

INTRODUCTION

There are mainly three most important materials requirements for a photochromic system which consists of photochromic dye and matrix material: high (acceptable) photochromic response to UV irradiation, high or very low fading rate of the coloured form for switching or memory devices, respectively, and high thermal and photochemical stabilities. The last requirement is especially a critical factor to practical applications. Mainly because of unsatisfactory thermal and photochemical stabilities, no large scale markets have been established that commercially exploit photochromic phenomena to date.

The fulfillment of the above requirements depends both upon exploitation of high-performance photochromic dyes and upon development of suitable matrix materials. SO dyes have been shown to possess much higher photochemical stability than spiropyrans (SP) by a factor of $\approx 10^3$, while exhibiting similar photochromic response and fading rate to the latter. N. Y. C. Chu [1~5] has published a series of original research papers on the SO-polymer photochromic systems. It turns out from these papers that the photochromic response of the dye is deeply suppressed so that a high dye concentration (> 1 wt.%) is necessary for obtaining a high enough photochromic response and the fading rate of the colour activated by UV light is largely slackened by a factor of > 10 as compared to the SO-ethanol solutions so that certain applications which require quick bleaching become impossible.

Porous solid materials derived by sol-gel processing, inorganic oxides or organic-inorganic composites (Ormocer), provide new possibilities of hosting photochromic dyes. There are a number of publications dealing with the incorporation of spiropyran (SP) [6~8] and 2,3-diphenylindenoneoxide (DPIO) [9] into sol-gel derived matrices, while little has been reported on SO

dyes. The results concerning SP and DPIO indicate strong matrix-dependence of the photochromism, but no data on the thermal and photochemical stabilities are available. We have been concentrating on SO-Ormocer photochromic systems for 2 years and the results already obtained about the photochromic response and fading rate are very encouraging: The photochromic response levels off during the wetgel-xerogel process and remains almost unchanged up to the present (8 months since preparation) at a satisfactory level with the colour-fading rate being the same as in ethanol [10, 11].

The objective of this work is to establish whether the thermal and photochemical stabilities of our SO-Ormocer system are comparable to those of the SO-PMMA system. The SO-Ormocer coatings were subjected to room temperature holding, heat treatment and UV irradiation (suntest) together with the SO-PMMA coatings for comparison. The photochromic intensity (ΔA_0) and half-life time ($t_{0.5}$) of the coloured form were monitored during these treatment processes. The results are very positive: the SO-Ormocer coatings exhibit similar thermal and photochemical stabilities to the SO-PMMA coatings while their photochromic response and fading rate are much more favourable to applications in switching devices than the latter.

EXPERIMENTAL

The preparation procedure of the SO-Ormocer gels and coatings is depicted in Fig. 1. Appropriate amounts of methyltrimethoxysilane (MTMS) and glydidyloxytrimethoxysilane (GPTMS) and water in the form of 0.1 N HNO_3 solution were first mixed by magnetic stirring for ten minutes in a plastic container (∅ 30x70 mm) and then subjected to 20 kHz ultrasonic radiation at a power of 20 W for 20 minutes. The ultrasonic wave was supplied by a SONIFIER Model 450 device (Branson Ultrasonics CT) through a standard horn tip immersed in the liquid mixture. The sols were then cooled down to room temperature, followed by the addition of appropriate amounts of additives and the introduction of dye-ethanol solution. After a 1h-magnetic stirring the sols were exposed to the open air with continuing magnetic stirring. When a final volume of 20 ml was reached the sols became viscous and the containers were then closed.

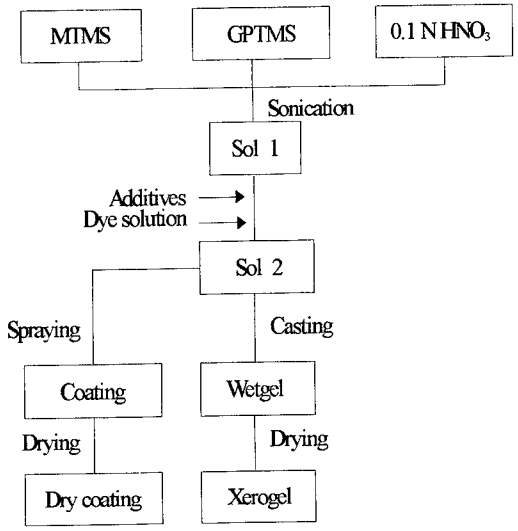

Fig.1: Preparation procedure of SO-doped Ormocer gels and coationg

Samples used for monitoring the evolution of the photochromism during RT-holding were prepared by pouring the viscous sols into polystyrene cell of 4 mm thick and keeping them open to the atmosphere. Coatings of various thickness for thermal (heat treatment) and photochemical (UV

irradiation) stability tests were produced by spraying appropriate volumes of the viscous sols on slide glass substrates.

The aluminosilicate samples were derived from di-iso-butoxy-aluminoxy-triethoxysilane (ASE) using iso-propanol (i-PrOH) as a solvent. At first, the H_2O-i-PrOH mixture was added to the ASE-i-PrOH mixture under vigorous magnetic stirring for 1h. Then the dye-ethanol solution was introduced slowly under vigorous stirring, too. After an additional 1h-stirring the resultant sols were transferred into polystyrene cells (10x10x45 mm) with stoppers and left to gel and age.

For the purpose of comparison, SO-PMMA coatings were also prepared by spraying on slide glass substrates the SO-PMMA-EA (ethylacetate) solution which contains 15 g PMMA in 100 ml ethylacetate.

Fig. 2 shows schematically the apparatus used for the real-time measurement of photochromism. UV irradiation is from a Hg-lamp and the Schott UV-pass filter UG5 is used to eliminate the influence of heat on the colouring-fading process. From the recorded transmission vs. time curves, photochromic intensity (ΔA_0) and half-life time ($t_{0.5}$) are evaluated. Their variations during RT-holding or after heat treatment at different temperatures and after UV irradiation for different lengths of time are used as a measure of the corresponding stabilities.

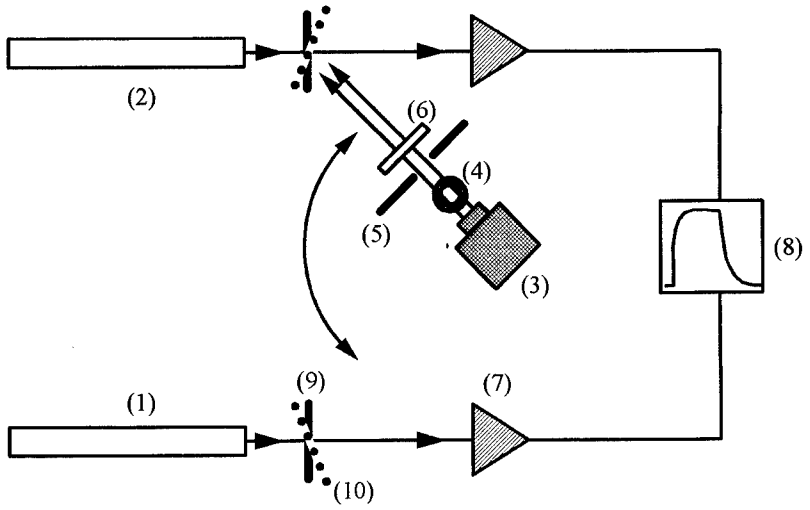

Fig.2: Schematic layout of the apparatus used for colouring-fading measurement
(1) green He-Ne-laser (2) red He-Ne-laser (3) Hg-lamp (4) Focussing system
(5) Shutter (6) UV-pass filter (7) Detector (8) Recorder
(9) Cell sample (10) Coating sample

A SUNTEST CPS (Heraeus) apparatus was employed to characterize the photochemical stability of the samples against UV irradiation at an intensity of 600 W/cm^2. Heat treatments were conducted in a MEMMERT model 100 electric furnace.

RESULTS AND DISCUSSION

Stability at room temperature

Fig. 3 demonstrates the severe degradation of the photochromic response of SO in ASE-gels during ageing. It is evident that the photochromic intensity decreases by a factor of $\approx$3 after 14 days and vanishes after 60 days ageing at room temperature. It is well known that SO dyes undergo ring-opening reactions under UV irradiation. During the ageing process of the ASE-gels the structural change of the SO-molecules would face greater and greater hindrance due to the increase of

condensation extent of the Al-O-Si network, therefore, the photochromic transformation is more and more heavily suppressed and finally nullified. Moreover, certain chemical bonding between Al in the matrix and O in the dye molecules may also be responsible at least partly for the degradation of the photochromic response.

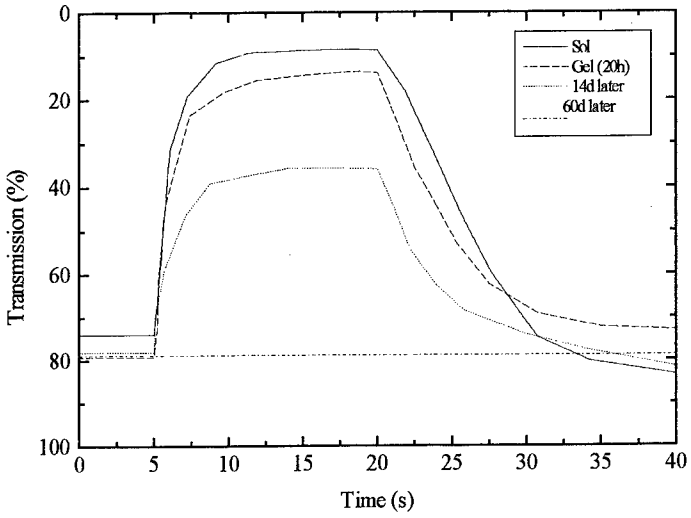

Fig.3: Colouring-fading curves of SO (C = $1x10^{-4}$ mol/l) in ASE-gel at different time after preparation (gelling time = 20h)

The RT-holding stability of SO is greatly improved by using Ormocer as matrix materials. This is clearly indicated by Fig. 4. Although ΔA_0 of the gel decreases at the early stages of the sol-gel transformation, it levels off in about one month after preparation.

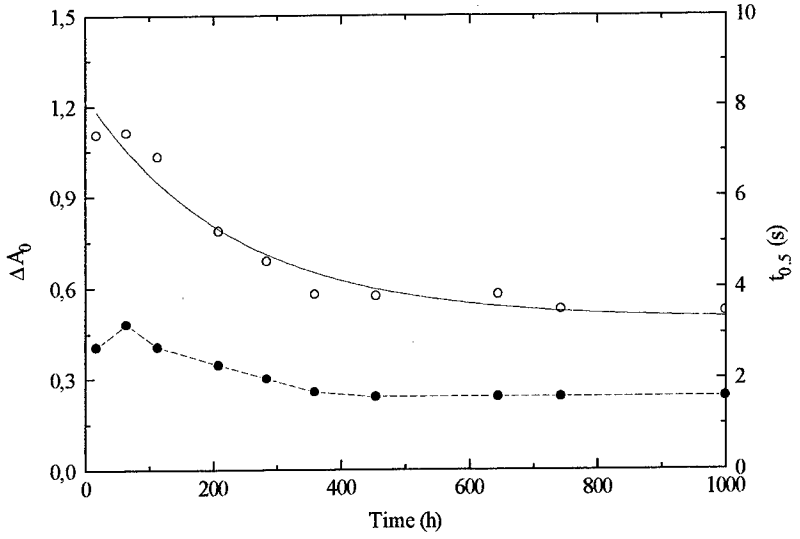

Fig.4: Variation of photochromic intensity (ΔA_0) and half-life time ($t_{0.5}$) of SO ($2.5x10^{-3}$ mol/l) in Ormocer gel during sol-gel transformation

Furthermore, the ΔA_0 remains almost constant (ca. 0.60) up to the present (6 months after preparation). Another interesting result is that $t_{0.5}$ increases in the early stage (within 100 h after preparation), then decreases and finally levels off in about one month, too. These results can be reasoned in terms of the viscosity increase before gelling and the difference in degree of freedom of the dye molecules entrapped in the pores and out of the pores. With the increase in the viscosity of the sol due to the progressive condensation, a greater and greater portion of dye molecules are more and more tightly confined so that the possibility of photochormic transformation decreases gradually in a statistical sense. Meanwhile, the fading speed of the coloured form decreases due to the increasing hindrance. At the gelling point, a certain portion of the dye molecules has been "killed" and loses its photochromic activity. Only those dye molecules caged in the pores in the gel matrix remain photochromically active and these molecules are completely free within the cages as in ethanol solution. Therefore, in the xerogel matrix both ΔA_0 and $t_{0.5}$ reach a steady value, ΔA_0 depends upon matrix composition while $t_{0.5}$ is equal to the value in ethanol solution ($\approx$ 1.5 s) independent of matrix composition.

Stability against heat treatment

The variation of $t_{0.5}$ and relative loss of ΔA_0 of the SO-Ormocer coating with heat treatment temperature is shown in Fig. 5, from which it can be seen that heat treatment has little influence on $t_{0.5}$ up to 120 °C and leads to limited increase in the relative loss of ΔA_0, ca 10% up to 120 °C. This result implies the possibility of curing the SO-Ormocer mterials thermally at around 120 °C without significant degradation of the photochromic performance as heat treatment is generally necessary in order to achieve desired flexibility (or rigidity) of the Ormocer matrices hosting photochromic dyes because the flexibility of the matrices is a conflicting factor which affects photochromic response and photochemical stability in opposite directions: higher flexibility is always favourable to the former but unfavourable to the latter.

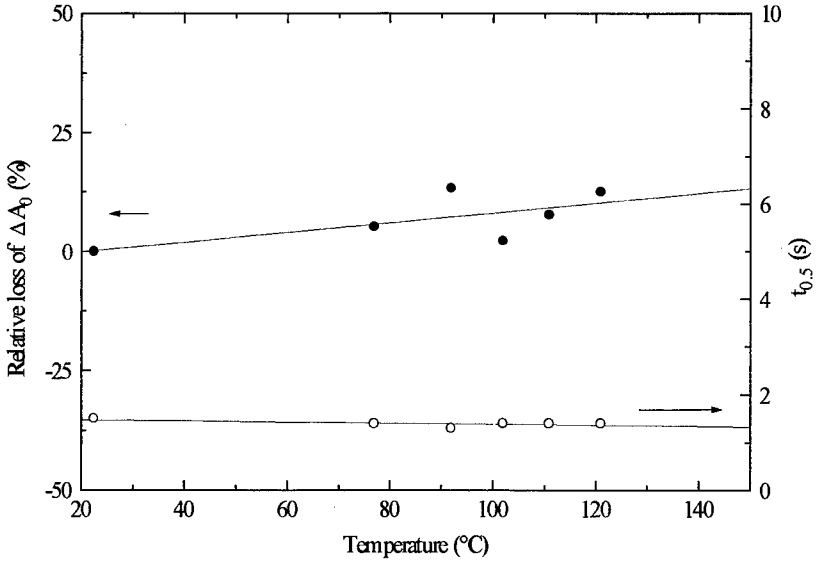

Fig.5: $t_{0.5}$ and relative loss of ΔA_0 of SO (2.5×10^{-3} mol/l)-Ormocer coating as a function of heat treatment temperature

Fig. 6 presents the variation of ΔA_0 and $t_{0.5}$ of SO-PMMA coatings with RT-holding time and heat treatment. It follows from this figure that ΔA_0 shows no significant decrease below 120 °C

while heat treatment at 140 °C for 6 h results in a relative loss of ΔA_0 less than 25% and the peeling-off of the coating. However, $t_{0.5}$ increases very rapidly with increasing heat treatment temperature, and even during RT-holding it increases slowly, too. Based on the results from Figs. 5 and 6 one may conclude that the thermal stability of ΔA_0 of the SO-PMMA system is a little better than the SO-Ormocer system whereas the thermal stability of $t_{0.5}$ of the SO-Ormocer system is much better than the SO-PMMA system. Or one can say that the thermal stability of the overall photochromic performance of the SO-Ormocer and SO-PMMA systems is similar.

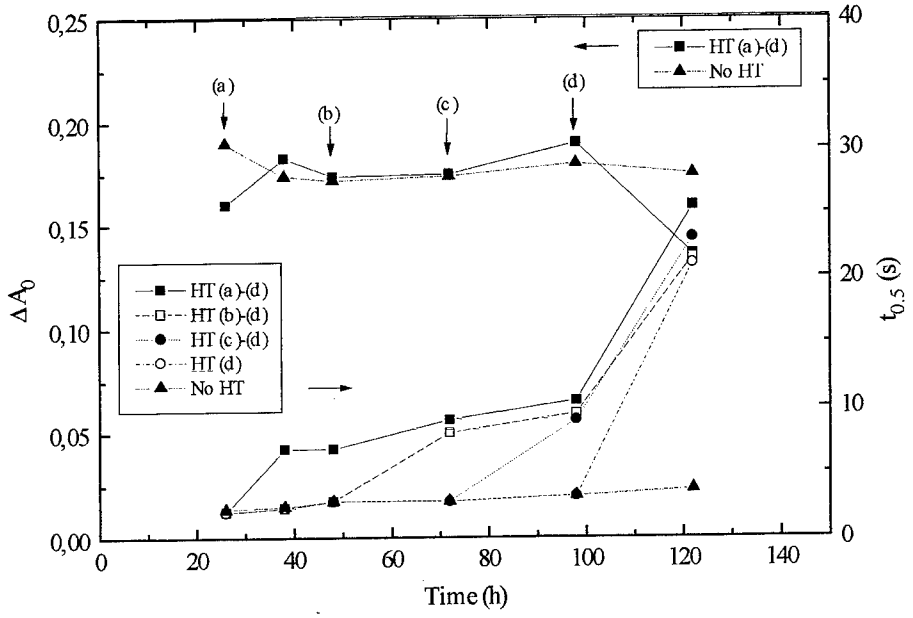

Fig.6: Variation of $t_{0.5}$ and ΔA_0 of SO ($1x10^{-3}$ mol/l)-PMMA coatings with RT-holding time and heat treatment (HT): (a) 100 °C / 12h, (b) 110 °C / 6 h, (c) 120 °C / 6 h, (d) 140 °C / 6 h

Photochemical stability against UV irradiation

Another conflicting factor to a photochromic material is the exposure to UV light. UV irradiation is indespensable to photochromism but harmful to the dye molecules. This is why solid matrices are preferred for photochromic dyes. The utilization of polymer matrices leads to significant enhancement of photochemical stability but at the same time poses a deep supression on both the photochromic response and the colour-fading rate. It has already been established that both the photochromic response and the colour-fading rate of SO-Ormocer gels and coatings are much higher than the SO-PMMA coatings. However, a comparison in the photochemical stability between the two materials must be made in order to confirm the feasability of practical applications of the SO-Ormocer material. Fig. 7 gives a comparison between SO-ethanol, SO-Ormocer and SO-PMMA. It turns out from this figure that (1) the photochemical stability of SO-Ormocer coating without any additives is between the SO-ethanol and SO-PMMA systems. (2) A small amount of an additive leads to a great improvement of the photochemical stability of SO-Ormocer coating, becoming considerably better than the SO-PMMA coating with the same SO concentration. (3) By increasing concentrations of SO in the SO-PMMA systems to $5x10^{-3}$ mol/l the photochemical stability is further enhanced. This suggests more elaborate research efforts to be made to further improve the

photochemical stability of our SO-Ormocer materials. Increasing SO concentration and introducing more effective additives may be helpful forthcoming steps.

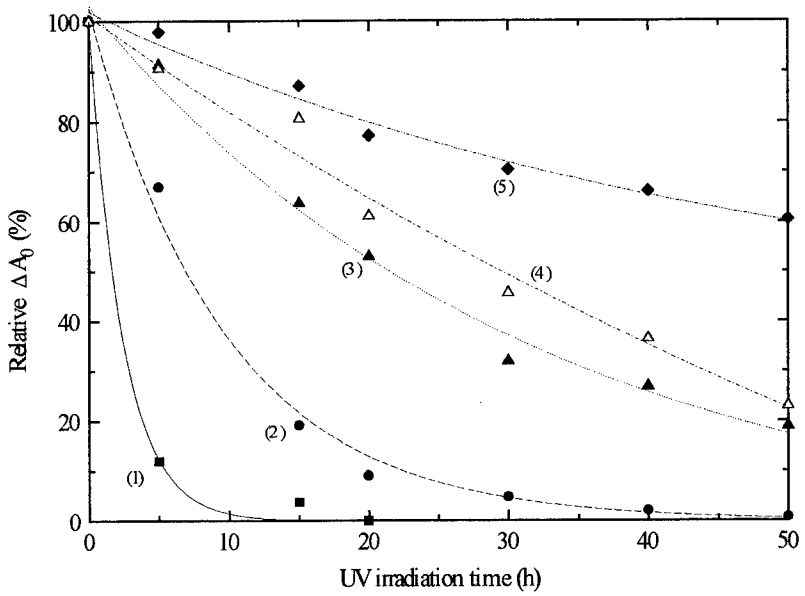

Fig.7: Decrease of ΔA_0 of SO with UV irradiation time in different matrices: (1) Ethanol (C = $4x10^{-3}$ mol/l), (2) Ormocer coating (C = $1x10^{-3}$ mol/l) without additives, (3) PMMA coating (C = $1x10^{-3}$ mol/l), (4) Ormocer coating (C = $1x10^{-3}$ mol/l) with an additive, (5) PMMA coating (C = $5x10^{-3}$ mol/l)

CONCLUSION

We are now in a position to tailor photochromic SO-Ormocer materials with the thermal and photochemical stabilities being comparable to, and both the photochromic response and the colour-fading rate much better than the SO-PMMA materials.

REFERENCES

[1] N. Y. C. Chu, SPIE's 29th Annual International technology Symposium Optical and Electrooptical Engineering **562-03**, 6 (1985)
[2] N. Y. C. Chu, Solar Energy Materials **14**, 215 (1986)
[3] N. Y. C. Chu, Optical Materials Technology for Energy Efficiency and Solar Energy Conversion VII, SPIE Vol. **1016**, 152 (1988)
[4] N. Y. C. Chu, Energy Res. Abstr. **14(10)**, No. 20059 (1989)
[5] N. Y. C. Chu, SPIE Institute Series **IS4**, 102 (1990)
[6] D. Levy and D. Avnir, J. Non-Cryst. Solids **113**, 137 (1989)
[7] D. Preston, J.-C. Pouxviel, T. Novinson et al., J. Phys. Chem. **94**, 4167 (1990)
[8] J. I. Zink and B. Dunn, J. Mater. Chem. **1**, 903 (1991)
[9] S. A. Yamanaka, J. I. Zink and B. Dunn, Proc. SPIE **1758**, 372 (1992)
[10] L. Hou, B. Hoffmann, M. Mennig and H. Schmidt, J. Sol-gel Sci. Techn. (in press)
[11] L. Hou, M. Mennig and H. Schmidt, Proceedings of the International Symposium on Glass Science and Technology, Oct. 6~8, 1993, Athens, Greece (in press)

Key Engineering Materials Vol. 150 (1998) pp. 49-66

Sol-Gel Coatings on Large Glass Substrates for Multilayer Interference Systems

E.K. Hussmann

Schott Glaswerke, Mainz, Germany

Keywords: Sol-Gel Coating, Process Parameters, Coating-Antireflective

0. Summary

Optical multilayer systems can be produced precisely and reliably on large substrates via sol-gel-dip coating. Critical points in the production sequence are discussed. The accuracy of the process is characterized.
Typical products and their properties are presented.

1. HISTORICAL BACKGROUND

Since more than 50 years Schott has developed techniques to deposit metallic and dielectric thin films. Many different methods were investigated. Besides vacuum evaporation[1] and chemical vapour deposition techniques[2] especially sol gel dip coatings were examined systematically. This research was carried out mainly by Geffcken and Schröder[2,3,4,5,6,7] and has been further extended by Dislich[8,9] and Arfsten[10]. Not so well known is the fact, that Geffcken made important contributions to the theory and design of interference layer systems. He is the "inventor" of the three layer antireflective systems[11].

Since 1953 Schott sells dip coated interference layer systems. These products were mainly for optical applications as for example heat mirrors, cold mirror, beam splitters and dielectric filters. Automotive rear view mirrors are produced since 1959 and antireflective interference layer systems since 1964.

1969 dip coated large window panes have been introduced to the market for sun-shielding window purposes. They are traded under the name CALOREX and IROX.

The latest product for architectural glazings is an antireflective shop-window glass which was started 3 years ago under the name AMIRAN.

2. CHEMISTRY AND PHYSICS OF SOL GEL DIP COATINGS

In the last two decades the chemistry and physics of sol gel processes were investigated thoroughly. So only a brief overview is given of the most important facts how to make coatings-especially multilayer interference coatings.

2.1 Coating solutions

The coating solution contains compounds from that element which later forms the transparent oxide film. These compounds should readily dissolve in an adequate solvent and build polymolecules. They should form gel-like films on the substrate when the solvent evaporates, with no tendency to crystallize. Hydrolysis and polycondensation take place. The solution should have a small contact angle to the substrate, to ensure good wettability.

There are many elements forming transparent oxide layers, especially: Al, In, Si, Ti, Zr, Sn, Pb, Ta, Cr, Fe, Ni, Co and some more rare earth elements. Mixed oxides can be made, as for example TiO_2 - SiO_2. Any refractive index in the range $1.45 < n < 2.30$ can so be realized. By incorporating metal colloids into SiO_2 or TiO_2 matrixes, the films can exhibit a wide range of absorption. The properties of these oxide films can be influenced by the composition of the atmosphere during baking. Baking in air or in a reducing gas atmosphere can lead to different oxidation stages.

2.2. Coating procedure

Sol gel coatings can be applied by spinning, lowering and dipping. For architectural coatings only the dipping techniqe is appropriate. It is the most economical method for large substrates.

The liquid film, adhering to the surface of the substrate is lifted up with the substrate and runs down partially back into the cuvette. At the same time the solvent evaporates in this "flow zone". An equilibrium is reached between these competing influences, and the film finally takes up a constant thickness along the lifting direction.

The thickness of the layers is therefore mainly a function of the lifting speed and the viscosity of the solution. The angle of inclination between the substrate and the surface of the liquid influences the thickness of the layers too.

It should be mentioned that the edges of dip coated plates show small irregular zones of 5-10 mm width, especially at the lower edge. These "trouble zones" have to be cut off.

After coating, the substrates are heated up to 100-180°C. Most coatings are then sufficiently stabilized so that the final firing can be performed later on in larger batches in an intermittently heated electric furnace, at 400-500°C.

The bonding strength between different coating materials is usually of the same order as the one between layers and glass substrates, and in some cases even considerably higher. Multilayer interference coatings can therefore be made easily by the dip coating process. The rate of diffusion of the various oxides into each other is imperceptible. The interfaces between the layers remain sharply defined. The statistical surface roughness of a film is not carried over to the surface of successive layers.

2.3 Peculiarities of the dip coating process

Both sides of a pane are coated simultaneously by dipping. It is even easier to coat both sides of a plate instead of one side only. The vacuum methods coat one side preferentially; to coat both sides involves much more effort. This constitutes an advantage for most products with antireflective coatings.

Another advantage is the good homogeneity of the dip coated layers. There is no great difference between coating small or large panes.

Dip coatings can be hard and scratch resistant and very durable against environmental influences.

Normally the dip coating process is confined to oxide layers. For example metal films are difficult to produce.

3. DIP-COATING-Facility

At SCHOTT the dipping procedure is the method mainly used to make sol-gel-coatings, especially for coating large panes.
Figure 1 shows a scheme of the oxide film formation.
SCHOTT operates many different ones from sizes 30 cm x 50 cm up to 3.21 m x 3.75 m for architectural coatings. Depending on the size and on the type of glass - floatglass, optical-glasses, borosilicate glasses the washing process varies. Small substrates are usually cleaned in ultra-sonic-washing facilities. Large substrates are washed under rotating brushes with cleaning agents. The coatings are heated up to 400°C - 500°C to convert them into transparent oxides. There are continuous ovens and batch ovens.

In figure 2 the sequence of production steps is shown. For multilayer coatings the sequence has to be passed repeatedly. Usually each layer has to be burned in seperately. Depending on the type of coating it is feasible to dry the coatings just mildly at about 200°C and apply the next layer. Then both are burned in together at 400°C - 500°C. This speeds up the production time considerably, since the firing step is the longest lasting step of the sequence given in figure 2.

4. INFLUENCE OF THE PROCESS-PARAMETERS UPON THE PROPERTIES OF THE COATINGS

Coatings - especially optical multilayer interference coatings - have many properties which have to be maintained within close boundaries in order to meet the required specifications. The spectral reflectance, transmittance and absorptance depend on the properties of the individual layers of multilayer system:

- thickness
- refractive index
- absorption
- scattering properties

Additional properties are significant for the complete system:

- mechanical strength
- chemical stability
- coating defects (pinholes, voids)
- internal stresses

The sol-gel-dip-coating process does not allow to monitor the optical properties directly, when the coating emerges from the solution. These properties can be judged only after baking the layer. Modern vacuum coating facilities are different, employing optical measuring systems.

Therefore optical multilayer interference coatings can be produced reliably only, if all the parameters are kept constant which influence the properties of the dip coated layers. These influences are discussed in detail.

4.1 WASHING PROCEDURE

Depending on the type of glass

- float glass
- optical glass
- borosilicate glass (PYREX, TEMPAX)

the washing procedure has to be adapted. There are washing procedures, which can leach the glass surface somewhat. Sodium-ions are taken out. The first coating on the substrate reacts chemically during the firing process with the glass. It is therefore important, to provide identically prepared surfaces. So it is necessary to stabilize the washing procedure in order to provide surfaces of constant "quality".

4.2 DRYING

There are different methods of drying the washed panes: Infrared heating or blowing-off the remaining water. In any case, it is important to prevent accumulation of dust on the freshly cleaned surfaces. Sometimes it is even necessary to free the dried surfaces from static electricity.

4.3 DIPPING SOLUTION

A good dipping solution provides the best compromise between lifetime, concentration, wettability, required optical and "durability" parameters and costs.

The concentration should be choosen in such a way, that high lifting speeds bring about the required film thickness. The viscosity of the solution is one of the major factors governing the required lifting speed. Since the viscosity is strongly dependend on the temperature of the solution, it is mandatory to keep the temperature of the solution constant.
In the normal production some solution has to be replaced. Each coating event consumes solution depending on the size of the plate. In addition solvent of the solution evaporates, which has to be replaced.

4.4 ATMOSPHERE IN THE DRAWING CHAMBER

The air in the drawing chamber should be exchanged constantly to remove the evaporating solvents of the emerging coating. The humidity and the temperature of this air has to be maintained exactly at the required values. Depending on the type of solution 4 g/m^3 - 15 g/m^3 absolute humidity are required.
Laminar air flow is essential for uniform, cloudless coatings. Only filtered dustfree air can be used.

4.5 DRAWING MACHINE

The mechanism used to lift the panes out of the solution has to provide and maintain the required lifting speed without any vibrations or oscillations. Lifting speed is in the range of 2 mm / sec - 15 mm / sec.

4.6 SUBSTRATE

It should be mentioned, that some glasses have surfaces with slightly differing properties, for example float glass. This can result in small differences of the optical properties of the coatings adhering directly on both surfaces of the substrate.

4.7 PARAMETERS INFLUENCING THE THICKNESS OF THE COATINGS

Besides the refractive index the thickness is the most important attribute. Therefore all influences are summarized again, even if mentioned already.

- concentration of the solution
- viscosity of the solution
- temperature of the solution
- lifting speed
- thickness of the substrate
- humidity of the atmosphere
- angle of inclination between the substrate and the surface of the liquid
- firing process

4.8 FIRING PROCESS

Many parameters influence the drying at 200°C and the firing process at 400°C - 500°C. Not only the end-temperature is of importance. Chemical reactions between the glass and the first coating involve diffusion - processes. Therefore the slope of the temperature increase against time and the baking time at maximum temperature strongly influence the properties (thickness, refractive index) of the coating[6]. Another parameter is the composition of the atmosphere in the oven. Reducing compounds (forming gas) in the atmosphere tend to generate suboxides or even metal clusters. The humidity of the atmosphere can affect the properties of the coatings too, in particular during the drying process at ca. 200°C.

5. ACCURACY OF THE DIP-COATING PROCESS

As outlined under heading 4, many parameters influence the properties - in particular the optical properties - of a multilayer coating. Are these parameters maintained within appropriate boundaries highly consistent multilayer coatings can be produced. Even on large panes the optical properties are uniform over the whole area. Figure 3 shows the refractive index and the thickness of a TiO_2 coating on a pane of 3.21 m x 3.75 m, measured at 9 positions. The mean values and standard deviations are:

thickness d_m = (65.53 ± 0.69) nm
refractive index n_m = 2.224 ± 0.003

An other example is shown in figure 4. The variation of x and y (tristimulusvalues of the CIE chromaticity diagram) of a dichroic filter illuminated with a black body radiation source of 3200 K is very small.This is valid for different positions on a single plate (60 cm x 50 cm) as well for different plates of a larger collective (25 panes). The dip coating process is very stable. Changes in the lifting speed to correct for alterations of the dipping solution (evaporation) are very small.

Switching from one product to an other one is easily done. Other thicknesses and sequences of layers can be realised instantly by an experienced operator of the dip coating facility.

6. PRODUCTS-OPTICAL MULTILAYER SYSTEMS

Two examples of optical multilayer inference coatings are given, produced regularly.

6.1 Antireflective coatings

Glasses with a refractive index n= 1.52 reflect 4 - 5 % at each interface against air. Light passing through a glass pane is therefore attenuated by 9 %. This loss of intensity is often of minor importance. The undesired reflection of cover glasses on instruments, pictures, showcases and other items can disturb an unhindered view and diminish the contrast.
Single or multiple interference layer systems permit a considerable reduction of these reflections. Figure 5 shows the reflection curves of two-layer and four-layer antireflection coatings compared with uncoated glass.
Again, the dip coating process is very well suited since the interference layer system is automatically applied onto both sides. This requires almost no special effort, even for very large panes.

Existing facilities for producing sunshielding glass were adapted to coat very large panes of clear and tinted floatglass with three or four layer antireflective systems.

These panes are mainly used for windows in shops with luxury goods as fine leather wear and jewelry. Panes can be coated up to sizes of 3.15 m x 3.75 m and thicknesses between 3 and 10 mm.

Nuclear reactors and other facilities dealing with intensive ionising radiation very often need thick radiation shielding windows which protect the workforce against radiation. These windows are assembled out of many single blocks. Most glasses used contain high percentages of lead. Therefore the refractive index is high which leads to high reflections. Antireflective coatings are therefore necessary.

A two layer system is sufficient (Figure 5), since the so called hot zone is illuminated by Na-gas-discharge-lamps. They emit monochromatic yellow light. A new facility was built which can handle windows up to 2 tons.

6.2 Dichroic filters

Today the film industry, television and theatre employ very large lighting apparatuses. Very often these lamps do not have the spectral radiation distribution which is required. Appropriately designed filters placed in front of such lamps convert the radiation to the spectral distribution necessary for illumination of the sets.
Such filters can be made using interference multilayer systems produced by dip coating process. These layer systems are preferably coated onto glass such as Duran 50 from SCHOTT. This glass has a low expansion coefficient and thus has a much greater tolerance of temperature differences. This is important since these filters are placed in front of very strong lamps. Such filters can raise or lower the color temperature.
Transmission curves of different color conversion filters are shown in Figure 6.

REFERENCES

1. Geffcken, W.: Angew. Chem., A 60, 1948, 1

2. Geffcken, W. und Berger E.; Verfahren zur Änderung des Reflexionsvermögens optischer Gläser, DRP 736 411 (1939)

3. Geffcken, W.: Glastechn. Ber. 24 (1951), 143-151

4. Schroeder, H.: Optica Acta, Vol. 9 (1962) Nr. 3, S. 249

5. Schroeder, H.: Int. Glaskongr. Brüssel (1965) Heft 1, 7.1-5

6. Schroeder, H.: Physics of Thin Films. Academic Press, New York-London, Vol. 5 (1969), S. 87-140

7. Schroeder, H.: Tenth Int. Kongr. on Glass, Kyoto, 8-118/8-130 (1975)

8. Dislich, H.: Angew. Chem. Int. Ed. Vol. 10 (1971) Nr. 6, S. 363-370

9. Dislich, H. und Hussmann E.: Thin Solid Films, 77 (1981) S. 129-139

10. Arfsten, N., J. Kaufmann, R., Dislich, H.: Sol-Gel-Derived Indium-Tin-Oxide Coatings. Ultrastructure Procesing of Ceramics, Glasses, and Composites, ed. by L. L. Hench and D. R. Ulrich, New York (1984), Chapter 15, 189-196

11. Geffcken, W.: DRP 758 767 (1940)

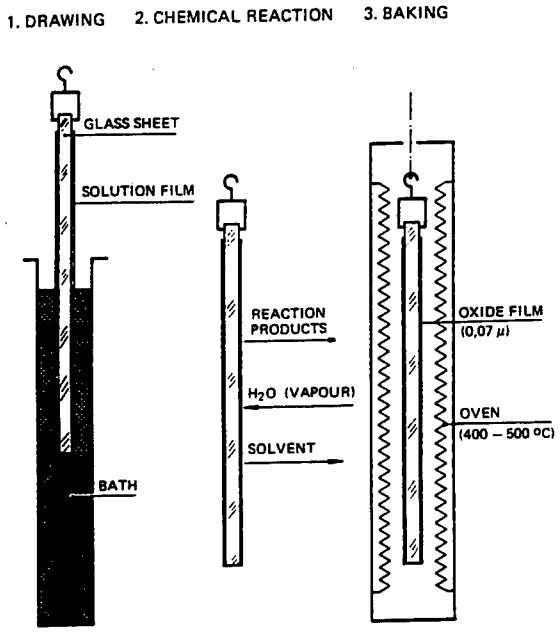
1. DRAWING
2. CHEMICAL REACTION
3. BAKING
GLASS SHEET
SOLUTION FILM
BATH
REACTION PRODUCTS
H_2O (VAPOUR)
SOLVENT
OXIDE FILM
(0,07 μ)
OVEN
(400 – 500 °C)

Figure 1

DIP - COATING - PROCEDURE

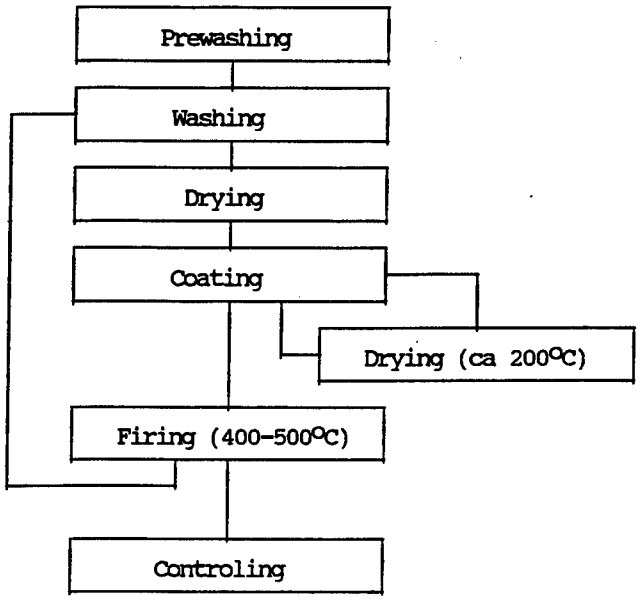

Figure 2

VARIATION OF REFRACTIVE INDEX AND THICKNESS OF A SINGLE TiO_2 - LAYER ON LARGE SUBSTRATES.

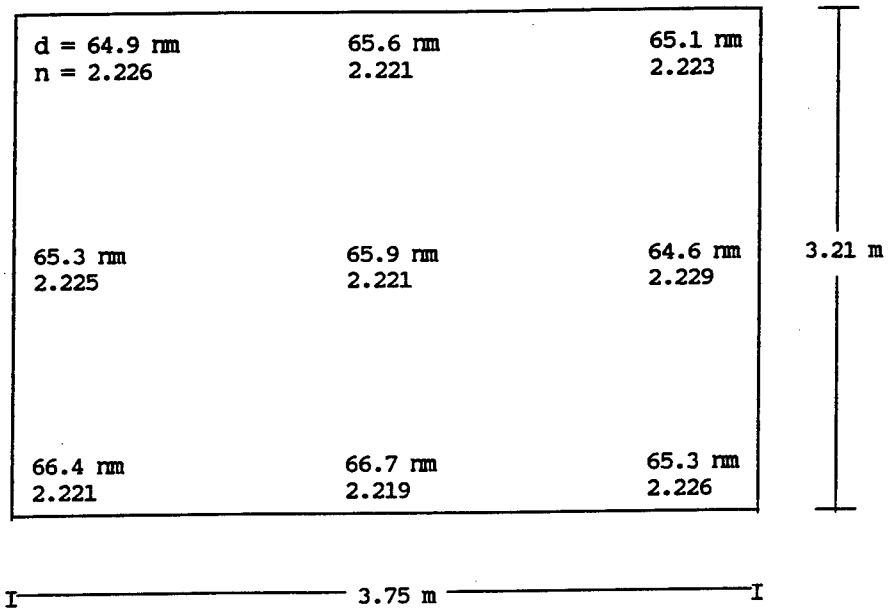

Mean values: d_m = (65,53 ∓ 0.69)nm
n_m = 2.224 ∓ 0.003

Figure 3

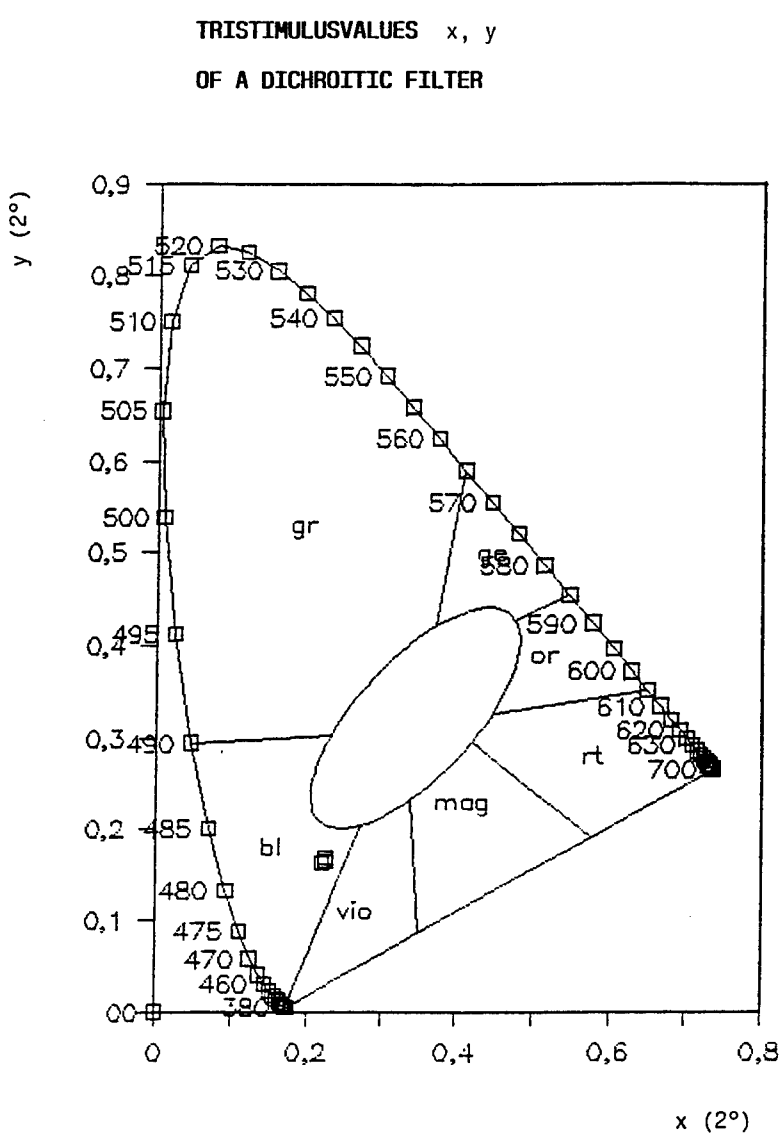
TRISTIMULUSVALUES x, y
OF A DICHROITIC FILTER
y (2°)
x (2°)
0,9
0,8
0,7
0,6
0,5
0,4
0,3
0,2
0,1
0
0,2
0,4
0,6
0,8
520
515
530
540
510
550
505
560
570
500
580
495
590
490
600
610
620
630
700
485
480
475
470
460
gr
or
rt
mag
bl
vio

Figure 4

REFLECTION OF ANTIREFLECTIVE COATINGS

TWO LAYER SYSTEM (———)

FOUR LAYER SYSTEM (-x-x-x-)

UNCOATED GLASS (- - -)

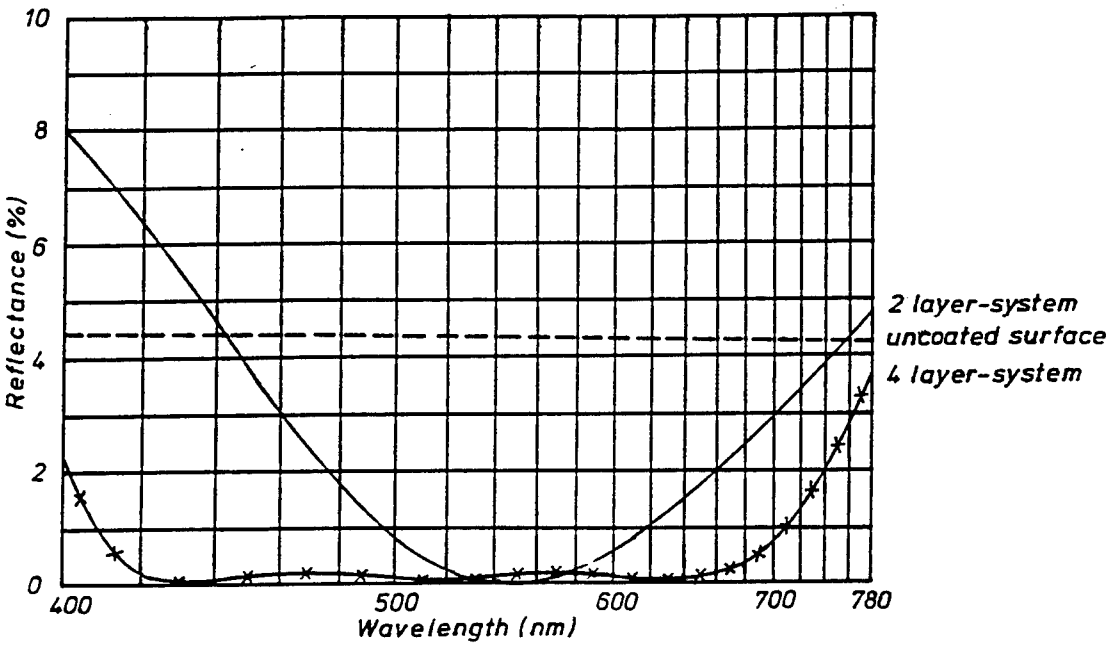

Figure 5

SPECTRAL TAANSMISSION OF COLOR CONVERSION FILTERS

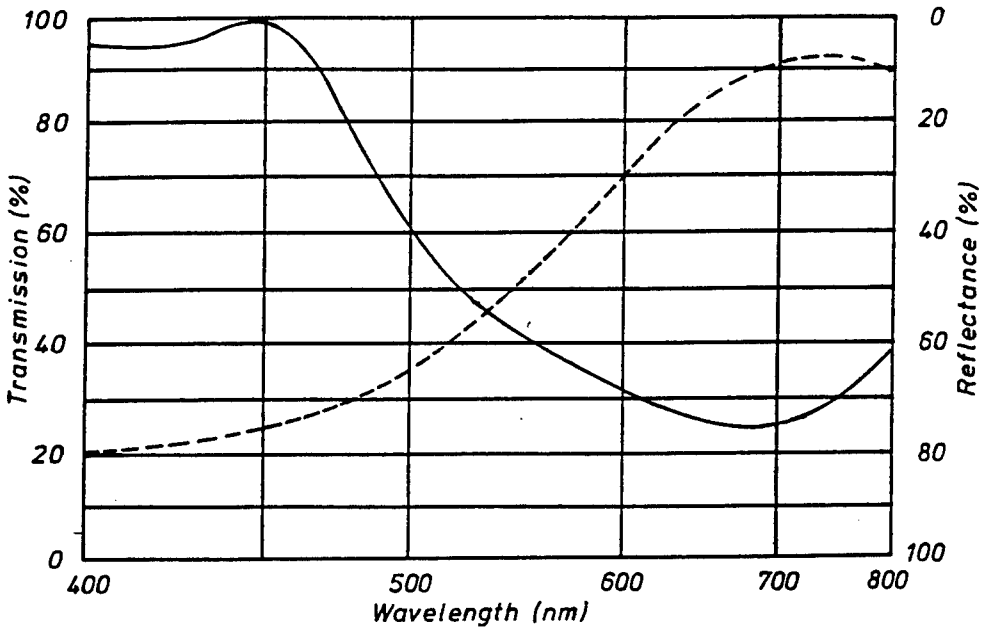

Figure 6

Key Engineering Materials Vol. 150 (1998) pp. 67-76

A SiO_2-ZrO_2 Gel Film Doped with Organic Pigments Made by the Sol-Gel Method for Contrast Enhancement of Color Picture Tubes

T. Itou and H. Matsuda

Toshiba Corporation, 1-9-2 Hatara-cho, Fukaya-shi, Saitama, Japan

Keywords: Color Picture Tube, Contrast, Color Purity, Filter, Organic Pigment, Color Bleaching, Sol-Gel Method, Spin Coating

Abstract: An organic pigment glass gel composite thin-filter made by the sol-gel method has been developed and commercialized for color picture tubes (CPT). It's formed on the outside of the CPT screen and provides remarkable improvements in contrast and color purity. It also has sufficient hardness and stability for practical use.

1. INTRODUCTION

One of the trends in color picture tube technology is a larger and wider screen. The size of the main products has been changing from 21" to 29" and it is beginning to shift to a 32" wide TV. There is a demand for the color picture tube to provide a better picture quality, that is, better color purity, contrast, brightness, and focus.

The authors have developed a new technology for improving the contrast and color purity simultaneously. We call this technology "Black Enhancer"[1]. This paper will describe this technology from the viewpoint of practical use.

2. SELECTIVE LIGHT ABSORPTION FILTER

(1) CPT screen

The screen structure of the CPT is shown in Fig. 1. The screen is constructed with three kinds of phosphor patterns which emit blue, green, and red light, respectively, and with black stripe patterns for contrast improvement. The newly developed technology is a selective light absorption filter formed on the outside of the face glass. This filter is made by the sol-gel method and it is a very thin film of about 0.2μm.

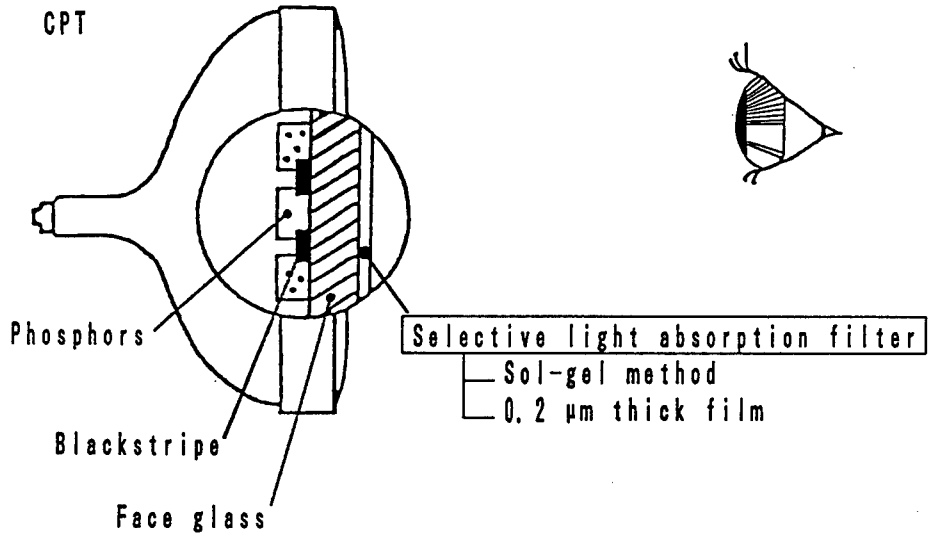

Fig. 1 New Technology for Improving Contrast and Color Purity

(2) Contrast

The contrast of CPT is defined by the next equation shown in Fig. 2. It is the ratio of brightness to a black level of the screen determined by reflectance. So, a brighter screen and/or a lower reflectance screen gives a better contrast.

● $\text{Contrast} = \frac{\text{B (Brightness)}}{\text{D (Reflectance)}}$

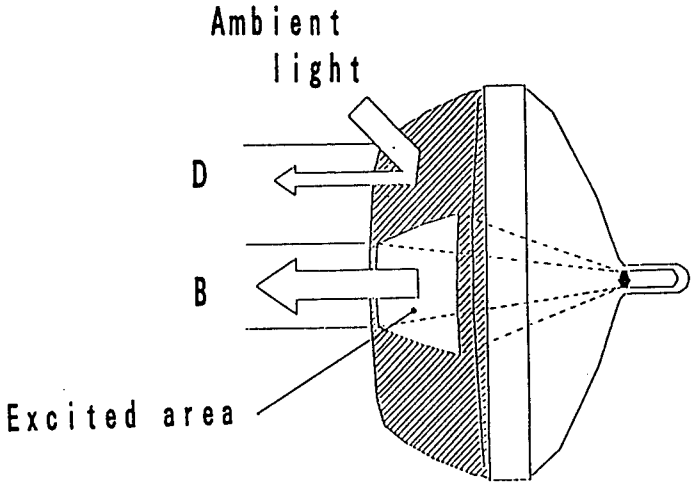

Fig. 2 Principle of Filter
for Contrast Enhancement

(3) Filter curve

The filter has a sharp absorption band at about 570nm, as shown in Fig. 3. Ambient light energy multiplied by luminosity index is maximum at this region. Therefore, the filter absorbs the ambient light effectively and provides a lower reflectance screen. The region is the ravine between the two fluorescence spectrum bands of green- and red-emmiting phosphors. Therefore, the filter absorbs only the sub-band part of the fluorescence. So there is little reduction in brightness. From this reason, the filter gives better contrast and color purity.

(a) Effective Absorption of Ambient Light (AL)

(b) Absorption of the Sub-band of Phosphor Fluorescence

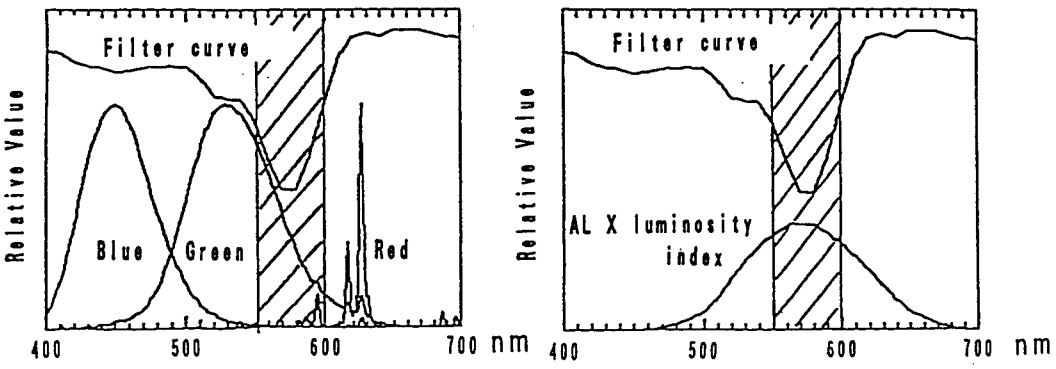

Fig. 3 Filter Curve

(4) Schematic structure

Fig. 4 is a schematic structure of the filter. Organic pigments are doped into inorganic amorphous gel films.

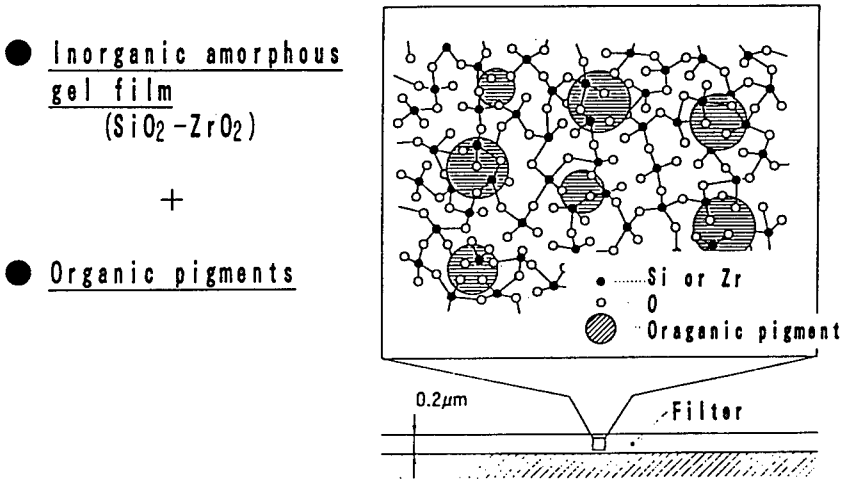

Fig. 4 Schematic Structure of Filter

(5) Characteristic

The filter has many superior properties. Inspite of a very thin film about 0.2 microns, it gives sufficient absorption, that is 60% transmittance at 570 nm. And it also gives sufficient hardness, 7 or 8H which is sufficient for practical use. These superior properties of the filter can be realized by combining the advantages of two techniques. One is organic pigments which give a suitable filter property and sufficient coloring ability. Another is the sol-gel method which gives a hard film even when made at a low baking temperature which is sufficiently low for organic pigments to withstand.

This film filter is prepared on the surface of the CPT by a simple and low cost coating method. These technique produces the "Black Enhancer" which has a better contrast , color purity, and low cost.

3. Coloring materials

(1) Requirements

First, it must give a sharp absorption around 570nm, because it directly determines the quality of contrast and color purity. Secondly, it must have sufficient coloring ability. The coating thickness which can be obtained by the sol-gel method is limited to 0.2μm max. So, it must give sufficient coloring ability even with this thin film. Thirdly, stability in the sol-gel process, that is, acid- and heat-proof properties, are also required. Forthly, the resistance to color bleaching is important. This has been a big problem for most practical use.

(2) Candidates

A few coloring materials, such as a xanthene series dyes and indigo series pigments were candidates. Among them, the indigo series pigments were selected because of their superior color bleaching property.

(3) Color bleaching

Fig. 5 shows the color bleaching results under UV ray for three kinds of candidates. The filter using the xanthene series dye showed severe bleaching. It was improved by the addition of nickel compounds, but still unsatisfactory. In contrast to these dyes, the organic pigment showed little reduction and excellent stability.

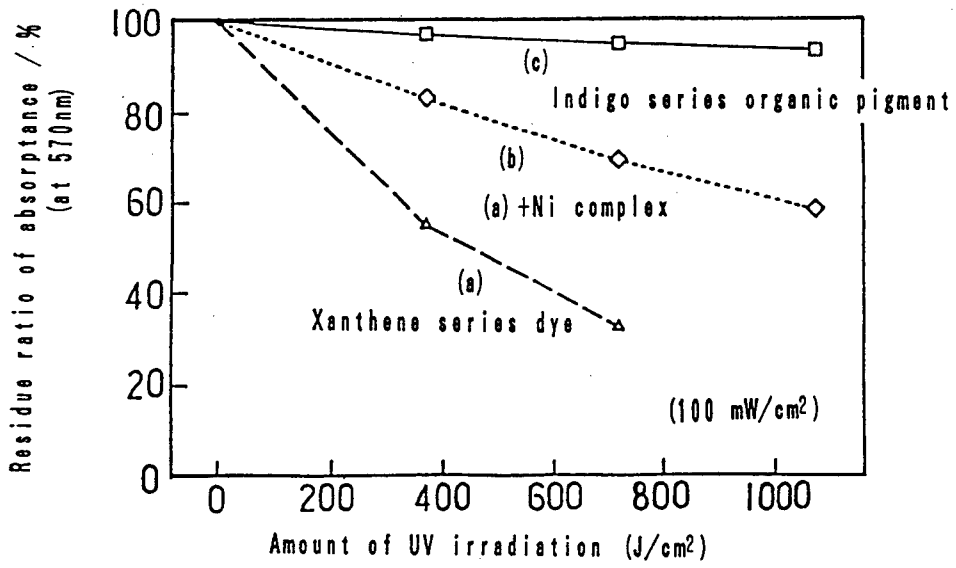

Fig. 5 Color Bleaching under UV Ray

(4) Particle size

The particle size of the organic pigments must be sufficiently small to form a transparent filter. One example of the average particle size of an organic pigment is shown in Fig. 6. A particle size of below about one-hundred nm is required.

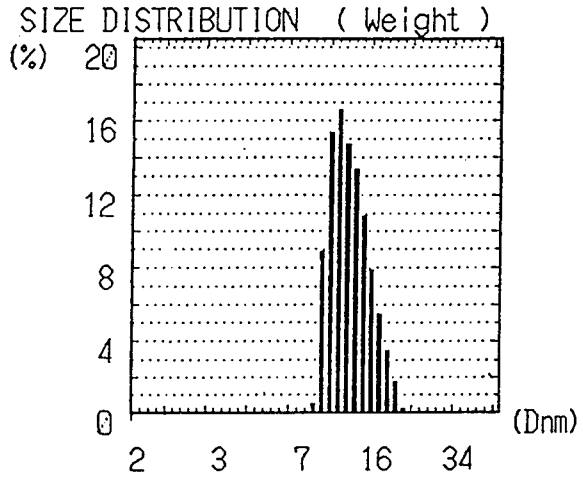

Fig. 6. Average Particle Size of Pigment

4. Sol-gel liquid

(1) Requirements

The requirements for the sol-gel method is that it gives a thin film with sufficient hardness and water-proof even when it is made at a low baking temperature. The SiO_2-ZrO_2 series was selected among various sol-gel film series.

(2) SiO_2-ZrO_2 series

The addition of zirconia to silica improved the film stability against water. Fig. 7 shows the film hardness as a function of the zirconia content after keeping it immersed in 60℃ water for 1 hour. More than about 10 mol% of zirconia to silica was needed for the required hardness.

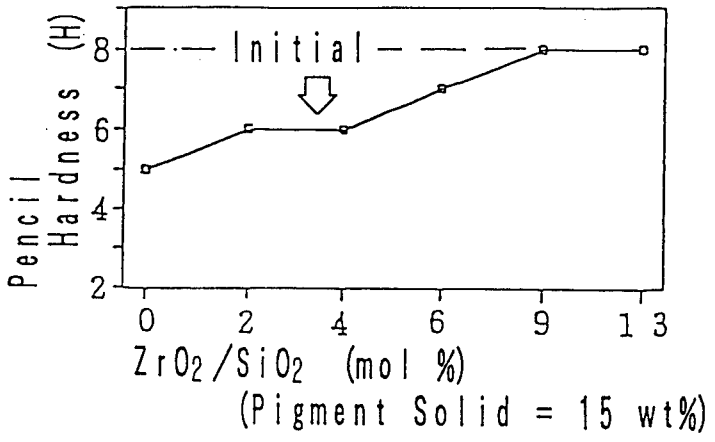

Fig. 7 Water Immertion Test (1 Hr in 60℃ Water)

5. Coating on CPT

(1) Process

The sol-gel liquid was applied on the CPT. The coating process was added to the final of the conventional CPT manufacturing proceses. First, the outside of the CPT face plate was washed with acid and water. Then, the film was formed by the spin coating method. After that, the coating film was heated at 190℃ for 10 min. Finally, inspection was done. A defective film was rejected and re-coverd easily by returning it to the cleaning position. So, this process actually gives an almost perfect yield. This is thought to be a simple and low cost process.

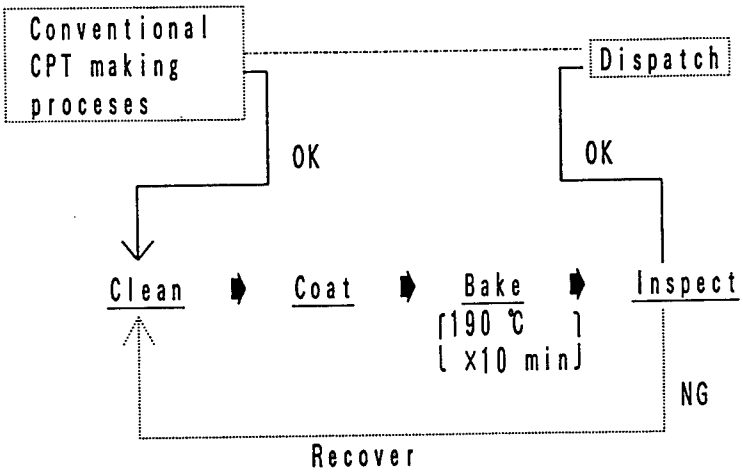

Fig. 8 Simple and Low Cost Coating Process

(2) Unevenness of coating

Spin coating is done as shown in Fig. 9. Due to the spherical shape of the face glass, the film is thicker at the corners (Fig. 10). One of the solutions for this problem is to increase the drying speed at the center portion to minimize the flow of the liquid to the corner portions. An uniform coating thickness is obtained with this method.

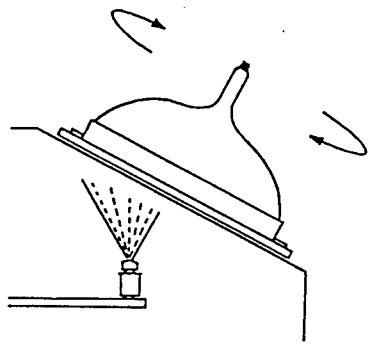

Fig. 9 Spin Coating

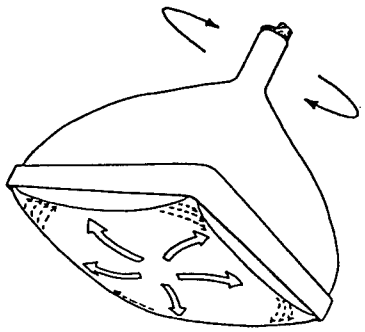

Fig. 10 Uneven Thickness of Coating

6. Improvements in Picture quality

Two kinds of improvements have been achieved simultaneously. One is the remarkable improvement in reprduciable black level (contrast) by 35% (Fig. 11). The other is the improvement in color purity. The color reproduction gamut was enlarged by 12% under 750 lx ambient light (Fig. 12).

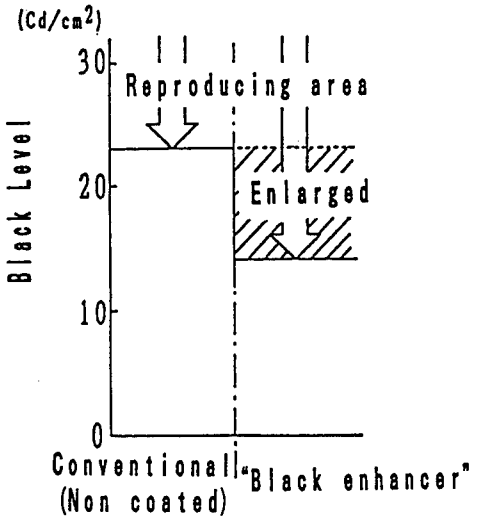

Fig. 11 Black Level (AL: 750 lx)

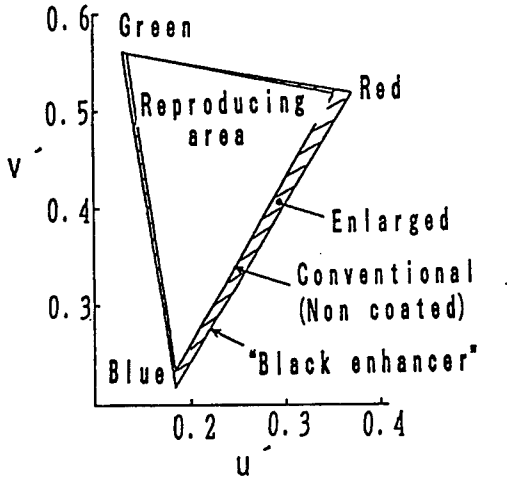

Fig. 12 Color Gamut (AL: 750 lx)

7. Production

The authors have produced a new "Black Enhancer" over one million pieces per year. Table 1 shows the amount of the ratio of the "Black Enhancer" to the total number of products (1992). This tecnology has been applied to most of Toshiba's products for larger size CPTs by the customers' request.

21"	25"	29"	34"	37"
16%	44%	87%	92%	100%

Table 1. Ratio of the "Black Emhancer" to Total Products

8. Conclusion

The authors have developed a new light-absorbing filter forming technique. The filter was made of organic pigment doped SiO_2-ZrO_2 amorphous gel films.

This filter forming technique has been applied to color picture tubes for improving its contrast and color purity. A better efficiency for contrast improvement than any other conventional techniques has been achievd. Sufficient hardness and stability against UV ray have also been realized.

Wide applications of this technique to other fields are possible because of the following advantages.

(1) A desired color can be selected.
(2) It can coat the substrate glass regardless of its shape.
(3) The colored film is sufficiently hard for most practical use.

REFERENCES

1) T. ITOU, et al. ; Proceedings of the Second International Symposium on Chemistry of Functional Dyes. 572 (1992).

Key Engineering Materials Vol. 150 (1998) pp. 77-88

Sol-Gel-Derived Coatings on Steel Sheets

K. Izumi, N. Minami and Y. Uchida

Nisshin Steel Co., Ltd., 5 Ishizu-nishimachi, Sakai-Shi, Osaka 592, Japan

Keywords: Sol-Gel Coating, Stainless Steel Sheet, Aluminized Steel Sheet, Corrosion Resistance, Oxidation Resistance, Adhesion, SiO_2, ZrO_2, Trifunctional Alkoxysilane, Organozirconium Compound, Hydrolysis

Abstract

Requirements for the sol-gel-derived coatings on steel sheets were discussed and the properties of coating films prepared from organozirconium compounds and trifunctional alkoxysilanes were mainly presented. ZrO_2 coating on stainless steel sheets was achieved in air successfully using zirconium tetraoctylate or zirconium acetylacetonate as starting materials instead of commonly used zirconium alkoxides. The oxidation resistance of stainless steel sheets at high temperature was improved by ZrO_2 coating, depending on the film thickness. Good adhesion of the coating film prepared from methyltrialkoxysilane to stainless steel sheets at the processed portions, such as bending, drawing and pressing, was obtained in a limited range of firing temperature from 200o to 300oC. This good adhesion was ascribed to a flexible structure of the films resulting from the remaining $Si-CH_3$ and Si-OH bonds.

1. Introduction

The sol-gel coating is receiving a great attention as one of the methods used to modify the surface properties of various substrates. This coating is commonly used for glasses or ceramics as the coating substrates[1,2], but, is also recognized to provide protective properties for metal substrates, such as stainless steel, aluminized and galvanized steel sheets[3,4]. However, a difference in thermal expansion coefficient between metal substrates and coating films often causes cracking and/or peeling. Therefore, a more care for the coatings on steel substrates is required than for those on glass substrates. A choice of steel substrates and their pretreatment are important for the sol-gel coatings. Understanding of hydrolysis for the starting materials and structure changes during firing are also necessary for obtaining a good coating film on steel substrates. In addition, steel sheets are usually subjected to the processing, such as bending, drawing and pressing in an actual use. Accordingly, it is necessary for the coating film to have a good adhesion to the substrates even at the processed portions. A poor elasticity of the sol-gel derived coating film on steel

sheets often causes peeling at these processed portions[5]. However, the coating film containing organic groups, which can be prepared from trifunctional alkoxysilanes, $R'Si(OR)_3$, where R' and R are alkyls[6,7], shows a potential for providing a flexible film[8].

In this paper, requirements for the sol-gel-derived coatings on steel sheets were discussed. The properties of coating films prepared from organozirconium compounds and trifunctional alkoxysilanes were mainly presented.

2. STEEL SUBSTRATE FOR SOL-GEL COATING

2.1 Type of steel

The steel substrate applying to the sol-gel coating is usually required a superior heat resistance, because it is generally subjected to a high temperature during the firing process after the sol-coating.

In addition, assuming the coating materials are used under a high-temperature environment in practical applications, the steel substrates must have a superior heat resistance themselves, as well as the coating films.

Figure 1[9] shows the weight gain curves of commercially produced metal coated and uncoated steels heated at 550°C in air. Galvanized and 5%Al-Zn alloy coated steels gain much weight by oxidation, though far less than the uncoated steel. In comparing 55%Al-Zn alloy coated and aluminized steels, the former material indicates a slightly larger weight gain. Therefore, the aluminized steel sheet can be a suitable substrate for the sol-gel coating among metal coated steels.

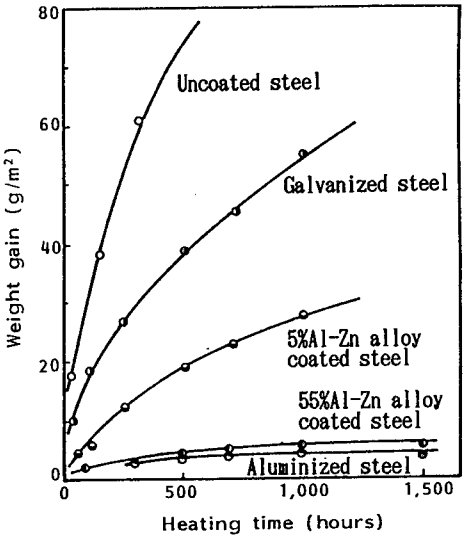

Fig.1 Weight gain curves of metal coated and uncoated steels after isothermal heating at 550°C.

The stainless steels have a further superior heat resistance against oxidation than the aluminized steel. Table 1 summarizes the oxidation resistance of various stainless steels[10]. Steel substrates coated by the sol-gel films should have not only heat resistance but also the desired characteristics in a practical use, such as corrosion resistance and mechanical property. Aluminized steel (Al coating weight:80g/m^2 on both side) and stainless steel(AISI 304) sheets of 0.4mm thick were mainly used as the substrates in the following results.

Table 1 The limiting temperature of oxidation for various stainless steels

Type of stainless steel	Limiting temperature (°C)	
(AISI)	Continuous heating	Intermittent heating
410	680	760
430	815	870
446	1,040	1,100
302B	930	870
304	870	800
309	1,100	1,000
310	1,100	1,050
316	900	815
321	870	800
347	870	800

2.2 Pretreatment of steel substrate

Steel substrates are commonly degreased for removing a rolling oil or sometimes a rust-preventing oil before subjecting to the coating. Organic solvents with a low boiling point, such as acetone, alcohol, or toluene can be used for the degreasing, preferably used together with the ultrasonic cleaning. Chromating is effective for improving the corrosion resistance of aluminized steel and the adhesion of coating film to the substrates. Physical polishing is useful for improving the adhesion of coating film to the stainless steel sheet. Chemical etching with a nitric acid, hydrofluoric acid or iron dichloride solution, and electropolishing are also suitable for the pretreatment of stainless steel.

3. HYDROLYSIS OF STARTING MATERIALS

3.1 Organozirconium compound for ZrO_2 coating

A choice of the starting materials for the ZrO_2 coating is most important from a viewpoint of a practical coating production, because their chemical properties have a great influence on the stability of coating solution in air and on the formation of the films. In general, a long time stability is required for the coating solution applying to the coating production. However, the hydrolysis rate of organozirconium compounds is generally very high and white turbidity or precipitation in their solution is readily formed in air; the precipitation is caused by the reaction of precursor compounds with moisture in air. Table 2[11] summarizes the stability of the coating solutions(ZrO_2 content of 0.038 mol/L) for different starting materials and solvents; the stability is defined as time(in hours) up to the formation of turbidity or precipitation. The stability of the solution of zirconium tetraisopropoxide or tetra-n-butoxide is less than 1.5h. However, the solutions of zirconium tetraoctylate and zirconium acetylacetonate are 30 times stabler than those of the alkoxides. Zirconium acetylacetonate is the most stable and suitable compound for ZrO_2

coating on steel sheet. This is because this compound has coordination bonds in the molecule[12], which retards the nucleophilic hydrolysis reaction with water molecule. The above finding indicates that the stability of the solution depends upon the hydrolysis rate of the starting materials and the larger the alkyl groups in alkoxides, the stabler the solution becomes.

Table 2 Influence of starting materials on stability

Starting material	Stability(h)				
	Methyl alcohol	Ethyl alcohol	Isopropyl alcohol	n-Butyl alcohol	Toluene
Zirconium tetraisoproxide	0	0.4	0.5	1.2	1.2
Zirconium tetra-n-butoxide	0	0.5	0.8	1.5	1.5
Zirconium tetraoctylate	12.0	15.0	24.0	48.0	>96.0
Zirconium acetylacetonate	>96.0	>96.0	>96.0	>96.0	>96.0

(ZrO_2 content:3.8×10^{-2})

3.2 Trifunctional alkoxysilane

The hydrolysis of trifunctional alkoxysilanes, $R'Si(OR)_3$, must depend strongly on R' as well as R, and thus their hydrolysis conditions may affect various properties of the resultant coating films on steel sheets. The influence of alkoxy groups in methyltrialkoxysilane on hydrolysis during ageing was tested. Figure 2[13] shows the relationship between the ageing time and the degree of hydrolysis;the degree of hydrolysis was determined from the alcohol amount of the aged solution by using a gas chromatograph. The degree of hydrolysis increases with ageing time for any alkoxysilanes. The hydrolysis rate, however, is strongly influenced by the type of alkoxy groups. These results show that methyltrialkoxysilanes with larger alkoxy groups are hydrolyzed more slowly, as already reported for tetra alkoxysilanes[14].

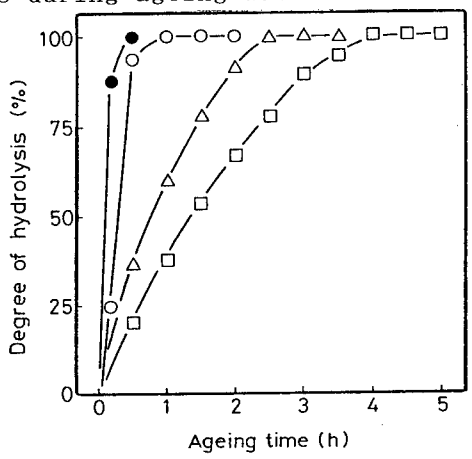

Fig.2 Relationship between degree of hydrolysis and ageing time of various methylalkoxysilanes:(●)$CH_3Si(OCH_3)_3$, (○)$CH_3Si(OC_2H_5)_3$, (△)$CH_3Si(OC_3H_7)_3$ and (□)$CH_3Si(O_4CH_9)_3$.

The influence of the alkyl groups in alkyl trialkoxysilanes on hydrolysis was then studied by using methyltriethoxysilane, MTES and phenyltriethoxysilane, $C_6H_5Si(OC_2H_5)_3$(PhTES). Figure 3 and 4 show the relationship between the degree of hydrolysis under HCl and NH_4OH catalysts, respectively. The hydrolysis rate of MTES under HCl catalyst is faster than that of PhTES. In contrast to these results under HCl catalyst, the hydrolysis rate of PhTES under NH_4OH catalyst is higher than that of MTES. These findings clearly show that whether alkyl groups in alkyl trialkoxysilanes are electron-donor or acceptor affects the hydrolysis rate.

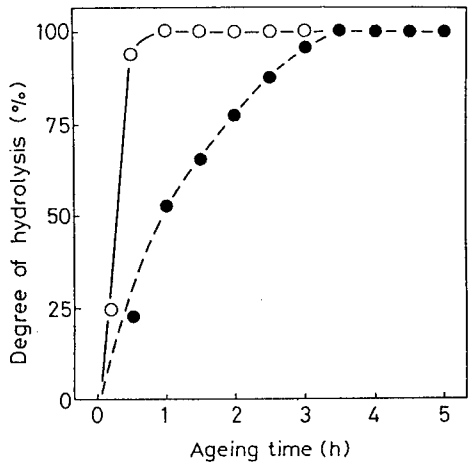

Fig.3 Relationship between degree of hydrolysis and ageing time of (○)MTES and (●)phTES under HCl catalyst.

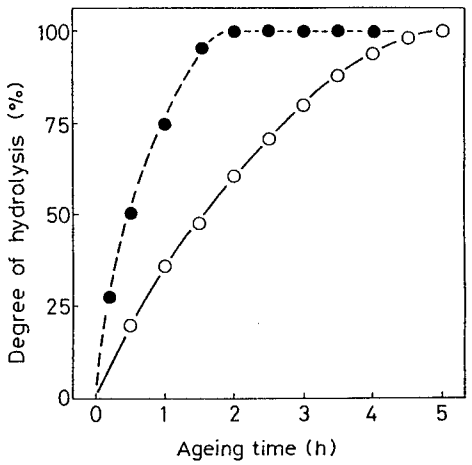

Fig.4 Relationship between degree of hydrolysis and ageing time of (○)MTES and (●)phTES under NH_4OH catalyst.

4. STRUCTURE CHANGE DURING FIRING

Structure and composition of the coating films obtained by the sol-gel method usually change with firing temperature, which could affect properties of the resultant coating films. Figure 5 shows the thermogravimetric and differential thermal analyses of the bulk gels from tetraethoxysilane ($Si(OC_2H_5)_4$,TEOS), MTES and zirconium tetra-octylate ($Zr(C_7H_{15}COO)_4$,ZTO) under a heating rate of 10°C/min. In the case of gel obtained from TEOS, a sharp exothermic peak and a weight loss are detected at around 280°C due to the combustion of remaining OC_2H_5 groups. An organic-free SiO_2 film can be obtained with firing at temperature higher than 300°C. In contrast, two exothermic peaks and two-step weight loss at around 250° and 450°C are observed in the gel from MTES. Judging from the result in SiO_2 film, a first exothermic peak at around 250°C is due to the burning of remaining OC_2H_5 groups. Relatively broad exothermic peak and weight loss are observed in the gel from ZTO from 200° to 400°C. This result suggests that the burning of bulky $C_7H_{15}COO$ groups of ZTO takes place more complex thermal process, compared with that of OC_2H_5 groups. An organic-free ZrO_2 coating film is also obtainable with firing at temperature higher than 400°C.

The structure of coating films prepared from MTES changes with firing temperature more complicatedly than that from TEOS or ZTO. Figure 6 shows Fourier-transformed infrared(FT-IR) spectra of the coating films from MTES with firing at temperatures from 150° to 500°C. The absorption peaks at around 1000cm^{-1} are assigned to Si-O-Si bonds. The absorption peaks at 1260, 1120 and 760cm^{-1}, which are observed in all the films fired at temperatures lower than 500°C, are due to $Si-CH_3$ bonds. The presence of these

absorption peaks clearly indicates that the CH_3 groups remain in a tree-dimensional Si-O-Si network[15,16]. However, from the result that the absorption peaks corresponding to Si-CH_3 bonds decrease extremely at the firing temperatures between 400° to 500°C, the second exothermic peak at around 450°C in the previous thermal analysis of the gel from MTES is due to the thermal decomposition of CH_3 groups.

From the above results, structures of the resultant films are summarized in Figure 7.

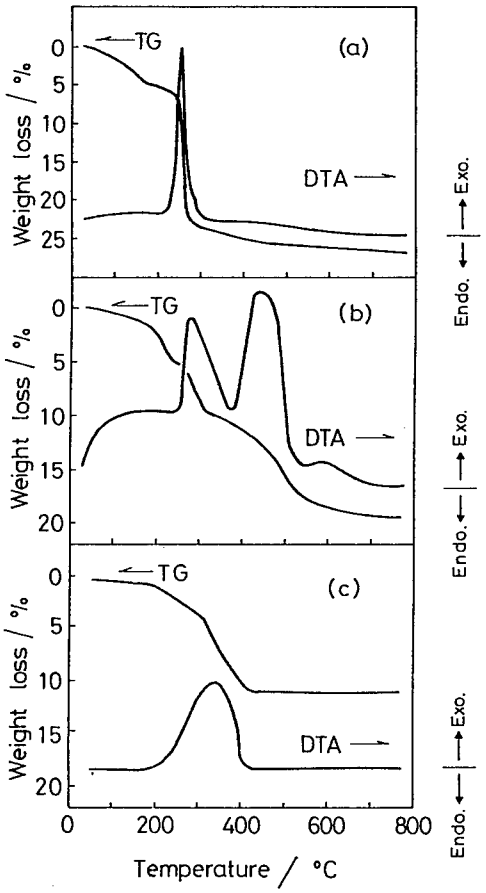

Fig.5 Thermogravimetric and differential thermal analyses of bulk gels prepared from TEOS(a), MTES(b) and ZTO(c).

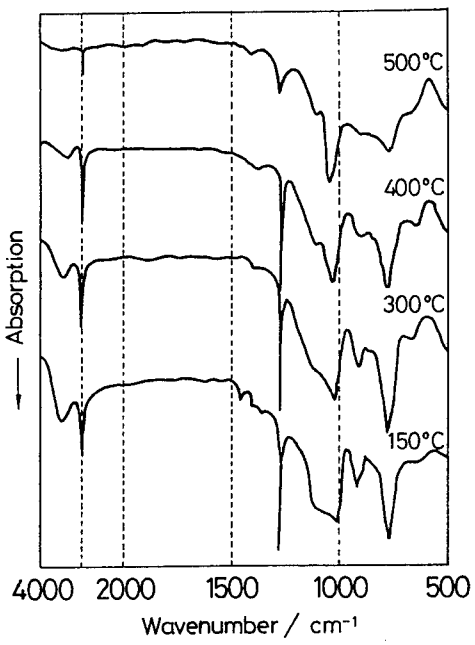

Fig.6 Fourier-transformed infrared spectra of coating films prepared from MTES with firing at 150° to 500°C on aluminized steel sheets.

Starting material	Firing temperature	Schematic structure of film
$Si(OC_2H_5)_4$ (TEOS)	300°C≦	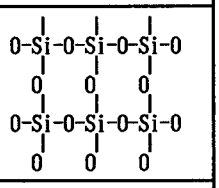
$CH_3Si(OC_2H_5)_3$ (MTES)	250°~450°C	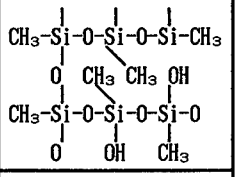
	450°C≦	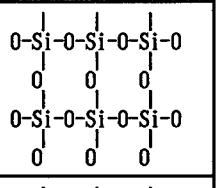
$Zr(C_7H_{15}COO)_4$ (ZTO)	400°C≦	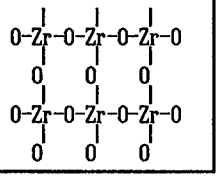

Fig.7 Firing temperature of coating films and schematic structure of resultant films.

5. PROPERTIES OF SOL-GEL DERIVED COATED STEEL SHEETS

5.1 Heat resistance of ZrO_2 coated stainless steel sheet against oxidation

Figure 8 illustrates the oxidation resistance of stainless steel sheets coated with different thickness of ZrO_2 films in testing at 800°C in air; the films were prepared from ZTO by firing at 400°C for 10min. The weight increase of stainless steel sheet at 800°C is suppressed by the application of the ZrO_2 coating, and this effect depends upon the thickness of ZrO_2 film coated. The weight increase of stainless steel sheet coated with ZrO_2 film of 1300Å thickness is about one-half of that of the stainless steel sheet without coating.

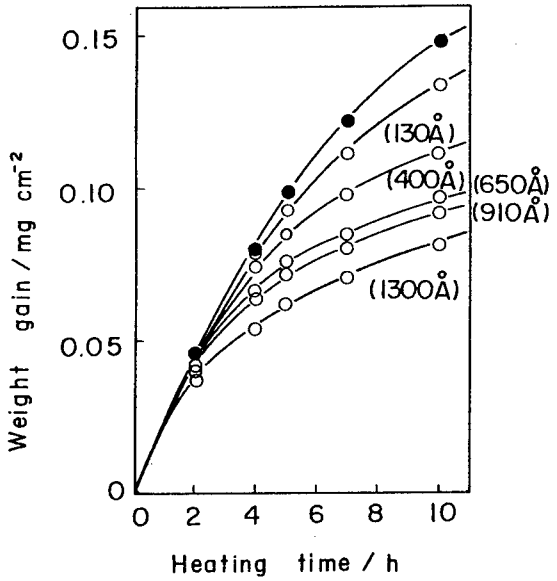

Fig.8 Effect of ZrO_2 thickness on weight gain by heating at 800°C in air:(●)uncoated stainless steel sheet and (○)ZrO_2 coated stainless steel sheet.

5.2 Influence of firing conditions on properties of film from MTES

Figure 9[19] shows the hardness and abrasion loss of the coating films(3μm thick) prepared from MTES on stainless steel sheets as a function of firing temperature.

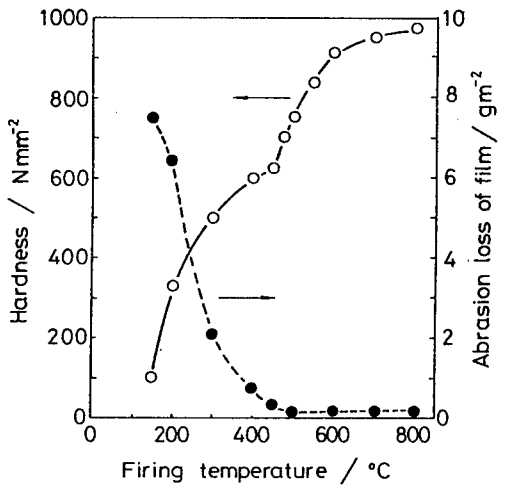

Fig.9 Hardness and abrasion loss of coating films prepared from MTES on stainless steel sheets as a function of firing temperature.

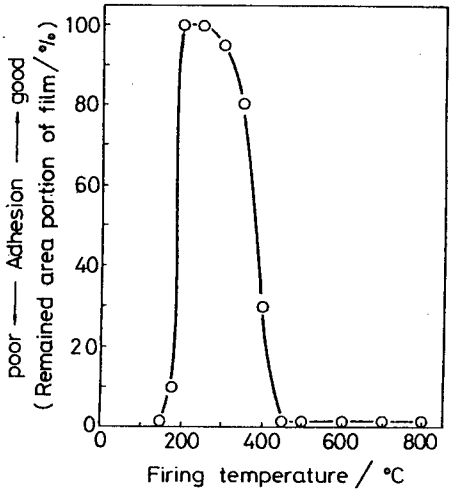

Fig.10 Adhesion of coating films to stainless steel sheets vs. firing temperature.

The hardness was determined with a dynamic ultra-microhardness tester and the abrasion loss was measured with an abrasion tester. The hardness of coating films increases logarithmically with an increase in firing temperature. A further increase of the hardness occurred at around 450°C. This suggests that the structure of coating film changes due to the burning of CH_3 groups occurring at this temperature. The abrasion loss of coating films decreases with an increase in firing temperature and reaches almost zero at temperatures higher than 500°C.

Figure 10 shows the effects of firing temperature on the adhesion of coating film at formed portions. The adhesion of coating film was evaluated by the following manner:stainless steel sheets with the coating films were subjected to the impact test and then the peeling test with scotch tape was carried out. The adhesion was evaluated from the remaining area of the film at the formed portion after the peeling test. At a firing temperature from 170° to 400°C, the coating films adhered to the stainless steel sheet even at the formed portions. An excellent adhesion is achieved in a limited range of firing temperatures from 200° to 300°C. This is caused by the flexible structure due to the remaining Si-OH and Si-CH_3 groups in the three dimensional Si-O-Si network.

5.3 Corrosion resistance

The wet and dry cyclic corrosion test (CCT) and the atmospheric exposure test were carried out for an evaluation of the corrosion resistance of aluminized steel sheets coated with SiO_2, CH_3-containing SiO_2 prepared from MTES, and ZrO_2 films.

Changes in surface appearance after 10 cycles of CCT are summarized in Table 3.

Table 3 Changes in appearance after 10 cycles of cyclic corrosion test(CCT)

Specimen	as-received aluminized steel sheet	SiO_2 coated	CH_3-containing SiO_2 coated	ZrO_2 coated
appearance	dark grayish rust no luster	no rust metallic luster	no rust metallic luster	dark grayish rust no luster

CCT; → Salt spraying at 35°C(4h)→Drying at 60°C(3h)→Humidifying at 50°C(14h) →

On the as-received aluminized steel sheet, dark grayish rusts are found and inherent metallic luster is lost after 10 cycles of CCT. In contrast, red-rusts are not observed; base steel is protected by the sacrificial corrosion effect of Al coating. On the other hand, aluminized steel sheets coated with SiO_2 and CH_3 containing SiO_2 films show an excellent corrosion resistance in this test. They have a metallic luster even after 10 cycles of CCT. On the aluminized steel sheets coated with ZrO_2 film, dark grayish rusts are observed after 10 cycles of CCT. The aluminized steel sheet coated with ZrO_2 film shows less corrosion resistance than that with SiO_2 and CH_3-containing SiO_2 films.

Figure 11 shows lightness changes on flat areas of the specimens during the atmospheric exposure test. The place of exposure is Sakai-city, Osaka-fu in Japan, which is in an industrial and marine environment. The lightness of as-received aluminized steel sheet is decreased by rusting at the surface with an exposure time. The metallic luster of as-received aluminized steel sheet is almost lost and the lightness becomes about a half of the initial lightness at a 6-year exposure. In contrast, decrease in lightness of SiO_2 and CH_3-containing SiO_2 films coated aluminized steel sheets are very slight even after 6 years of the exposure test. These results correspond to the results in the accelerated corrosion test.

Figure 12 shows polarization curves in 5%NaCl solution at 35°C for aluminized steel sheets with CH_3-containing SiO_2 and ZrO_2 films. The corrosion potentials of all the specimens show a constant value of about -740mV(vs. S.C.E.). The coatings of CH_3-containing SiO_2 and ZrO_2 films have an effect on preventing cathodic current of the aluminized steel sheet without coating. Corrosion current densities(Icorr) measured from these polarization curves for as-received, CH_3-containing SiO_2 and ZrO_2 films coated specimens are 5.0, 0.5 and 2.0μA/cm^2, respectively. It is found that CH_3-containing SiO_2 coating is more effective for inhibition of an oxygen reduction reaction than ZrO_2 coating. It has been reported that ZrO_2 film prepared by the sol-gel method consists of fine particles[18,19]. Accordingly, it is considered that CH_3-containing SiO_2 film has a more compact structure than ZrO_2 film.

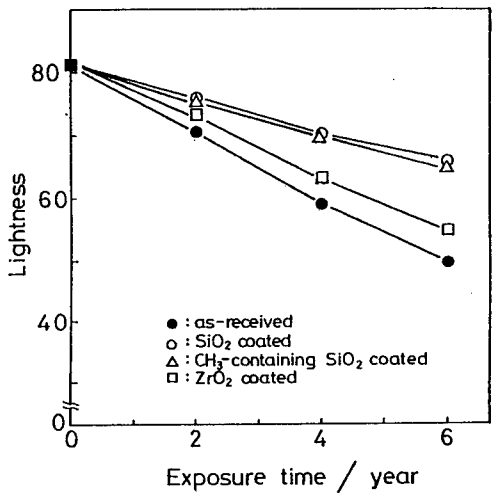

Fig.11 Change of lightness on surface of aluminized steel sheets coated with various coating films during atmospheric exposure test.

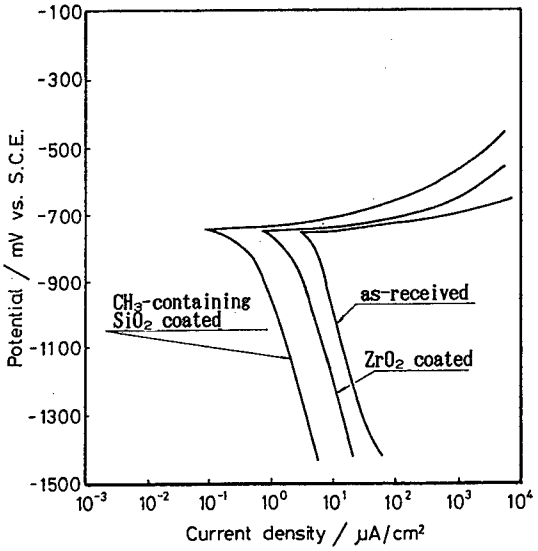

Fig.12 Polarization curves in 5%NaCl at 35°C for CH_3-containing SiO_2 film and ZrO_2 film coated aluminized steel sheets.

CONCLUSION

In this work we have described the suitable steel substrates and the pretreatment of the substrates, hydrolysis of starting material and structure changes of coating films during firing for the sol-gel-derived coating on steel sheets. Furthermore, properties of the steel sheets with coatings have been introduced. It is concluded that the sol-gel-derived coating improves the various surface properties of steel sheets, such as oxidation resistance and corrosion resistance. Moreover, the coating films prepared from MTES show good adhesion even at the formed portion. Application of the sol-gel-derived coating to the steel sheets will continue to expand.

ACKNOWLEDGMENT

The authors acknowledge Professors Tsutomu Minami of Osaka Prefecture University and Noboru Tohge of Kinki University for their many helpful comments and suggestions.

REFERENCE

[1]B.D.Fabes and D.R.Uhlmann, J.Am.Ceram.Soc. **73**, 978(1990).
[2]F.Orgaz and H.Rawson, J.Non-Cryst.Solids **82**, 378(1986).
[3]M.Atik and M.A.Aegerter, J.Non-Cryst.Solids **147&148**,813(1992).
[4]O.Desanctis, L.Gomez, N.Pellegri, C.Parodi, A.Marajofsky and A.Duran, J.Non-Cryst.Solids **121**, 338(1990).
[5]M.Guglielmi, D.Festa, P.C.Innocenzi, P.Colombo and M.Gobbin, J.Non-Cryst.solids **147&148**,467(1992).
[6]I.Hasegawa, S.Sakka, Y.Sugihara and K.Kuroda, J.Ceram.Soc.Jpn. **98**,647(1990).
[7]K.Kamiya, T.Yoko, K.Tanaka and M.Takeuchi, J.Non-Cryst.Solids **121**,182(1990).
[8]M.Murakami,K.Izumi, T.Deguchi, A.Morita, N.Tohge and T.Minami, J.Ceram.Soc.Jpn **97**,86(1989).
[9]J.Sumiya, Y.Uchida and Y.Hirose, SAE-Paper, No.850006(1985).
[10]M.Hasegawa, "Handbook of stainless steel" Nikkankogyo sinbunshya, 459(191976).
[11]K.Izumi,M.Murakami,T.Deguchi,A.Morita, N.Tohge and T.Minami, J.Am.Ceram.Soc. **72**,1465(1989).
[12]K.Kamiya, T.Yoko,K.Tanaka and H.Itoh, J.Ceram.Soc.Jpn,**95**,13(1987).
[13]K.Izumi, H.Tanaka, Y.Uchida, N.Tohge and T.Minami, J.Mater.Sci.**12**,724(1993).
[14]T.Mizuno, J.Phalippou and J.Zarzycki, Glass Technol.,**26**,39(1985).
[15]E.F.Riebling, J.Mater.Sci.,**7**,40(1972).
[16]H.Yoshino, K.Kamiya and H.Nasu, J.Non-Cryst.Solids,**126**,68(1990).
[17]K.Izumi, H.Tanaka, Y.Uchida, N.Tohge and T.Minami, J.Non-Cryst.Solids, **147&148**,483(1992).
[18]A.Negishi, J.Ceram.Soc.Jpn., **93**,566(1985).
[19]Y.Takahashi, K.Niwa, K.Kobayashi and M.Matsuki, J.Ceram.Soc.Jpn.,**95**,942(1987).

Key Engineering Materials Vol. 150 (1998) pp. 89-96

Preparation of High Sinterable $Ba(Mg_{1/3}Ta_{2/3})O_3$ Powders by Hydrolysis of Metal Alkoxides

S. Katayama, I. Yoshinaga, T. Nagai and M. Sugiyama

Advanced Materials & Technology Research Laboratories, Nippon Steel Corporation, 1618 Ida, Nakahara-ku, Kawasaki 211, Japan

Keywords: $Ba(Mg_{1/3}Ta_{2/3})O_3$, Metal Alkoxides, Low-Temperature Synthesis, Chemical Processing, Microwave Ceramics

Abstract

$Ba(Mg_{1/3}Ta_{2/3})O_3$ {BMT} perovskite powders have been prepared at extremely low temperatures (~100°C) by hydrolysis of Ba, Mg, and Ta ethoxides. The alkoxides were hydrolyzed with a large amount of water (H_2O : alkoxy group molar ratio = 10) under refluxing to precipitate a crystalline powder with the BMT pseudo-cubic perovskite structure. The BMT powder was calcined at 1000°C for 3h to yield a suitable powder for pressing and sintering. The calcined powder has high sinterability to provide a high-dense sintered body with the density of 94.0-98.0% at a low firing-temperature of 1400°C.

1. INTRODUCTION

Microwave ceramics have been developed with the progress of broadcasting and communication via geostationary satellites. Some complex perovskite ceramics, $A(B_{1/3}B'_{2/3})O_3$, exhibit low dielectric losses (high Q, Q is defined as $1/\tan\delta$) at microwave frequencies and can thus be used as microwave dielectric resonators[1-8]. Especially, $Ba(Mg_{1/3}Ta_{2/3})O_3$ {BMT} ceramics have high Q values (36000 at 10 GHz)[6]. However, it is difficult to sinter BMT powders prepared by the conventional solid-state reaction method because of its low sinterability. Thus, the densification has been accomplished by addition of sintering aids[1,7] or by rapid heating ($1600°C min^{-1}$)[6]. Even these techniques require high sintering temperatures of ~1600°C.

The chemical processing provides fine oxide powders with high sinterability, as well as high purity and homogeneity. This method can also be used for the preparation of fine BMT powders with high sinterability. There are some reports on the sol-gel preparation of BMT powders[9-11], in which the perovskite phase has been formed at calcination temperatures of 590°C or above. One of the present authors found that the hydrolysis of Ba, Mg, and Ta ethoxides can provide BMT perovskite phase at extremely low temperatures (around 100°C)[12].

This paper describes the hydrolysis condition for the precipitation of crystalline BMT powders at low temperatures and the sintering behavior of the BMT powers.

2. EXPERIMENTAL

Penta-ethoxy tantalum {$Ta(OC_2H_5)_5$}, cobalt(II) acetylacetonate {

$Co(CH_3COCHCOCH_3)_2 \cdot 2H_2O$}, Ba metal, and Mg metal were used as starting materials. $Ta(OC_2H_5)_5$ and $Co(CH_3COCHCOCH_3)_2 \cdot 2H_2O$ were commercially available (High Purity Chemicals Co. and Tokyo Chemical Industry C., Ltd., respectively). $Ta(OC_2H_5)_5$ and Mg metal were added to dried ethanol, followed by refluxing for 48h in dry nitrogen. A transparent solution was obtained possibly because of the formation of a double alkoxide $Mg\{Ta(OC_2H_5)_6\}_2$ [12,13]. Ba metal was further dissolved to the above solution in the stoichiometric ratio of BMT. For Co-doping, $Co(CH_3COCHCOCH_3)_2 \cdot 2H_2O$ was added to the BMT alkoxide solution. The metal alkoxides in ethanol were hydrolyzed by addition of CO_2-free water diluted in ethanol (50wt%) in the water : alkoxy group molar ratio (r) of 1-100 under refluxing at ~100°C or stirring at room temperature to yield a white precipitate. The precipitates were separated by ultrafiltration and dried under reduced pressure. The powders were calcined at various temperatures for 3h. A BMT powder was also prepared by the conventional solid-state reaction method. $BaCO_3$, MgO, and Ta_2O_5 were mixed and calcined at 1250°C for 4h to give a BMT powder, which was compared with the alkoxide-derived BMT powders. The BMT powders were uniaxially pressed at 100MPa with polyvinyl alcohol (PVA) binder or isostatically pressed at 200MPa without binder to form green bodies like a disk. The green bodies were fired at various temperatures.

Phases of samples were identified by X-ray diffraction analysis using Cu$K\alpha$ radiation with a monochromater. The high density of sintered samples was measured by the Archimedes method. The low density of green bodies and sintered samples was estimated by measuring the weight and volume (diameter and thickness) of the disks. The morphology of BMT powders and the fracture surfaces of the sintered bodies were examined by scanning electron microscopy (SEM). The microwave dielectric properties were measured by Hakki and Coleman's method[14] improved by Kobayashi and Tanaka[15].

3. RESULTS AND DISCUSSION

3.1 Effect of hydrolysis condition on direct formation of crystalline BMT

Figure 1 shows X-ray diffraction patterns of powders prepared by hydrolysis with water in the ratio of r=1(a), 2(b), 10(c), and 100(d) under refluxing. Although the powders precipitated in the ratio of r=1 and 2 are amorphous, the hydrolysis in the ratio of r=10 and 100 give a crystalline powder with the BMT pseudo-cubic perovskite structure. The stoichiometric amount of water for hydrolysis and condensation reactions of Ba, Mg, and Ta ethoxides to form the BMT oxide corresponds to only a half mole of alkoxy groups (r=0.5), according to the followed reaction equation.

$$Ba(OEt)_2 + 1/3Mg(OEt)_2 + 2/3Ta(OEt)_5 + 3H_2O \longrightarrow Ba(Mg_{1/3}Ta_{2/3})O_3 + 6EtOH \quad (1)$$

Despite hydrolysis with over the stoichiometric amount of water (r>0.5), the formation behavior of the BMT phase depends on the amount of water. In the hydrolysis condition of non-refluxing, amorphous powders were obtained, even in the ratio of r=10 and 100. Therefore, the hydrolysis with a large amount of water

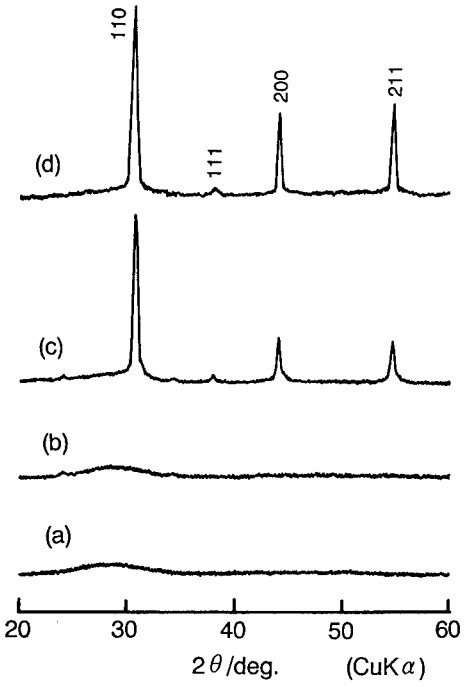

Fig. 1 XRD patterns of BMT powders prepared by hydrolysis with water in the ratio of r=1(a), 2(b), 10(c), and 100(d) under refluxing. hkl indices indicate diffraction peaks of the BMT pseudo-cubic perovskite.

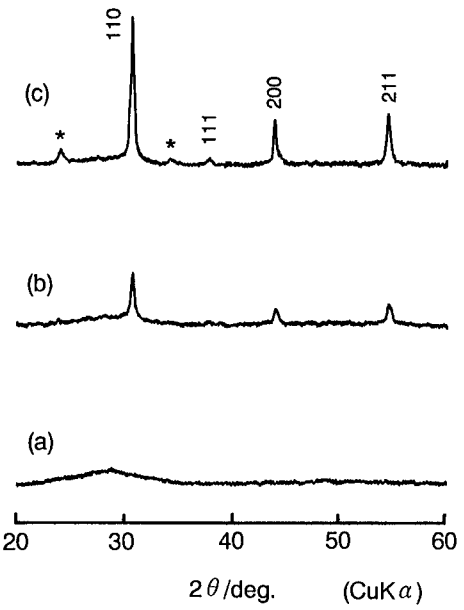

Fig. 2 XRD patterns of BMT powders prepared by hydrolysis with water in the ratio of r=10 and refluxing for 0(a), 1(b), and 12h(c). hkl indices indicate diffraction peaks of the BMT pseudo-cubic perovskite. * indicates diffraction peaks of $BaCO_3$.

under refluxing is effective to precipitate a crystalline BMT powder.

BMT alkoxides were hydrolyzed with water in the ratio of r=10, followed by refluxing for 0(a), 1(b), and 12h(c). X-ray diffraction patterns of the obtained powders are shown in Fig. 2. Whereas amorphous powders are precipitated under non-refluxing (0h), the crystalline BMT phase is formed under refluxing just for one hour. The BMT powder prepared for a long refluxing-time of 12h exhibits stronger diffraction peaks of the perovskite structure than that prepared for a refluxing-time of 1h. It is assumed that the BMT perovskite is crystallized from the hydrolyzed amorphous product under refluxing.

3.2 Sintering behavior of alkoxide-derived BMT powders

BMT powders were prepared by hydrolysis with water in the ratio of r=10 under refluxing and calcined at various temperatures for 3h. Figure 3 shows SEM

micrographs of the as-prepared BMT powder(a) and BMT powders calcined at 800(b), 1000(c), and 1100°C(d). The as-prepared BMT powder is composed of ~50nm particles with rough surface. It was difficult to press it into a dense green body possibly because of the rough surface of the very fine particles. The surface of the particles turns out to be smoother with higher calcination temperature. In the BMT powder calcined at 1100°C, the significant neck-growth between particles is also observed. The calcined powders were uniaxially pressed and fired at 1400°C for 4h. The relative densities of green and fired bodies are shown in Fig. 4, where the value of $7.628 gcm^{-3}$ is used as the theoretical density of BMT. The green densities increase with an increase in calcination temperature. However, the densities of the sintered bodies exhibits a maximum at a calcination temperature of 1000°C. The calcination can control the morphology of particles to give a dense green body, from which BMT ceramics with high density are prepared. Despite the high density of the green body from the BMT powder calcined at 1100°C, the BMT powder yields a low-dense sintered body. The high calcination temperature may reduce the sinterability of BMT powders.

The BMT powder calcined at 1000°C was uniaxially pressed and fired at temperatures from 1200 to 1600°C for 4h. The BMT powder prepared by the solid-state reaction method was also treated in the same manner. The relative

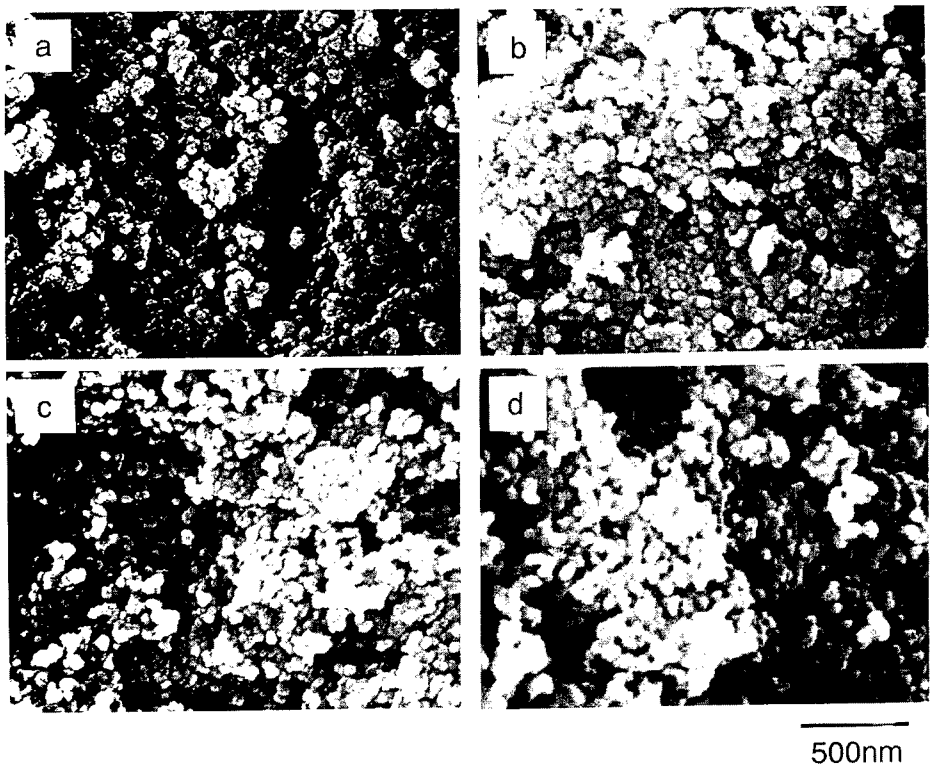

Fig. 3 SEM micrographs of as-prepared BMT powder(a) and BMT powders calcined at 800°C(b), 1000°C(c), and 1100°C(d) for 3h.

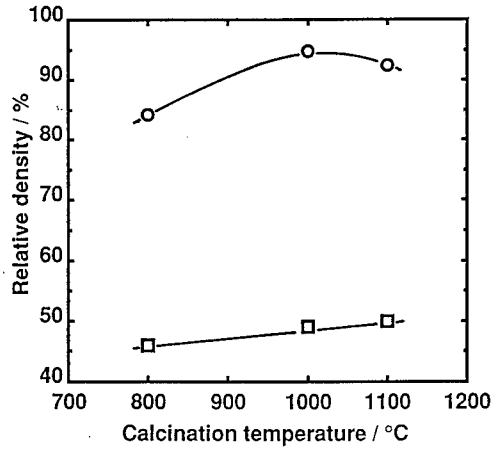

Fig. 4 Relative densities of green (□) and fired (○) bodies prepared from BMT powders after calcining alkoxide-derived powder at various temperatures for 4h. The green bodies were prepared by uniaxially pressing at 100MPa with PVA binder, followed by firing at 1400°C for 4h.

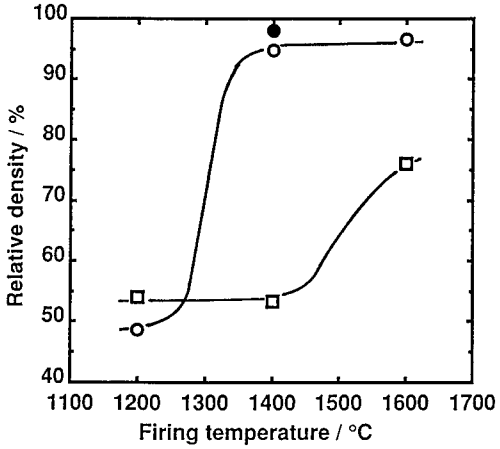

Fig. 5 Relative densities of BMT ceramics prepared from alkoxide-derived powder (○) and solid-state reaction powder (□). They were fired at various temperatures for 4h. ● indicates the density of the sample prepared by isostatically pressing at 200MPa without binder and fired at 1400°C for 8 h.

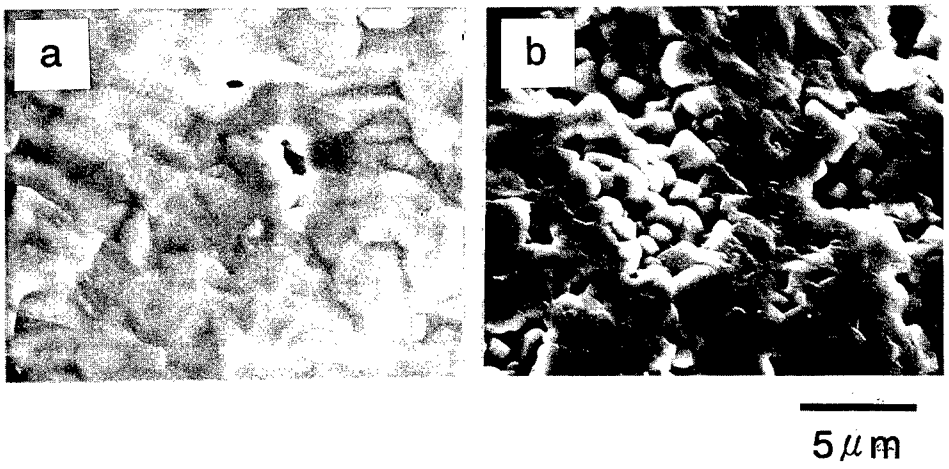

Fig. 6 SEM micrographs of fracture surfaces of BMT ceramics prepared from alkoxide-derived powder(a) and solid-state reaction powder(b). (a) and (b) were fired for 4h at 1400°C and 1600°C, respectively.

densities of these samples are shown in Fig. 5. The alkoxide-derived BMT powders are sintered into a high-dense body with the relative density of 94.7% at a firing temperature of 1400°C, whereas there is little densification at a firing temperature of 1200°C. The BMT powder prepared by the solid-state reaction method exhibits no densification up to 1400°C where the density is almost identical to that of the green body. Even at the high firing temperature of 1600°C, the obtained body has a lower density of 76.0% than that of the alkoxide-derived BMT. The alkoxide-derived BMT powder is highly densified even at a low firing-temperature of 1400°C. The calcined BMT powder was also isostatically pressed and fired at 1400°C for 8h. The sintered body has the highest density of 98.0% shown as a closed circle in Fig. 5. Figure 6 shows SEM micrographs of fracture surfaces of the BMT ceramics prepared from the alkoxide-derived powder(a) and solid-state reaction powder(b). The BMT ceramic prepared from the alkoxide-derived powder at a low firing-temperature of 1400°C is composed of several micrometer grains in close contact, whereas grains are not in close contact with each other in the BMT body prepared from the solid-state reaction powder at a high firing-temperature of 1600°C. Thus, the chemical process by hydrolysis of metal alkoxides provides a higher sinterable BMT powder than that of the conventional solid-state reaction method.

3.3 Microwave dielectric characterization of alkoxide-derived BMT ceramics

Table 1 shows microwave dielectric properties of alkoxide-derived BMT ceramics. The dielectric constant ε_r increases with an increase in density, as described by Banno et al.[4]. The Q・f product of alkoxide-derived BMT ceramics (No.1 and 2) was ~35000, being lower than the value of BMT ceramics prepared by the conventional solid-state reaction method[6]. However, the relative high Q・f value of 103100 was obtained in the sample No.3 containing Co as a partial substitution for Mg in the ratio of $Ba\{(Co_{0.125},Mg_{0.875})_{1/3}Ta_{2/3}\}O_3$.

Table 1 Microwave dielectric properties of alkoxide-derived BMT ceramics

No.	firing condition	relative density(%)	ε_r	Q・f(GHz)
1	1400°C 64h	96.7	24.3	35100
2	1600°C 64h	95.4	23.8	34700
3	1600°C 64h	92.2	22.7	103100

The sample No.3 contains Co in the ratio of $Ba\{(Co_{0.125},Mg_{0.875})_{1/3}Ta_{2/3}\}O_3$.

4. CONCLUSIONS

BMT perovskite ceramics have been prepared at extremely low temperatures by the chemical processing comprised of the hydrolysis of Ba, Mg, and Ta ethoxides.

(1) The crystalline phase with the BMT pseudo-cubic perovskite structure is formed at ~100°C by the hydrolysis with a large amount of water under refluxing.

(2) The alkoxide-derived BMT powder exhibits high sinterability. The BMT powder calcined at 1000°C provids a sintered body with the relative density of

94–98% at a low firing-temperature of 1400°C, although such a high dense body is not obtained by the conventional solid-state reaction method even at a firing temperature of 1600°C.

The authors would like to thank K. Nieda for his experimental assistance and M. Hatakeyama for the XRD measurement.

5. REFERENCES

[1] S. Nomura, K. Toyama, and K. Kaneta, Jpn. J. Appl. Phys., 21(10)L624–L626(1982).
[2] M. Onoda, J. Kuwata, K. Kaneta, K. Toyama, and S. Nomura, Jpn. J. Appl. Phys., 21 (12), 1707–10(1982).
[3] S. Kawashima, M. Nishide, I. Ueda, and H. Ouchi, J. Am. Ceram. Soc., 66 (6), 421–23(1983).
[4] M. Banno, F. Mizuno, T. Takeuchi, T. Tsunooka, and K. Ohya, Jpn. J. Appl. Phys., 24 , Suppl. 24-3, 87–89(1985).
[5] S. Nomura, and K. Kaneta, Jpn. J. Appl. Phys., 23(4), 507–508(1984).
[6] K. Matsumoto, T. Hiuga, K. Takada, and H. Ichimura, Proc. 6th IEEE Int. Symp. on Applications of Ferroelectrics, Bethlehem, PA, June, 118–21(1986).
[7] M. Sugiyama, T. Inuzuka, and H. Kubo, in Ceramic Transactions: Materials and Processing for Microelectronic System, ed. K. M. Navi, R. Pohanaka, and R. C. Buchanan, Am. Cream. Soc., Westervill, 153–166(1990).
[8] T. Nagai, T. Inuzuka, and M. Sugiyama, Jpn. J. Appl. Phys., 31(9B), 3132–35(1992).
[9] M. Schnoeller and W. Wersing, in Processing Science and Advanced Ceramics, ed. I. A. Aksay, G. L. McVay. and P. R. Ulrich, Mater. Res. Soc. Symp. Proc. Vol.155, Mater. Res. Soc. Pittsburgh, 45–52(1989).
[10] M. Schnoeller and W. Wersing, in European Mater. Res. Soc. Monographs 5 (Eurogel '91), ed. S. Vilminot, R. Nass, and H. Schmit, Elsevier Science Publishers, North-Holland, 255–263(1992).
[11] O. Renoult, J.-P. Boilot, F. Chaput, R. Papinernik, L. G. Hubert-Pfalzgraf, and M. Lejeune, J. Am. Ceram. Soc., 75(12), 3337–40(1992).
[12] S. Katayama and M. Sekine, J. Mater. Chem., 2(8), 889–90(1992).
[13] S. Govil, P. N. Kapoor, and R. C. Mehrotra, J. Inorg. Nucl. Chem., 38, 172–3(1976).
[14] B. W. Hakki and P. D. Coleman, IRE Trans. Microwave Theory Tech., 8, 402–10(1960).
[15] Y. Kobayashi and M. Katoh, IEEE Trans. Microwave Theory & Tech., 33(7), 586–92(1985).

Key Engineering Materials Vol. 150 (1998) pp. 97-110

Development of HUD Combiner for Automotive Windshield Application

K. Makita, H. Inaba and H. Sakai

Glass Research Center, Central Glass Co., Ltd.,
1510 Ohokuchi-cho, Matsusaka City, Mie Pref., 515, Japan

Keywords: Head-Up Display, Windshield, Transmittance, Reflectance, TiO_2-SiO_2, Sol-Gel Metal Alkoxide, Dielectric Film, Durability

ABSTRACT

The Head-up Display system (HUD) has been developed for the windshield of Nissan Motor's passenger car '88 model of 240SX. Since that, for the past 5 years, over 150 thousands HUD system have been used for a few car models.

The concept of HUD system is conveying vital information to a driver in a visible form without requiring him to take his eyes off the road. This system provides nice visibility of the speed in a three-digit reading at the position of one meter or more far from driver's eye focus even under the bright sunlight.

The system consists of an ultra-high bright vacuum fluorescent tube (VFT), a reflective mirror, a set of optical lenses, a transparent curved aperture cover and a combiner as the special screen. The combiner has to have high transmittance as well as high reflectance so that a driver can see both foreground object and display reading at the same time. The optical design of the combiner is based on these two concepts:

(1)Visible light transmittance shall be 70% or more in accordance with a legal requirement.
(2)Taking both peak wavelength of VFT and sensitivity characteristics of human eyes into consideration, 530nm wavelength is chosen as a reflective light.

The combiner consists of a dielectric thin layer of $TiO2$-SiO_2 system. Its basic structure is decided by simulation with matrix method of the resultant waves. The coating film is applied on the restricted area of

the inside surface of the laminated windshield by newly developed sol-gel coating process using a metal alkoxide solution with a long storage life. The dielectric films being achieved was chemically and physically strong, and satisfy the durability requirements based on ANSI or JIS such as abrasion resistance and weathering resistance.

1. INTRODUCTION

HUD was originally developed as the display devices for the use of aircraft, and in recent years, its advantage has also aroused automotive industry's interest [1].

Central Glass Co. and Nissan Motor Co. have jointly developed a HUD system for the purpose of applying it to the passenger car. The combiner windshield manufactured by Central Glass and the optical element developed by Nissan Motor were successfully combined into the world first commercial HUD system for '88 model of 240SX [2]. This HUD system have been installed in 150 thousands cars for past 5 years. Since our HUD system have introduced in the market, HUD system is gradually and widely recognizing as a new automotive display system.

2. HUD COMBINER

The display image of the HUD system is shown in Fig.1. The combiner, 115x75mm size, is the dielectric layer formed on the inside surface of the windshield. The location of combiner at the windshield is designed so that a driver can get the driving information such as vehicle speed being projected on the combiner without leaving his line of sight from the foreground.

The optical system of HUD is shown schematically in Fig.2. It consists of ultra-high bright vacuum fluorescent tube as a display light source, optical lenses focused at long optical distance, reflective mirror, transparent curved aperture cover and combiner made by sol-gel coating method. The concept of this system is to convey vital information to a driver in a visible form without requiring him to take his eyes off the road. The actual size of this system is about two pieces of cigarette boxes. The combiner was designed from two optical concepts. Firstly, this combiner has to meet the regal requirement of minimum transmittance of 70% for normal incident light. Secondly, as the incident angle of display light

onto the combiner is required from 60 ° to 70 °, light reflectance of combiner surface at the wavelength of 530nm shall be more than 25% obtain good recognizability of displayed information. Because of taking both peak wavelength of VFT and sensitivity characteristics of human eyes into considerations, the wavelength of 530nm shall be selected as a peak wave length of reflected light. The luminance of VFT which human eyes feel may be expressed as the product of the spectral luminous efficiency and the spectral distribution of radiant flux of VFT as shown in Fig.3 [3,4].

Furthermore, the combiner shall satisfy general requirement on the durability for practical automotive use.

Fig.1 Displayed image by HUD system

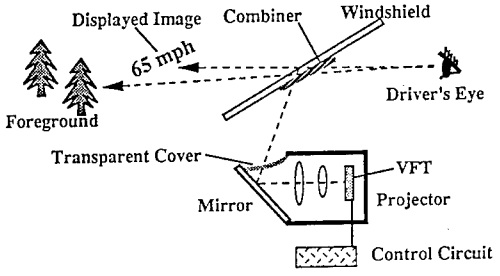

Fig.2 Optical design of HUD system

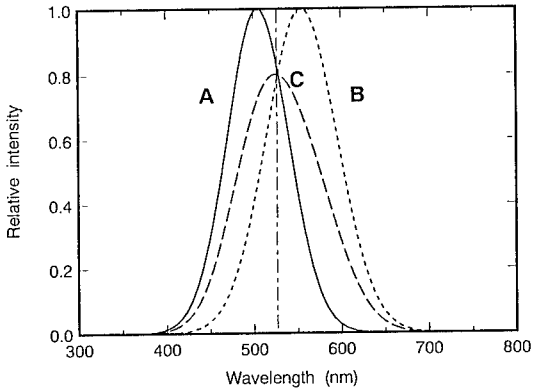

A : luminance of VFT
B : sensitivity characteristics of human eyes
C : reflectivity being required on combiner

Fig.3 Luminance of a VFT corrected by sensitivity characteristics of human eyes

3. OPTICAL DESIGN

Necessary refractive index and thickness of optical thin film for the combiner were calculated by computer simulation program. Fig.4 shows one of the result for the Nissan's 240SX car. In this case, we obtained refractive index 2.05 and the physical thickness 220nm at the incident angle 66 ° from the calculated result. Also it was understood that these optical properties were able to be realized by single layer of thin film. Fig.5 shows the simulated reflectance of the combiner at the incident angle of 66 °. As seen from this figure, the peak wavelength is about 530nm and peak reflectance is about 35% or more. And furthermore, we can see that this simulated curve of the selective reflective combiner shows good agreement with experimentally measured reflection curve of the combiner installed in 240SX as shown in Fig.5.

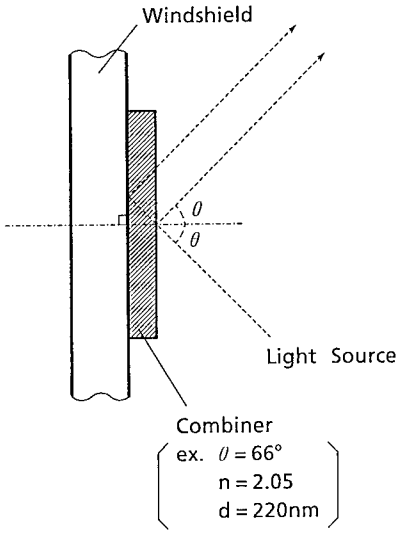

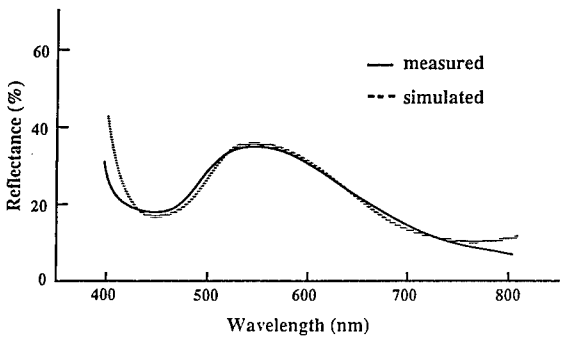

Fig.5 Reflectance of the combiner

Fig.4 Simulated design for HUD combiner

4. MANUFACTURING

4.1 Thin film by sol-gel coating

The manufacturing process is based on a sol-gel coating method using a metal alkoxide solution. It has three major advantages as the following:

(1)Easy control of film thickness. In the case of dip coating, required film thickness can be obtained by simply controlling of withdrawal rate.

(2)Easy control of refractive index.

Our actual combiner consists of a dielectric thin film. By means of sol-gel coating, in general, we can obtain high refractive index about 2.25 from TiO_2 and low refractive index about 1.45 from SiO_2. Fig.6 shows the refractive index of TiO_2-SiO_2 binary system as a function of the molar proportion of TiO_2. In this figure, X-axis is the molar proportion of TiO_2 and Y-axis is the refractive index of films. In the case of the combiner for the 240SX, it needs the refractive index of 2.05. It can be easily understood from this figure that refractive index 2.05 can obtain at the molar ratio of 80% TiO_2 and 20% of SiO_2. In Fig.6, we show a comparison of our experiment result in solid line and Dr. Schröder's result [5] in dotted line. Both lines agree well.

(3)By heat-treatment at higher enough temperature, it can be expected that TiO_2-SiO_2 binary system film will have high chemical durability and good mechanical property such as abrasion resistance and scratch resistance.

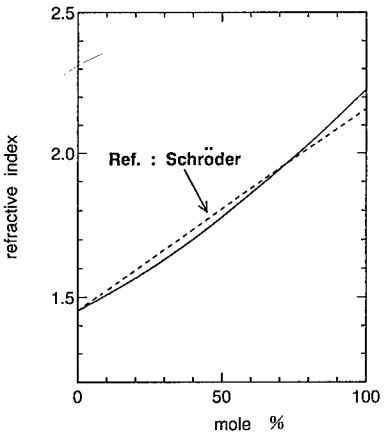

Fig.6 Composition dependence of refractive index in the TiO_2-SiO_2 system

H.Schröder; Physics of Thin Films, 5, 87, 87-141 (1969)

4.2 Preparation of alkoxide solution

Preparation procedure is shown in Fig.7. As starting materials of the coating solution, we use originally developed Ti-alkoxide and SiO_2 sol which have longer storage life. Stability of chemicals is one of the most important point to maintain high level of products quality and reproducibility of production at the manufacturing of sol-gel coating products.

In the first stage, Ti-alkoxide and SiO_2 sol are mixed and stirred. And next stage, iso-propanohol as the major solvent and small quantity of

Hydroxi-Propyl-Cellose (HPC) are added to the solution. With this, we obtain alkoxide solution mix for the coating. This solution contains almost no water, consequently hydrolysis mainly occurs by the moisture in atmosphere.

In the sol-gel coating process, it is well known that addition of small quantity of HPC to the alkoxide solution is very useful and effective to obtain thicker film. An effect of HPC at the sol-gel coating process is shown in Fig.8 [6]. In this figure, Y-axis represents film thickness and X-axis is viscosity of alkoxide solution. In the case of SiO_2 sol containing HPC, the maximum thickness of about 0.5 μm is obtained.

However, during above process, we often encountered with serious problem that coated film, being heated at higher temperature than 500-600 °C, should poor chemical and mechanical durability in spite of good appearance of the film. A microscope photograph of the surface of the obtained film is shown in Fig.9. It can observed that many micro cracks of smaller than 0.1mm size are studded. It was considered that partial thermal-shock caused by oxidation of HPC at the specific temperature during heat-treatment of the film gave these micro cracks which might be cause of the poor durability of film.

As the solution of this problem, it was very effective to use two kinds of HPC which had different decomposition temperature respectively for reducing thermal-shock cause by oxidation of HPC. One of our result on the study of HPC mixture is shown in Fig.10. In this study, we used a mixture of HPC-M and HPC-L (by Nippon Soda Co.). The molecular weight of HPC-M is larger than that of HPC-L. Decomposition temperature of HPC-M is slightly higher than that of HPC-L. This figure shows the number of micro cracks vs ratio of HPC-M to total HPC. X-axis is quantity of HPC-M and Y-axis is the number of micro cracks in $100cm^2$ area observed by 200 magnification. In this figure unsymmetrical curve are observed. In the case of total quantity of HPC is 0.34 wt%, no crack formation is observed at weight ratio of HPC-M about 0.9 [7].

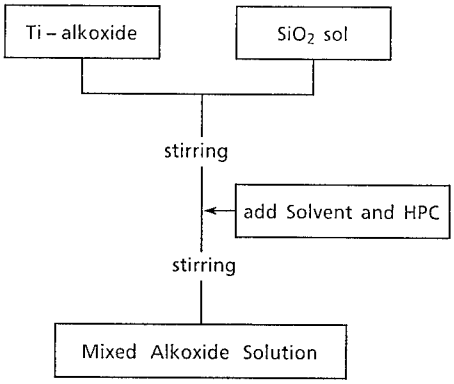

Fig.7 Preparation procedure of the mixed alkoxide solution

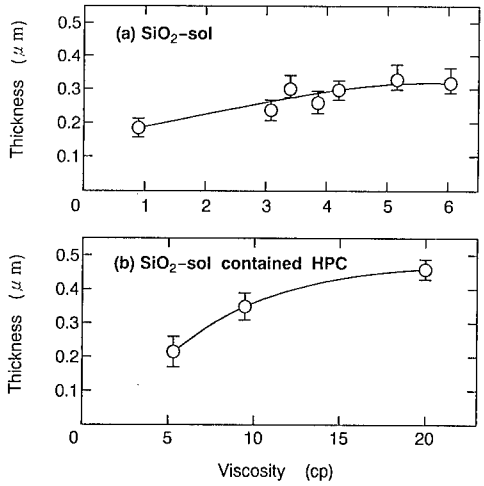

Fig.8 Relation between thickness of SiO_2 film and viscosity of SiO_2 sol

Y.Yamamoto, K.Kamiya and S.Sakka ; J.Ceram.Soc.Japan, 90, 328-333 (1988)

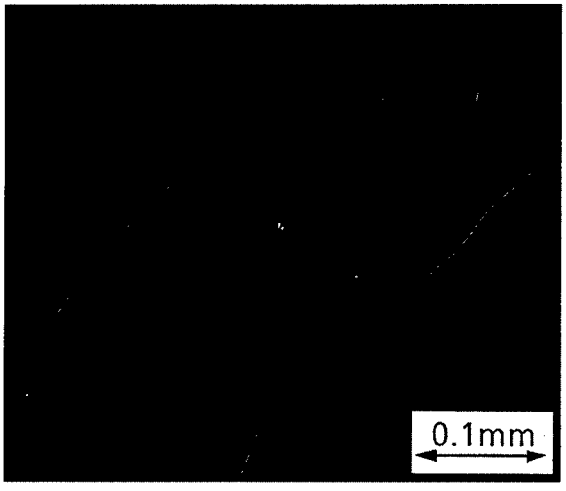

Fig.9 Microscope photograph of the film surface

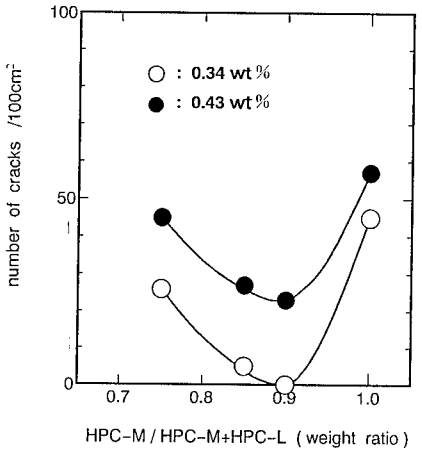

Fig.10 Relation between the number of micro cracks and the HPC-M/(HPC-M+HPC-L) ratio

4.3 Newly developed sol-gel coating process

In sol-gel coating, dip-coating is very well known method. But by this method, coating films are always applied to the both surfaces of the substrate. Therefore, regular dip-coating is not appropriate method for combiner production. Single side coating method such as spray coating, flow coating, roller coating and spin coating are also not good method for combiner production, because film is always applied to whole area of substrate surface. As I mentioned before, combiner has to be applied to restricted area at one side surface of substrate. In general, screen printing or pad printing are also useful method, but at combiner production, film thickness has to be strictly controlled for optical purpose. The both methods don't give enough thickness accuracy for optics of selective reflective combiner.

Our newly developed coating method for the combiner production is shown in Fig.11 schematically. Coating process of this method is explained as the follows:

(1)A washed and dried sheet glass is set to the newly developed apparatus, and a container of coating solution which has an opening at one side is tightly contacted to the sheet glass, so that the opening of the container is closed by the sheet glass to become complete box.

(2)After that, a coating solution in the reservoir tank is transferred to the container through flexible connecting tube until the solution in the the solution in the container reaches to predetermined level. By this manner, any desired area of sheet glass surface is directly exposed to metal alkoxide solution.

(3)Application of solution to the glass surface can be done by lowering the reservoir tank at constant rate, that is, lowering the solution, while glass substrate is stationary.

The relation between the number of coating glasses and coating rate, that is, lowering late of alkoxide solution level at commercial plant is shown in Fig.12. X-axis is the number of treated glasses and Y-axis is coating rate. The thickness t of the coating film is mainly a function of the concentration C, the viscosity of the solution respectively and coating rate V at which the sheet glass is coated. This relation in the actual plant can be empirically expressed as the from of Eq.1 :

$$t = 150 \cdot C^{4/5} \cdot \eta^{7/12} \cdot V^{7/12} \quad (1)$$

If C and η are fixed, the thickness t is proportional only to seven twelves power of V. But in actual production, C and η increase gradually during production due to evaporation of solvent and increasing of water contents of solution. C and η can be expressed by Eq.2 and Eq.3 respectively:

$$\eta = 6.85 + 0.0033X \quad (2)$$

$$C = 0.463 + 0.000128X \quad (3)$$

where 6.85 and 0.463 are the initial viscosity and the concentration of solution respectively. 0.0033 and 0.000128 are the increasing rate of the viscosity and the concentration respectively. X is the number of repeating of coating. With these practical measure, we can obtain the appropriate film thickness meeting the required optical specification.

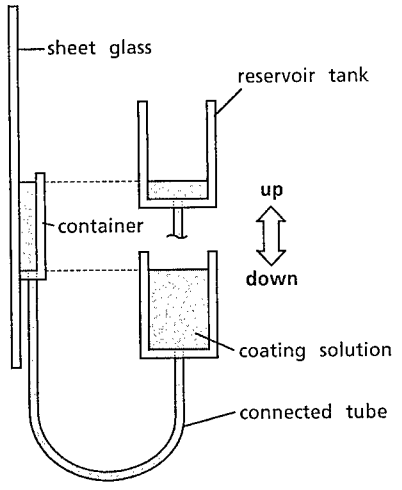

Fig.11 Schematic illustration of newly developed coating process

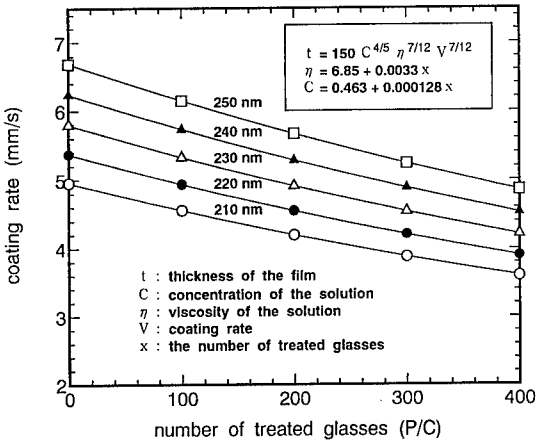

Fig.12 Relation between the treated glasses and coating rates

4.4 Newly developed patterning process

The photograph of windshield with combiner is shown in Fig.13. It can see the gradation area at the periphery of combiner. This gradation area

shall be necessary owing to the legal requirement for distinguish the combiner from patched plastic film on the surface of the windshield. We also have developed new patterning method for gradation shown in Fig.14 schematically. A process of this method is explained as follows :

(1)Originally developed etching paste are screen printed on the unnecessary part of dried gel film.
(2)Gel film and printed paste are heat-treated together.
(3)The paste and unnecessary part of the film can be removed at the same time, because the film under the paste has already attacked and decom posed by the paste.

By this technique, we can make any pattern of sol-gel coating such as any figure, letters and dotted pattern, etc. Some example are shown in Fig. 15. All of these coatings are made by patterned TiO_2 film on glass substrate. Coated film have high reflectivity, high transparency and different color depending on difference of the film thickness.

(4)Finally, a sheet glass being coated and patterned at the restricted area is bent to windshield in the electric furnace at higher temperature over 600 °C. The above glass is laminated with another regular bent glass.

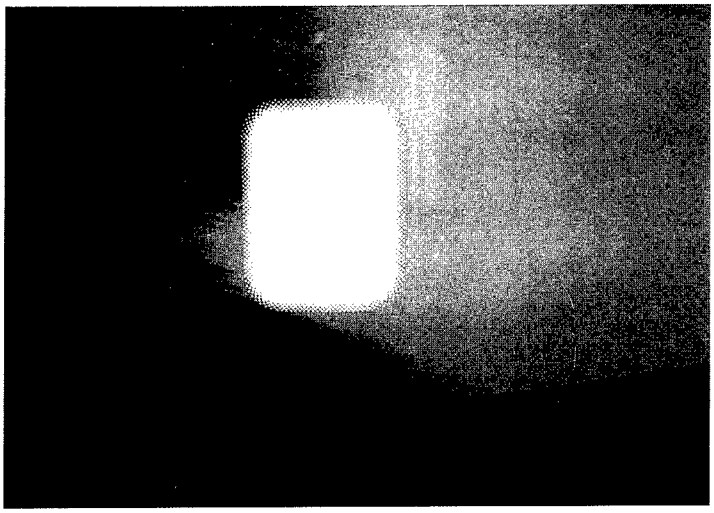

Fig.13 Windshield with the combiner in HUD system

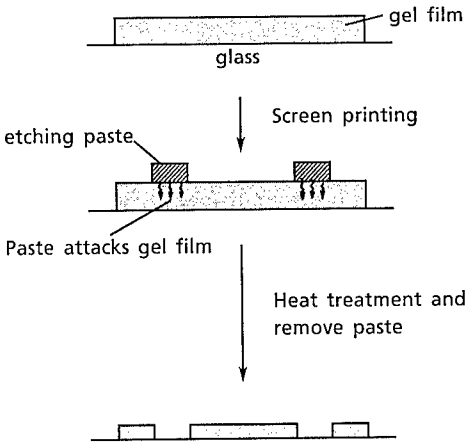

Fig.14 Schematic procedure of the patterning process

Fig.15 Transparent ornaments made by sol-gel method

5. EVALUATION

5.1 Optical properties

We have already know that the peak wavelength and peak reflectance of the combiner at the incident angle of 66 ° made by actual plant is 530nm and 35% or more respectively as seen in Fig.5. For the measurement of the reflectance at the specific incident angle, we use Spectra Multi Photo Detector (MCPD) which has multi photo diode array detector developed by Otsuka Electronics Co. in Japan.

5.2 Durability

The results of typical durability test on the combiner windshield in accordance with standards such as American National Standard in Z26.1 and Japan Industrial Standards RS2311 are shown in Table 1. Chemical and mechanical properties of the combiner film have satisfied all the requirements for the practical use.

Table 1 Results of durability tests

Test items	Procedures	Results
Heat resistance	keep 2 hrs. in boiling water	No change was recognized
Light resistance	irradiate with 750 watts UV lamp for 2 weeks	No change was recognized
Humidity test	keep 2 weeks in high humidity of 50°C/95%RH	No change was recognized
Acid resistance	immerse in 1% H_2SO_4 for 30 min	No change was recognized
Alkali resistance	immerse in 1% NaOH for 24 hrs.	No change was recognized
Gasoline resistance	immerse in regular gasoline for 24 hrs.	No change was recognized
Heat cycle	90°C/4hrs.~-40°C/1.5hrs. for 10 cycles	No change was recognized
Weathering test	Sunshine Weather Meter for 2000 hrs.	No change was recognized
Abrasion test	Taber abrasion test; 100 revolutions on combiner surface	Haze; less than 4%

6. CONCLUSION

HUD combiner for automotive windshield which is a light-selective reflective dielectric thin film has been developed by means of the following techniques:

(1)Optical design of thin film

(2)Preparation of longer storage life metal alkoxide solution

(3)Newly developed sol-gel coating technique

(4)Original patterning process of sol-gel thin film

(5)Appropriate selection of film baking condition

(6)Processing of sheet glass for automotive windshield

It is expected that applications of this type of HUD may be spread to any other windshield besides automobiles such as air craft, train, etc.

ACKNOWLEDGMENTS

We would like to express our appreciation to Professor Sumio Sakka of Institute of Chemical Research of Kyoto University for his useful advice and suggestion to us on sol-gel science.

REFERENCES

1.S.Okabayashi, M.Sakata *et. al.*; "Development of Practical Head-Up Display for production Vehicle Application", SAE International Congress and Exposition 890559 Feb./March(1989)

2.A.Hattori, K.Makita and S.Okabayashi; "Development of HUD Combiner for Automotive Windshield Application", SPIE Current Developments in Optical Engineering and Commercial Optics Congress and Exposition Proceedings, Vol.1168 272-282 Aug.(1989)

3.J.Tsujiuchi; Kougaku Gairon 1, 62-73, Asakura Shoten, Tokyo, 1979

4.N.Ohba *et. al.*; Kougakuteki-sokutei Handbook, 427-438, Asakura Shoten, Tokyo, 1981

5.H.Schröder; "Oxide Layer from Organic Solution", Physics of Thin films, Vol.5, 87-141(1969)

6.Y.Yamamoto, K.Kamiya and S.Sakka; Yogyo-Kyokai-shi, 90, 328-333(1982)

7.K.Makita and S.Yamazaki; The Glass Division of the Ceramic Society of Japan, The 31st Symposium on Glass Proceedings 135-136 Aug./Sep.(1990)

Key Engineering Materials Vol. 150 (1998) pp. 111-120

Optical Disk Substrate Fabricated by the Sol-Gel Method

A. Matsuda[1], Y. Matsuno[1], Y. Mitsuhashi[1], N. Tohge[2] and T. Minami[3]

[1] Tsukuba Research Laboratory, Nippon Sheet Glass Co., Ltd.,
5-4 Tokodai, Tsukuba, Ibaraki 300-26, Japan

[2] Department of Metallurgy, Kinki University,
3-4-1 Kowakae, Higashiosaka, Osaka 577, Japan

[3] Department of Applied Materials Science, Osaka Prefecture University,
1-1 Gakuen-cho, Sakai, Osaka 593, Japan

Keywords: Sol-Gel Method, Coating, Fine-Patterning, Optical Memory Disk

ABSTRACT

Pregrooves for optical memory disks have successfully been fabricated in sol-gel derived SiO_2 films on glass substrates of 130 mm in diameter, using a newly developed fine-patterning process. The patterning is carried out under vacuum by pressing a stamper against the SiO_2 gel film containing poly(ethylene glycol), PEG, and then the gel film is pre-heat treated with being pressed by the stamper. After the gel film becomes hard, the stamper is removed and the glass disk substrate with patterned gel film is finally heat-treated at 350°C to decompose PEG and to be densified. The process time is shortened to the practical fabrication level by optimizing the pre-heat treatment temperature and the amount of PEG added on the basis of the hardening properties of the gel films. The pregroove depth and pitch of the glass disk substrates fabricated show almost constant values at a given radius. The mechanical characteristics of the glass disk substrates satisfy the international standard(ISO/IEC 10089). The noise levels of the fabricated glass disk substrates are also low enough for the practical use. It is noted that the sol-gel pregrooved glass disk substrates have excellent weathering resistance compared with even the conventional glass disk substrates by the photo-polymerizable resin method or by the dry etching method.

Considering the fact that optical disk industry is progressing in many ways, several applications of the sol-gel pregrooved glass disk substrates are proposed. The authors believe that increasing demand of high reliability and large storage capacity for various optical memory disks will require the sol-gel pregrooved glass disk substrates.

1. Introduction

Optical memory disks are high-density and mass storage media with potential of wide application in computer and information systems[1]. Rewritable optical memory disks such as magneto-optical type and phase-change type have been put into practical use and gaining popularity in the systems. In typical rewritable optical memory disks, fine-patterns with a pitch of 1.6μm and a depth of 40 to 100 nm, so called pregrooves, are required at the surface of the substrates. Pregrooves are focused and tracked by the laser beam during the reading and writing operation. Generally polycarbonate substrates are employed for optical memory disks in spite of such drawbacks as gas permeability and water adsorptivity, since pregrooves are fabricated at the surface of the substrates at low cost by the injection molding which is economical process for mass production. Glass substrates are intrinsically superior to plastics for optical memory disks, since they are optically isotropic and highly stable against weathering. A serious problem associated with glass substrates is, however, the difficulty in formation of pregrooves. Pregrooves are conventionally formed by the lithographic techniques consisting of laser beam cutting or contact printing of photoresist, and subsequent etching of the glass substrate[2-5].

These techniques, however, involve complicated processes and need expensive equipment. To overcome these problems, we have developed a new technique to form fine patterns in submicrometer order on glass substrates, based on the sol-gel coating process[6,7] and successfully fabricated pregrooves[8-10] and CD-ROM pit patterns[11] on glass disk substrates by this technique. The key point of the fine-patterning technique developed is the embossing by pressing a stamper against the gel films, the hardness of which is controlled by the incorporation of organic polymers such as poly(ethylene glycol), PEG.

In this paper, the pregrooving process is described from the viewpoint of hardening of gel film and some characteristics of the pregrooved disk substrates obtained are reported. In addition, promising applications of the sol-gel pregrooved optical memory disk are proposed.

2. Experimental Procedure

a) Preparation of Coating Solution

The pure SiO_2 system was chosen in the present study to evaluate the fundamental characteristics of the glass disk substrates pregrooved by the sol-gel fine-patterning process. The coating solution was prepared in the following manner. Silicon tetraethoxide, $Si(OEt)_4$, in ethanol, EtOH, was hydrolyzed with water containing 0.1 wt% HCl at room temperature for 30 min, the molar ratios of EtOH and water to $Si(OEt)_4$ was 5 and 6, respectively. The solution obtained was diluted with EtOH to control the film thickness. PEG, average molecular weight of which was 600, abbreviated as PEG600, was then added to the solution and stirred for 10 min. The clear and homogeneous solution obtained in this way served as the coating solution.

b) Measurement of Gel Film Hardness

A soda-lime-silica glass plate was coated with the PEG-containing solution by the dipping-withdrawing method in an ambient atmosphere for the hardness measurement. The thickness of the gel films was about 800 nm. The hardness of the gel film was measured using a dynamic ultra-microhardness tester (DUH50, Shimadzu).

c) Pregrooving on Glass Disks

Figures 1(a) and (b) show the flow chart and the schematic drawing of the present pregrooving process, respectively. A chemically strengthened glass disk, which was 130 mm in diameter and 1.2 mm in thickness, was coated with the PEG-containing solution in a spinning method in an ambient atmosphere. A polycarbonate, PC, work stamper with pregrooves of 1.6 μm in pitch was pressed against the resultant gel film under the vacuum of about 10^{-3} Pa using a pressing equipment (Fig.2) under the average pressure of 5 MPa. While being pressed by the stamper, the glass disk with the gel film was then heat-treated at various temperatures ranging from 18 to 120℃. After this pre-heat treatment, the stamper was removed and the patterned gel film was heat-treated at 350℃ for 15 min in air using a clean oven to decompose PEG in the gel film and to be densified. The thickness of the pregrooved SiO_2 layer is about 250 nm after the heat-treatment. Through the above processes, the pregrooved glass disk with the negative pattern of the stamper was obtained.

d) Evaluation of Pregrooved Glass Substrates

Uniformity of groove dimensions such as depth and pitch was evaluated for the pregrooved disk substrates using a groove dimension measurement equipment (PGM100, Nikon) in a reflection mode based on a diffraction theory. Physical and mechanical characteristics of pregrooved disk substrates such as dynamic axial runout, radial acceleration, circularity and tilt were measured using a mechanical characteristic test system (LM100, Ono-sokki). Signal characteristics such as head position signals, tracking signals and noise levels were also measured using a conventional optical memory disk tester (LDT3050, EST). The weathering tests for the pregrooved glass disk substrate were carried out using a temperature- and humidity-controlled equipment and changes in mechanical and signal characteristics of the substrates during the test were measured. The weathering tests were also carried out for a glass disk substrate with pregrooved photo-polymerizable(2P) resin layer and a glass disk substrate pregrooved by a dry etching(DE) method for comparison.

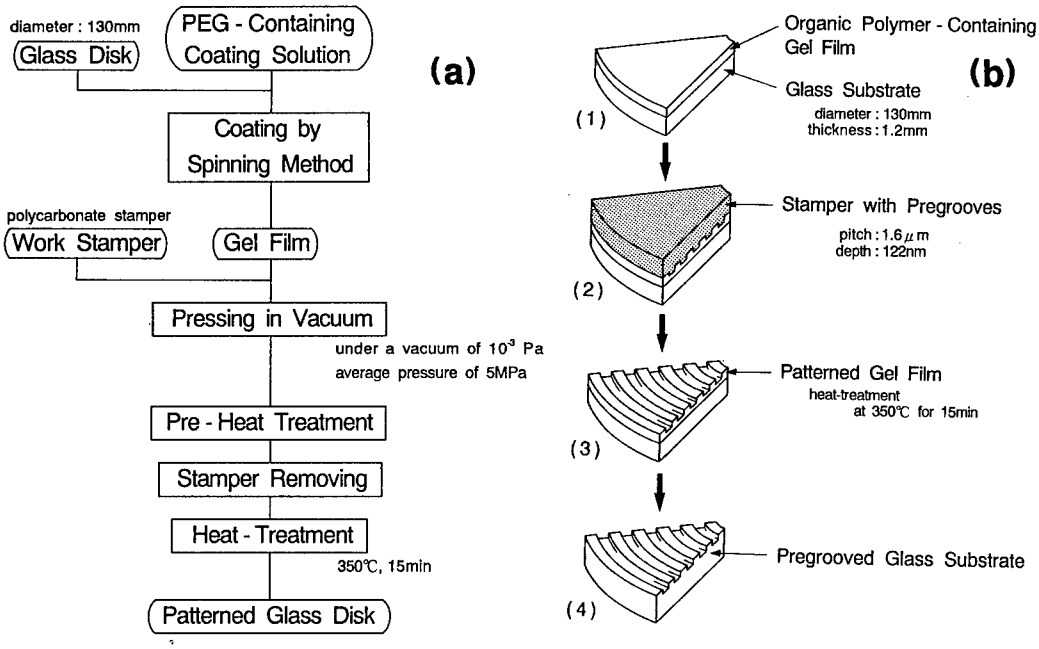

Fig.1. Sol-Gel pregrooving process. (a) is the flow chart and (b) the schematic drawing.

3. Results and Discussion

a) Hardening of Gel Films and Fine-Patterning Process

The feasibility and productivity of the patterning depends on the hardness and hardening rate of the gel films, which are greatly affected by the amount of PEG added and the process temperature. It is, thus, very important to investigate the influences of these factors on hardening of the gel film.

Figure 3 shows the variations in hardness of the gel films containing different amounts of PEG during heat-treatment at 130℃. Open, half-closed and closed circles represent PEG/SiO_2 ratios of 0, 0.5 and 1.0, respectively. PEG added remains in the films at 130℃ because it decomposes over 250℃[6]. The films with the addition of smaller amounts of PEG harden more quickly than those with the addition of larger amount of PEG. At a given heat-treatment time, the hardness of the film containing smaller amounts of PEG is higher than that of the film containing larger amount of PEG.

Figure 4 shows the variations in hardness of the gel films heat-treated at different temperatures as a function of heat-treatment

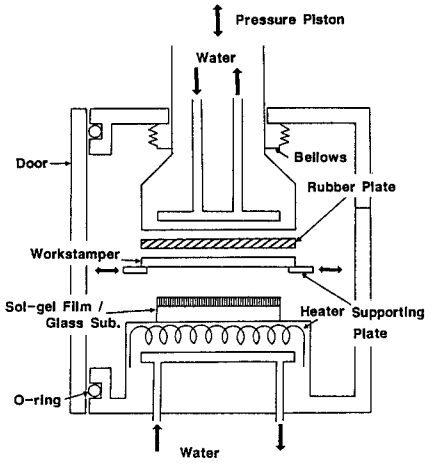

Fig. 2. Pressing equipment used in the present work.

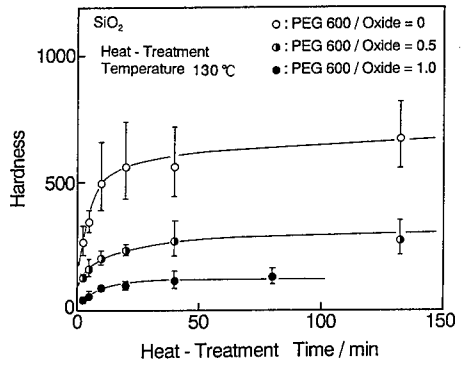

Fig. 3. Variations of hardness of the gel films containing different amounts of PEG as a function of heat-treatment time at 130°C. Open, half-closed and closed circles represent the PEG/SiO_2 weight ratio of 0, 0.5 and 1.0, respectively.

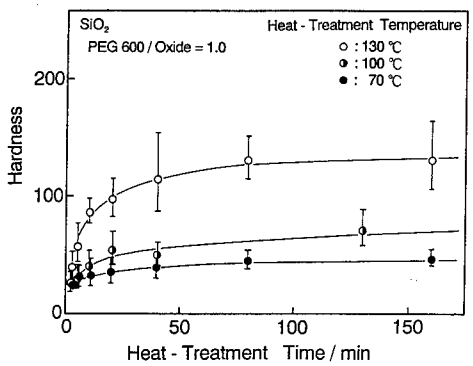

Fig. 4. Variations of hardness of the gel films heat-treated at different temperatures as a function of heat-treatment time. The weight ratio of PEG to SiO_2 was unity. Open, half-closed and closed circles represent the gel films heat-treated at 130, 100 and 70°C, respectively.

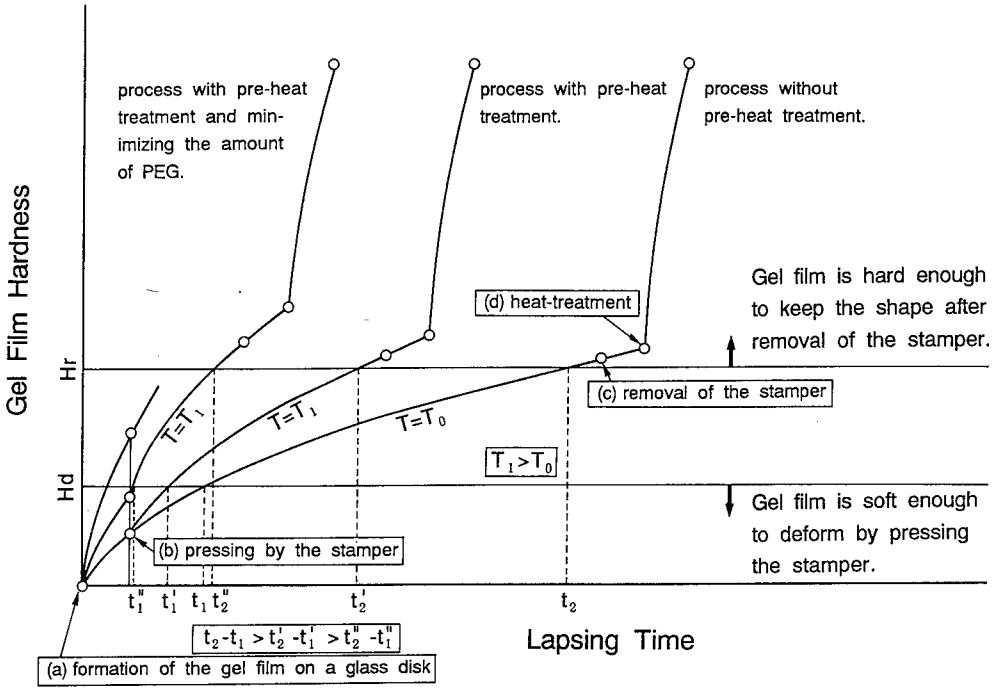

Fig. 5. A model of the fine-patterning process from the viewpoint of gel film hardness. (a) formation of the gel film, (b) pressing by the stamper, (c) removal of the stamper and (d) heat-treatment. H_d and H_r are defined as the maximum hardness to deform by the press and the minimum hardness to keep the shape of the pattern after removal of the stamper, respectively.

time. For all the films the PEG/SiO_2 weight ratio is unity. Open, half-closed and closed circles represent the films heat-treated at 130, 100 and 70°C, respectively. The higher heat-treatment temperature gives the steeper increase in hardness of the gel films.

From the results shown in Figs. 3 and 4, a model of the fine-patterning process is described from the viewpoint of gel film hardness as shown in Fig.5. The process consists of the following steps: (a) formation of the gel films on a glass substrate, (b) pressing a stamper against the gel film, (c) removal of the stamper and (d) heat-treatment to decompose PEG in the film. It is essential in this process to press a stamper against the gel film while it is soft enough to deform by the press and to remove the stamper from the gel film after it becomes hard enough to keep the shape of the patterns formed. The specific values of hardness of the gel film in Fig.5, H_d and H_r, are defined as the maximum hardness to deform by the press and the minimum hardness to keep the shape of the pattern after removal of the stamper, respectively.

In order to apply this process to the industrial fabrication, a shortening of the process time is necessary. Among the above steps (a) through (d), the period from (b) to (c) takes the longest time, since in this period each substrate must be pressed with a stamper individually. The pre-heat treatment during the pressing time is very effective for shortening the process time and it is expected that the process time decreases with an increase in the pre-heat treatment temperature. Moreover, it is obvious that there is a lower limit in the amount of PEG needed to deform the gel film by pressing a stamper and the lower limit of the PEG addition provides the largest hardening rate and hence the shortest pressing time to obtain the accurate patterns at a given pre-heat treatment temperature.

b) Shortening of the Pressing Time

Figure 6 shows the evaluation of glass disk substrates with pregrooves fabricated at various pre-heat treatment temperatures and for various periods. The weight ratio of PEG to SiO_2 is 0.625 which is almost the lower limit to deform the gel films by pressing a stamper, i.e., the optimum weight ratio to shorten the pressing time. Open and closed circles represent the glass disk substrates with accurate patterns and with dull patterns, respectively. As the pre-heat treatment temperature increases, the pressing time needed to obtain the accurate patterns

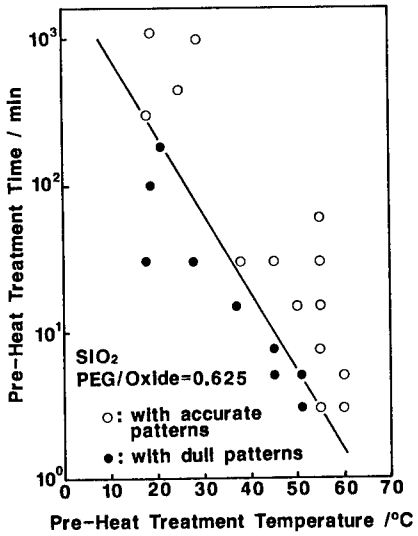

Fig. 6. Evaluation of glass disk substrates with pregrooves fabricated at various pre-heat treatment temperatures and periods. The weight ratio of PEG to SiO_2 is 0.625. Open and closed circles represent the glass disk substrates with accurate patterns and with dull patterns, respectively.

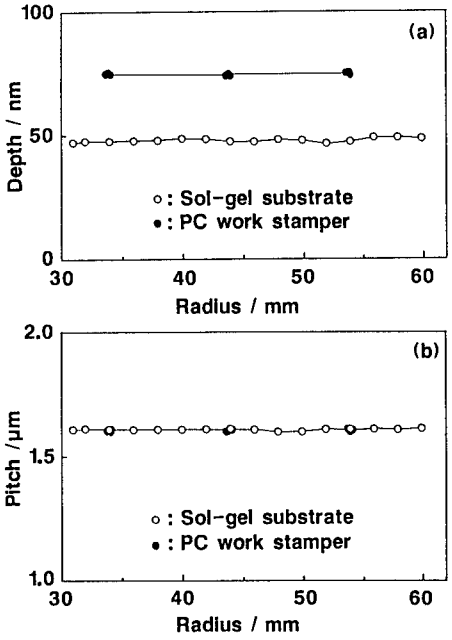

Fig. 7. Radial variation of pregroove dimensions of the sol-gel pregrooved glass disk substrate and the PC work stamper. (a) is for groove depth and (b) for groove pitch. Open and closed circles represent the results of the sol-gel pregrooved glass disk substrate and the PC work stamper.

decreases drastically. This finding proves the expectation mentioned in the previous section (a). A pressing time for 3 min is sufficient at 60°C, while 300 min is needed at room temperature. A pressing time for 3 min is probably short enough to apply this process to the practical industrial fabrication. In addition, the temperature 60°C for pre-heat treatment is low enough to avoid the thermal deterioration of the stamper.

c) Dimensions of Pregrooves Formed

Figures 7(a) and (b) show the radial variation of pregroove dimensions of a glass disk substrate fabricated and a PC work stamper used. (a) is for groove depth and (b) for groove pitch. In each figure, open and closed circles represent the results of the sol-gel pregrooved glass disk substrate and the PC work stamper, respectively. The depth of the fabricated pregrooves is 48 nm, which corresponds to about 64 % of that(75nm) of the PC work stamper. On the other hand, the pitch of the pregrooves fabricated is 1.6 μm, which precisely coincides with that of the stamper. These results indicate that the pregrooved gel film mainly shrinks in the vertical direction to the substrate during the heat-treatment. The groove depth and pitch of the fabricated glass disk substrate show almost constant values at a given radius, which means that the very uniform pregrooves are formed in the whole surface area of the glass disk of 130 mm in diameter.

d) Physical and Mechanical Characteristics

Table 1 summarizes the mechanical characteristics of the sol-gel pregrooved glass disk substrate and the PC work stamper referring to International Standards (ISO/IEC 10089: 130 mm rewritable optical disk cartridges for information interchange, 1991). All the mechanical characteristics of the glass disk substrate fabricated satisfy the requirements as an optical memory disk substrate in International Standards, so that the sol-gel pregrooved glass disk substrates are applicable to the practical fabrication of the optical memory disks.

The dynamic axial runout of the sol-gel pregrooved glass disk substrate is much smaller than that of the PC work stamper. This result can be ascribed to the flatness of the glass disk substrate itself, i.e. the glass disk substrate is much flatter than the PC work stamper. On the other hand, the dynamic radial runout, maximum radial acceleration and the

Table 1. Mechanical characteristics of the sol-gel pregrooved glass disk substrate and the PC work stamper and International Standards (ISO/IEC 10089)

Characteristics	Sol-gel substrate	PC work stamper	ISO/IEC standard
Dynamic axial runout (μm)	6.8	32	<300
Maximum axial acceleration (m/s^2)	2.2	3.5	<20
Dynamic radial runout (μm)	19	27	<50
Maximum radial acceleration (m/s^2)	1.3	1.2	<6.0
Circularity (μm)	3.5	4.1	---
Tilt (mrad)	0.67	1.9	<5.0

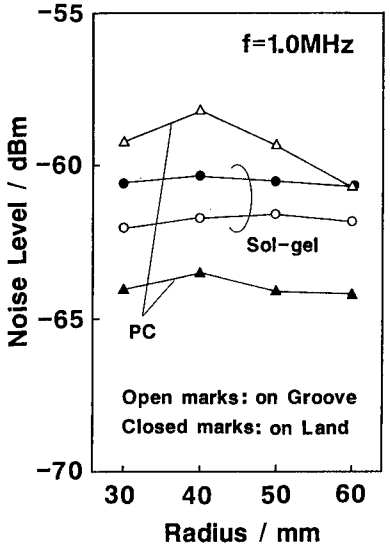

Fig. 8. Radial variation of noise levels for the sol-gel pregrooved glass disk substrate and the PC work stamper in 1.0 MHz at 1800 rpm. Open and closed circles show the noise levels on groove and on land of the sol-gel pregrooved glass disk substrate, respectively. Open and closed triangles show those on groove and on land of the PC work stamper, respectively.

circularity of the pregrooved glass disk substrate are almost equal to those of the PC work stamper. These results indicate that the mechanical characteristics in the radial direction of the PC work stamper can be transferred to the gel film on the glass disk substrate without degradation by the present fine-patterning technique. The tilt of the pregrooved glass disk substrate is again smaller than that of the PC work stamper. The smaller tilt can also be ascribed to the higher flatness and higher rigidity of the glass disk substrate than those of the PC work stamper.

e) Signal Characteristics

Figure 8 shows the radial variation of noise levels for the sol-gel pregrooved glass disk substrate and the PC work stamper in 1.0 MHz at 1800 rpm. Open and closed circles show the noise levels on groove and on land of the pregrooved glass disk substrate, respectively. Open and closed triangles show those on groove and on land of the PC work stamper, respectively. Pregrooves fabricated on glass disk substrates are the negative patterns of the PC work stamper, i.e. the dimensions of groove and land of the pregrooved glass disk substrate correspond to those of land and groove of the PC work stamper. The noise levels of the sol-gel pregrooved glass disk substrate show almost constant values at a given radius, which means that the uniform pregrooves are formed on the whole surface area of the disk of 130 mm in diameter. Both noise levels on groove and on land of the glass disk substrate fabricated are between the noise levels on groove and on land of the PC work stamper for the radius of 30 to 60 mm and those are low enough for the practical use. The difference in noise levels between the sol-gel pregrooved glass disk substrate and the PC work stamper can mainly be ascribed to the differences in groove depth and in refractive index of the grooves.

f) Weathering Resistance

Changes in mechanical and signal characteristics of pregrooved glass disk substrates during the weathering test were measured. Among the characteristics examined, the noise level of the pregrooved glass disk substrates was found to increase in an environment of high temperature and high humidity whereas the other characteristics showed almost no change.

Figure 9 shows changes in noise level of several kinds of pregrooved glass disk substrates during the weathering test. Open circles are for the sol-gel pregrooved disk substrate, open squares for the glass disk substrate with pregrooved photo-polymerizable (2P) resin layer and open triangles for the glass disk substrate pregrooved by the dry etching (DE) method. For all the glass disk substrates, the back side of the substrate was coated with SiO_2 films of 200 nm in thickness as a protective layer for by a sputtering method. The weathering tests were carried out at 85 °C and 90 % R.H. up to 1300 h. The noise levels of the glass disk substrate fabricated by the DE method and the substrate with 2P resin layer increase during the weathering test. The increase in noise level of the substrate with 2P resin layer is smaller than that of the substrate fabricated by the DE method. On the other hand, no change in the noise level is seen during the weathering test for the substrate fabricated by the sol-gel fine-patterning technique .

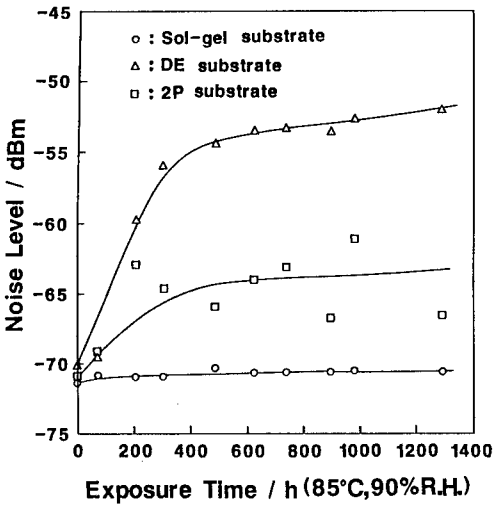

Fig. 9. Changes in noise level of pregrooved glass disk substrates during the weathering test at 85 °C and 90% R.H. Open circles are for the sol-gel pregrooved glass disk substrate, open squares for the glass disk substrate with pregrooved 2P resin layer and open triangles for the glass disk substrate pregrooved by DE method.

The weathering of glass substrates proceeds with the reaction of alkalis in the substrates with carbon dioxide and water in the atmosphere to form salts such as Na_2CO_3[12]. The pregrooved 2P resin layer and the pregrooved sol-gel layer are considered to serve as a protective layer for glass disk substrates. It is noted that the pregrooved sol-gel layer in 250 nm thickness is much more effective than the 2P resin layer in 20-50 μm thickness for the weathering resistance improvement of the glass disk substrates.

g) Applications of Sol-Gel Pregrooved Optical Memory Disks

It is evident from the viewpoints of dimensional, physical, mechanical characteristics and weathering resistance that a glass substrate is superior to a plastic substrate. Among glass substrates, the sol-gel pregrooved glass substrate has the best weathering resistance. In other words, the glass substrate is the most suitable for an optical memory disk which requires long storage life. The main reason for a glass substrate of not to be widely used at the present time is the difficulty to form pregrooves on the substrate. The pregrooving on glass substrate by DE and 2P processes is much more time consuming than the injection molding process applied for a plastic substrate. Thus the cost of DE or 2P glass substrates become much higher than that of plastic substrates. However, it is expected that the sol-gel fine-patterning technique can supply low cost pregrooved glass substrates.

Sol-gel pregrooved optical memory disks can be expected to be applicable, especially to the following fields:

- **300 mm write-once optical memory disks** which require long archival storage life,
- **calibration disks** to calibrate servo-characteristics of drives for interchangeability among many disks and drives, which need stable mechanical characteristics,
- **reference disks** for future international standardization of optical memory disks,
- **rewritable optical memory disks of phase-change type** which need higher writing power and require substrates with a high heat-resistance,
- **rewritable optical memory disks of magneto-optic type as an advanced type** which will use a garnet film, a short wavelength of laser and high temperature initialization process and thus require substrates with a high heat-resistance,
- **smaller optical memory disks**, for example, of diameter less than 2 inch, which might use thinner substrates for volumetric efficiency and thus require rigid glass substrates.

4. Summary

The sol-gel fine-patterning process was described from the viewpoints of hardness and hardening of the gel film. By optimizing the amount of PEG added and applying the pre-heat treatment at 60°C, the pressing time was shortened to 3 min which was probably short enough to apply this process to the practical and industrial fabrication of the pregrooves for optical memory disks. The depth and pitch of the pregrooves fabricated showed almost constant values in the whole surface area of the disk substrate of 130 mm in diameter. The mechanical characteristics of the sol-gel pregrooved glass disk of 130 mm in diameter satisfy the specifications required by the international standard (ISO/IEC 10089: 130 mm rewritable optical disk cartridges for information interchange). The sol-gel pregrooved glass substrate verified the most excellent weathering resistance among the substrates examined.

The sol-gel pregrooved glass disk substrates are useful for 300 mm write-once optical memory disks, calibration disks, reference disks, and rewritable optical memory disks of phase change type and advanced magneto-optic type. The authors believe that increasing demand of high reliability and large storage capacity for various optical memory disks will require the sol-gel pregrooved glass disks.

5. References

[1] V. B. Jipson, *Proc. of SPIE vol. 1499 Optical Data Storage '91,* 2 (1991).
[2] K. Ohta, J. Hirokane, T. Inui, A. Takahashi, T. Deguchi and T. Okamoto, *J. Vacuum Soc. of Jpn.*, **28**, 77 (1985).

[3]. M. Miyagi, A. Iwasa and H. Yamasaki, *Proc. Int. Symp. on Optical Memory, Jpn. J. Appl. Phy.*, **26** Suppl. 26-4, 83 (1987).
[4] K. Ohta, Y. Nagahara, J. Hirokane, K. Van and T. Inui, *Extended Abstracts (The 35th Spring Meeting); The Japan Society of Applied Physics and Related Societies*, No.3 29a-ZQ-2, 869 (1988).
[5] J. Hirokane, Y. Nagahara, K. Van, A. Takahashi, T. Inui and K. Ohta, *Extended Abstracts (The 35th Spring Meeting); The Japan Society of Applied Physics and Related Societies*, No.3 29a-ZQ-3, 869 (1988).
[6] N. Tohge, A. Matsuda, T. Minami, Y. Matsuno, S. Katayama and Y. Ikeda, *J. Non-Cryst. Solids*, **100**, 501 (1988).
[7] N. Tohge, T. Minami, A. Matsuda, Y. Matsuno, S. Katayama and Y. Ikeda, *J. Ceram. Soc. Jpn.*, **96**, 1127 (1988).
[8] Y. Matsuno, A. Matsuda, S. Kataoka, S. Katayama and T. Tsuno, *Proc. 1st Japan International SAMPE Symposium*, 295 (1989).
[9] A. Matsuda, Y. Matsuno, S. Katayama, T. Tsuno, N. Tohge and T. Minami, *Proc. of SPIE vol. 1328 Sol-Gel Optics*, 62 (1990).
[10] Y. Mitsuhashi, A. Matsuda and Y. Matsuno, *Proc. of SPIE vol. 1758 Sol-Gel Optics II*, 105 (1992).
[11] H. Yamaguchi, Y. Tsukamoto, F. Watanabe, A. Sato, M. Saito, H. Honda, M. Murahata, M. Yanagisawa and T. Tsuno, *Proc. of SPIE vol. 1499 Optical Data Storage '91*, 29 (1991).
[12] P. B. Adams, "Glass Corrosion," *J. Non-Cryst. Solids*, **67**, 193 (1984).

Key Engineering Materials Vol. 150 (1998) pp. 121-128

Preparation of Lithium Chloroboracite from Alkoxides

T. Nagase, H. Wada, K. Sakane and T. Kitamura

Shikoku National Industrial Research Institute,
2-3-3 Hananomiya-cho, Takamatsu, Kagawa 761, Japan

Keywords: Lithium Chloroboracite, Preparation, Alkoxide, Lithium Borate

Lithium chloroboracite ($Li_4B_7O_{12}Cl$), known as a lithium-ion conductor, was prepared from lithium methoxide and boron methoxide with hydrochloric acid or ammonium chloride as a chlorine source. The effects of the amount of chlorine source and heating temperature on phases in products were investigated. Pure $Li_4B_7O_{12}Cl$ was obtained at the heating temperature of 923 to 973 K and at the Cl/Li ratio in the sol solution (Rc) of 0.675 with the addition of hydrochloric acid or at Rc of 0.675 to 0.825 with the addition of ammonium chloride. A smaller Rc than the above values resulted in the formation of lithium tetraborate due to a lack of chlorine, caused by the evaporation of chlorine during heating. On the other hand, a larger Rc led to lithium metaborate formation, because of the evaporation of boron during drying. Heating above 1023 K resulted in a partial decomposition of $Li_4B_7O_{12}Cl$ into lithium borates.

There was a difference in reaction sequence between hydrochloric acid and ammonium chloride addition. With hydrochloric acid addition, $Li_4B_7O_{12}Cl$ formed through an intermediate of lithium tetraborate. With ammonium chloride addition, however, lithium tetraborate did not form as an intermediate and $Li_4B_7O_{12}Cl$ formed at a temperature approximately 50 K lower than with hydrochloric acid addition. The reason for this difference was discussed.

1. Introduction

Lithium boracites $Li_4B_7O_{12}X$ (X=halogen) are known as lithium-ion conductors. The representative compound $Li_4B_7O_{12}Cl_{0.68}Br_{0.32}$, which is a solid solution of chloroboracite and bromoboracite, shows a high conductivity of 2×10^{-6} Scm^{-1} at 298 K [1]. This value is comparable with 4×10^{-6} to 5×10^{-6} Scm^{-1} at 298 K of solid solutions of lithium phosphate and lithium silicate (x Li_3PO_4 - (1-x) Li_4SiO_4), which are prominent lithium-ion conductors of the oxyacid salt type [2,3]. Lithium boracites are also stable in air and insoluble in water. Thus the lithium boracites have a potential application to the solid electrolyte of a thin film battery. Such an application needs a film of the lithium boracites. However, the flux or hydrothermal methods give only crystals of a microscopic or millimeter size. It is also difficult to grow a larger crystal from melt or to sinter powder into a body, because lithium boracites decompose at high temperatures.

Synthesis from alkoxides generally has the advantage of easily permitting various forms of

materials. We planned to use this method to synthesize a film of lithium boracites. Lithium chloroboracite ($Li_4B_7O_{12}Cl$) was selected as a representative of lithium boracites. As the first step of its synthesis, we tried to prepare $Li_4B_7O_{12}Cl$ powder from lithium methoxide and boron methoxide with hydrochloric acid (HCl) or ammonium chloride (NH_4Cl) as a chlorine source. This paper describes the effects of the amount of chlorine source and heating temperature on phases in products. The reaction process during heating was also examined with differential thermal analysis - thermogravimetric analysis (DTA-TG) and high-temperature X-ray diffraction analysis (high-temperature XRD).

2. Experimental Method

2.1 Preparation

The whole process for preparing $Li_4B_7O_{12}Cl$ is shown in Fig. 1. Lithium methoxide was prepared by dissolving 1.39 g of metallic lithium (purity>99%) into 200 ml of methanol cooled in an ice bath. Boron methoxide was prepared by Schlesinger's method [4] with a slight modification. Seventy

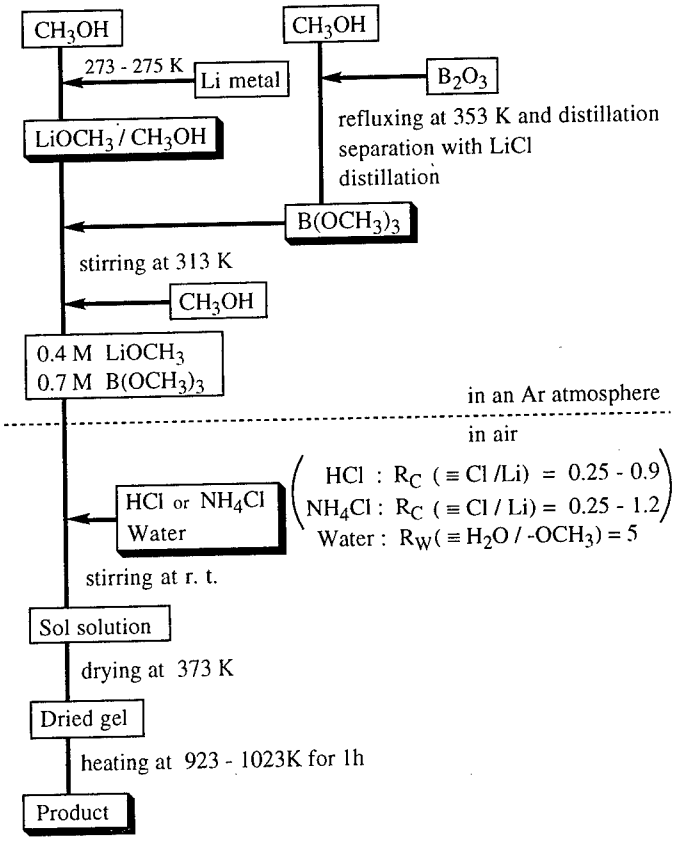

Fig. 1. Flowchart for preparing $Li_4B_7O_{12}Cl$

grams of boron oxide were dissolved into 250 ml of methanol. After refluxing the methanol solution for 6 h, the solution was distilled and the fraction with a boiling point range of 328 to 333 K was collected. Eighteen grams of lithium chloride were dissolved into 150 g of the distillate and then it was settled to allow phase separation. The upper layer was further distilled and the fraction with a boiling point of 340 K (lit., 341 K) was collected. Its boron content was 10.3 wt% and agreed well with the theoretical value of 10.4 wt% for boron methoxide.

The boron methoxide was added slowly to the methanol solution of lithium methoxide at room temperature to adjust the molar ratio of boron to lithium to 7/4, the stoichiometric value for $Li_4B_7O_{12}Cl$. The mixed alkoxide solution was stirred for 1 d at 313 K. All operations up to this step were performed in an argon atmosphere. The resulting solution was diluted to a concentration of 0.4 M lithium methoxide and 0.8 M boron methoxide with methanol. Water and various amounts of HCl or NH_4Cl were then added. The molar ratio of chlorine to lithium in the solution (abbreviated as Rc below) was varied from 0.25 to 0.9 with HCl addition and from 0.25 to 1.2 with NH_4Cl addition. The molar ratio of water to the total methoxide groups in lithium methoxide and boron methoxide was fixed of 5. Stirring the solutions further for 1 d at room temperature gave a clear sol solution. The sol solution was transferred to an oven for drying at 373 K. The dried gel thus obtained was heated at a temperature from 923 to 1023K for 1 h to give products.

2.2 Chemical Analysis and Identification

Lithium, boron and chlorine in the dried gels and the products were determined by atomic absorption spectrometry, ICP emission spectrometry and ion chromatography, respectively. The products were also identified by powder X-ray diffraction analysis (XRD, CuKα). To examine the reaction process during heating, the dried gels were analyzed by DTA-TG with a heating rate of 5 K/min. The samples obtained by preheating the dried gels at 673 K for 1 h were also analyzed by high-temperature XRD at temperature steps of 50 K from 573 to 973 K. The heating rate was 5 K/min and the holding time for each step was 20 min.

3. Results and Discussion

3.1 Effect of amount of chlorine source on phases

Dried gels with various amounts of chlorine source were heated at 973 K for 1 h. The obtained products were identified by XRD. The results showed that $Li_4B_7O_{12}Cl$ formed with by-products depending on the amount of chlorine source (Rc). The by-products, lithium tetraborate ($Li_2B_4O_7$), lithium metaborate ($Li_2B_2O_4$), lithium chloride (LiCl) and a trace of an unknown compound were observed. In Fig. 2 the intensities of the unique peaks of $Li_4B_7O_{12}Cl$, $Li_2B_4O_7$ and $Li_2B_2O_4$ (32.84°, 21.78° and 30.56° in 2θ for CuKα radiation, respectively) are plotted versus Rc in order to estimate the amount of these phases. In the case of HCl addition (Fig. 2A), the main phase at Rc=0.25 was $Li_2B_4O_7$. However, the intensity of $Li_2B_4O_7$ became weaker with increasing Rc and its diffraction peak disappeared at Rc=0.675. In contrast, the diffraction peak of $Li_2B_2O_4$ appeared at Rc=0.75 and its intensity increased with increasing Rc. Thus the main phase at Rc=0.9 was $Li_2B_2O_4$. LiCl and its hydrate were also detected by XRD in the product at Rc=0.9 and the product was deliquescent. These

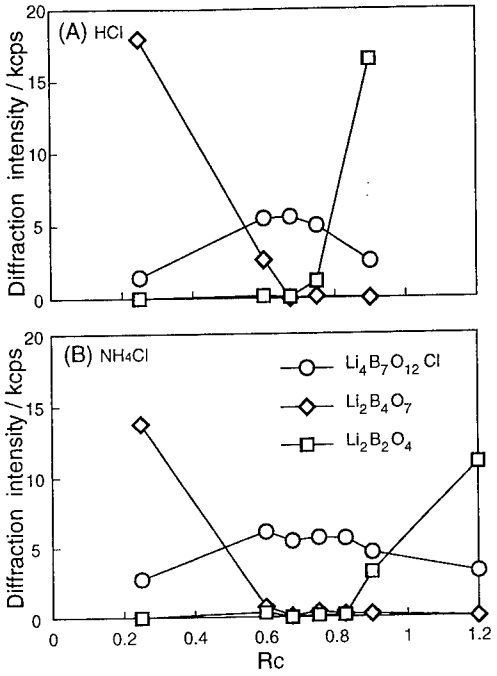

Fig. 2. Changes in diffraction intensities of phases in products with amount of chlorine source : (A) with HCl addition and (B) with NH4Cl addition. The products were obtained by heating at 973 K.

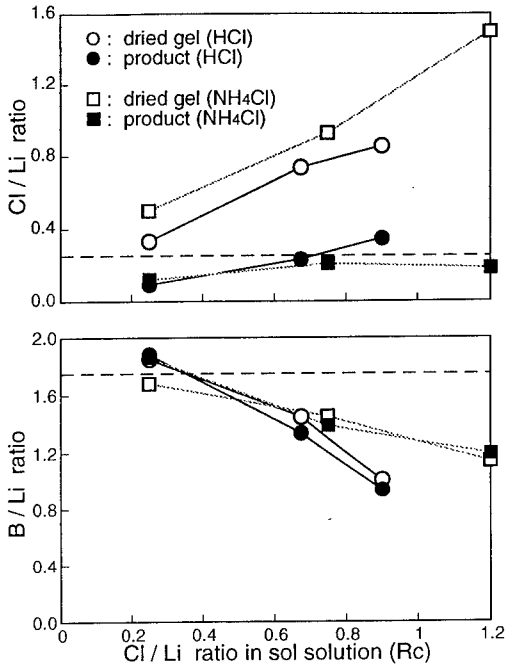

Fig. 3. Changes in elemental composition in dried gels and products with amount of HCl and NH4Cl. The products were obtained by heating at 973 K. The broken lines show the stoichiometric ratios for Li4B7O12Cl.

findings suggest the by-product formation of LiCl at Rc=0.9. At Rc=0.675 neither $Li_2B_4O_7$, $Li_2B_2O_4$ nor LiCl was observed and the intensity of $Li_4B_7O_{12}Cl$ was strongest. In the case of NH_4Cl addition (Fig. 2B), the tendency of the formation of by-products was similar to that with HCl addition. The formation of $Li_4B_7O_{12}Cl$ without by-products was observed at Rc=0.675 to 0.825.

The contents of lithium, boron and chlorine in the dried gels before heating and the products were determined. From the results, the molar ratios of chlorine to lithium (Cl/Li) and boron to lithium (B/Li) are plotted versus Rc in Fig. 3. In the case of HCl addition, the Cl/Li ratios in the dried gels were nearly the same as those in the sol solution (=Rc) irrespective of the Rc value, but those in the products were less than their corresponding Rc's. This result shows that chlorine did not evaporate in drying the sol solution, but did evaporate during heating. In contrast, the the molar ratio of boron to lithium (B/Li) ratios both in the dried gels and in the products were the same. At Rc=0.25, the B/Li ratios both in them were the same as the ratio in the sol solution (7/4=1.75). In other words, the full amount of boron added was remained in the product at Rc=0.25. But at Rc>0.25, the B/Li ratios both in them decreased considerably with increasing Rc. These results show that at Rc>0.25 boron evaporated in drying but not during heating and the amount of boron evaporated increased with increasing Rc. Nearly the same trend in the changes of the molar ratios was observed in the case of NH_4Cl addition, also. However, the amount of the boron evaporated was smaller with NH_4Cl

addition than with HCl addition at Rc≥0.9.

We will first discuss the effect of the amount of chlorine source with HCl addition (Fig. 2A and 3). The Cl/Li ratio corresponding to the stoichiometric value for $Li_4B_7O_{12}Cl$ is 0.25. However, Fig. 2A shows that at Rc=0.25 $Li_2B_4O_7$ formed in preference to $Li_4B_7O_{12}Cl$. Fig. 3 shows that the Cl/Li molar ratio in the product at Rc=0.25 was much less than 0.25. This lack of chlorine will depress the formation of $Li_4B_7O_{12}Cl$. The reason why $Li_2B_4O_7$ formed in preference to other lithium borates is that the B/Li ratio in the product was 1.88 and closest to the ratio for $Li_2B_4O_7$ of 2.

When Rc exceeded 0.675, $Li_2B_2O_4$ and LiCl began to form and the formation of $Li_4B_7O_{12}Cl$ was depressed again (Fig. 2A). Fig. 3 shows that boron evaporated during drying and the B/Li ratio in the product at Rc=0.9 was only 0.93, which was smaller than that for $Li_4B_7O_{12}Cl$ of 1.75 and nearly the same as that for $Li_2B_2O_4$ of 1. This can explain the formation of $Li_2B_2O_4$ and the depression of $Li_4B_7O_{12}Cl$ formation. The depression would result in residual LiCl. The evaporation of chlorine at all Rc's and of boron at high Rc's results in the amount of HCl reaching a proper level at Rc=0.675 to obtain pure $Li_4B_7O_{12}Cl$.

Next, the case of NH_4Cl addition will be discussed (Fig. 2B and 3). The tendency of the formation of by-product and the change of the Cl/Li and B/Li ratios were similar to those in HCl addition. However, the range of Rc required to produce pure $Li_4B_7O_{12}Cl$ was broader than that with HCl addition; from 0.675 to 0.825 with NH_4Cl addition but only 0.675 with HCl addition. Also the amount of $Li_2B_2O_4$ formed at Rc=0.9 is smaller with NH_4Cl addition. These results were caused by the fact that the amount of the boron evaporated was smaller with NH_4Cl addition than with HCl addition. This difference is likely to be due to the depolymerization of polyborate species caused by the lower pH of the sol solution with HCl addition [5]. Actually, the pH of the sol solution at Rc=0.9 was 5.7 with HCl addition and lower than 8.7 with NH_4Cl.

3.2 Effect of heating temperature on phases

The dried gels obtained with HCl addition (Rc=0.675) or with NH_4Cl addition (Rc=0.75) were heated at 923, 973 and 1023 K for 1 h. The obtained products were identified by XRD. The results showed that $Li_4B_7O_{12}Cl$, $Li_2B_4O_7$ and $Li_2B_2O_4$ formed depending on heating temperature. The diffraction intensities of the unique peaks of the above phases are plotted versus the heating temperature in Fig. 4, where the same peaks are

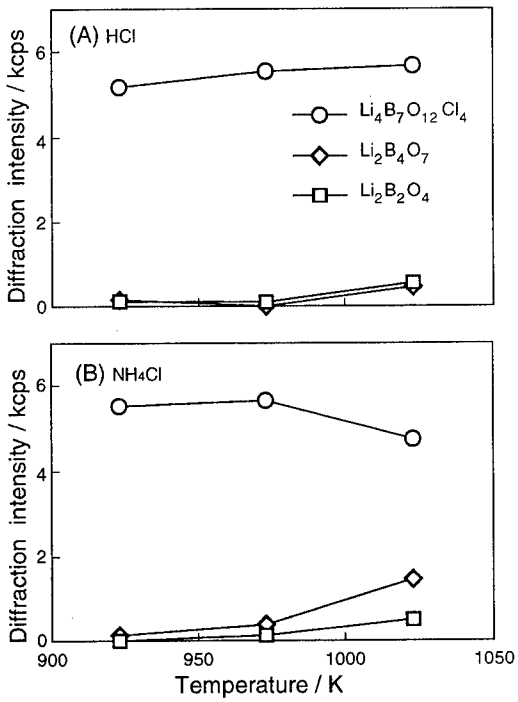

Fig. 4. Changes in diffraction intensities of phases in products with heating temperature : (A) with HCl addition (Rc=0.675) and (B) with NH4Cl addition (Rc=0.75).

used as in Fig. 2. Fig. 4 shows the formation of by-products was negligible at 923 and 973 K both with HCl addition and NH_4Cl addition. With NH_4Cl addition, the intensities of $Li_2B_4O_7$ and $Li_2B_2O_4$ increased from 973 to 1023 K and the intensity of $Li_4B_7O_{12}Cl$ decreased. This shows that a part of $Li_4B_7O_{12}Cl$ already decomposed into $Li_2B_4O_7$ and $Li_2B_2O_4$ at 1023 K. This temperature was lower than DTA-TG results described below. This discrepancy was probably due to differences in heating conditions. With HCl addition, the extent of this decomposition seems to be smaller than with NH_4Cl addition. In any case, the heating temperature of 923 to 973 K was appropriate for obtaining pure $Li_4B_7O_{12}Cl$.

3.3 Reaction process during heating

The two dried gels obtained with HCl (Rc=0.675) or NH_4Cl addition (Rc=0.75) were analyzed by DTA-TG, the results of which are shown in Fig. 5. Both gels showed similar DTA-TG curves except for an endothermic peak at 531 K. The following peaks were easily identified: 370~415 K (endo), evaporation of methanol and water; 883 K (endo), melting of LiCl (lit.,879 K); 1155 K (endo), decomposition of $Li_4B_7O_{12}Cl$(lit., around 1140 K) [1], where the terms of endo and exo in parentheses refer to endothermic and exothermic peak, respectively. In addition to these peaks, some unknown peaks were also observed: 690K (endo), 828 ~ 855 K (exo) in the both cases and 531 K (endo) with NH_4Cl addition only.

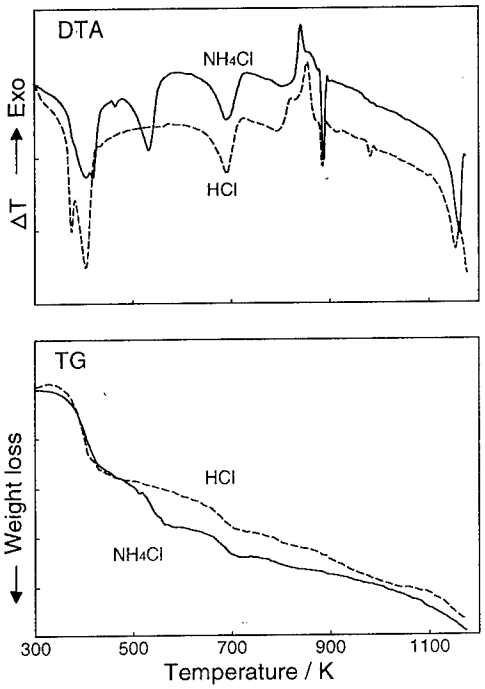

Fig. 5. DTA and TG curves of dried gels obtained with HCl addition (Rc=0.675) or NH4Cl addition (Rc=0.75).

The change of phases during heating was examined by high-temperature XRD. The samples for the high-temperature XRD were obtained by preheating the dried gels at 673 K for 1 h. The result showed that $Li_2B_{10}O_{16}\cdot H_2O$, LiCl, $Li_4B_7O_{12}Cl$ formed in each case while $Li_2B_4O_7$ formed only with HCl addition. The thermal changes in diffraction intensities of the unique peaks of these phases is shown in Fig. 6. The plotted peaks are 26.35° for $Li_2B_{10}O_{16}\cdot H_2O$, 30.09° for LiCl, 32.84° for $Li_4B_7O_{12}Cl$ and 21.78° for $Li_2B_4O_7$. With HCl addition (Fig. 6A), LiCl was already present in the preheated gel. Its diffraction intensity did not change below 773 K, but it began to decrease abruptly above 823 K and the peak finally disappeared at 973 K. The hydrate $Li_2B_{10}O_{16}\cdot H_2O$ was also present in the preheated gel, although it disappeared at 723 K. $Li_2B_4O_7$ began to form at 723 K and its intensity increased with increasing temperature, reaching a maximum at 823 K. It then decreased and the peak finally disappeared at 973 K. $Li_4B_7O_{12}Cl$ began to form at 773 K following the formation of $Li_2B_4O_7$ and the intensity of $Li_4B_7O_{12}Cl$ increased considerably from 773 K to 873 K. At 973 K it

reached a maximum asymptotically without other phases. With NH_4Cl addition, different behaviors were observed (Fig. 6B).$Li_2B_4O_7$ did not form during heating at all. The formation of $Li_4B_7O_{12}Cl$ was observed in the preheated gel and its diffraction intensity increased considerably from 723 to 823 K. These temperatures were about 50 K lower than those with HCl addition.

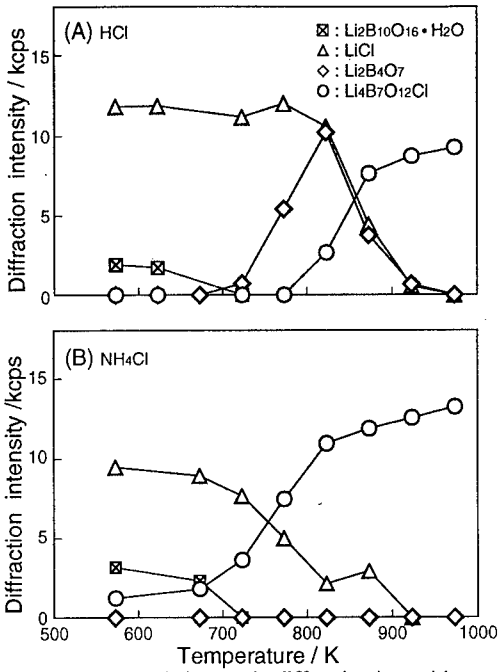

Fig. 6. Thermal changes in diffraction intensities of phases : (A) with HCl addition (Rc=0.675) and (B) with NH4Cl addition (Rc=0.75).

We will first discuss the reaction process during heating with HCl addition with respect to the results of DTA-TG (Fig. 5A) and high-temperature XRD (Fig. 6A). The first thermal event was the evaporation of methanol and water at temperatures of about 370 to 400 K. Then at 690 K an endothermic reaction occurred, which can be identified as the decomposition of the hydrate $Li_2B_{10}O_{16}\cdot H_2O$ from the disappearance of its diffraction peak at 723 K (Fig. 6A). Assuming that the weight loss at this endothermic reaction is due to the evaporation of water in $Li_2B_{10}O_{16}\cdot H_2O$, the weight loss suggests that almost all of the boron was present as the hydrate under 690 K. At the same temperature of 723 K the peak of $Li_2B_4O_7$ appeared (Fig. 6A). This disappearance of the hydrate and the appearance of $Li_2B_4O_7$ at 723 K show that the decomposition of the hydrate caused the formation of $Li_2B_4O_7$. Further, at the temperature of 828 to 855 K, an exothermic reaction occurred. Fig.6A shows that at 823 K the diffraction intensity of $Li_2B_4O_7$ reached a maximum and the peak of $Li_4B_7O_{12}Cl$ appeared. These exothermic reaction could be identified as the formation of $Li_2B_4O_7$ and $Li_4B_7O_{12}Cl$. At a temperature above 823 K the diffraction intensity of $Li_2B_4O_7$ also decreased with that of LiCl. This results suggest that the reaction between LiCl and $Li_2B_4O_7$ caused the formations of $Li_4B_7O_{12}Cl$. A tentative reaction sequence to form $Li_4B_7O_{12}Cl$ would be as follows:

$$Li_2B_{10}O_{16}\cdot H_2O \rightarrow Li_2O\cdot 5B_2O_3(glass) + H_2O \quad \text{(Eq. 1)}$$

$$Li_2O\cdot 5B_2O_3(glass) \rightarrow Li_2B_4O_7 + 3B_2O_3(glass) \quad \text{(Eq. 2)}$$

$$3/2\ Li_2B_4O_7 + LiCl + 1/2\ B_2O_3(glass) \rightarrow Li_4B_7O_{12}Cl \quad \text{(Eq. 3)}$$

With NH_4Cl addition there were differences in the reaction sequence from that with HCl addition. One of differences is the presence of the endothermic reaction at 531 K. This endothermic reaction was identified as the decomposition of NH_4Cl by a spot test of ammonium ion and XRD. This decomposition would lead to the formation of a small amount of $Li_4B_7O_{12}Cl$. Under this 'seeded' circumstance, the decomposition of $Li_2B_{10}O_{16}\cdot H_2O$ probably results in the formation of $Li_4B_7O_{12}Cl$ rather than $Li_2B_4O_7$. This sequence can account for why $Li_4B_7O_{12}Cl$ formed in an appreciable amount

at a temperature approximately 50 K lower with NH_4Cl addition than with HCl, and why $Li_2B_4O_7$ did not form as an intermediate with NH_4Cl addition.

4. Conclusion

The preparation of $Li_4B_7O_{12}Cl$ from lithium methoxide and boron methoxide with HCl or NH_4Cl as a chlorine source was investigated. Particular attention was paid to the effects of the amount of chlorine source and heating temperature on phases in products. The results are summarized as follows:

1) Pure $Li_4B_7O_{12}Cl$ is obtained at the heating temperature of 923 to 973 K and at the Cl/Li ratio in the sol solution (Rc) of 0.675 with HCl addition or 0.675 to 0.825 with NH_4Cl addition.

2) A smaller Rc than the above values results in the formation of $Li_2B_4O_7$ by-product, while a larger Rc leads to $Li_2B_2O_4$ formation.

3)With HCl addition, $Li_4B_7O_{12}Cl$ forms through an intermediate of $Li_2B_4O_7$. With NH_4Cl addition, however, $Li_2B_4O_7$ does not form as an intermediate and $Li_4B_7O_{12}Cl$ forms at a temperature approximately 50 K lower than with HCl addition.

References

[1] W. Jeitschko,T. A. Bither and P. E. Bierstedt, Acta Cryst. B**33**, 2767 (1977).

[2] Y-W. Hu, I. D. Raistrick and R. A. Huggins, J. Electrochem. Soc., **124**, 1240, (1977).

[3] K. Miyauchi, *et al.*, Extended Abs. 161 st Electrochem. Soc. Meet., 1138, (1982).

[4] H. I. Schlesinger, H. C. Brown, D. L. Mayfield and J. R. Gilbreach, J. Am. Chem. Soc., **75**, 213 (1953).

[5] C. J. Brinker, K. J. Ward, K. D. Keefer, E. Holupka and P. J. Bray, 57 in Aerogels (Ed. J. Fricke), Springer-Verlag, Berlin (1986).

Key Engineering Materials Vol. 150 (1998) pp. 129-134

Local Repairing of Lining Glass Layer by the Alumina Powder Composite Sol-Gel Method

R. Ota[1], T. Hara[1], T. Wakasugi[1], J. Fukunaga[1] and A. Miyake[2]

[1] Kyoto Institute of Technology, Matsugasaki, Sakyo-ku, Kyoto 606, Japan

[2] Shinko Pantec Co. Ltd., Murotani 1-1-4, Nishi-ku, Kobe 651-22, Japan

Keywords: Sol-Gel Method, Glass Lining, Alumina Powder, Gelation, Shrinkage, Durability, Na_2O-ZrO_2-SiO_2 Gel

Alumina powder composite sol-gel method has been applied for repairing a damaged part of glass lining. Excellent physico-chemical properties of the composite gel-derived glass were shown. The feasibility of the alumina powder composite gel-glass route was confirmed by the standard tests for airtight, permeation, adhesion strength, thermal shock strength and thermal fatigue strength. The durability against organic solvents was found equivalent to lining glass but the durability against water, acid or alkali aq. solution was less than the lining glass. The composite gel-glass proved to be durable for at least 6 month period. The characteristic feature of the alumina powder composite sol-gel technique includes (a) accelerated gelation in the presence of solid fine particles, (b) very small volume shrinkage of powder composite gel-derived glass during drying or heating and (c) low working temperature for repairing processes at 300 °C.

1. Introduction

Figure 1 shows a glass lined vessel which has suffered a partial damage to the glass lining layer. Repairing the damaged parts may be done by substitutional materials which include organic materials, metals and glasses. Glasses are superior over other substituents in several aspects: non-permeabiltiy, chemical durability, thermal shock strength, and adhesion strength etc. Repairing must be done at relatively low temperature not exceeding 300 °C, because thermal expansion gap between metal substrate and the glass lining layer gives rise to cracks at the repairing part.

In the present study local repairing by sol-gel method was studied and the feasibility of the finished product was tested.

The prerequisites for suitable repairing technique are (a) volume shrinkage as small as possible to suppress crack formation during drying or heating treatment, (b) enough wear resistance, durability against water, acid or alkali solution for at least 6 month period, and enough thermal shock strength, thermal fatigue strength and adhesion strength etc, (c) short gelation time to ensure short repairing time. Hara et al [1] showed that alumina powder composite sol which consists of Na_2O-ZrO_2-SiO_2 sol and alumina powder of 50/50 weight ratio exhibits a very small volume shrinkage on drying and heating. The solid powder composite sol-gel ethod satisfies item (a) of the prerequisites. By adjusting the ZrO_2 content chemical durability against alkali solution can be insured. Item (b) of the prerequisites could be achieved by the solid powder composite sol-gel method which can incorporate potential solid powder such as alumina, titania and yttria etc. Hara et al. [1] observed in conducting the alumina powder composite sol-gel technique that gelation took place much faster than in solid powder-free sol solution. It was suspected that gelation was accelerated by the catalytic work

of the solid surface, probably due to the presence of -OH groups on the solid surface. With respect to item (c) the prerequisites solid powder composite sol-gel method looks very much promising.

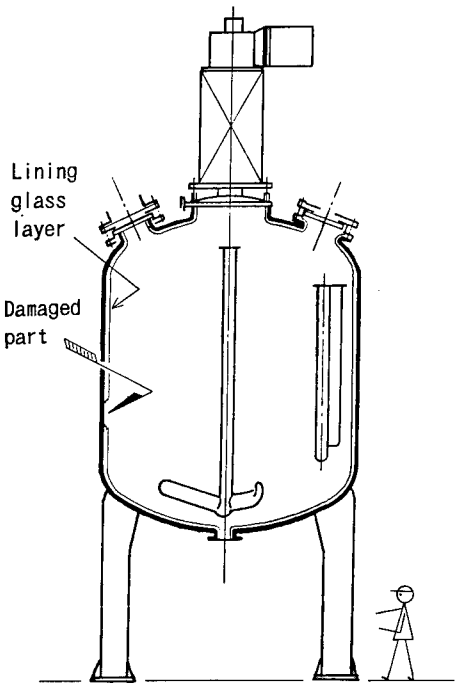

Fig.1 Damaged part of a glass lined vessel

2. Experimental

2.1 Solid powder composite sol-gel method as a repairing technique of damaged part of the glass lining

Application of alumina powder composite sol-gel method as a repairing technique of damaged part of the glass lining was studied (Fig.1). The procedure of repairing a glass lining on the metal substrate (SS400) of 3.2 mm thickness includes (a) preparation of sol solution, (b) mixing of alumina powder with the sol solution, (c) pre-treatment of metal substrate, (d) coating of the composite sol followed by sol impregnation, and (e) drying and heat-treatment of the composite sol and gel.

(a) As starting materials for the gel of composition $7Na_2O$-$6ZrO_2$-$87SiO_2$ (mol%), siliconethoxide ($Si(OC_2H_5)_4$), zirconium n-propoxide ($Zr(O\cdot n\text{-}C_3H_7)_4$) and sodium ethoxide($NaOC_2H_5$) were employed. Ethanol was used as a solvent. Water was not added to the solution to avoid an unnecessarily quick hydration of zirconium propoxide and sodium ethoxide. The weight ratio of alkoxides over alcohols was kept constant at 40:60. The sol solution was kept in a sealed container until it is used within a week.

(b) Reagent grade alumina powder (a-alumina) of particle size of 44-74 mm was used as the solid powder. Cleared in pure water and rinsed in ethanol, the alumina powder was dried for 2 hours at 200 °C. Just prior to the coating operation, 50 g of the sol was mixed with 50 g of alumina powder. The composite sol preparation procedure is shown in Fig.2.

(c) Pre-treatment of the metal substrate was done by applying a specially prepared solution consisting of siliconethoxide, ethanol, water and 85% phosphoric acid.

(d) The metal substrate was coated with powder composite sol solution 0.5 mm Thick at one time using a brush, then powder-free sol was impregnated.
(e) 10 minutes were allowed for gelation and drying at room temperature after each coating of composite sol and sol impregnation and 5 min for heat-treatment by a hot air dryer. The dried composite gel was heated up to 300 °C using the flexible furnace [2] at a rate of 10 °C/min and kept 10 min at 300 °C.

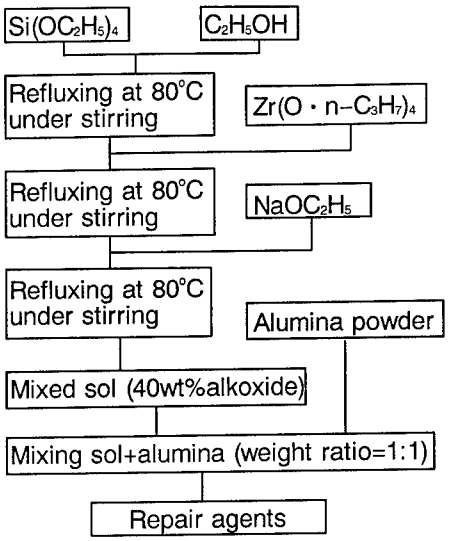

Fig.2 Flow diagram of preparation of an alumina composite sol in the Na_2O-ZrO_2-SiO_2 system.

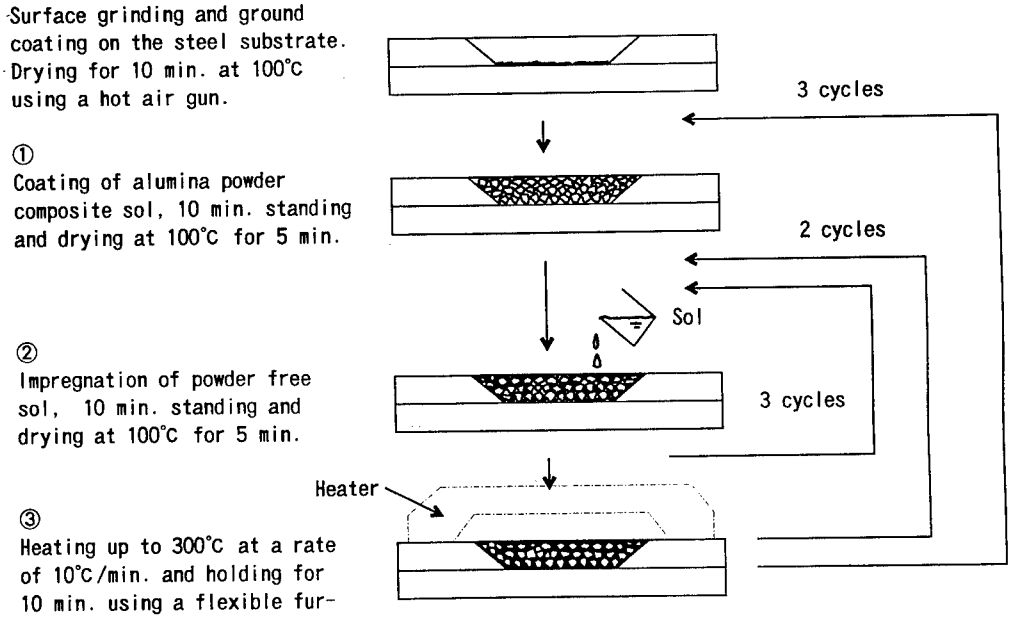

Fig.3 Unit operations for repairing process of lining glass layer by the alumina powder composite sol-gel method.

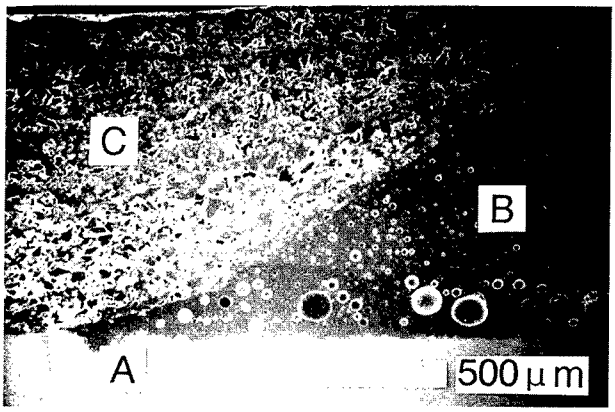

Fig.4 SEM photograph of cross section of repaired part of glass lining (B) with an alumina composite glass layer (C). (A) is the metal substrate.

Figure 4 shows a SEM photograph of the cross section of thus repaired glass lining. (C) indicates the composite glass layer. Numerous small pores of about 20 μm in diameter are observed in the gel glass layer.

2.2. Feasibility tests of repaired glass lining from physico-chemical aspects

The feasibility of physico-chemical properties were evaluated on specimens prepared by the procedures described in 2.1 according to the standardised testing method. The measuring items (a) airtight, (b) permeability, (c) durability against water, acid or alkali aq. solution and organic solvents, (d) thermal fatigue strength, (e) adhesion strength, (f) thermal shock strength.

(a) Air tight test was conducted to detect pass-through pores in the specimen. Electric conductivity was measured between the stainless steel electrode an a 1% phosphorous acid aq. rinsed fiter paper pasted to the gel-glass surface and the metal substrate beneath the gel-glass layer. Evacuation test was also conducted for the air tight test.

(b) Permeability test was conducted by exposing the repaired surface of gel-glass layer deposited on the metal substrate to 0.01 N hydrochloride acid aq. Solution for 6 month or more at 80 °C. The ferro-oxyl method (JIS H8617) was used to detect dissolved ferrous (Fe^{2+}) as well as ferric (Fe^{3+}) ions in the solution.

(c) Chemical durability test was done by measuring the weight loss in water (100 °C), 0.1 N HCl aq. solution (80 °C), 0.1 N NaOH aq. solution (80 °C), toluene (b.p. 110.6 °C, ethanol (b.p. 78.3 °C) and methanol aq. solution (80 °C).

(d) Thermal fatigue strength was evaluated from exfoliation of the gel-glass layer during the cyclic thermal treatment in toluene by warming up to 110.6 °C (b.p. of toluene) and cooling to room temperature every 5 hours.

(e) Adhesion strength of the repaired glass layer was measured by observing an exfoliation to occur when a steel ball of 36.51 mm diameter and 200 g weight was dropped vertically from a 45 cm height onto the gel-glass layer.

(f) Thermal shock strength test was conducted by immersing the specimen from 100 °C environment to ice-water (0 °C) within 2 sec and the damage of the specimens surface was observed with an optical microscopy.

3. Results and discussion

3.1 The feasibility tests for the physico-chemical properties of the repaired composite gel-glass layer

The test results are summarized in Table 1. (a) By airtight test it was found that there are no pass-through pores in the gel-derived glass layer despite the numerous pores visible in the SEM photo (Fig.4) Evacuation test showed that pressure leak after a week was less than 1 Torr under a vacuum of 10 Torr. (b) In the permeability test either ferrous or ferric ions were not detected after 6 month's period. (c) The durability against water-vapor, acid and alkali aq. solution were inferior to that of the glass lining, but the durability against organic solvents were equivalent to those of the glass lining. (d) After 6 months of cyclic fatigue test iron ions were not detected by the ferro-oxyl method. This means that no break off took place at the boundary between the gel-glass layer and the glass lining. (e) Dropping of a steel ball gave no exfoliation on the repaired gel-glass surface as confirmed by observations by naked eyes as well as by an optical microscopy. (f) By repeated thermal shock treatments there were no apparent exfoliation or cracks formed on the gel-glass surface. After all 6 month's usage was assured for the alumina composite gel-glass layer as was shown from the rate of erosion by the water-vapor, acid or alkali solution.

Table 1 The feasibility tests of an aluminum composite gel-glass layer.

Items	Specimens	Procedure and condition	Results
Permeability test	Substrate: SS400 3.2x100x100 mm^3 Thickness of glass layer: 1.5 mm	Detecting of Fe- ion from SS400 soaked in HCl solution of 80 °C, pH = 2	Fe-ion was not detected after 6 month.
Corrosion resistance test	Bulk sample Ø 25.4x1mm^2	Water-vapor (100 °C) 0.1 N HCl solution (80 °C) 0.1 N NaOH solution (80 °C) Toluene (b.p. 110.6 °C) Ethanol (b.p. 78.3 °C) Mixed solution (80 °C) (CH_3OH/H_2O = 3/7, wt)	Average corrosion rate: gel-glass (lining glass) = 0.4 (0.04) = 0.2 (0.008) = 0.6 (0.6) = <0.008 (<0.008) = <0.008 (<0.008) = <0.008 (<0.008) (mg/cm^3·day)
Thermal cycle test	Substrate: SS400 3x100x100 mm^3 Thickness of glass layer: 1.5 mm	Interval corrrosion test of toluene vapor (b.p. 110.6 °C) at intervals of 5 hr.	No exfoliation was observed after half a year.
Adhesion test	Substrate: SS400 6x100x100 mm^3 Thickness of glass layer: 1.5 mm	Dropping a steel ball vertically. Ball weight:~ 200 g Ball size: Ø 36.51 mm (JIS R 4201)	H = 0.45 m; No exfoliation (pass of JIS R 4201)
Thermal shock test	Substrate: SS400 3.2x80x80 mm^3 Thickness of glass layer: 1.5 mm	Quenching of specimens from high temperature oven tinto cold water. (JIS R 4201)	Δ T= 100 °C; No exfoliation (pass of JIS R 4201)

3.2. Accelerated gelation in the powder composite sol-gel technique

Figure 5 illustrates the schematic drawing of the apparatus to estimate the gelation time of the alumina composite sol. An alumina composite sol of alumina/sol weight ratio of 1.4:1 on a polystyrene film was placed on a flat plate with a hole in the centre, through which an edge pushes up the composite sol-gel specimen. The breaking strength of the wet composite sol-gel was measured as a function of standing time Gelation time was estimated to be 5-10 minutes when composite sol is open to air, while 1 hour when composite sol is sealed off from the air in a polystyrene envelope.

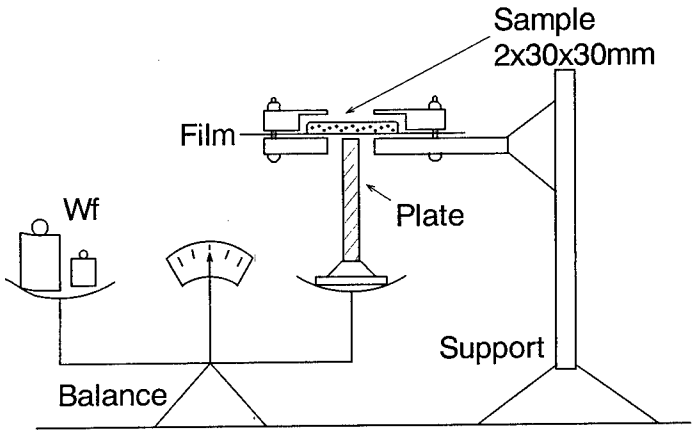

Fig.5 Apparatus for gelation time measurement

Possibla reasons for the accelerated gelation in the alumina composite sols include (a) enlarged surface are as the solvent evaporates from the composite sol solution, prompting the hydration due to the humidity in the air, (b) work of -OH units connected to the solid surface or adsorbed water at the solid surface, (c) change of sol composition which favours prompt gelation due to a possible adsorption of some of the sol components. Among them (b) should be the main reason.

4. Conclusion

The alumina powder composite sol-gel method proved to be an useful technique to repair the damaged part of glass lining, because of ist accelerated gelation, low working temperature and small volume change on drying and heating.

Reference

[1] T. Hara, R. Ota, J. Fukunaga, T. Wakasugi and A. Miyake, Proc. 35th Japan Congress on Materials Res., 83 (1992).

[2] T. Hara, S. Uegaki and K. Wada, U.S. Patent 5,175,414 (1992)

Key Engineering Materials Vol. 150 (1998) pp. 135-140

Flat Ceramic Ultrafiltration Membranes and Modules Coated by the Sol-Gel Technique

K. Pflanz[1], N. Stroh[1] and R. Riedel[2]

[1] Fraunhofer-Gesellschaft IGB, Nobelstrasse 12, D-70569 Stuttgart, Germany

[2] TH Darmstadt, Fachbereich Materialwissenschaften, Hilpertstrasse 31, D-64295 Darmstadt, Germany

Keywords: Inorganic Ultrafiltration, Membrane, Spinel $MgAl_2O_4$, Sol-Gel Technique, Filtration Module Design

1 Objectives

Sol-Gel techniques are common in preparing inorganic ultrafiltration membranes [1-5]. Since applicable membranes should exhibit improved chemical and thermal stability with respect to phase transition, pore size and particle growth, we developed a new method for preparing an inorganic ultrafiltration membrane made of magnesium aluminium spinel, $MgAl_2O_4$. This membrane is supported by a flat ceramic microfilter (α-Al_2O_3) produced via the tape casting process, which offers the opportunity of improved processing techniques and new module concepts compared to the widely used extruded multi channel modules. Membrane characteristics and filtration behaviour will be shown.

2 Experimental Results and Discussion

The membrane preparation procedures have already been reported [6] and will be briefly summarized.

The colloidal sol-gel approach was used to prepare the $MgAl_2O_4$ spinel membranes. As precursor a mixed alkoxide with the general formula $MgAl_2OR_8$ (R = 2-butyl or *i*-propyl) was chosen to obtain the required stoichiometric ratio for spinel formation within the sol particles. Acidic peptization (HNO_3) resulted in a stable sol with a mean particle size of 30 nm in diameter. This opalescent sol was modified with additives to adjust the viscosity for the subsequent slip-casting procedure of the flat porous disc (Kerafil™; Ø: 9 cm, thickness: 1 mm, pore size: 2 µm in Ø). After calcining supported ultrafiltration membranes with controllable pore sizes in the range of 5 nm to 20 nm and a thickness of 2 µm can be obtained. The final pore size is related to the temperature achieved in the calcining program. Up to 600 °C the mean pore diameter is about 7 nm. Calcining at 1200 °C results in pore diameters around 20 nm. Pore sizes were determined by BET (Nitrogen adsorption). With increasing temperature the porosity decreases and the pore size distribution broadens. Therefore the adjustable pore size range to be used in filtration applications is limited.

In Figure 1 the surface of a supported membrane (500 °C) analysed by atomic force microscopy [7] is shown. The globular particle structure and the gaps between can be seen. Due to the needle dimensions the resolution in depth is limited.

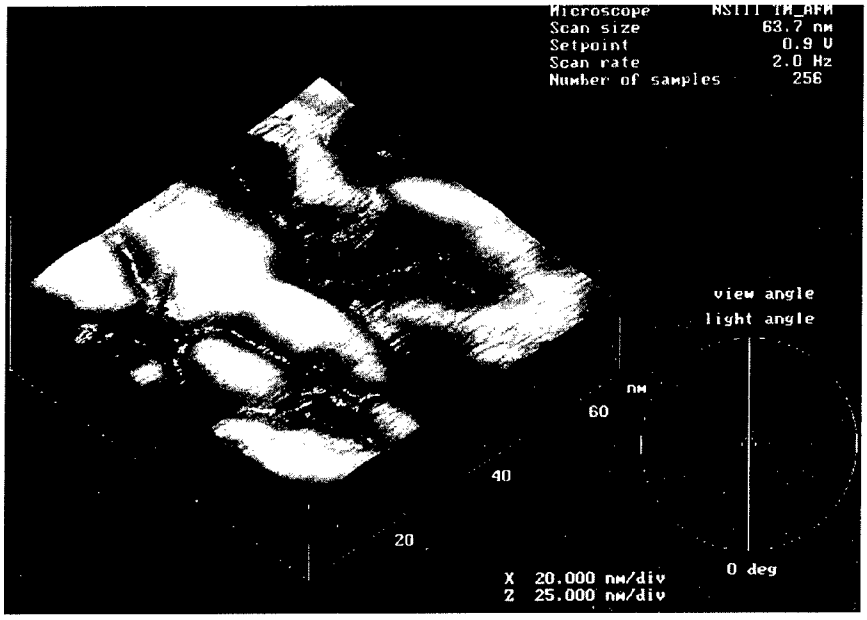

Figure 1: AFM micrograph of the membrane surface.

A corresponding SEM micrograph of the supported membrane is given in Figure 2.

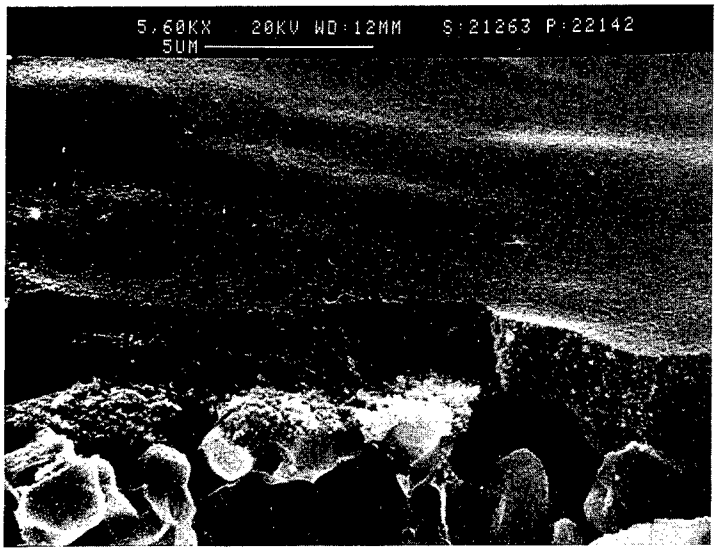

Figure 2: SEM micrograph of the supported membrane.

To ensure membrane quality for separation, filtration experiments were carried out with Dextran standard solutions [8] as well as a fermentation process medium. For the filtration experiments a cross-flow test cell especially designed for the coated flat ceramic Kerafil™ discs was used.

According to the adjusted membrane pore size different Cut-Off values should be expected. The diagram in Figure 3 shows the obtained retention of dextran standards (conc. 0.4 %) versus their molecular weight. The membrane prepared at 700 °C offers smaller Cut-Offs (≈15 kD) compared to the 900 °C membrane (≈25 kD). Corresponding water flux (bidest.) for both membranes resulted in ≈250 l/hm^{2}bar, but decreased to ≈30 l/hm^{2}bar for the filtration of the dextran mixture according to concentration polarisation and fouling effects.
Dextran blue solution (MW 2 000 kD, 0.1 %) shows less fouling and therefore a flux of more than 120 l/hm^{2}bar combined with a retention of 100 %. After treatment with a commercial alkaline cleaning agent (Ultrasil® P 54, 1-2%) the initial water flux can be completely restored.

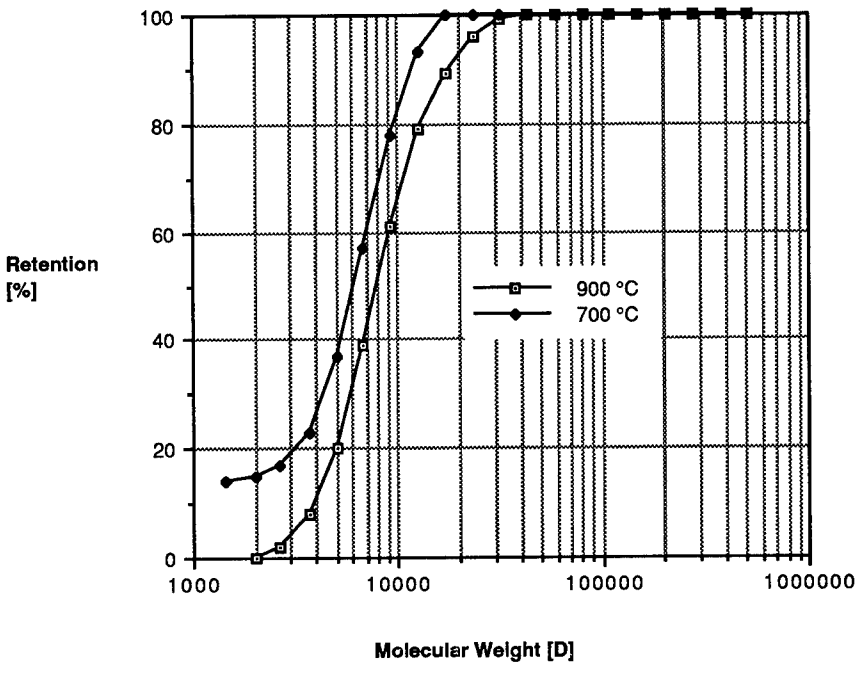

Figure 3: Retention of Dextrane molecules by spinel ultrafiltration membranes (900 °C preparation compared to 700 °C preparation).

But for generalization of the obtained Cut-Off values it has to be taken in account that process conditions (e.g. pH, concentration, cross flow velocity) and properties of the filtration media can

shift the retention quality and therefore for every application problem the appropriate pore size and other filtration parameters have to be determined.

Filtration of a lactobacillus whey fermentation medium (5% dry weight) resulted in a strung flux decline, due to the crude mixture of all kinds of molecules, which leads to a strong fouling tendency. Trans membrane flux decreased from ≈300 l/hm^{2}bar to ≈20 l/hm^{2}bar in about 6 hours. Because of the high contents of calcium hydrogen phosphate acidic and alkaline cleaning is necessary. Subsequent washing procedures with nitric acid (0.5 M) and sodium hypochlorite (2500 mg/l active chlorine, pH ≥ 12), combined with the use of commercial cleaner (Ultrasil P 54) restored the initial flux.
Considering this aggressive medium, even 4 hours rinsing didn't influence the quality of the membrane structure, which could be proofed by filtration test and SEM micrograph comparison before and after the cleaning procedure. The membrane characteristics (e.g. retention, flux) were not influenced and no blocked pores could be detected.

For technical purpose high membrane areas are necessary to obtain sufficient filtration performance. Single flat filter discs do not fit this requirement. Therefore a self supporting module design was developed. It combines two discs separated through an intermediate layer from the same material, which acts as a supporting spacer. All parts can be easily cut from the casted green tape and will bind during the sinter step to an all ceramic filter. The filtrate is collected in the center, where the modules can be stacked easily. This design offers large membrane surfaces in a small housing, which overcomes one main disadvantage of the tubular ceramic filters.

3 Conclusion

Flat ceramic filters coated with spinel ultrafiltration membranes show a sharp Cut-Off combined with a high flux. The membranes are resistant against aggressive cleaners and therefore their initial characteristics can be recovered even after severe fouling. The flat support filter offers new opportunities in module design.

4 References

[1] R. Bhave (Ed.): Inorganic Membranes, van Nostrand & Reinholdt, New York (1991).
[2] Veyre R., Richard S., Pejot F., Grangeon A., Charpin J., Plurien P., Rasneur B., FR Pat. 2550953 B1 (1977).
[3] Anderson M. A., Gieselmann N. J., Xu Q., J. Membr. Sci., **39**, 243 (1988).
[4] Larbot A., Fabre J.P., Guizard C., Cot L., J. Membr. Sci. **39**, 203 (1988).

[5] Leenaars A. F. M., Keizer K., Burggraaf A. J., J. Mat. Sci. **19**, 1077 (1984).

[6] Pflanz K. B., Herstellung und Charakterisierung einer Spinell-Ultrafiltrationsmembran, Fortschrittberichte **5**(323), VDI, Düsseldorf 1993.
Pflanz K. B., Riedel R., Chmiel H., Adv. Mater. **4**(10), 662 (1992).

[7] Picture taken with an AFM Nanoscope III, by LOT, Darmstadt, Germany. Due to the required surface smoothness the membrane was supported by a flat glass substrate.

[8] Schock G., Miquel A., Birkenberger R., International Congress on Membranes and Membrane Processes, Tokyo, 8.-12.6.1987.

Key Engineering Materials Vol. 150 (1998) pp. 141-152

Emerging Applications of Sol-Gel Technology

E.J.A. Pope

MATECH 31304, Via Colinas Ste.102, Westlake Village, CA 91362, USA

Keywords: Coatings, Ultrafilters, Monoliths, Porosity, Microspheres, Flatpanel Color Displays, Diamond-Containing Ceramics

INTRODUCTION

The first documented alkoxide-based gel-formation was obtained by Ebelman in 1846 [1]. Since that time, alkoxide-based gels have been researched and, occasionally, exploited at a relatively lethargic rate up until the post-World War II era. Since the 1940's, both research and commercialization of sol-gel has increased exponentially until the late-1980's. Due, in part, to a substantial investment of public funds, most notably those of the Air Force Office of Scientific Research under the direction of the late Dr. Donald Ulrich, sol-gel processing has matured into a full-fledged discipline, repleat with numerous international conferences, symposia, and workshops. As is often the case, commercialization has lagged behind scientific progress.

In considering both the prospects and the opportunities for the future commercialization of sol-gel technology, several lessons can be gleamed from the activities of the past few decades. Most of the successful applications of sol-gel processing to date are in the areas of thin films and coatings, fibers, and particulate materials, including microspheres. Few, if any, commercial products are now available for monolithic products with dimensions exceeding a few centimeters, at the largest. This is in no small measure due to the continuing difficulty in obtaining high yields of large monoliths without cracking, or without resorting to costly and production-rate limiting procedures, such as the hypercritical drying process.[2]

Despite a disproportionate amount of research dollars having been allocated to these areas, no commercial successes have been achieved in exotic optical applications, such as high-power-laser glasses, non-linear optic materials, gradient-index (grin) glasses, solid-state organic dye lasers, etc. In each of the aforementioned cases, the performance requirements greatly exceed the current "state-of-the-art" capabilities of the sol-gel derived materials.

Most successful commercializations of the sol-gel process to date are either in applications for which the performance requirements are relativily modest, or for which the sol-gel process is "naturally" suited. There are at least three characteristic or "intrinsic" properties of gel-derived materials. First, the sol-gel process favors the formation of materials with small dimensions, such as films, fibers, particles, and small monoliths. Second, most sol-gel products

are initially porous with moderate to large surface areas. Finally, gel-derived materials typically contain high levels of hydroxyl and organic impurities. Applications for which these characteristics are desirable, or at least tolerable, have a much greater likelihood of success than applications for which these characteristics must be overcome. For example, the fabrication of large, dense, hydroxyl-free laser glass or optical fiber preforms both require that all of these "intrinsic" characteristics be surmounted. It should, therefore, come as no surprise that no such products are yet commercially available, despite substantial research on both topics.

In this paper, four examples of products in development are presented which, to a large degree, take advantage of the "inherent" characteristics of the sol-gel process. These are: 1) high temperature ceramic coatings for satellite positioning and apogee thrusters; 2) Porous ceramic ultrafilters for molecular filtration and biomedical applications; 3) Optically-active sol-gel microspheres for flat-screen color display technology, and; 4) Diamond-containing ceramic composites for cutting tools.

HIGH TEMPERATURE CERAMIC COATINGS FOR COMPOSITE SATELLITE THRUSTERS

Satellites used for communications and surveillance typically possess both an apogee thruster and at least several positioning thrusters. The apogee thruster is responsible for moving the satellite from low earth orbit (LEO), where it is delivered by the primary launch systems, to a higher orbit, such as geosynchronous orbit. Apogee thrusters typically deliver a thrust of 100 pounds. Positioning thrusters are responsible for maneuvering the satellite once it attains it's final orbit and for realigning the satellite periodically or upon the instructions of ground control. These much smaller thrusters usually produce a thrust of about five pounds, depending upon the size and mass of the satellite and number of thrusters.

The challenge for materials scientists is to develop new thruster material systems which are both longer-lived, higher performance, and lighter weight. Most thruster materials, such as high temperature metals and alloys, graphite, and carbide ceramics, are susceptable to corrosion, ablation, and oxidation due to the excessively high temperatures and the oxidizing conditions of combustion. Peak combustion temperatures can easily exceed 2000°C. This poses severe limitations on the useful lifetime of conventional thruster materials.

In order to enhance the useful lifetime of non-oxide composite thrusters, high temperature oxide systems have been proposed [3]. The sol-gel process is ideally suited for the impregnation and coating of porous CVI-derived composite thrusters, due to its low temperature processing requirements and ability to coat complex geometries. In figure 1, an yttrium zirconium

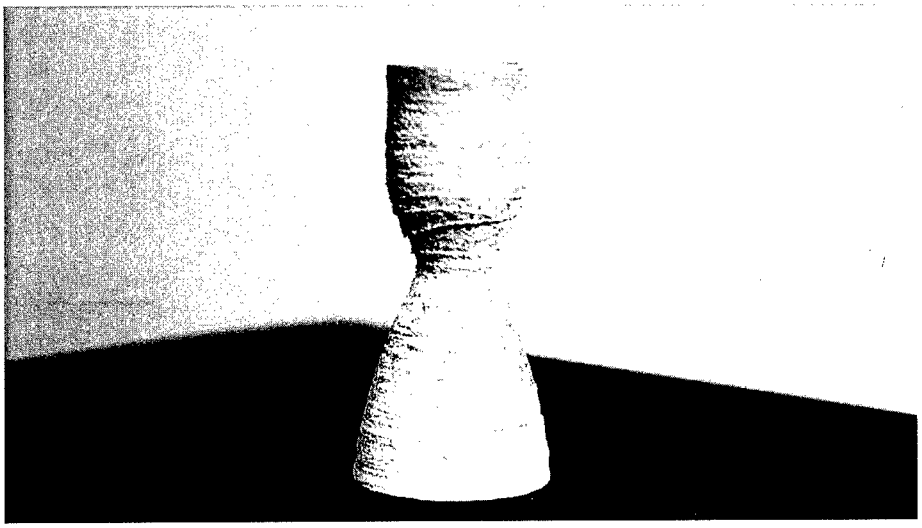

Figure 1: Photograph of sol-gel coated satellite positioning thruster.

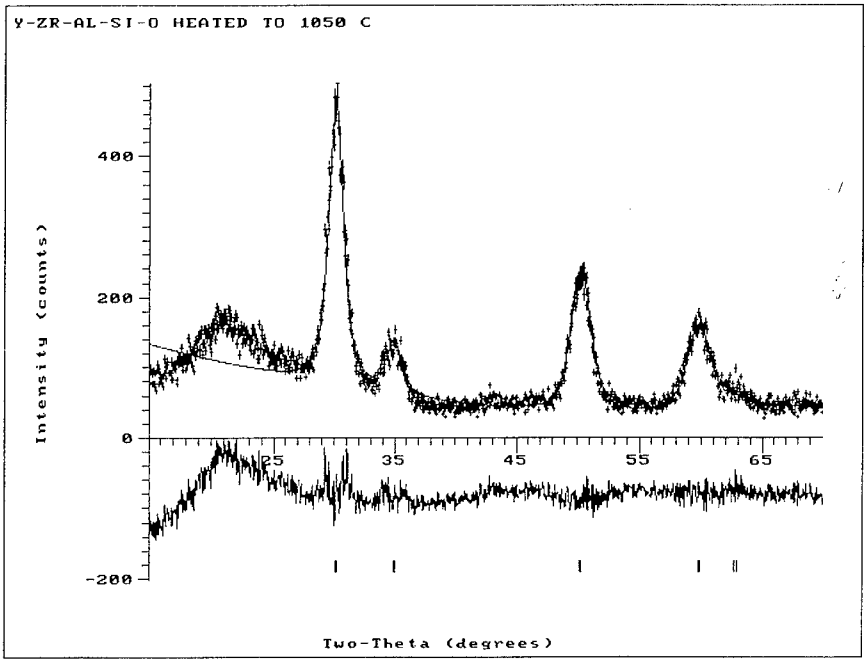

Figure 2: X-ray diffraction pattern of Y-Zr-Al-Si-O gel after heat treatment at 1050°C for 1 hour.

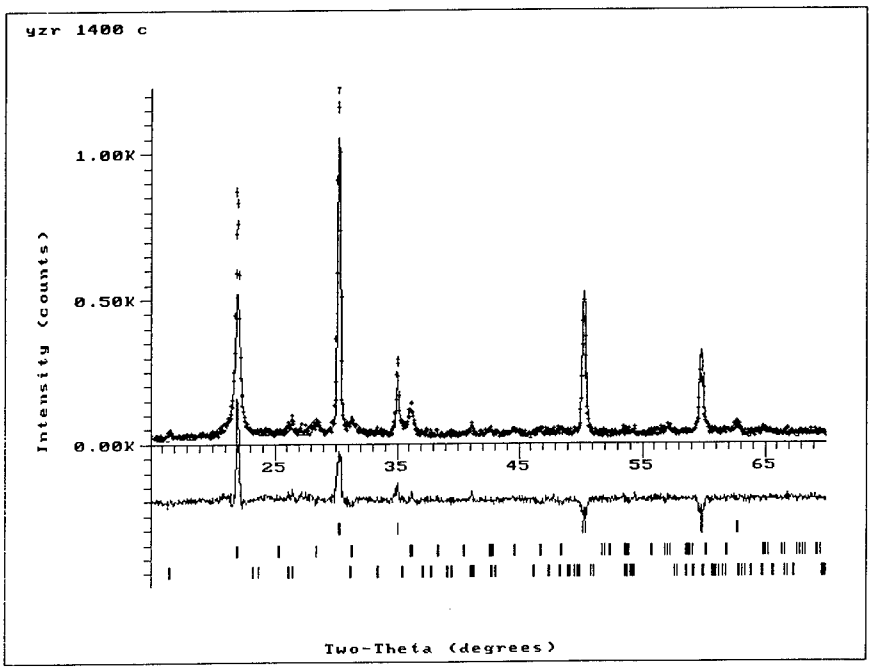

Figure 3: X-ray diffraction pattern of Y-Zr-Al-Si-O gel after heat treatment at 1400°C for 1 hour.

TABLE I: FIVE CLASSES OF POROUS CERAMIC FILTERS

Type I	Continuous monomodal "fine" porosity (1.0-100.0 nm) e.g. porous silica gel.
Type II	Continuous monomodal "coarse" porosity (>0.1 micron) e.g. fritted filter glass.
Type III	Continuous "fine" porosity with isolated "coarse" porosity.
Type IV	Continuous "fine" and "coarse" porosity.
Type V	Multilayer ceramic membrane.

aluminosilicate coated positioning thruster is presented. Using Rietveld analysis, the phase formation of this system has been followed by XRD up to 1400°C [4-6]. When heat treated up to 850°C, for 6 hours, the multicomponent coating appears completely amorphous to X-rays. The first evidence of crystallization appears at 1050°C (see fig. 2), at which temperature only cubic zirconia appears. By Scherer analysis, crystallite size is of the order of 90-100 nanometers. The unit cell dimension was estimated to be 5.123 angstroms. When compared with XRD diffraction reference data, this corresponds to an yttria substitution of roughly 15 percent, giving the nominal composition of $Y_{0.15}$ $Zr_{0.85}$ O_2 [7]. Upon heating to 1400°C, the coating becomes substantially crystallized (see fig. 3). Rietveld analysis yields the nominal composition of 40% stabilized cubic zirconia, 30% cristobalite, 10% mullite, and 20% amorphous phase with crystallite sizes in the range of 1300-1500 A.

Preliminary test-firing of the ceramic oxide coated thruster showed no observable degradation up to 10 hours at 1700°C.

MONOLITHIC ULTRAFILTERS

Typically, ceramic ultrafilters are prepared by depositing a thin layer of nanoporous sol-gel derived oxide on top of a microporous ceramic support [8,9]. These supported membrane filters can be tailored to filter to the nanometer level [9]. Due to their thinness, relatively high flow rates can also be realized. Unfortunately, pinhole defects can destroy the filter's effectiveness.

The notions of creating monolithic ultrafilters is relatively new. Porous gel-derived ceramics are ideal for filtration. Conventional gel monoliths, however, exhibit extremely low fluid flow rates and high pressure drops accross the porous ceramic.

Recently, a new approach to designing gel-derived ceramics has been proposed which substantially improves flow rates without compromising filtration properties [10]. By producing porous ceramics with bimodal pore size distributions, it is possible to attain ultrafiltration with high fluid flow rates. In table I, five classifications of porous ceramic filters are presented. Type III, which contains continous "fine" porosity, below 1000 angstroms, and isolated "course" porosity, exhibits the behavior of a multilayer supported ultrafilter. In fig. 4, type I, type III, and type V porous ceramic structures are schematically presented.

In figure 5, the pore size distribution for a porous type III composite is shown. This composite was used to filter rhodamine--B organic dye from ethanol sol'n (fig 6) and aldolase from aqueous solution (fig 7) [10]. The pore size and porosity of the fine pores can be controlled by varying the initial solution and aging conditions of the gel [11,12]. The course porosity

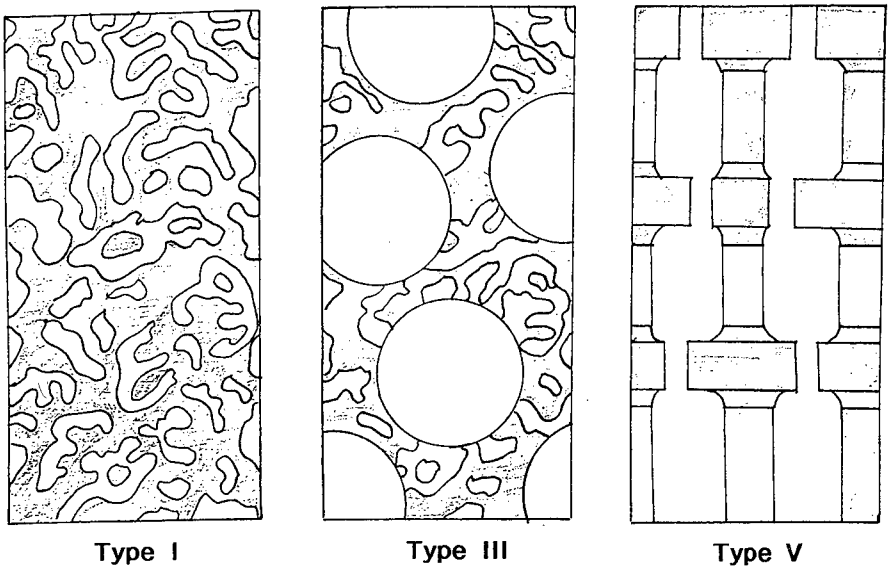

Figure 4: Schematic representation of type I, type III, and type V porous ceramic filters.

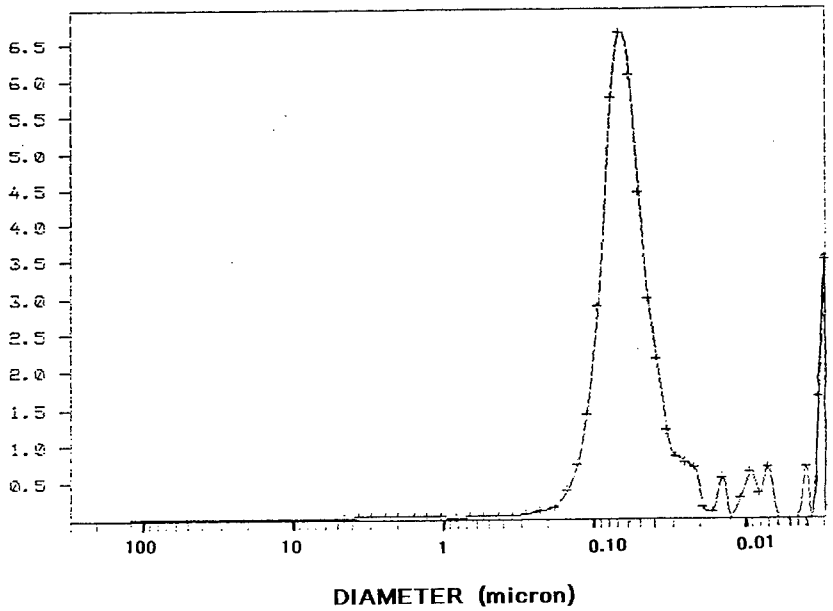

Figure 5: Mercury porosimetry pore size distribution for SiC-SiO_2 composite type III. Peak pore sizes are 3.0 nm and 70.0 nm.

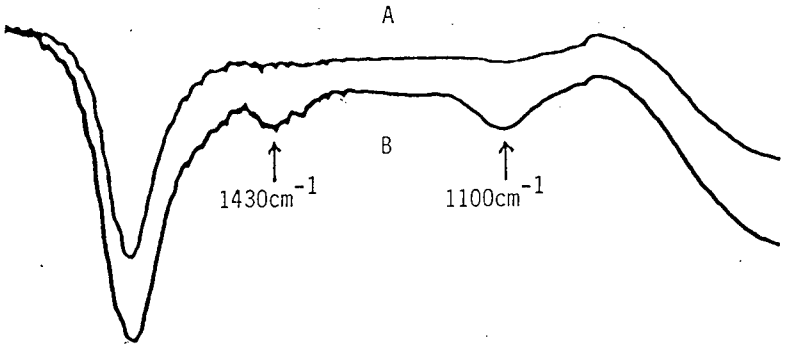

Figure 7: Infrared absorption spectra of the aqueous solution containing aldolase (MW = 142,000) before (B) and after (A) filtration with SiC-SiO_2 ceramic ultrafilter.

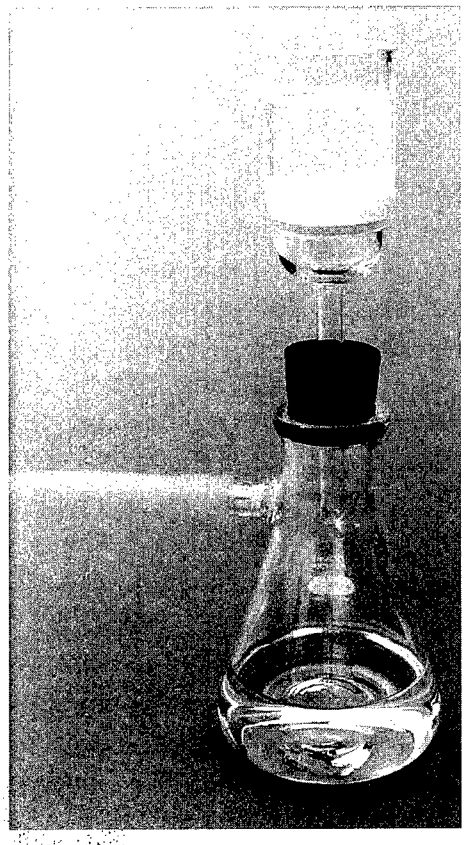

Figure 6: Ultrafiltration of rhodamine-B from ethanol (top reservoir is red, flask at bottom is colorless).

is produced by the addition of organic "filler" materials (e.g. polymer beads, sawdust, carbon black or graphite, paper pulp, etc.) which can be subsequently oxidized, leaving large voids [10].

FLAT-PANEL DISPLAYS

Large, optically-active silica microspheres can be fabricated by the Sol-Gel process [13-15]. Sphere diameters ranging from only a few microns to as large as several millimeters have been made. One potential application of fluorescent dye-doped microspheres is in flat-panel display technology [15,16]. By appropriately arranging microspheres which fluoresce red, blue, and green to align with liquid crystal light valves, a color display can be fabricated [15]. In fig. 8, a large scale prototype is shown back illuminated with ultraviolet light. For a standard format 10" screen with 640 by 480 individual pixels, sphere diameters of approximately 200 microns are required.

Unlike conventional displays, in which light is simply transmitted through colored filters, the newly disclosed technology uses optically-active microspheres as luminescent radiators. The microspheres, can be doped with a wide range of both organic and inorganic species, such as laser dyes or lanthanide elements.

Similar to conventional liquid crystal based displays, this new technology also relies upon a liquid crystal to act as a light valve. The light which reaches the viewer, however, is produced by luminescence of the optically-active microsphere. It is, therefore, not the same light which traveled through the liquid crystal layer.

Typically, conventional flat-panel color displays are composed of liquid crystal (LC) multilayers doped with organic dyes, which act as filters. In this technology, only one LC layer is required, thereby significantly reducing alignment problems during fabrication. Another fundamental difference is that instead of filtering a white background light, the new technology converts the "pump" light, blue or UV, into the desired wavelength, such as red, blue, or green, via luminescence. Given the high luminescence conversion efficiency of today's fluorescent dye molecules, this can lead to a 50 to 100% increase in brightness, depending upon the assumptions used in the calculation. Flat-panel displays produced by this technology will be viewable from wide angles, much like conventional CRT displays. This results from emitted light radiating evenly from the spherical surface of the luminescent pixels across an entire 180 degrees. The emitted light is also de-polarized, thereby eliminating optical interference.

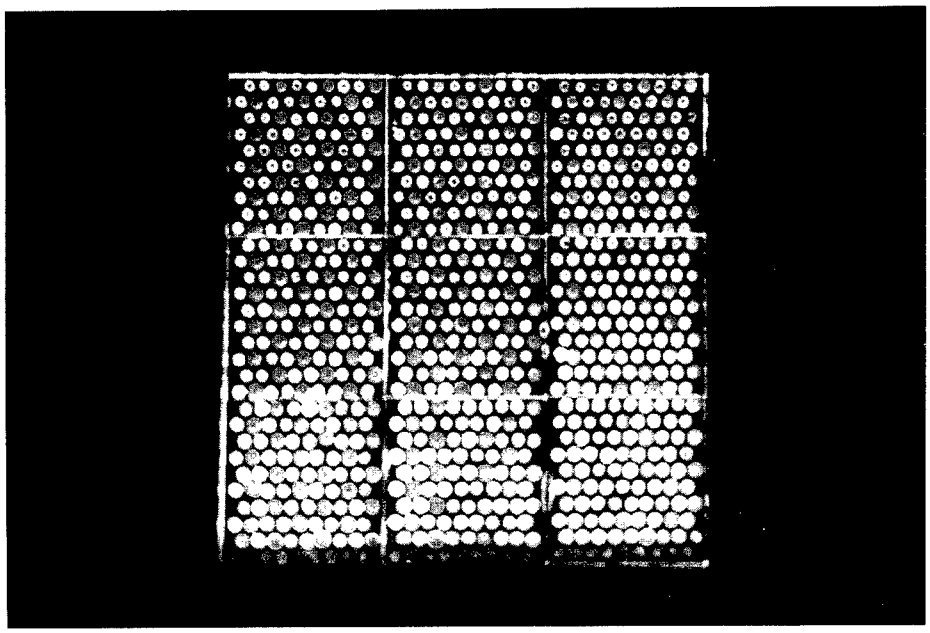

Figure 8: UV back illuminated microsphere color array. Alternating sequences of red, blue, and green fluorescent spheres. A total of 810 individual pixels.

DIAMOND-CERAMIC COMPOSITES

Diamond is the hardest known material [17]. It has been used as a grinding and polishing media for precision optics and ceramic polishing. Making diamond-containing ceramics with high diamond content by conventional ceramic processing techniques is extremely difficult, mainly due to the relatively low processing temperatures required to suppress graphitization of the diamond phase. Recently, the sol-gel route has been successfully demonstrated as a route to synthesizing dense diamond-containing ceramic oxides [18]. For example, a dense sodium silicate glass containing 5 v/o diamond was prepared by mixing sodium methoxide, tetramethoxysilane, methanol, water, Cab-O-Sil "fumed" silica, and 9 micron industrial diamond [18]. After gelation, the samples were dried at 60°C and densified in vacuum at 1100°C. The relative components are 5.0 v/o diamond, 20 v/o Cab-O-Sil, and 75 v/o alkoxide-derived sodium silicate glass. Samples of diamond-containing silica glass with as much as 33 w/o diamond and less than 3.0% porosity have been prepared from HF-catalyzed TEOS sintered in vacuum to 1013°C [18]. Styluses produced from such samples can scratch 99.9% dense aluminum oxide ceramic.

SUMMARY

Four examples have been selected in which the "intrinsic" properties of sol-gel processing have been exploited. The sol--gel process is more readily adapted to products in which at least one dimension is relatively small, such as coatings, fibers, spherical particles, and small monoliths. Thus, the high temperature ceramic coatings and luminescent microspheres both take advantage of these attributes. Because the optically--active microspheres are tailored for use in the visible part of the spectrum, hydroxyl impurities are of negligible importance. Gel-derived materials typically possess large amounts of nanoscale porosity, ideally suited for filtration applications. The low sintering temperatures typical of gel--derived materials has been exploited to produce dense ceramic composites of diamond, which otherwise cannot be processed much beyond 1100°C. These diamond-ceramic composites may be used for cutting and machining tools, in which easily produced small monoliths are suitable.

AKNOWLEDGEMENTS

I would like to thank Dr. Sam Iyengar for helpful discussions and analysis of XRD data, Mr. Ed Johanson for comments and suggestions regarding microspheres, Mr. Alex Almazan for sample preparation, and Mrs. Barbara M. Pope for manusctipt preparation.

REFERENCES

[1] J.J. Ebelman, Ann. 57 (1846) 331

[2] S.S. Kistler, J. Phys. Chem. 36 (1932) 52.

[3] J.R. Strife and J.E. Sheehan, Amer. Ceram. Soc. Bull. 67 [2] (1988) 369; D.P. Stinton, et al. ibid, 350.

[4] H.M. Rietveld, Acta Cryst. 22 (1967) 151.

[5] H.M. Rietveld, J. Appl. Cryst. 2 (1969) 65.

[6] D.L. Bish and J.E. Post,"Modern Powder Diffraction", (Mineralogical Society of America, Washington, DC: 1989) 279-308.

[7] JCPDS-ICDD No. 30-1468. Pfoertsch, McCarthy, JCPDS Grant-in-aid report (1977)

[8] L. Cot, et al, in "Ultrastructure Processing of Advanced Ceramics", ed by J.D. Mackenzie and D.R. Ulrich (Wiley Interscience, New York: 1988) 211.

[9] C. Guizard, et al, in "Chemical Processing of Ceramics", ed by B.I. Lee and E.J.A. Pope (Marcel-Dekker, New York; 1994) in press.

[10] E.J.A. Pope and J.D. Mackenzie, patent pending.

[11] E.J.A. Pope and J.D. Mackenzie, J. Non-Cryst. Sol.,87 (1986) 185.

[12] E.J.A. Pope, et al, U.S. Patent 5,023,208 (June 11, 1991).

[13] E.J.A. Pope, "Sol-Gel Optics II,"ed by J.D. Mackenzie, SPIE Symp. Proc. vol. 1758, (Soc. Photo-optic Instrumentation Engineers, Billingham WA; 1992) p. 360

[14] E.J.A. Pope J. Amer. Ceram. Soc., submitted.

[15] E.J.A. Pope, patent pending.

[16] E.J.A. Pope, J. Sol-Gel Sci. & Tech, in press.

[17] D.W. Richerson, "Modern Ceramic Engineering" (Marcel-Dekker,New York: 1982).

[18] J.D. Mackenzie and E.J.A. Pope, U.S. Patent No. 5,215,942 (June 1, 1993).

Key Engineering Materials Vol. 150 (1998) pp. 153-160

Sol-Gel Optical Fiber Preforms

A. Sarkar, F. Kirkbir and S. Raychaudhuri

YTC America Inc., 550 Via Alondra, Camarillo, CA 93012, USA

Keywords: Fiber Optics, Preforms, Sol-Gel

Abstract:

Attempts to fabricate optical fiber preforms by the sol-gel process have been continuing at different industrial research laboratories for more than a decade with very limited success. This review paper summarizes the requirements of optical fiber preforms, the status of the vapor deposition processes currently used in production, the potential advantages of the sol-gel process and the current status of this field. This paper also addresses the key technical hurdles that need to be overcome for this process to be a commercial success.

Introduction:

Optical fiber preforms are essentially glass rods fabricated by homogeneous chemical vapor deposition processes [1,2,3] developed in the seventies and commercialized in the eighties. Fibers drawn from these preforms are used in optical communication systems for telephony, data transmission, CATV and multitude of other applications.

The technical requirements of optical fiber preforms are numerous. The preform must have a structure consisting of a central core and a concentric outer cladding of a lower refractive index for it to be a waveguide and transmit optical signals [4]. It must have low transmission loss to be able to transmit signals over long distances required particularly for application in telecommunication. The transmission loss in fibers [5] depend on some intrinsic material characteristics of the glass, its Rayleigh scattering coefficient, absorption loss due to extension of the uv absorption band into the

wavelength range of interest and additional absorption loss due to the infrared absorption band edge. Furthermore, commercial fibers exhibit extrinsic losses caused by absorption or scattering of light. Absorption of light is caused by impurities such as transition metal ions and residual hydroxyl ions in the glass. Extrinsic scattering losses are caused by structural defects in the fibers.

In addition to transmission loss, practical fibers have to have i) stringent control of refractive index profiles of the fiber, to minimize distortion of the transmitted signal that limits its bandwidth [6]; ii) control of fiber geometry to minimize splicing and connectorization losses [7] and iii) control of mechanical properties to ensure integrity of the fiber through the cable manufacturing steps, during installation of the cable and its 20 to 30 year specified operating life [8].

Status of vapor deposition processes:

"Optical Fiber Communications" Volume 1, Fiber Fabrication, Academic Press, edited by T. Li covers the fundamentals of the vapor deposition processes. The predominant design is a germania doped silica core, silica clad fiber with Raleigh scattering coefficients less than 1.0 dB/Km.um^4 [9]. Vapor deposited glass fibers have been able to lower the harmful transition metal ion impurities to a level that abosrption losses due to their presence are not detectable. Residual hydroxyl ion content of less than 1 ppb has been reported [10]. The core-clad interface is typically a layer of soot deposited on another. In other words it is a soot-soot interface with very few defects. The standard deviation of fiber diameter is controlled to less

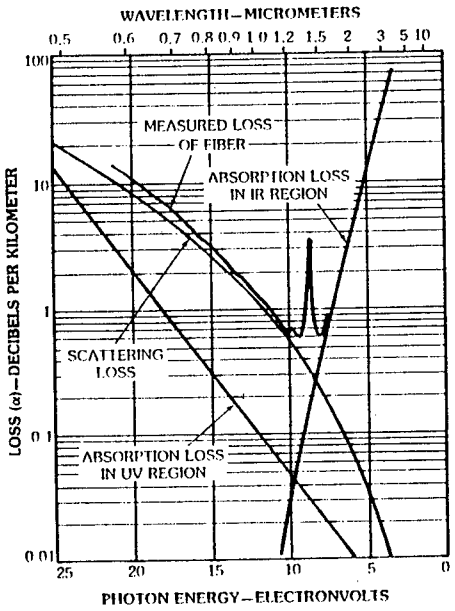

Fig. 1. Spectral loss curve of germania-silica core optical fiber separated into intrinsic loss components [5]

than 0.1 um. Thus as shown in Fig. 1, the excess loss of typical vapor deposited fiber is within 0.03 dB/km of its intrinsic loss limit.

The vapor deposition processes are also very flexible in terms of refractive index profile control and produce a multitude of fiber designs, as shown in Fig. 2. The nominal value of the maximum refractive index difference between the core and the cladding is dictated by stresses generated in preforms due to mismatch of expansion coefficient and glass transition temperature between the core and cladding and is limited to about 2.0% or a numerical aperture of 0.29.

Fibers can be produced to extremely tight geometrical tolerances due to the radially symmetric nature of the vapor deposition processes, permitting automated splicing with losses of less than 0.1 dB/splice [11]. Mechanical properties of the fibers are predominantly a function of the fiber drawing process and are expected to be common for both vapor deposited and sol-gel preforms.

Finally, the cost of vapor deposited preforms has been decreasing rapidly, as the deposition rates increased to greater than 20 gm/min and preform sizes increased to greater than 7 Kg [12]. The price of preforms is now in the range of 1.00 $/gm, which is almost the same as other synthetic fused silica products. The vapor deposition processes can now be considered as established technologies and further cost reductions are expected to follow patterns of mature technologies.

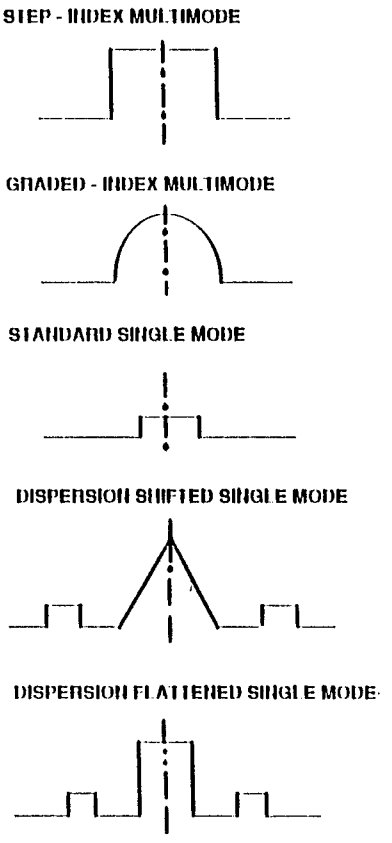

Fig. 2. Typical refractive index profiles of vapor deposited fibers

Potential advantages of sol-gel process:

In addition to the commonly cited merits of the sol-gel process [13], there are some specific potential advantages of sol-gel process for producing optical fiber preforms. The sol-gel process has more compositional flexibility; in other words, many elements such as alkali metal ions which are difficult to introduce into glass by vapor deposition process can be produced by the sol-gel process. Thus in theory, glasses with scattering losses less than that of high silica glasses [14] can be fabricated by the sol-gel process. Similarly, for the same compositional flexibility, it may be possible to produce sol-gel fibers with higher numerical aperture than by vapor deposition processes.

From a manufacturing point of view, in contrast with the vapor deposition processes which have about 50% materials collection efficiency, the sol-gel process converts all of the precursor materials into usable glass. It does not require expensive vapor deposition equipment and eliminates the need for investment in pollution control systems which are required to dispose the effluents of hydrochloric acid and uncollected glass soot produced in the vapor deposition processes. It is therefore postulated that even though the materials cost is higher, sol-gel glass would be significantly cheaper than those produced by the vapor deposition processes [13].

R&D status of sol-gel preforms:

One of the approaches has been to attempt to produce the entire preform by sol-gel process. In this most of the effort to date has been in compositions that are produced by vapor deposition processes. Scherer has reported [15] producing step index multimode germania doped silica core silica clad preforms by a colloidal gel process, with losses slightly above that obtained by vapor deposition process, approximately 4.0 dB/km at 850 nm wavelength of light.

Silica core-fluorine doped silica clad preform has been produced by Shibata et al [16] using the sol-gel process; by producing the rods and tubes separately and collapsing the tube on the rod using a glass lathe. This approach has produced the lowest loss of 1.8 dB/km at 1.6 micron wavelength of light. Also, fibers produced by this approach had the lowest reported hydroxyl ion content of less than 1 ppm; absorption peaks at 1385 nm being around 20 dB/km.

Germania doped silica core rods were prepared by K. Susa et al [17]. In this approach sol was composed of a mixture of metal alkoxide precursors and the gels were dried under atmospheric pressure. The germania silica rod was drawn into a fiber using a rod in tube drawing process, where a specially prepared high purity silica tube with a vapor deposited borosilicate layer was used as the cladding material. The losses were greater than 10 dB/km, primarily due to the very high hydroxyl ion content.

Kirkbir et al [18] produced sol-gel fiber, also using alkoxides of silica and germania to produce the gel, but dried the gels using a supercritical drying process to obtain larger pore size distribution. The expectation was to be able to dry larger size gels and obtain a lower water containing glass by chlorinating the gel more effectively prior to sintering. Fibers were drawn using the rod in tube approach. Bubble free fibers were drawn for fiber numerical aperture up to 0.21. The losses were of the order of 10-12 dB/km at 660 nm, but hydroxyl ion content remained greater than 10 ppm, resulting in high losses at longer wavelengths of light. Tensile tests of the fiber showed mechanical properties of the fiber to be similar to that of vapor deposited fibers.

Sol-gel tubes for optical fiber preforms:

A second research effort in the sol-gel process has been to produce a low water high quality silica tube. The concept has been to use a vapor deposited central rod consisting of the core and part of the cladding to be surrounded by a cheaper sol-gel silica tube to form the preform. Since the outside 95% of fiber material does not function as a transmission media, but primarily acts to improve its rigidity to minimize excess loss caused by external perturbations, it was postulated that this approach should not impact the optical performace of resulting fiber. The best results obtained using this approach has been at AT&T Bell Laboratories [19]. Aqueous colloidal gel tubes of greater than 1 kg have been fabricated and used to overclad vapor deposited rods to form preforms. However, the fibers drawn show losses a little higher than vapor deposited fibers. Most probably it is for the aforementioned reason alone that the process is yet to be commercialized.

To summarize, it is clear that, to date, the sol-gel process has been used to produce compositions that can be produced by vapor

deposition; designs that have the lowest degree of difficulty in refractive index profile control; and have not matched vapor deposition processes in performance or cost.

Hurdles for commercialization of sol-gel preforms:

High loss glass fibers offer system designers no benefit similar to plastic fibers, that remain flexible at relatively large diameters and can be connected to low cost electro-optical components. Furthermore, preform cost is of the order of 5% of a typical installed fiber optic communication link. Thus, even if sol-gel preforms are marginally cheaper, it is unlikely that these preforms will be commercialized unless there is some performance benefit.

To match performance of vapor deposition fibers, the sol-gel process must produce preforms with hydroxyl ion content of <30 ppb. In addition, this must be done in a processing approach that will produce preforms with defect free core clad interface. If the above can be done in a cost effective way, sol-gel process will have just matched vapor deposition process in cost and performance. For successful commercialization, sol-gel fiber must either have lower loss due to use of a lower scattering glass composition or have a higher numerical aperture. At this time, it is believed unlikely that sol-gel process will ever be commercialized for optical fiber preform manufacturing. Consequently the number of institutions involved in this field has been shrinking.

References:

[1] A. J. Morrow, A. Sarkar, P. C. Schultz, Optical Fiber Transmission, Vol. 1, ed. T. Li, Academic Press, 65-95 (1985)
[2] J. B. MacChesney, J. B. O'Connor, H. M. Pressby, Proc. IEEE 62, 1278-1279 (1974)
[3] T. Izawa, S. Kobayashi, S. Sudo, F. Hanawa, Integr. Opt. Opt. Fiber Commun. Tech. Dig. Cl-1, 375-378 (1977)
[4] C. K. Kao, G. A. Hockman, Proc. IEEE, Vol. 133, 1151 (1966)
[5] H. Osanai, T. Shioda, T. Moriyama, S. Araki, M. Horiguchi, I. Izawa, H. Takata, Electron. Lett. 12, 549-550 (1976)
[6] K. Okamoto, T. Okoshi, IEEE Trans. Microwave Theory Tech. Vol. MTT-24, 213-221 (1977)
[7] A. Sarkar, Optical-Fiber Trnasmission, ed. E. E. Basch, Howard W. Sams & Co., 65-91 (1986)

[8] F. V. DiMarcello, C. R. Kurkjian, J. C. Williams, Optical Fiber Transmission, Vol. 1, ed. T. Li, Academic Press, 179-248 (1985)
[9] M. Oshashi, K. Shiraki and K. Tajima, J. Lightwave Tech., Vol. 10, 539-543 (1992)
[10] F. Hanawa, S. Sudo, M. Kawachi and M. Nakahara, Electron. Lett. 16, 699-700 (1980)
[11] T. Tanifuji and Y. Kato, Opt. Fiber Commun. Tech. Dig. MG3, 14-15 (1983)
[12] M. Ito, M. Takagi, T. Danzuka, H. Yokota and M. Watanabe, European Conf. Opt. Commun. Conf. Pub. No. 292- Part 1, 453-456 (1988)
[13] J. D. Mackenzie, Ultrastructure Processing of Glasses, Ceramics, and composites, eds. L. L. Hench and D. R. Uhlrich, Wiley, 15 (1984)
[14] D. A. Pinnow, L. G. V. Uitert, T. C. Rich, F. W. Ostermayer and W. H. Grodkiewicz, Mat. Res. Bull. 10, 133 (1975)
[15] G. W. Scherer, Us Patent 4574063 (1986)
[16] S. Shibata, K. Takeshi and M. Horiguchi, J. Non-Cryst. Solids 100, 269-273 (1988)
[17] K. Susa, I. Matsuyama and S. Satoh, J. Non-Cryst. Solids 128, 118-125 (1991)
[18] F. Kirkbir and S. Ray Chaudhuri, SPIE, Vol. 1758, 160-172 (1992)
[19] J. B. MacChesney, SPIE, Vol. 988, 131-134 (1988)

Key Engineering Materials Vol. 150 (1998) pp. 161-170

Production of Dispersible Aluminas and their Use in Different Applications

J. Schimanski

CONDEA Chemie GmbH, Überseering 40, D-22297 Hamburg, Germany

Keywords: Alumina Production, Alumina Hydrate, Boehmite, Colloidal Alumina, Dispersible Alumina, Alumina Sol, Liquid Alumina System, Ziegler ALFOL-Process, Colloidal Coating, Mixed Oxide Synthesis, Inorganic Binder

KEYWORDS

alumina production, alumina hydrate, boehmite, colloidal alumina, dispersible alumina, alumina sol, liquid alumina system, Ziegler ALFOL-process, colloidal coating, mixed oxide synthesis, inorganic binder.

ABSTRACT

Since 1964, alkoxide-derived hydrated aluminas have been commercially available. These alumina hydrates are recovered in the form of boehmite-type powders (AlO(OH)) with a defined grade of crystallinity. In the presence of diluted aqueous monovalent acids, boehmite forms colloidal alumina particles (sols). The particle sizes of the dispersed alumina hydrates can be adjusted in the nanometer range from below 30 to 500 nm. Some properties of these liquid alumina systems (sols), e.g. translucency, charge or particle diameter, are determined by the crystallinity of the starting boehmite alumina powder. Application examples are given to show that such materials are already used commercially for colloidal sol-gel processes and meet with increasing interest for other applications.

INTRODUCTION

In nature, aluminas occur abundantly mainly in the form of impure hydroxides that are main constituents of bauxites and other minerals. In addition, a smaller alumina quantity appears in the form of crystals in the mineral corundum, as ruby and sapphire, and as emerald.

Industrially, the access to alumina hydroxides of higher purity than that occuring in nature was established by the Bayer process [1]. Here, bauxite ore is dissolved in aqueous NaOH and, after addition of e.g. acid, alumina hydrate crystallizes in the form of gibbsite ($Al(OH)_3$). Traditionally, the main quantity (>95 %) of the world's alumina consumption is derived by that process. All aluminium metal is made from Al_2O_3 that is calcined from ($Al(OH)_3$) [1].

In 1964, CONDEA Chemie started a process for the production of fatty alcohols and high-purity alumina hydrates. This production process is based on the hydrolysis of aluminium-organic precursors characteristically derived from the Ziegler ALFOL-process [2]. The resulting alumina hydrate crystallizes in the form of microcrystalline boehmite (AlO(OH)). Boehmite-type aluminas, in addition to their elevated chemical purity, have some interesting physical properties compared to standard aluminas. The commercially available quantity of this grade (sol-gel alumina) now is 55,000 mt. That is approx. 0.15 % of the world's synthetic alumina production.

ALUMINA PRODUCTION FROM AL-ALKOXIDES AT CONDEA CHEMIE

In the 1950s, the development of the low-pressure polymerisation process for the production of polyethylene was patented by the German Nobel Prize winner Prof. Karl Ziegler. The process was based on aluminium-organic intermediates. In conjunction with this research work, Prof. Dr. Ziegler and his coworkers also used aluminium-organic intermediates for the synthesis of straight-chain linear alcohols [2].

Fig. 1: Ziegler ALFOL and ALUMINA Process

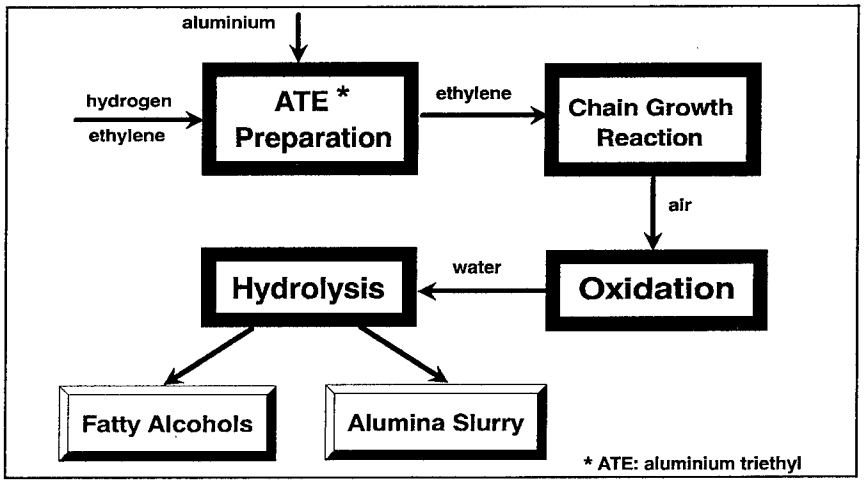

The flow chart for the Ziegler ALFOL-process (see Fig. 1) shows that, in a four-step synthesis, the process leads to synthetic straight-chain fatty alcohols and alumina hydrates. Starting from aluminium metal, ethylene and hydrogen as base materials, aluminium triethyl (ATE) is formed. Upon addition of ethylene to ATE, long-chained aluminium alkyls build up (oligomerisation). The effluent is oxidized with air to form Al-alkoxides. After hydrolizing the Al-alkoxides with water, the straight-chain linear fatty alcohols are recovered from the upper organic phase. The lower aqueous phase consists of high-purity alumina slurry. Following hydrolysis, the alumina slurry is dried. Depending on the application in which the alumina will be used, various drying techniques (e.g. spray drying) are applied.

The X-ray diffraction pattern of the resulting alumina powders shows bands similar to pseudo-boehmite and/or boehmite. Boehmite is a well-defined crystalline inorganic structure, where - in the direction of the a-axis - two (O-Al-OH)-chains are arranged in antiparallel double layers to form a kind of inorganic polymer molecule (see Fig.2). Sometimes it happens that the packing of the double layers is affected by excess water molecules. These structural fragments are called pseudo-boehmite structures [3].

It can be easily deduced from the flow chart and the product balance that the Ziegler ALFOL-process was not designed to produce aluminas. Historically, it is most interesting that these 'exotic' high-purity aluminas entered literature as a 'by-product' of linear alcohol production [4].

Fig. 2: Boehmite and Pseudo-Boehmite Structures (simplified models)

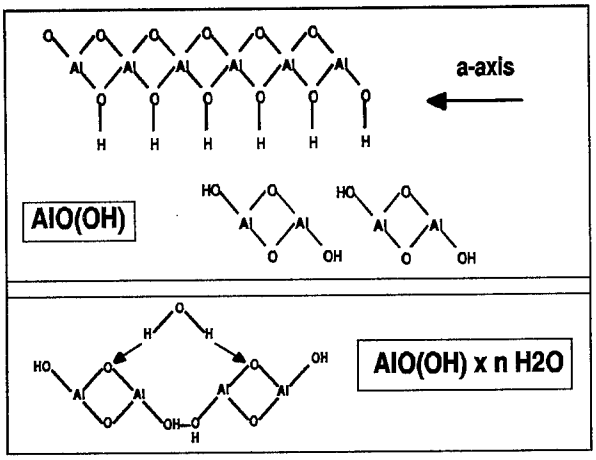

At the end of the 70s, it became apparent that market requirements of aluminas would exceed existing compulsory production capacity. Therefore, a separate process for the production of aluminas of the same quality independent of fatty alcohols was developed [5].

As described in (EQ. 1), the on-purpose alumina production process also starts from aluminium metal. Aluminium metal reacts with alcohol to form Al-alkoxide. This is hydrolized in the same way as in the Ziegler ALFOL-process to form boehmite alumina (EQ. 2). The alcohol from this reaction is recovered and recycled. The only by-product of this process (compare EQ. 3) is hydrogen of high purity which can be used elsewhere. The on-purpose alumina process was first commercialized in Germany in 1983. The worldwide accepted quality led to a second alumina capacity expansion in 1991 when the on-purpose alumina plant capacity was doubled.

Stoechiometry of On Purpose Alumina Process			
$Al + 3\ R\text{-}OH$	--->	$Al(OR)_3 + 3/2\ H_2$	(EQ.1)
$Al(OR)_3 + 2\ H_2O$	--->	$AlO(OH) + 3\ R\text{-}OH$	(EQ.2)
$Al + 2\ H_2O$	--->	$AlO(OH) + 3/2\ H_2$	(EQ.3)

CONDEA Chemie in the meantime has become part of RWE-DEA, the management company for petroleum and chemicals within the RWE Group. In 1992, VISTA Chemicals, the former chemical division of CONOCO Inc., was acquired by RWE-DEA. This group now represents a total capacity of 55,000 mt of organo-metallic-based alumina.

PHYSICAL PROPERTIES OF BOEHMITE ALUMINA POWDERS

The physical properties of boehmite alumina powders are related to their microcrystalline structure. CONDEA Chemie and VISTA Chemicals have established patented process know-how to adjust the microcrystalline structure of these aluminas [6, 7]. The inorganic alumina polymers are available in the range of amorphous (below 4 nm) to highly crystalline boehmites (above 60 nm) [7a].

In Fig. 3, the product called DISPERAL® SOL represents a low-crystalline size (approx. 4 nm) and the product called DISPERAL® 400 a high-crystalline one (approx. 40 nm). The degree of microcrystallinity affects other physical properties, such as surface area.

Fig. 3: Physical Properties of Alumina Powders (Crystallinity and Surface Area)

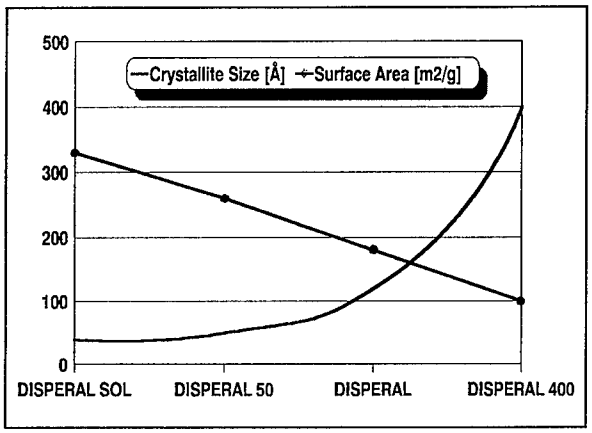

The surface area in the diagram decreases from 320 to 90 m^2/g and is inversely proportional to crystallite size [8].

Differences in crystallinity also have a great impact on phase transition temperatures. The thermal decomposition of the a.m. two alumina powders is shown in Fig. 4. Above 250°C, the boehmite-type structures decompose. As the temperature increases, the gamma alumina phase formation takes place.

Fig. 4: Thermal Decomposition of Aluminas

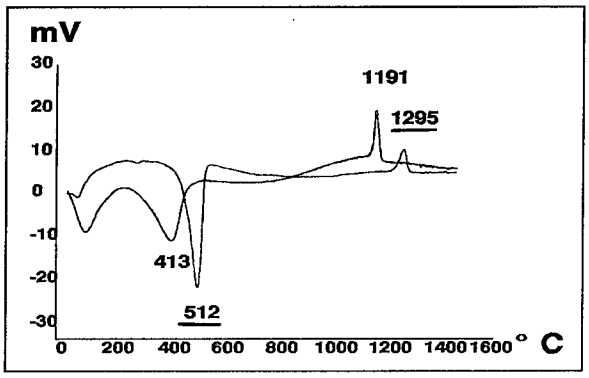

For lower-crystalline alumina, the gamma transformation is completed halfway at 413°C. Higher-crystalline alumina converts at 512°C. For alpha conversion the same temperature difference (approx. 100°C) is observed. It might be interesting to compare this effect of lowering crystallization temperatures with reported seeding methods [9, 10].

PHYSICAL PROPERTIES OF LIQUID BOEHMITE ALUMINA SYSTEMS

Colloid science is a very extensive field and cannot be covered in depth in this paper. However, over the last ten to fifteen years, as sol-gel processes have become a key subject, for instance in high-performance ceramics [11], some fundamentals have to be mentioned.

By definition, sol is the descriptive name of a two-phase colloidal system where the continuous phase is liquid, whereas the disperse phase is solid [12]. If the solid particles aggregate or polymerize to form a giant aggregate or molecule that extends throughout the sol, the substance is said to be a gel. Simply speaking, a sol can be transformed into a gel and sometimes vice versa. If we consider the boehmite alumina powder from the above-mentioned synthesis as alumina network structure comparable to a gel, we can generate a sol (a liquid alumina system) by reducing the size of the alumina network in the presence of a liquid.

Fig. 5: Boehmite Dispersing Process (simplified)

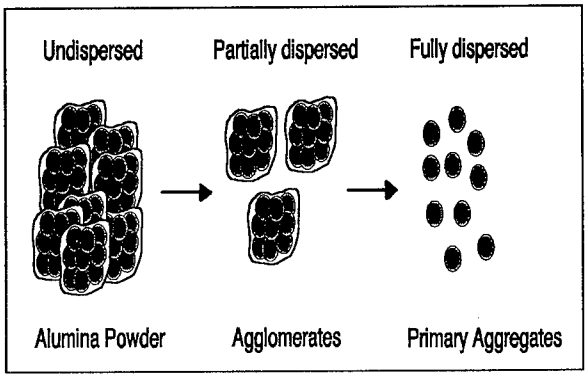

It is one of the most important properties of boehmite-type alumina powders that such a size reduction can be achieved by chemical attack. For example, in the presence of dilute monovalent acids, boehmite powders easily redisperse down to the colloidal dimensions.

Fig. 5 is a simplified illustration of the main steps describing such a dispersion process. When alumina powder is poured into a diluted monovalent acid, the chemical attack causes the alumina particles to break down into smaller fragments. These fragments are called agglomerates. The chemical attack of the acid solvates the agglomerates and, furthermore, enables them to generate smaller primary aggregates. A further effect of the acid is to provide all the primary aggregates with a positive charge. This charge produces electrostatic repulsion between the individual particles in solution and prevents them from settling. The particle charge that is obtained in e.g. 10 %wt. Al_2O_3 containing sols is plotted in Fig. 6. It demonstrates that the resulting charge of the alumina particles in a sol, achieved by chemical attack, is inversely proportional to the crystallite size of the alumina in the powder.

A special property of colloidal sols is that the charged stabilized solid particles cannot be removed by standard filtration. In other words, the particles in the liquid alumina system must be very small indeed as they can pass so easily through a filter. And, in fact, the particle sizes are in the colloidal range, between 100 and 10000 Angstroem (compare Fig. 6) [13].

Fig. 6: Physical Properties of Dispersible Aluminas (Crystallite Size, Charge and Particle Diameter)

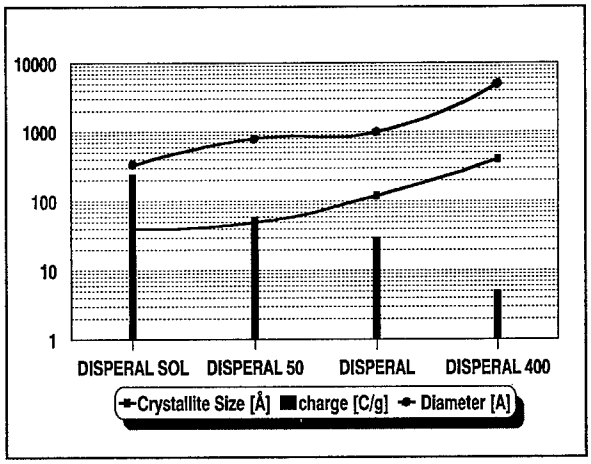

The analysis of the particle size (diameters) of the liquid alumina systems with the crystallite sizes of the corresponding alumina powder confirms that the primary aggregates of the sol are larger by roughly a factor of 10. Of course, the measured particle sizes correspond also to the optical appearance of the different sols. Along with the larger particle size of the primary aggregates, the permeability for light decreases. Many of these sols are translucent (compare Fig. 7).

Fig. 7: Transmission Values [%] of Alumina Dispersions

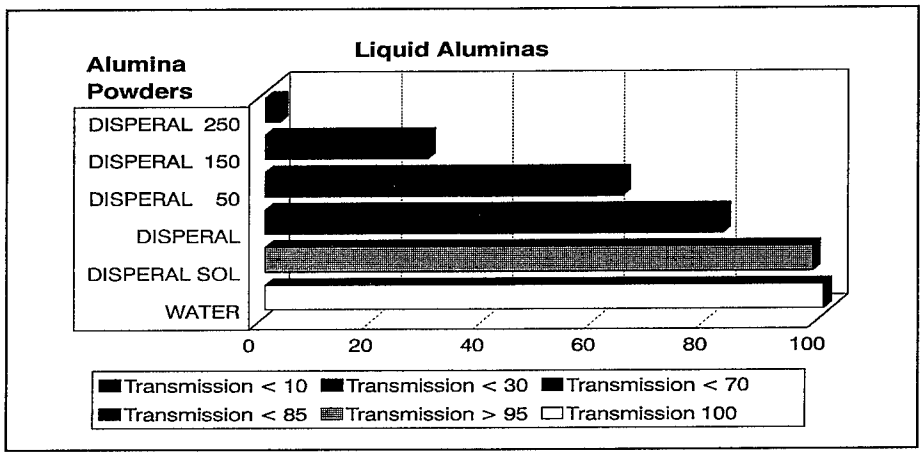

From all these considerations, it is obvious that the boehmite alumina powder properties correspond to the properties of liquid alumina systems. From a scientific point of view, colloidal dispersions have interesting features. But a more important question is, which way can such properties be utilized? Which reactions occur with these tiny primary aggregates?

Fig. 8: Reactions of Primary Aggregates

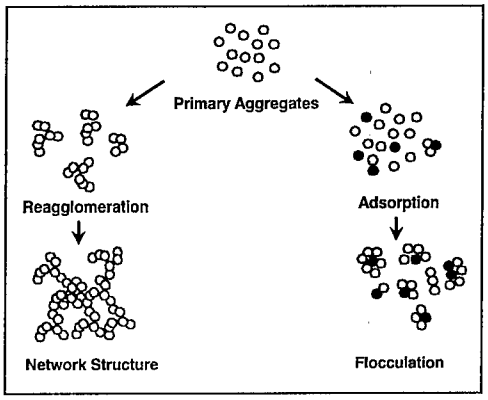

Fig. 8 shows that primary alumina aggregates can attach themselves to other particles. For this reagglomeration, it does not matter whether the particles are of the same kind or of different kinds (e.g. different diameters). Depending on chemical and physical conditions, larger network structures can be generated. On the other hand, alumina aggregates can be used to adsorb other substances. Particle charge has a great impact on the selectivity of adsorption processes.

APPLICATIONS

One strength of dispersible boehmite aluminas is that they originate from reproducible production processes which enable the manufacture of alumina powders with adjustable physical properties in reproducible consistency. Hence, boehmite aluminas can be used in a great many different applications. Fig. 9 arbitrarily divides the non-catalytic applications of aluminas into low-temperature and high-temperature applications. In the area of low-temperature applications, aluminas are frequently used at ambient temperature, for instance as viscosity improvers to thicken paints. Most of the applications mentioned are based on the

reactions of primary aggregates, regardless of whether the adsorption properties of the liquid alumina systems are applicable to inorganic or organic molecules.

Fig. 9: Boehmite Alumina Applications

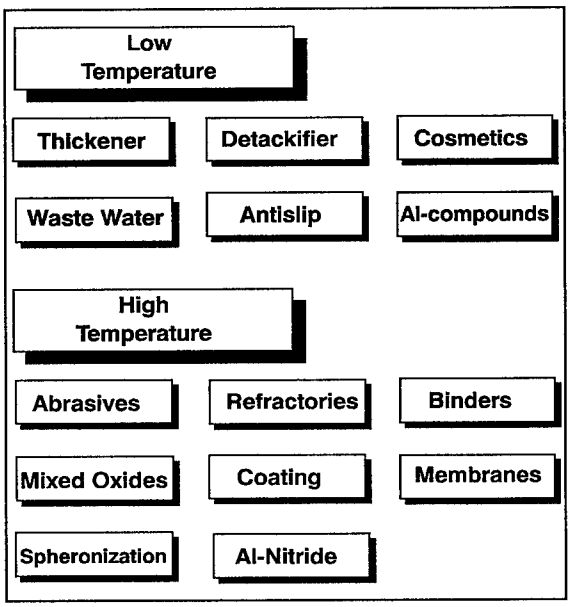

The strong adsorption properties of boehmite aluminas are taken into account in applications like purifying waste water [14] or detackifying paint from spray boosts in the automobile industry [15]. High-purity aluminium compounds can be made from dispersible aluminas due to their out-standing purity.

The front-runner in established high-temperature applications still is the parent compound of all dispersible aluminas, DISPERAL®. As described in a number of patents, it can be used in the production of abrasives [9, 16-20]. There, non-fused aluminium-oxide-based abrasive minerals are processed into microcrystalline corundum abrasive sintered bodies which are used in high-performance grinding wheels and belts. The latest revolutionary inventions in the field of abrasives are based on the systematic approach to combining in-depth know-how of colloidal chemistry with new process technology. For instance, the combination of sol-gel processing and reaction-sintering can be used to prepare dense non-oxide abrasive grits which have performance properties equivalent to premium oxide abrasives [21].

In refractories and specialty ceramics, dispersible aluminas can be used as binders for casting molds, for fiber materials, and in the extrusion of electroceramics. In this area, binders containing Al_2O_3 are gradually replacing traditional organic binders and those containing silica. The conversion to aluminium oxide-containing binders is occuring both for safety reasons, since silicas are suspected to produce silicosis in some applications, and due to performance considerations, since aluminium oxides are considered superior in withstanding the high temperatures in firing furnaces.

Reverting to the reactions of primary aggregates, it is easy to understand that dispersible aluminas are ideal raw materials for producing mixed oxide compounds. By adjusting the charge and the particle diameter of the raw materials, the co-precipitation of the mixed oxide compound can be controlled. Based on this knowledge, for instance, mullites and spinels are produced [9, 22-23].

The group of coatings includes more than just automotive catalytic converter coatings, although this area still is the domain of alumina powders which are used to coat ceramic or

metallic based honeycombs. Today, coating is also a catchword when it comes to applying special inorganic liquid systems based upon colloidal translucent alumina sols. If thin film coatings without organic solvents are required, aqueous alumina sols can easily be used in all kinds of coating applications, such as glass, metal or alumina itself. Of course, all coating procedures - whether water-based or based on organic solvents - have advantages and disadvantages. The decision on which solvent to use depends on the benefits attained for the application.

Inorganic membranes based on boehmite can be used as filter materials to purify process and waste gases, and as filters in food processing technology (as an alternative to asbestos) [24, 25].

By using special techniques, alumina sols can be transformed into small beads. Such spheronization processes are based on patented know-how [26]. It is known that alumina beads are used in some catalytic applications, for instance catalytic carriers. Those beads are often superior because of their high porosity and low attrition compared to spheres attained by agglomerization processes. Applying colloidal chemistry, it is possible to produce alumina beads of low porosity and very low attrition. New applications may come up in the ceramics industry if markets demand such alumina beads, for instance as grinding tools. Such materials might be advanced compared to standard products.

FUTURE ASPECTS

Over the past 30 years, CONDEA Chemie and VISTA Chemical Co. have established continuous production processes for special aluminas. Using on-purpose alumina plants, the capacity for bulk high-purity synthetic aluminas has been expanded. "Semi-commercial process units" have been designed to increase process flexibility and to be able to meet future customer needs. In these process units, aluminas can be tailored to the requirements of customers. For instance, specialties like co-precipitates can be continuously manufactured in smaller quantities. Such processes are the basis for the development of commercially available specialties in the future.

LITERATURE

[1] H. Ginsberg and Fr.W. Wrigge, Tonerde und Aluminium, Teil 1, Die Tonerde; de Gruyter, Berlin (1964).
[2] K. Ziegler et al., Angew. Chem. **67**, 425 (1955), Liebigs Ann. Chem. **629**, 121 (1960), Liebigs Ann. Chem. **629**, 241 (1960).
[3] B.C. Lippens, Structure and Texture of Aluminas, p. 52ff; Editor Waltman, Delft (1961).
[4] Ch. Misra, Industrial Alumina Chemicals, Monograph **184**, p. 48; American Chemical Society, Washington (1986).
[5] G. Albert et al., German Patent No. DE 3244972 C1, Feb. 9 (1984), assigned to Condea Chemie GmbH (Germany).
[6] A. Meyer et al., German Patent No. DE 3823895 C1, Dec. 21 (1989), assgined to Condea Chemie GmbH (Germany).
[7] B.E. Leach et al., United States Patent No. 4,676,928-A, June 30 (1986), assigned to Vista Chemical Company (USA).
[7a] The crystallite size of boehmite is determined by the line broadening of the (021)-reflex according to the Scherrer equation.

[8] Surface area is measured by B.E.T. technique on activated aluminas (3h at 550°C) according to ASTM D 4567-86.
[9] Y. Suwa, R. Roy and S. Komarneni, J. Am. Ceram. Soc. **68**, C-238 (1985).
[10] J.L. McArdle and G.L. Messing, J. Am. Ceam. Soc. **69**, C98 (1986).
[11] D.L. Segal, J. Non-Crystalline Solids **63**, 183 (1984).
[12] P.C. Hiemenz, Principles of Colloid and Surface Chemistry, p. 11; Editor Marcel Dekker, New York (1986).
[13] Particle sizes of submicron polymeres in liquid systems are measured by laser light scattering method.
[14] H.L. Fleming, Environmental Progress **5**, 159 (1986).
[15] A. Meyer et al., United States Patent No. 4,992,199, Feb. 12 (1991), assigned to Condea Chemie GmbH (Germany).
[16] M. Leitheiser et al., United States Patent No. 4,314,827, Feb. 9 (1982), assigned to Minnesota Mining and Manufacturing Company (USA).
[17] M.G. Schwabel and P.E. Kendall, Am. Ceram. Soc. Bull. **70**, 1596 (1991).
[18] R. Bauer et al., United States Patent No. 4,797,139, Dec. 16 (1987), assigned to Norton Company (USA).
[19] M. Tamamaki et al., United States Patent No. US 5,190,567, March 2 (1993), assigned to Japan Abrasives (Japan).
[20] K. Miyazaki et al., German Patent No. DE 3913810, April 26 (1989), assigned to Showa Denko K.K. (Japan).
[21] J.P. Mathers, T.E. Forester and W.P. Wood, Am. Ceram. Soc. Bull. **68**, 1330 (1989).
[22] J.C. Huling and G.L. Messing, J. Am. Ceram. Soc. **72**, 1725 (1989).
[23] M.G.M.U. Ismail et al., Int. J. High Technology Ceramics **2**, 123 (1986).
[24] A. Larbot et al., Int. J. High Technology Ceramics **3**, 143 (1987).
[25] R. Soria, lecture during the Sol-Gel-Conference in Saarbrücken Germany (1993), see this book.
[26] A. Meyer et al., Europian Patent No. EP 0090994 B1, July 8 (1987), assigned to Condea Chemie GmbH (Germany).

Key Engineering Materials Vol. 150 (1998) pp. 171-176

Sol-Gel Applications for Membranes

R. Soria

SCT/U.S. Filter, BP 1, F-65460 Bazet, France

Keywords: Mineral Membrane, Sol-Gel, Zirconia, Titania, Streaming Potential, Nanoparticles, Mesoporous, Microporous

Abstract: Sol gel is a versatile technique which allows to produce membranes working by size exclusion mechanism such as meso-and microporous layers, or by specific interaction such as modified membranes of SCT.

1. INTRODUCTION

Inorganic membranes were first developed for a nuclear application: separation of uranium isotopes by gas diffusion. Today, they cover a broad range of industries: chemical and petrochemical industry (catalyst recovery, solvent clean up), pharmaceutical (metabolites and antibiotic extraction, cell-harvesting), food and beverages (clarification and sterilization of fruit juices), dairy (cold pasteurization of milk, cheese making), potabilization of water and clean up of waste streams (oil-water treatment, dye recovery). Membranes split the feed into a clear filtrate and a retentate which is a concentrated suspension. This comes from the concept of crossflow filtration, that is circulation of the liquid to be filtered (feeding product) under pressure tangentially to the surface of the membrane, so as to deplete it of the liquid phase, that permeates through the membrane. The separation takes place at the surface of the top-layer. It is deposited at the surface of a macroporous support and its pore size is well defined. The role of the support is to give shape and mechanical strength to the filtration element. This support is a ceramic block pierced by several parallel channels, the inner surface of which is covered by the top-layer (often called the membrane).

2. APPLICATION OF SOL-GEL PROCESS IN MEMBRANE TECHNOLOGY

The efficiency of the top-layer depends on its basic properties such as pore size distribution or surface chemistry. The sol-gel technique is well adapted for mastering or modifying these properties.

Three types of sol-gel applications are recorded in membrane field:

- Particle production to create a slip for mesoporous layer deposition,
- Direct layer deposition by destabilization of colloïdal sol

(DCS) which induces mesoporous layer, or by polymerization of molecular species (PMS) for microporous or dense structure, or by the ormosil/ormocer technology,

- Coating with thin film (by PMS) to adapt physico-chemistry properties of the membrane in terms of corrosion, selectivity or flux performance to the feed characteristics.

3. PARTICLE PRODUCTION FOR LAYER DEPOSITION

This point can be illustrated by the production of zirconia particles.

Zirconia particles can be obtained by thermohydrolysis of different compounds. In particular, it is possible to obtain monoclinic zirconia from an acetate sol.

Thermohydrolysis of a colloidal sol of zirconium acetate gives two types of product:

- amorphous monolith gel
- sol of crystallized zirconia.

The temperature of the transition (gel-crystallized sol) is 200°C and the gelification takes place at 45°C. IRFT , thermal studies and SAXS measurements show that the sol-gel transition is obtained by elementary cluster aggregation. This aggregation induces the production of more and more compact and voluminous particles (Rg increases from 1 upto 9 nm and the fractal dimension from 1 upto 2.6). So the gelification works by physical aggregation without hydrolysis of acetate group. This hydrolysis occurs during the second transition (gel-crystallized sol).

The hydrolysis of acetate groups allows the condensation of molecules to form Zr-O-Zr structure. Zirconia crystallizes under a monoclinic structure.

Size of crystallite increases with increase of the temperature and duration of the thermohydrolysis but the particle size decreases when the concentration of colloidal sol increases. Particles with a 45 nm diameter are obtained from a 10 % sol whereas particles with a 25 nm diameter are obtained from a 25 % sol.

These slurries of nanometric particles are used to produce a mesoporous layer with a pore diameter of 20 to 50 nm and a porosity around 60 % .

4. Direct layer deposition

The sol transition can be realized directly in place at the surface of the porous support.

Three different techniques have been used:

- Ormosils/ormocers give microporous or dense layers with gas separation properties.

- PMS technique produces microporous layers for nanofiltration or gas separation.

- DCS technique induces the deposition of mesoporous layers.

This last process can be illustrated by the gamma alumina example. Aluminum butoxide is hydrolyzed by water, then peptized with nitric acid. So a stable boehmite sol is obtained. Introduction of a binder allows to increase the viscosity of the sol upto the required level for the layer deposition which is obtained by coating.

The porous structure of support sucks water of the sol and the gelification takes place by colloid destabilization. Drying and sintering allow inorganic layer production. In this case, at 450°C, a gamma alumina layer with a 2 nm pore diameter is obtained. The pore diameter evolves with the sintering temperature and a 100 nm pore diameter layer is obtained at a 1200°C sintering temperature.

5. Layer modification

The layer modification is realized to improve the flux in particular conditions (i.e. non aqueous feed), to improve the selectivity (i.e. extraction of one particular molecule in a mixture) or to improve the chemical resistance (i.e. filtration of fluorhydric acid solution). These modifications allow the development of intelligent membranes by controlling the interaction membrane surface and the feed components.

Sol-gel technique can be used to modify the streaming potential (IEP) of the membrane. The goal is not just to adapt the electrical charge at the interface membrane feed but to treat all surfaces in contact with the liquid (feed and permeate) which present full pore wall surface. In this purpose we deposit a very thin film around every particles of the membrane. Sol-gel techniques are well adapted to this challenge. A three-component sol is realized with a metal alkoxide, a modifier (with a high molecular weight) and an alcohol. The role of the modifier is to reduce the hydrolysis kinetics (to prevent precipitation of particles and to allow the self-cicatrization of the film), and to increase the sol viscosity (to induce homogeneous film).

The role of the solvant is to adjust the metal alkoxide concentration to obtain a homogeneous and defect-free film. Modified alkoxide is hydrolysed by the air moisture to create a gel film. The hydrolysis rate decreases, air water must pass through the film to react with modified alkoxide. If the gel film cracks the alkoxide reacts easylier to repair the film. Drying in well-controlled conditions (humidity and temperature) and sintering give a continuous oxide film. Depending on the metal nature, different structures are obtained: gamma structure for aluminum, monoclinic for zirconium, rutile for titanium. The obtained oxide film (1 nm thick) modifies the streaming potential of the membrane in fuction of the feed pH. The isoelectric point (IEP) is the pH value of the feed with a streaming potential equal to zero. For the initial alumina membranes the IEP is 8, after zirconia modification IEP decreases downto 5.7 and 5.5 in the case of titania coating, IEP of

silica modified membranes is 4.5 (see figure 1).

The influence of the IEP modification has been tested on fresh orange juice. As shown in figure 2, flux increases when IEP decreases (35 l/h m^2 for alumina membranes upto 82 l/h m^2 for titania modification). Membrane fouling is decreased by IEP reduction. Simultaneously the quality of juice is modified. Juice obtained by filtration on zirconia modified membranes contains a larger quantity of molecules generating flavour than "titania juice" (321 components versus 213).

6. Conclusion

Sol-gel is a key process for membrane production. The versatility of this technique allows the preparation of particles (for mesoporous layers) or polymeric network (for dense and microporous layers) and the modification of membrane chemistry for the preparation of "intelligent" membranes.

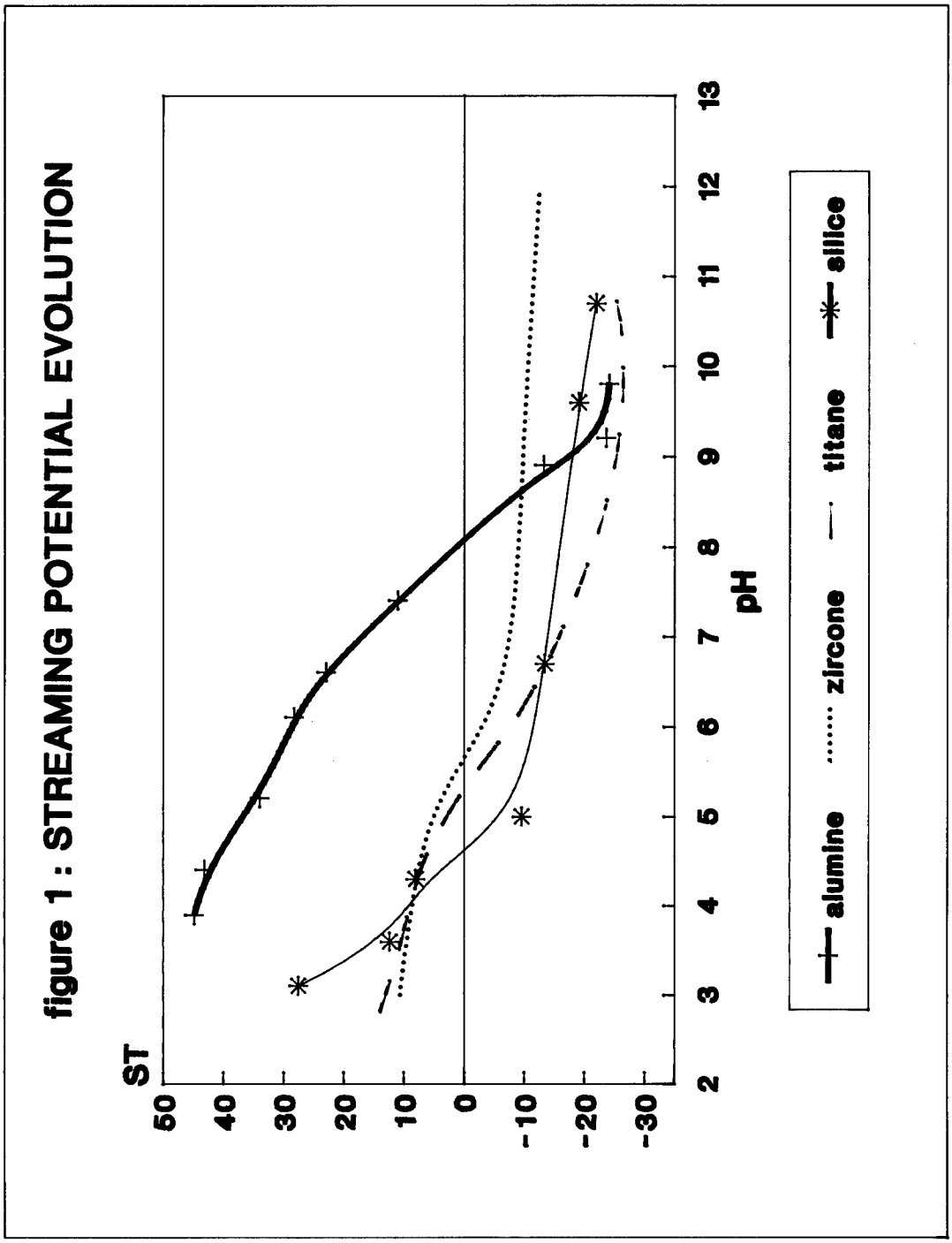
figure 1 : STREAMING POTENTIAL EVOLUTION
ST
50
40
30
20
10
0
-10
-20
-30
2
3
4
5
6
7
8
9
10
11
12
13
pH
alumine
zircone
titane
silice

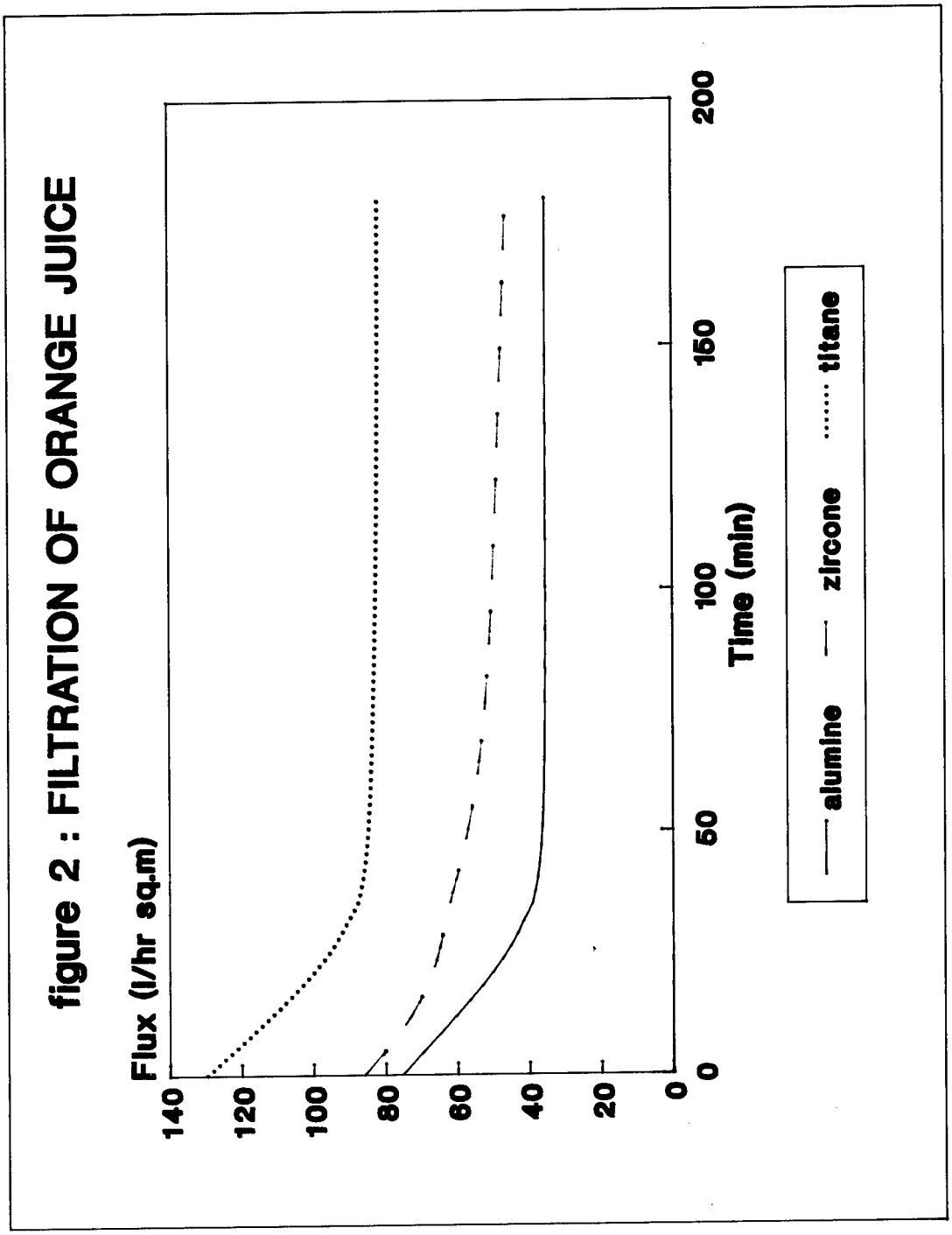
figure 2 : FILTRATION OF ORANGE JUICE
Flux (l/hr sq.m)
140
120
100
80
60
40
20
0
0
50
100
150
200
Time (min)
alumine
zircone
titane

Key Engineering Materials Vol. 150 (1998) pp. 177-184

Development of Wet Chemical Processing in Nippon Sheet Glass

K. Takemura[1], K. Doushita[1], K. Yokoi[1] and T. Mizuno[2]

[1] R & D Group, Central Research Laboratory, Nippon Sheet Glass Co., Ltd.,
1-Kaidoshita, Konoike, Itami 664, Japan

[2] R & D Department, Nippon Sheet Glass Co., Ltd.,
Shinbashi, Sumitomo Bldg., 11-3, 5-Chome, Shinbashi, Minato-ku, Tokyo 105, Japan

Keywords: Liquid Phase Deposition (LPD), Silica Film, Alkali Diffusion Barrier, Sol-Gel Method, Ultra-Thin Silica Glass Flake, Titania Dispersed Ultra-Thin Silica Glass Flake, Photocatalytic Activity

Abstract

The liquid phase deposition (LPD) is a film coating process developed in Nippon Sheet Glass (NSG). Silica thin film can be grown by an equilibrium reaction in aqueous solution. The formation of silica film on a glass substrate was found in hexafluorosilisic acid (H_2SiF_6) solution supersaturated with silica in 1982. The film thus obtained showed extremely smooth surface and high density while formed at near room temperature. The LPD has been applied to the process of a manufacturing substrate glass for a liquid crystal display (LCD) since 1986. Recently, another application of the LPD has been proposed in the fabrication process of ULSI circuits. We found organic dye-doped silica films can be also prepared by the LPD. NSG has been developing in the various industrial applications.

Ultra-thin silica glass flakes were prepared by the sol-gel method. The flakes were manufactured by sintering silica gel flakes which were peeled from a sol-coated substrate. These silica glass flakes were not only very thin but have a sharp thickness distribution. The titania dispersed silica glass flakes absorbed UV light perfectly, and showed less toxicity in comparison with the conventional UV absorbing materials. We have recently started distributing the samples to mainly cosmetic manufacturers.

1. Introduction

The liquid phase deposition (LPD) is a film coating process developed in Nippon Sheet Glass (NSG). Silica thin film can be formed by an equilibrium reaction in aqueous solution. The film thus obtained shows extremely smooth surface and high density while formed at near room temperature [1,2,3].

The LPD has been applied to the process of a manufacturing substrate glass for a liquid crystal display (LCD). Silica film on the glass was used as a barrier to prevent diffusion of alkali ions from the glass to the indium tin oxide (ITO) layer.

Recently, we have developed a glass flake manufacturing process using the sol-gel method [4]. Ultra-thin silica glass flakes were prepared by sintering gel flakes which were peeled off from a sol-coated substrate. These flakes have a sharp distribution in thickness compared with commercially available glass flakes.

In order to add UV-light protection function to the flakes, Ultra-fine titania particles were dispersed in the flakes [5]. These flakes showed high transparency in visible light region, but absorbed UV-light perfectly. The flakes also showed less toxicity in comparison with the conventional UV absorbing materials.

In this paper, we describe the procedure and features of the above wet chemical processings,

and also review briefly the background of our R & D work on the processes. Furthermore, typical properties of the titania dispersed flakes will be introduced.

2. Liquid Phase Deposition

2-1. Process and mechanism

A schematic diagram of the LPD process is shown in Fig.1. This process is mainly consist of following 3 steps:

Step1; Hexafluorosilicic acid (H_2SiF_6) solution is saturated with silica by dissolving silica gel.

Step2; The saturated solution is turned to the supersaturated solution by means of additives such as aluminum.

Step3; Silica film is formed on a substrate in the supersaturated solution at near room temperature.

In step 2, the additives are like reaction initiators and play an important role in silica film formation. The mechanism of the LPD process is considered to be described by the following two equilibrium rections [6]:

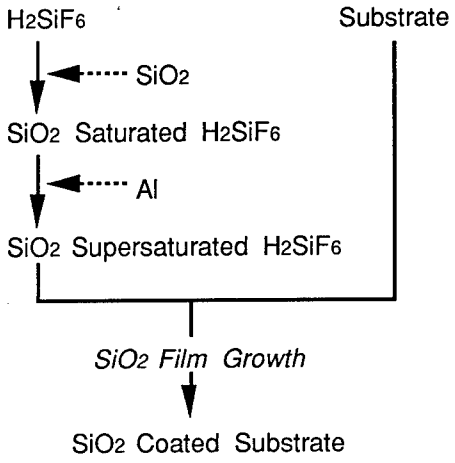

Fig. 1. Schematic diagram of the LPD.

$$H_2SiF_6 + 2H_2O = SiO_2 + 6HF \quad (1)$$

$$6HF + Al = H_3AlF_6 + 3/2H_2 \quad (2)$$

From the above mentioned process, it is clear that the LPD process is not similar to the conventional wet chemical processings such as the sol-gel method. One of the most remarkable differences is that silica film is grown on a substrate surface. Therefore, contrary to the sol-gel method, immersion time of the substrate ditermines film thickness. Hishinuma et al. reported the almost linear increase in thickness of silica film against time [6].

Table 1
Etching rates of SiO_2 films

Type of SiO_2	Etching rate(at 25°C) (nm/s)
LPD-SiO_2 (30-35°C)	1.8 - 2.1
e-Beam evaporation (400°C)	2.8 - 3.3
CVD (450°C)	1.0 - 2.5
Reactive sputtering (600°C)	0.35 - 2.1
RF sputtering (100 - 450°C)	0.4 - 1.2
Thermals(980°C)	0.2

Etching solution
48%HF : 70%HNO_3 : H_2O = 3 : 2 : 60 in volume

Another difference is the film formation reaction is completely finished in the supersaturated aqueous solution without sintering process. . The etching rates of various types of silica films are shown in Table 1 [6]. Since the etching rate of the LPD silica film shows same order with the other films formed by higher temperature process, it is considered that the density of the LPD film is extremely high as a near room temperature process. Those differences seems to be derived from a dehydration rection of the silica gel accelerated by fluorine in the supersaturated H_2SiF_6 solution with silica.

2-2. Historical background

The history of our R & D work on the LPD process is shown in Fig.2. H_2SiF_6 has been used as the surface treating solution to manufacture anti-reflective glasses such as a cover glass for solar collector and a visual display tube (VDT) filter. In this process, a kind of porous silica layer was formed on a soda-lime glass in the saturated solution.

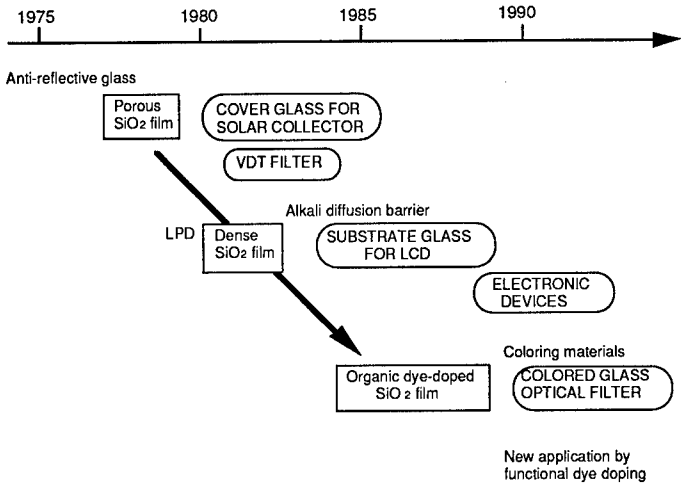

Fig. 2. History of R & D work on the LPD.

The LPD was found in 1982 as an unusual phenomenon of the above surface treatment. We applied this process to an alkali diffusion barrier silica coating for soda-lime glass. It was well known that a sodium ion was a harmful impurity to a transparent electrode such as ITO, because it reduced the conductivity. Silica coating manufactured by the sol-gel method was the most general material for the diffusion barrier at that time. After 3 years of R & D, a pilot plant was installed at our Sagamihara factory in 1985. As a result, we started the production of the substrate glass for LCD in 1986. Fortunately, the production of the glass reaches over 40,000 m^2/month at the present day.

2-3. Application

As can be seen from Fig. 2, another application of the LPD has been reported in the fabrication process of ultra-large scale integrated (ULSI) circuits. T.Homma et al. used the LPD process in a fully planarized multilevel interconnection technology, and they succeeded in reduction of the processing time [7,8]. In their process, silica film was formed on the spacings between photoresist patterns selectively, but not formed on the patterns. It is interesting to notice that this selectivity due to the demerit of wet chemical processing, namely, nothing can be coated on a solvent repellent surface.

Recently, we have developed a new colorful coating method using the LPD process [9]. Some kind of organic dyes in the saturated or supersaturated H_2SiF_6 solution were directly doped in the LPD film. The film thus obtained showed higher durability in comparison with the conventional films.

Since silica film incorporated with organic molecules has been considered to be a most promising optical and photonic material, we hope the LPD process will be a major technology in this field.

3. Silica Glass Flakes

3-1. Historical background

The sol-gel method is a very attractive technology for glass manufacturer, since it has many advantages such as low processing temperature. The reseach of the method began in our laboratory about 10 years ago aiming at a silica plate glass production. After several years of R & D, we developed a unique process which could make a silica plate glass 15 cm by 15 cm for only 5 days.

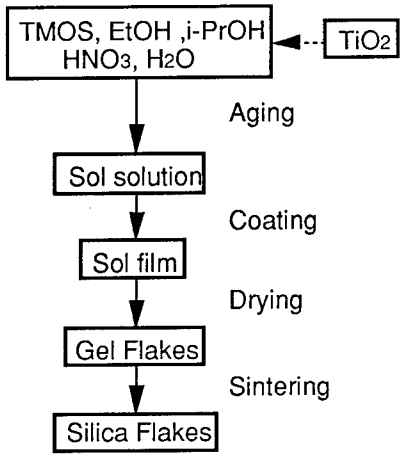

Fig. 3. Schematic representation of the flake manufacturing process.

3-2. Manufacturing Process

Fig.3 shows a schematic representation of the manufacturing process of glass flakes by the sol-gel method. Tetra methoxysilane(TMOS), ethanol, isopropanol, nitric acid and water were mixed and stirred for few hours at room temperature. In order to manufacture TSG flakes, titania sol (titania fine particles dispersed in water) was added and dispersed in the mixture. Then, the solution was kept at 50 to 60 °C for 20 to 30 hours to be desired viscosity. The sol thus obtained was coated on a stainless sheet substrate by dipping method.

The coated sol with the substrate was dried at 120 to 150 °C for few minutes. During this process, the sol turned to the gel film and then peeled off from the substrate as the gel flakes. It is considered that the flakes are peeling off by means of large shrinkage and less interaction at the gel/substrate interface. In order to attain this flake formation without a scraper, we had to determine optimum processing parameters such as the silica concentration in the sol. These gel flakes were finnally sintered at 900 to 1200 °C for few hours to convert gel to glass.

The production cost, however, was not lower than that of the conventional process, we gave up the silica glass production using the sol-gel method. As a result, we were looking for a new research target of the method at that time.

On the other hand, our company has been a single supplier of a soda-lime silicate glass flake in Japan. Therefor we could find market demands for ultra-thin glass flake, but it was difficult to make thiner glass flake by the conventional molten glass process.

The sol-gel method was applied to the manufacturing process of the ultra-thin glass flakes in the above mentioned circumstances. In following discussion, we will introduce typical data of silica glass (SG) flakes and titania dispersed silica glass (TSG) flakes.

Table 2
Typical properties of SG flakes and TSG flakes

	SG flakes	TSGflakes
Titania content (wt.%)	0	9.3
Density (g/cm3)	2.2	2.35
Refractive index	1.458	1.53
Loss on ignition (%)	0.055	0.055

Fig. 4. SEM photograph of the TSG flakes.

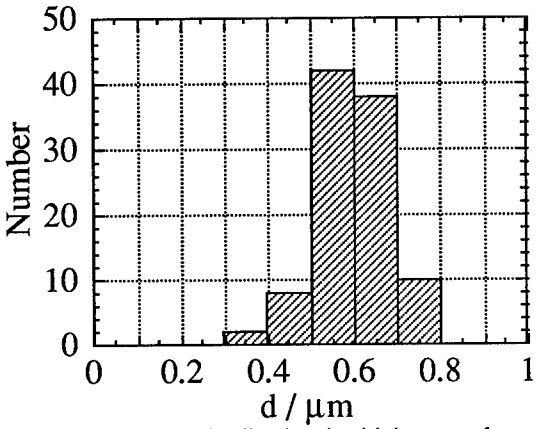

Fig. 5. Distribution in thickness of the TSG flakes.

was 0.588 μm, standerd deviation was 0.081 μm (n=100). It seems this narrow distribution can not be achieved by conventional or natural flake materials, such as mica.

Fig. 6 shows a X-ray diffraction pattern of the TSG flakes. As can be seen from this figure, the flakes are composed of crystalline titania (anatase form) and amorphous silica. A TEM photograph of the flakes indicate the titania srystals are uniformly dispersed in the silica matrix, and their diameters are 40 to 50 nm. Since these diameters are

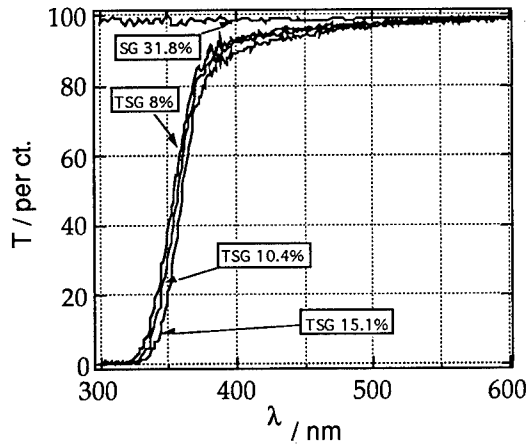

Fig. 7. UV-VIS spectra of the flakes.

3-3. Characteristics

Typical properties of our glass flakes are listed in Table 2. Refractive index and density of the SG flakes sintered at 1000 °C are 1.458 and 2.2 respectively, which are equivalent to commercially available silica glasses. On the other hand, those values of the TSG flakes containing 9wt.% titania are 1.53 and 2.35, respectively.

Fig. 4 is an SEM photograph of the TSG flakes. The flake surface is very smooth and its thickness is less than 1 μm.

Thickness of the flakes were measured by an interferometer. Distribution in thickness of the TSG flakes is shown in Fig. 5. In this case, the average thickness

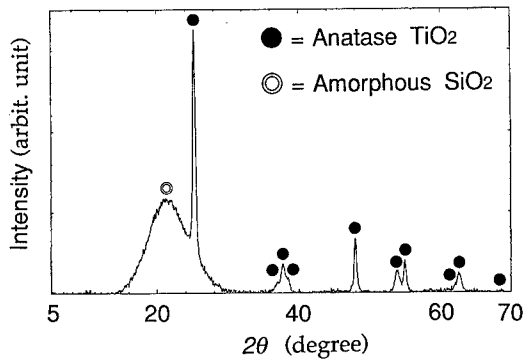

Fig. 6. X-ray diffraction pattern of the TSG flakes.

same as those in the starting sol, it is considered that titania particles are incorporated in the silica glass flake without an undesirable aggregation.

Transmittance spectra of the flakes dispersed transparent polymer films are shown in Fig. 7. Spectrum of the SG flakes indicate a very high and flat transmittance over UV-visible region. It is considered that this is due to high purity of the SG flakes. On the other hand, UV light up to 350 nm is absorbed or scattered by the TSG flakes. These UV absorbing properties are caused by the energy band gap of titania crystal and the scattering on the interface between titania and silica matrix.

3-4. Photocatalytic activity

It is well known that titania is not only a high performance white pigment but an excellent UV absorbing material in a

cosmetic application. Recentry, it has been pointed out that a human skin may be damaged by the photocatalytic activity of titania. Therefore, silica-alumina coated titania particles are widely used in a cosmetic application these days.

The photocatalytic activity of the TSG flakes is compared with those of the commercially available titania perticles in Fig. 8 [10]. The activityies were determined by measuring the decomposition rates of formic acid solutions which contain same quantity of titania [11]. The vertical axis represents the amount of CO2 evolved from the formic acid with UV light irradiation, and the large value indicates high photocatalytic activity. As can be seen from this figure, the activity of the TSG flakes is about one tenths of that of anatase form titania. It is considered that most of titania particles in the TSG flakes are covered with silica matrix. The activity of the flakes is also less than that of the commercially available silica-alumina coated titania.

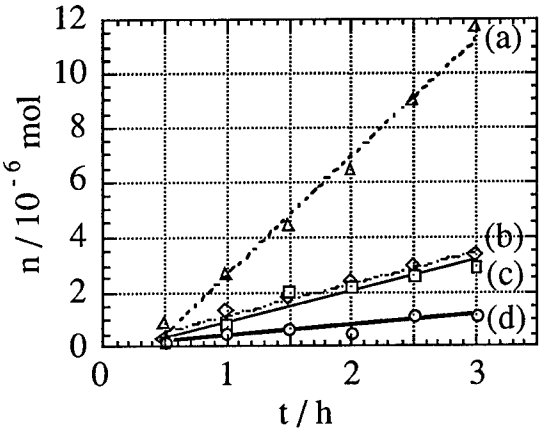

Fig. 8. Amounts of CO_2 evolved as a function of photoirradiation time.

(a) Anatase TiO_2
(b) Rutile TiO_2
(c) Silica-Alumina coated Rutile TiO_2
(d) TSG flakes/TiO_2=9.8wt.%

3-5. Application

It is believed that the TSG flakes are promising UV absorbing materials in a cosmetic application. Table 3 summarizes typical features of the flakes. Particularly, the less toxicity will be the most important criteria for the future.

Table 3
Typical features of the TSG flakes

(1) Transparent but perfect UV light protection
(2) Less toxicity agaist skin
• Inoganic material
• Low photocatalytic activity

4. Conclusion

Two wet chemical processings developed in NSG were reviewed here. The LPD has already industlialized as the manufacturing process of the substrate glass for LCD. New applications have been proposed in many fields recently. On the other hand, the ultra-thin glass flakes have just manufactured by a pilot plant installed at our laboratory. We have started distributing the flakes to mainly cosmetic manufacturers.

References

[1] H. Nagayama, H. Honda and H. Kawahara, J. Electrochem. Soc. 135, 2013 (1988).
[2] T. Goda, H. Nagayama, H. Honda, A. Hishinuma and H. Kawahara, Mat. Res. Symp. Proc. 105, 283 (1988).
[3] H. Kawahara, T. Goda, H. Nagayama, H. Honda and A. Hishinuma, Int. Congr. Opt. Sci. Eng. 24 (1989).
[4] K. Yokoi, T. Mizuno, K. Doushita and T. Yamagishi, Bol. Soc. Esp. Ceram. Vid., **31-C**, 7, 69 (1992).
[5] T. Mizuno, K. Doushita, K. Yokoi and K. Takemura, IUMRS-ICAM-93, in press.
[6] A. Hishinuma, T. Goda, M. Kitaoka, S. Hayashi and H. Kawahara, Appl. Surf. Sci., 48/49,

405 (1991).
[7] T. Homma, K. Katoh, Y. Yamada, J. Shimizu and Y. Murao, NEC Res & Dev., **32**, 315 (1991).
[8] K. Kanba, T. Horiuchi, T. Homma, Y. Murao and K. Okumura, IEDM Tech. Dig., 637 (1991).
[9] J. Ino, K. Takemura and H. Kawahara, Rivista della Staz. Sper. Vetro n. 1, 15 (1992).
[10] K. Doushita, K. Yokoi, K. Takemura and T. Mizuno, *Abstracts of Papers*, Shikizai Kenkyu Happyokai, 2B-29 (1993).
[11] H. Tada, K. Miyata, H. Yoshida and H. Kawahara, J. Japan Soc. Colour Material, **61**, 665 (1988).

Key Engineering Materials Vol. 150 (1998) pp. 185-192

Commercial Development of Sol-Gel Technology in Australia

G.E. Tulloch and S.M. Tulloch

Silicon Technologies Australia Limited,
11 Aurora Avenue, Queanbeyan NSW 2620, Australia

Keywords: Sol-Gel, Thin Films, Low E, Sensors, Smart Windows

ABSTRACT

A consortium of Australian companies, universities, and government laboratories was formed in 1989 to expand existing sol-gel ceramic oxide film research, for the development and commercialisation of

- Advanced Coatings and Coated Products
- Advanced Window Systems.

The development of sol-gel formulations has been directed towards optimisation of reactions in solution and preparation of stable solutions. The chemistry and processes have been particularly well developed for the preparation of spinel and perovskite compounds. A variety of application techniques have been developed. Processes have been developed to produce thin films with oriented crystal structures. Techniques and equipment for scratch resistant have been developed.

- Products at various stages of commercialisation include:
- Energy saving coatings on glass;
- Abrasion and corrosion resistant coatings on glass, stainless steel, aluminium and low temperature alloys;
- Thin film sensors for defence surveillance equipment;
- SMART Windows, which are electrically switchable, based on electrochromic films;
- Stealth Coatings;
- Powder for composite sensors.

BACKGROUND

The work described in this paper has been the result of an inter-disciplinary team.

The key consortium organisations are Silicon Technologies Australia Limited (STA), the lead commercial collaborator responsible for applications development and manufacturing; Monash University, responsible for chemistry research; and University of Technology Sydney, responsible for physics and ceramic engineering. Other researchers include ANSTO (Australian Nuclear Science and Technology Organisation), Defence Science and Technology Organisation Materials Research Laboratory, and Sydney University. Major funding has been provided by the Australian Government through the Department of Industry Technology and regional Development, the Energy research and Development Corporation and the Department of Defence. Government funding has been matched by contributions from the corporate and laboratory partners.

ENERGY SAVING COATINGS ON GLASS

The objective in application of sol-gel technology for production of energy saving coatings on glass has been to produce materials which reflect/absorb IR while maximising transmission in the visible band. An added objective has been to produce films which can be utilised on the external surface of glass. The major market to be addressed by the sol-gel coated glass is the residential and small commercial window market in Australia and S. E. Asia. This market, which is predominantly between the Tropic of Cancer and the Tropic of Capricorn is characterised by generally temperate to hot conditions with medium to high insolation. While the use of energy efficient glass is in its infancy in these regions, the potential for application of low cost heat reflective glass is very high. A smaller, but more immediately accessable section of the market in southern Australia and New Zealand is based on the temperature climate with cool to cold winters, where single glazed low E glass would provide benefits.

Consequently, the first priority has been to produce low E coatings for use in single and double glazed windows in the cooler climates. The performance of a spectrally selective heat reflective coating is directly related to the electronic conductivity of the coating. Unfortunately, the best conductors - being the noble metals - can only be deposited by vacuum technology, are soft, and reflect visible light. There are both aesthetic and safety problems with coatings which reflect visible light. In the first instance, coloured reflective/absorbing glass is not considered architecturally pleasing in the residential market place. In the second instance, the reflective nature of the glass renders it internally reflecting at night - a problem recognised in CBD offices - and a security hazard in the residential environment. In addition, heat absorbing glass is not energy efficient when used in single glazing. Finally, authorities are increasingly regulating against the use of glass with high visible reflection.

The Australian research had commenced some ten years ago with the manufacture of cadmium stannate. Obviously, this market can no longer be applied for commercial glass due to the cadmium safety hazards. However, the extensive research carried out over a period of seven years provided an excellent basis for development of other transparent conductive oxide coatings. The ligand chemistry of the cadmium stannate system was developed on the basis of maximising reactions in solution and production of stable solutions. Processing to produce

coatings with resistivity of about 100 ohms/sq involved post curing in vacuum or reducing atmospheres. Solutions remained stable for over two years.

The recognised material for maximum electronic conductivity is Indium Tin Oxide (ITO). The production of ITO is more complex than production of cadmium stannate due to the moisture sensitivity of the precursors and the consequentially reduced stability of solutions. The STA developments have involved utilisation of both inorganic and organic precursors. Minimum sheet resistivity achieved has been 10 ohm/sq. These films have a hazy appearance and are inappropriate for commercialisation. Films with adequate visible light transmission have minimum sheet resistivity of about 20-30 ohms/sq. The processing conditions require strict control of humidity during deposition. To prevent crazing, the films are hydrolysed at low humidity. Several coats are applied and each coat is partially cured before deposition of the next layer. The final treatment involves a controlled reduction of the ITO to maximise electronic conductivity.

Figure 1 shows typical spectral response curves for glass coated with approximately 1 micron ITO with sheet resistivity in the range 30 to 50 ohms/sq. The coatings are relatively hard having diamond scratch resistance (3g load) similar to that of uncoated glass. The manufacture of these coated products is in pilot production with market entry planned for 1994/95.

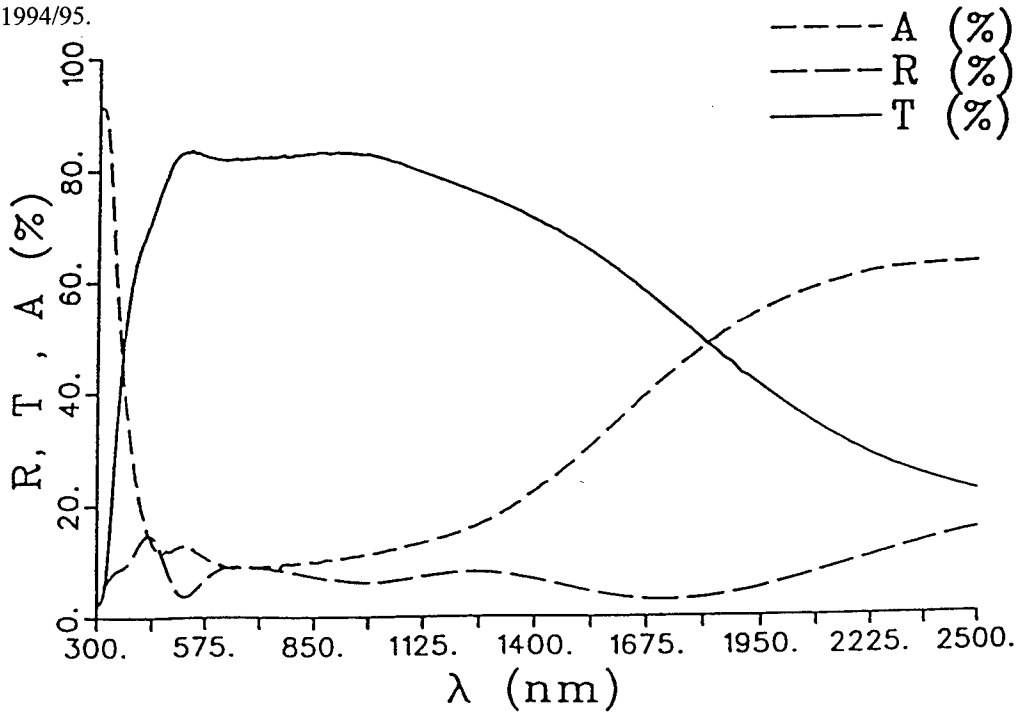

FIGURE 1
Typical Spectral Response Curves for glass coated with approx. 1 micron ITO

STA is also developing sol-gel angular selective coatings for application in solar IR reflection. The coatings are based primarily on Silica/Titania layers. Other oxides such as Zirconia can also be used. The objective is to bring these products to the market in !995/96. The design involves sequential coats of silica and titania on the glass to produce an angular selective filter for operation in the low and medium IR ranges from approximately .8 micron wavelength. Coating and processing regimes are being studied to provide the conditions for preparation of a range of products to suit the requirements at different latitudes.

CORROSION RESISTANT COATINGS

Sol-gel technology is a cost effective means of depositing continuous defect free oxide coatings on metals for prevention of corrosion. STA has deposited alumina, magnesium aluminate, silica, zirconia, barium titanate and barium zirconate films on a range of metals including aluminium, titanium, stainless steel, nickel, brass and 'antique' brass to protect the base metal from discoloration and more serious corrosion. The coatings can also be used for decorative effects. The coatings on aluminium foils have demonstrated up to 5 times resistance to attack by HCl compared to uncoated materials. The coatings are also used for planarising of metal substrates and, in the case of aluminium, the films, cured at less than 300 degrees C, provide adequate corrosion resistance and significant improvement to surface finish.

THIN FILM FLEXIBLE CERAMIC SENSORS AND DIELECTRICS

STA has proven sol-gel processing technology for new generation, low cost sensors which have excellent integrity and high performance. The products are thin film ceramic sensors which can be configured for the widest range of requirements from integration with microelectronics to flexible large area conformal arrays and continuous metal foil dielectrics. The sensors have the potential to be formulated and configured to detect within a broad wavelength range, from IR to acoustic.

A range of pure and doped compositions has been produced based on Barium Titanate, Lead Titanate, and Lead Zirconate Titanate. Breakdown strength tends to mirror the behaviour of bulk piezoelectric ceramics. The technology has recently been successfully applied to the production of PZT sonar sensors under contract to the Australian Department of Defence. Techniques have been developed and proven for a revolutionary poling.

Some of the key features of these new sensors are:

- The sensors are resistant to damage. Bending and even more serious physical damage does not significantly affect properties. Typical hysteresis is shown in Figure 2.
- The sensors have an effective dielectric constant of up to 500 depending on final crystallisation conditions. This translates to a substrate area of about 1 sqcm per microfarad of capacitance for double sided devices.
- Polarisation is unaffected by temperature in normal processing ranges.

- Sensor films have been deposited on substrates up to 100mm x 70mm indicating that large area sensors could be made with continuous or large batch production equipment. Large area sensors could be mechanically or laser scribed to produce arrays.

- The large pyroelectric effect is shown qualitatively by the low Q doped PZT and lead titanate devices indicates that sensors could be produced for a range of heat detection applications.

To demonstrate the technology, sensors have been manufactured for assembly into a four vane hydrophone and as miniature benders. Sensitivity of better than -200 dB re 1V/mPa is forecast for optimised devices. The lack of obvious resonance of the vane hydrophones in the sonar frequency range indicates that the continuos film hydrophones may be most suitable for broad range low-medium frequency operation. High frequency and ultrasonic applications of the sensor technology will involve selective deposition or post deposition scribing to produce the miniaturised sensors.

The developments have demonstrated the efficacy of the technology and the viability of development of sol-gel film sensors for acoustic and pyroelectic applications. Continuous deposition of sol-gel thin film high dielectric constant films provides an opportunity for introduction of a new range of high energy dielectrics.

Hysteresis Curve of a PZT ferroelectric
J series

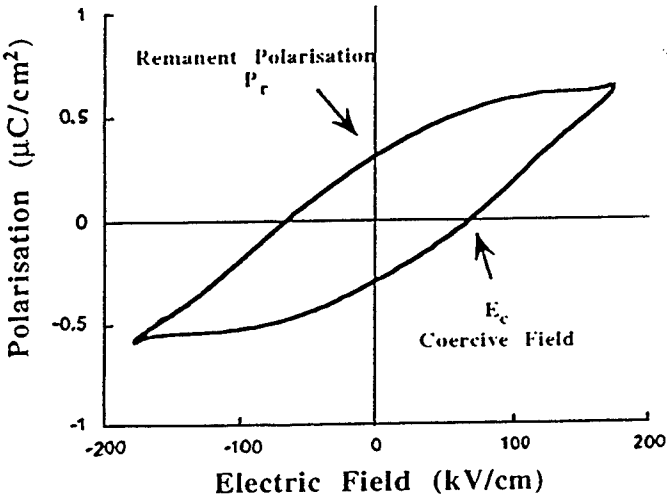

FIGURE 2
Typical hysteresis of thin film piezoelectric on metal foil

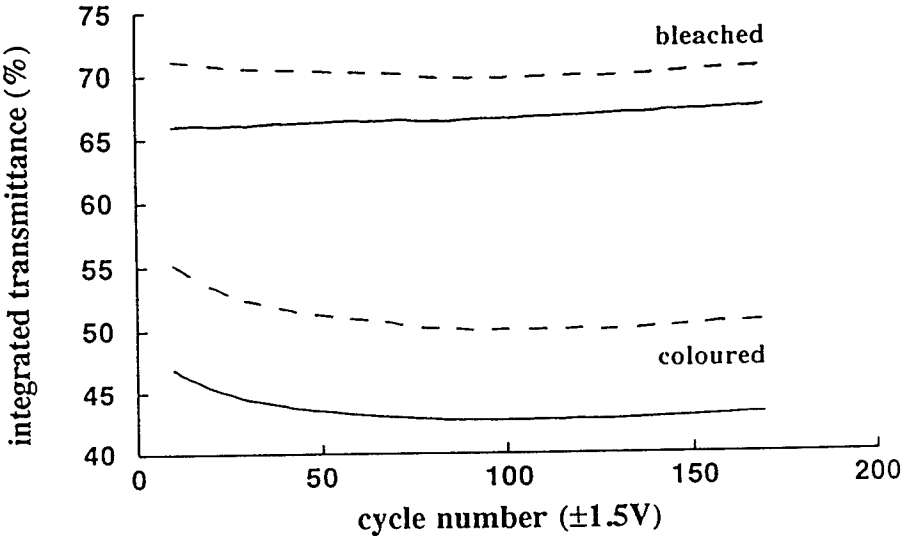

FIGURE 3
The performance of an electrochromic device based on sol-gel deposited WO_3 and sol-gel deposited V_2O_5 as the counter electrode under continued cycling, luminous transmittance; solar transmittance. This device is very consistent over time, and shows an increase in the dynamic range up to 50 cycles. Spectra were recorded every 10 cycles.

SMART WINDOWS

For the past four years, STA has been sponsoring development of SMART WINDOWS at the University of Technology Sydney and Monash University, under a major Energy Research and Development Corporation programme. The research team is developing a window system which is electronically switchable to reduce transmission of solar energy in weather and admit solar energy and reduce loss of internal warmth in the cold weather. Energy savings maximum use of natural light and pleasing aesthetics are the goals. The programme utilises electrochromic sol-gel films. The second phase which will involve building a one square metre pilot SMART WINDOW system was commenced in early 1993. For this phase, the research consortium has been expanded. The project is due for completion in 1996 and commercialisation in 1997.

The electrochromic device performance and reliability have been demonstrated (Figure 2). The development work has two current facets. The first involves increasing the conductivity of the transparent ITO conductor layers to below 10 ohm/sq by means of improved ITO processing in association with novel composite conductor techniques. The second involves investigating both organic and inorganic ionic electrolytes. The organic electrolyte technology involves conducting polymers with improved UV stability.

The project has required extensive investigation of the organometallic behaviour of tungsten, particularly with respect to effects of purity of precursors, moisture content, and processing conditions.

The performance of a laboratory device is shown in Figure 3.

CONCLUSION

Across a wide range of applications, a consortium of Australian research organisations and companies has achieved significant progress over the past five years. The focus of the work has been optimisation of reaction in solution, particularly for the preparation of films of perovskite and spinel compounds, and coatings for glass. Future emphasis will shift towards production techniques.

Key Engineering Materials Vol. 150 (1998) pp. 193-198

Novel Corrosion Resistant Hard-Coatings for Metal Surfaces

G.W. Wagner, S. Sepeur, R. Kasemann and H. Schmidt

Institut für Neue Materialien gem. GmbH,
Im Stadtwald, Gebäude 43, D-66123 Saarbrücken, Germany

Keywords: Corrosion Protection, Ormocers, Coatings, Mechanical Protection

Abstract: Using the sol-gel process, novel inorganic-organic composites (ormocers) were synthesized. By controlled hydrolysis and condensation of an epoxy modified alkoxide, a propyl modified alkoxide and an aluminum alkoxide in the presence of fluoride ions, stable sols can be produced. These can be applied by conventional coating techniques (e. g. spray-, spin-, dip-coating) on metal surfaces (Al, Zn, Mg) and cured thermally. The high corrosion inhibitant properties are explained by a special metal/coating interface. The transparent coatings show good adhesion, corrosion protection and a high wear resistance avoiding chemical pretreatement (e. g. chromating). These new coatings open a wide field of applications.

Introduction

The mechanical and corrosive protection of metal surfaces are questions of current interest. Usual coating materials based on organic polymers show low scratch- and abrasion resistance as well as a lack of resistance to corrosive impact. In several applications pretreatment steps which cause environmental problems (e. g. pickling, etching, chromating) are necessary. Incorporation of inorganic fillers leads to increased scratch and abrasion resistance of the polymer coatings but the resulting coatings are no more transparent. Sol-gel processing of inorganic-organic nanocomposites with molecular or nano-scaled phase dimensions ($\leq$ 5 nm) opens the possibility to achieve transparent coatings with improved properties. The basic principles of the sol-gel processing of inorganic-organic composites by incorporation of organic groupings (network modifiers: alkyl, aryl....; network formers: methacryl, epoxy....) linked to the inorganic backbone formed by hydrolysis and condensation (e. g. starting from alkoxides) are described elsewhere [1-7]. Objective of the present study is to synthesize a transparent sol-gel inorganic-organic composite coating with high scratch and abrasion resistance due to in-situ generation of nano-particles and the achievement of good adhesion and corrosion inhibition by a tailored metal/coating interface.

Experimental

The synthesis of the coating material is shown in figure 1:

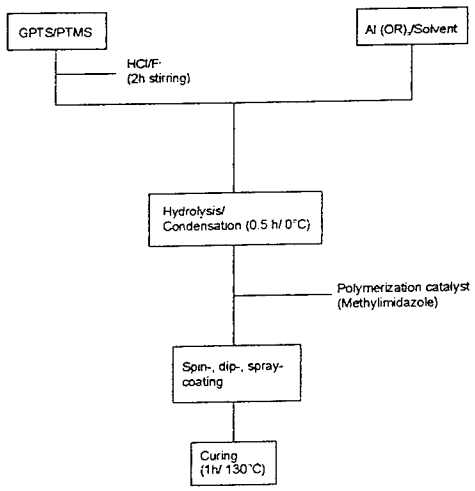

Fig. 1: Synthesis scheme of the coating material [8]

Hydrolysis and condensation were followed by ^{29}Si-NMR spectroscopy [8] and by photon-correlation spectroscopy (PCS) [8, 9] for determination of the synthesized particles in the sol-phase. Coating experiments were carried out by common coating techniques like spin-, dip- or spray coating on the metal surfaces previously degreased with an alkaline surfactant. Curing was carried out at 130 °C/1h.

Results and discussion

γ-glycidyloxipropyltrimethoxysilane (GPTS), propyltrimethoxysilane (PTMS) and an aluminum alkoxide (ASB) were chosen as starting materials for the synthesis. The epoxy group of GPTS generates a poly ethylene oxide network beside the inorganic backbone by organic polymerisation . The propyl containing PTMS is used as an network modifier to increase the relaxation behavior of the material to achieve a more hydrophobic behavior of the material. For determination of the particle growth PCS measurements were performed. No particle generation could be detected during the measurements using HCl catalysis for hydrolysis and condensation of the alkoxides. When a HCl/F$^-$ catalysis was used particle growth was detected within 6h reaction time up to particle sizes of 5 nm (Fig. 2).

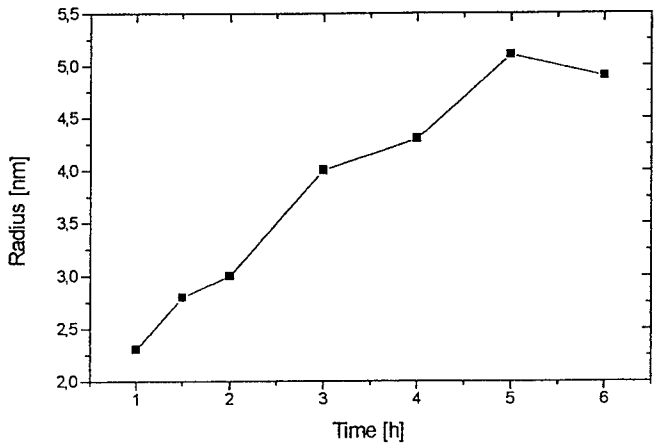

Fig. 2: Particle growth detected by PCS measurements in the system GPTS, PTMS, ASB catalyzed by HCl/F^-

The particle growth caused by the fluoride ions [10, 11] is due to the known behavior of fluoride ions as condensation catalyst.

The coating material was applied by conventional coating techniques (e. g. dip-, spray-coating) on the metal surfaces (Al, zinced steel, Mg) and cured thermally at 130° C. The thickness can be adjusted by variation of the viscosity and the coating conditions between 5 and 25 μm. The transparent coatings show very good adhesion proven by cross cut/pull-off test (DIN 53 151). The adhesion is unaffected after 4 weeks of wet climate test (DIN 50017). The very good wet climate stability is due to the hydrophobic behavior of the propyl chains within the network. Because of the very good adhesion environmentally damaging surface pretreatments like chromating can be avoided. The excellent adhesion can be explained by chemical links formed by condensation of surface hydroxyl groups of the metal with alkoxides as shown in fig. 3.

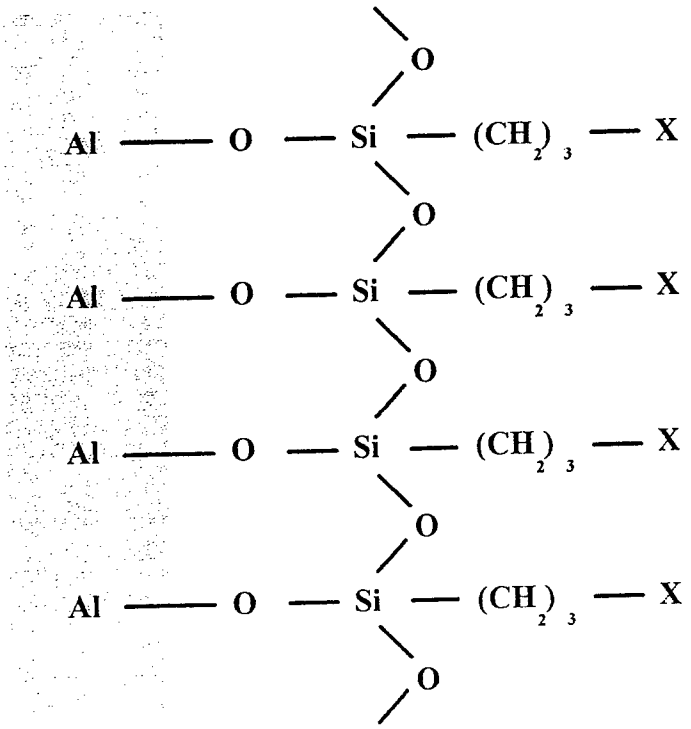

Fig. 3: Scheme of the interface layer metal/coating

The scratch resistance of the coatings was measured by a modified Erichsen test (load on a diamond that is moved on the surface when the first visible scratch on the microscope is detected). The scratch resistance is in the range of 8 to 10 g for the inorganic-organic composite coating in comparison to ≤ 1g for conventional 2-component-epoxy polymer coatings. The abrasion resistance was determined by surface roughness measurements before and after the taber abrader test (100 cycles taber abrader, DIN 52 347) and compared to the 2-component-epoxy coating (fig. 4).

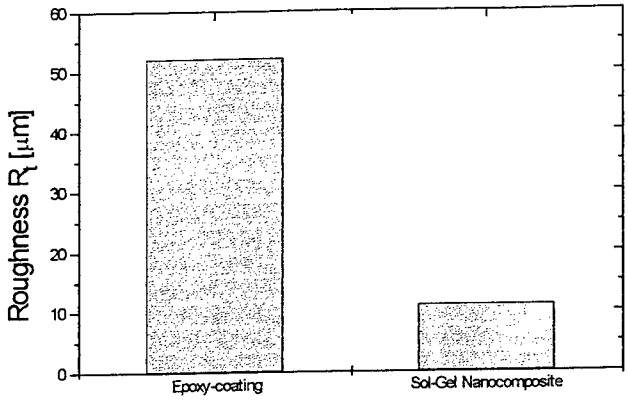

Fig. 4: Surface roughness after taber abrader test for the nanocomposite and the 2-component-epoxy coating (R_t of both coatings before test: 1,2 µm)

The low surface roughness of the nanocomposite coating compared to the epoxy polymer coating (fig. 4) shows the high abrasion resistance of the coating. The high scratch and abrasion resistance of the nanocomposite coating is due to the inorganic backbone and the nanoparticles in the coating.
The corrosion protection properties of the coatings are determined by salt-spray test (DIN 50 021/53 167). Epoxy coated and nanocomposite coated samples with applied cross-cuts before the test, were exposed to salt-spray test for 2 weeks. The epoxy coating shows a high corrosive attack whereas the nanocomposite shows no corrosion. The cross-cuts show no corrosion along the interface of coated and destroyed regions and thereby corrosion inhabitant properties (fig. 5). The reason for this is the very stable tailored metal/nanocomposite interface which act as a chemical link between the metal and the coating.

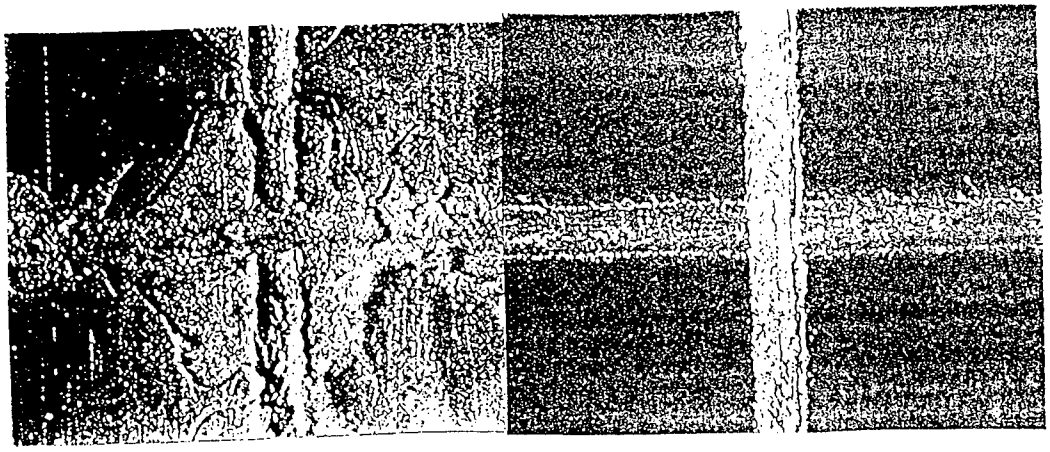

Fig. 5: Comparison between cross-cuts in epoxy coating system (left) and nanocomposite coating on aluminum after 2 weeks salt-spray test

Conclusion

Coating materials for metal surfaces based on inorganic-organic composites could be synthesized by controlled hydrolysis and condensation. The transparent coatings show very good corrosion protective properties because of tailored interface between metal and coating by oxygem bridges. The good scratch and abrasion properties are attributed to the inorganic backbone in combination with in-situ generated particles. These properties open a wide field of applications for example in the car and aircraft industries.

Acknowledgement

The authors want to thank the state of Saarland for financial support.

References

[1] H. Schmidt, B. Seiferling, G. Philip and K. Deichmann; in: Ultrastructure of Processing of advanced Ceramics, J.D. Mackenzie and D.R. Ulrich (eds.), John Wiley & Sons, New York (1988), p. 651.
[2] H. Schmidt; Mat. Res. Soc. Symp. Proc. **171** (1990)3.
[3] H. Schmidt; in Chemical Processing of Advanced Materials, L. L. Hench and J. K. West (eds), John Wiley & Sons, New York (1992).
[4] H. Schmidt, H. Scholze and G. Tünker; J. Non-Cryst. Solids **80** (1989) 557.
[5] H. Schmidt; in Chemical Spectroscopy and Applications of Sol-Gel Glasses; R. Reisfeld, C. K. Joergensen (eds.), Springer, Berlin, Heidelberg (1992).
[6] C. Sanchez; J. Non-Cryst. Solids **147/148** (1992)1.
[7] E. J. A. Pope and J. D. Mackenzie; J. Non-Cryst. Solids **87** (1986) 185.
[8] G. W. Wagner; Master´s Thesis, Saarbrücken (1992).
[9] S. E. Bott; ACS Symposium Series **332** (1985).
[10] J. C. Brinker, G. W. Scherer (eds.); Sol-Gel Science, Academic Press, London (1990).
[11] P. W. J. G. Wijnen, R. A. Van Santen et al., J. Coll. Interface Sci. **145** (1991) 370.

Key Engineering Materials Vol. 150 (1998) pp. 199-208

Characterization of Aluminium Phosphate Gel

Ch. Weber, R. Field and H.H. Höfer

Research & Development Silica/Adsorbents,
Grace GmbH, In der Hollerhecke 1, D-67545 Worms

Keywords: Aluminium Phosphate, Porosity, Thermal Stability, Mechanical Strength

Abstract

The studies presented focus on amorphous aluminum phophate gel (APG) with a P/Al atomic ratio near unity. APG samples were prepared via the inorgnic sol–gel technique. APG has been characterized by composition, nitrogen adsorption, mercury porosimetry, SEM, XRD and TGA/DTA. The effects of heat and ultrasonic treatment on the thermal and mechanical stability have been investigated.

Results: APG materials with pore volumes of 0.80–2.0 $cm^3 \cdot g^{-1}$ and specific surface areas of 240–270 $m^2 \cdot g^{-1}$ remain amorphous upon heat treatment up to 1273 K. Most of the pore volume and specific surface area are maintained after heat treatment at 1073 K. Particle size analysis after ultrasonic exposure reveal that APG particles are mechanically stable.

1 Introduction

The use of amorphous aluminum phosphates with near stochiometric composition has been described in various catalytic applications such as skeletal isomerisation [1] , alkylation [2,3], and dehydration [4]. In a review, Moffat [5] relates the structure of various orthophosphates including $AlPO_4$ to their catalytic properties. Reference [6] discloses zeolite/$AlPO_4$ containing fluid cracking catalysts that are particular selective for the production of C_3 and C_4 olefins. The regioselective liquid phase 1,4−hydrogenation of benzylidene ketones using $Rh/AlPO_4$ is described by Cabello et al. [7]. $Cr/AlPO_4$ systems for the polymerization of olefins have been investigated by McDaniel [8,9]. Besides catalytic applications, aluminum phosphate gels (APG) have been found useful as starting materials for the synthesis of aluminum phosphate molecular sieves [10−12].

In this work, we focus on the characterization of large−pore APG materials which have most of their surface area and pore volume in highly accessible pores. Furthermore, we investigate the thermal stability and mechanical strength of APG since high thermal and mechanical stability is required in many industrial catalytic operations.

2 Experimental

2.1 Preparation

The aluminum phosphate gels were prepared as in Reference [13]. A typical preparation procedure is given in Figure 1:

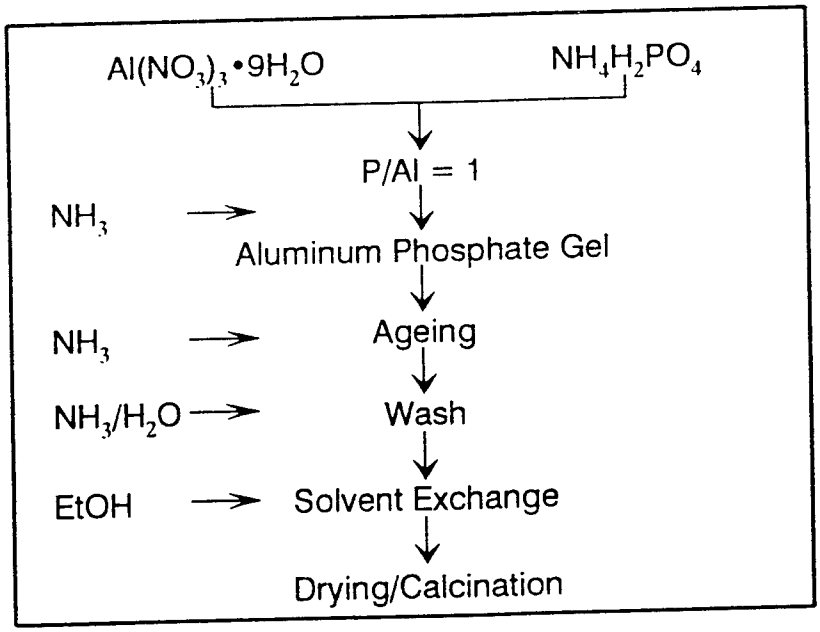

Fig. 1 Typical preparation of APG

2.2 Analyses

Elemental analyses were performed by ICP–AES using a 3580 ARL instrument. The specific surface areas and pore volumes in the pore diameter range 16–600 Å were measured by nitrogen adsorption at 77 K with a Micromeritics ASAP 2400. The specific surface area was calculated according to the BET method [14]. The N_2 pore volume was calculated at a relative pressure of 0.967 according to Reference [15]. The surface area and pore volume distributions were calculated according to the BJH method [16]. The pore volume of macropores between 600–10.000 Å has been measured by Hg porosimetry with a Micromeritics Autopore 9220 (Hg contact angle: 140 °; Hg surface tension: 0.485 $N \cdot m^{-1}$).

Scanning electron microscopy was carried out using a JEOL JXA–840A (coating: Au/Pd; accelerating voltage : 5 kV; working distance: 14 mm).

APG samples (ca. 20 g each) were calcined in a Nabertherm N50 muffle furnace at various temperatures between 873–1273 K for 1 h. XRD patterns were recorded with a Siemens D500TT Diffraktometer (Cu K_{alpha} ; 30 mA/42 kV; 3–70 ° 2 *theta*).

Thermal analyses were carried out using DuPont Instruments 951 Thermogravimetric Analyzer (TGA) and 910 Differential Scanning Calorimeter (DTA) applying a 10 $K \cdot min^{-1}$ heating rate in the temperature range of 293–1373 K (TGA) and 293–1273 K (DTA) respectively.

The mechanical stability of APG was investigated by exposing 2 % (w/w) aqueous suspensions to ultrasonic radiation, using a Branson Sonifier B–12 (20 kHz/65W) followed by particle size analysis using a Coulter Counter TAII (560 μm orifice).

3 Results and Discussion

Reported in Table 1 are properties of three APG materials with similiar composition but increasing porosities.

Tab. 1 Physico–chemical properties of APG samples

Sample		APG–1	APG–2	APG–3
N_2–PV *	$cm^3 \cdot g^{-1}$	0.85	1.16	1.38
Hg–PV #	$cm^3 \cdot g^{-1}$	0.05	0.21	0.61
PV_{total} $	$cm^3 \cdot g^{-1}$	0.90	1.37	1.99
N_2–BET	$m^2 \cdot g^{-1}$	240	269	256
P/Al	atomic ratio	0.96	0.99	0.99

* N_2 pore volume in the pore diameter range of 16–600 Å

Hg pore volume in the pore diameter range of 600–10.000 Å

$ Sum of N_2 and Hg pore volume

Figure 2 shows scanning electron micrographs of the irregularly shaped APG−1 and APG−3 particles.

(a) APG-1 single particle

(b) APG-1 general area micrograph

(c) APG-3 single particle

(d) APG-3 general area micrograph

Fig.2 Scanning electron micrographs

Figure 3 demonstrates that most of the pore volume and specific surface area of the samples is associated with pore diameters larger than 100 Å.

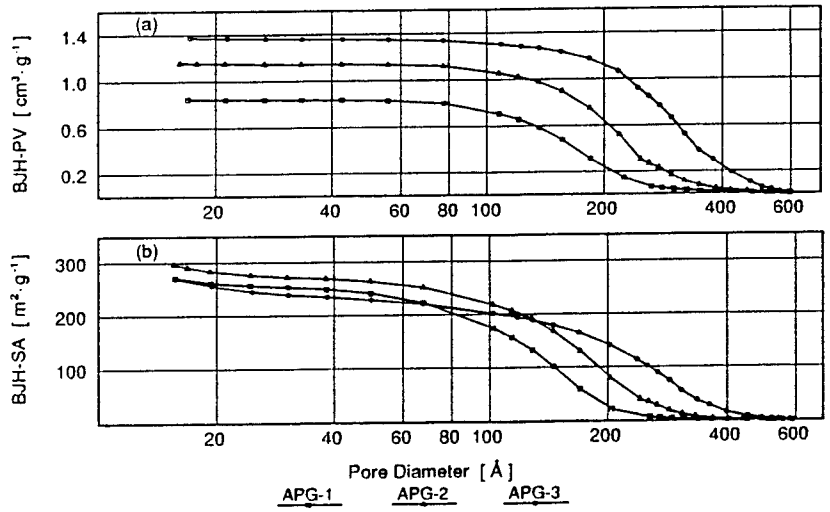

Fig. 3 BJH cummulative nitrogen pore volume (a) and surface area (b) distributions

In Figure 4 the cumulative N_2 pore volume distributions are compared to the respective distributions obtained by Hg intrusion porosimetry.

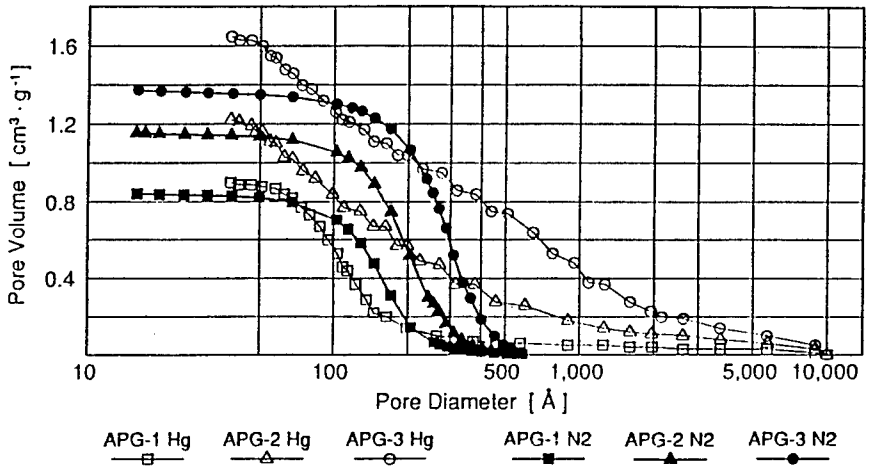

Fig. 4 Cummulative N2 and Hg pore volume distributions

From the Hg intrusion curves it can be seen that APG−2 and APG−3 exhibit some porosity associated with pores larger than 600 Å diameter, as also evidenced by the N_2 adsorption isotherms given in Figure 5, which shows non−saturated curves for samples APG−2 and APG−3 at a relative pressure of 1.

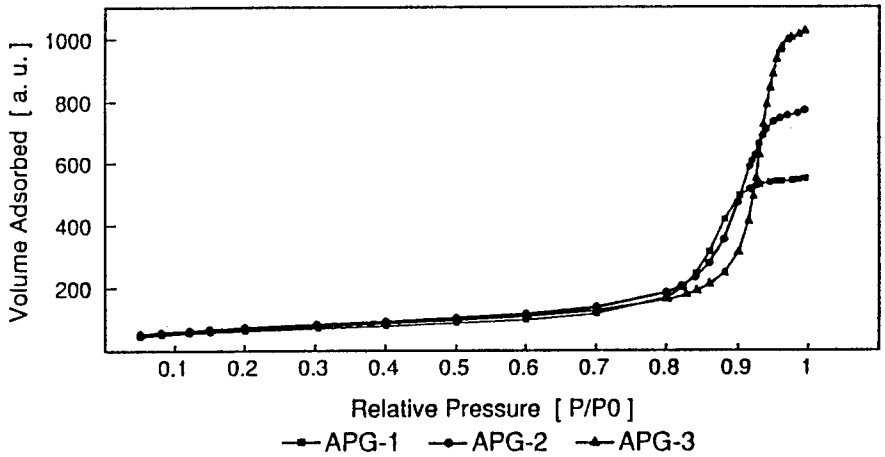

Fig. 5 Nitrogen adsorption isotherms

The Hg pore volume distributions deviate from the N_2 curves in the pore diameter range below 600 Å for reasons discussed in [17−19]. The higher the pore volume, the less agreement is observed especially in the pore diameter range below 100 Å where according to [19] the high pressures exerted are causing compaction or damage the porous structure.

The TGA profiles for APG–1 and APG–3 are depicted in Figure 6. For both materials, a single mass loss step is observed due to the release of adsorbed water. At low temperatures, a small moisture uptake can be seen. The corresponding DTA profiles (Figure 7) of both gels are also qualitatively equivalent. However, the broad endotherm of APG–3 centered at 372 K versus 393 K observed for APG–1 reflects the release of water at a lower temperature from the more open pore structure of APG–3.

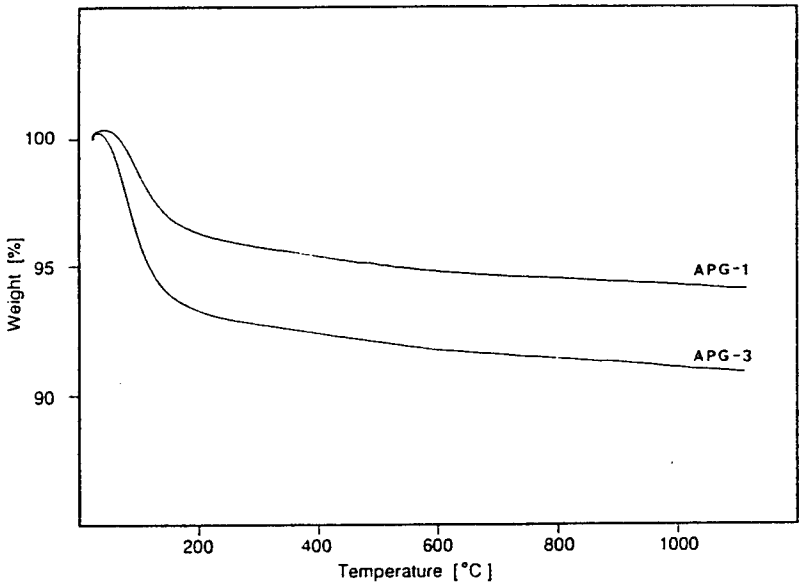

Fig. 6 TGA profiles of APG–1 and APG–3

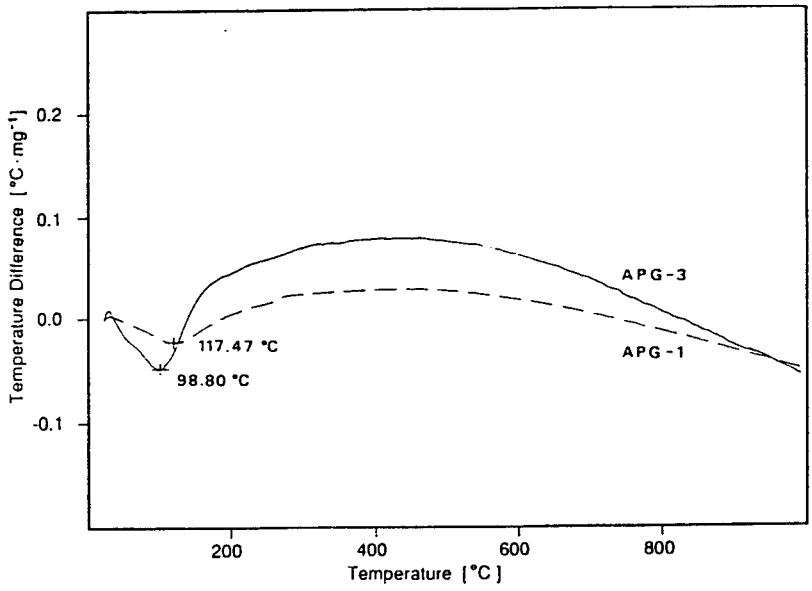

Fig. 7 DTA profiles of APG–1 and APG–3

As depicted in Figure 8, the surface area and the pore volume remain unchanged upon calcination up to 1073 K. Beyond that temperature sintering occurs .

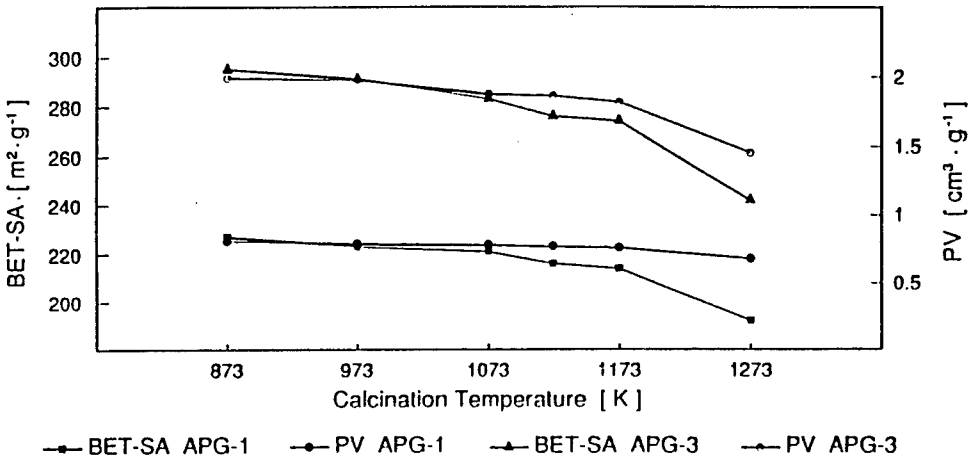

Fig. 8 Effect of calcination temperature on PV and BET-SA

The XRD patterns given in Figure 9 demonstrate the isostructural relationship of APG with silica gel. It also confirms the DTA results: no phase transformations are observed upon calcination up to 1273 K. APG remains amorphous up to this temperature.

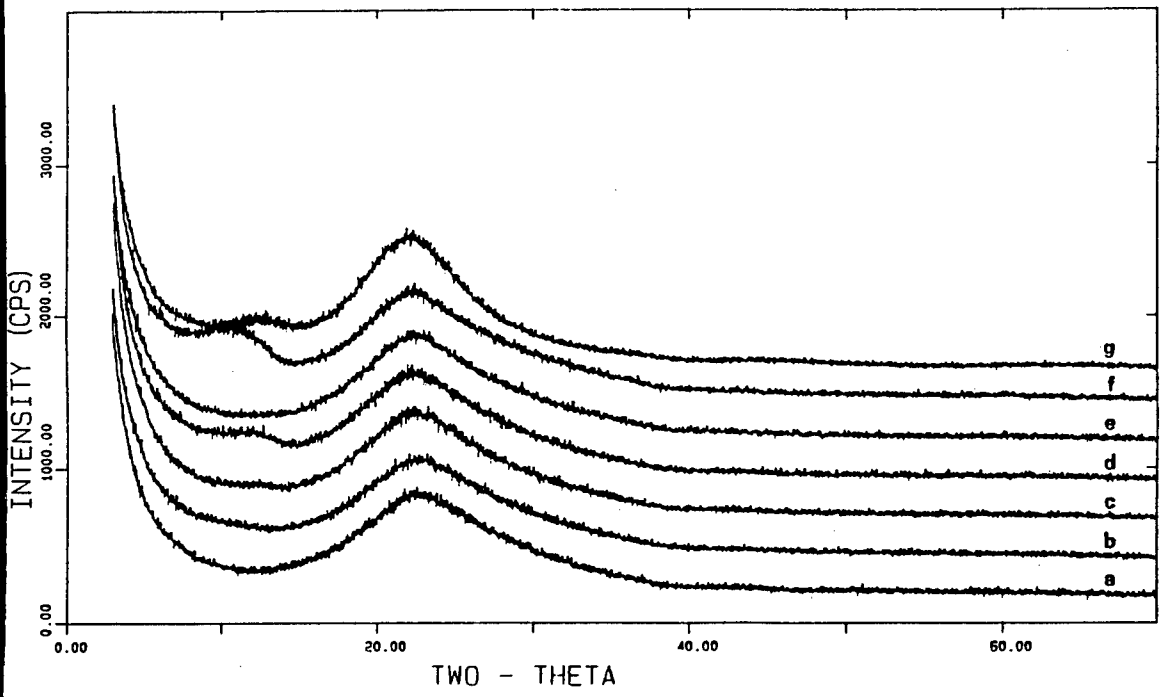

Fig. 9 XRD patterns of APG–1 calcined at 873 K (a), 973 K (b), 1073 K (c), 1123 K (d), 1173 K (e), 1273 K (f) and Grace Davison Silica Grade 332 as a reference (g)

Figure 10 depicts the effect of ultrasonic exposure on the median particle size (d_{50}) of the APG−1 and APG−3 samples. For comparison, the corresponding data for a silica gel carrier known to have good attrition resistance in polyolefin catalysis are also given. As can be seen the median paricle sizes are not affected indicating that aluminum phosphate gels are mechanically at least as stable under the given conditions as a conventional silica carrier for polyolefin catalysts.

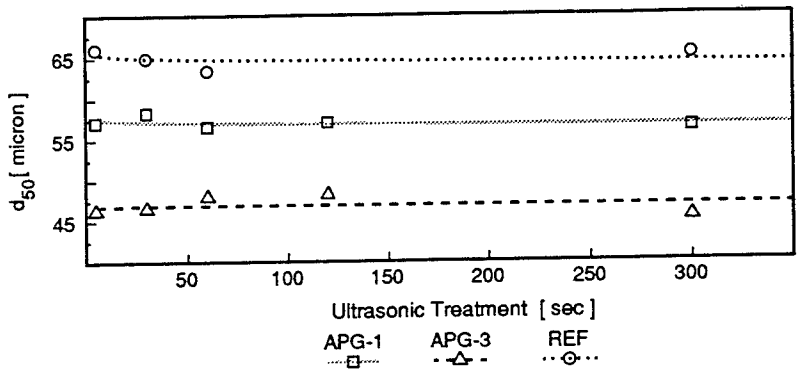

Fig. 10 Effect of ultra sonic treatment on median particle size (d_{50})

4 Conclusions

Aluminum phosphates prepared by precipitation usually do not possess large pores nor do they have sufficient mechanical strength to be used in industrial catalysis. However, the aluminum phosphate gels prepared by the aqueous inorganic sol−gel route have pore volumes in the range of 0.80−2.0 $cm^3 \cdot g^{-1}$ and exhibit most of their specific surface area (240−270 $m^2 \cdot g^{-1}$) in accessible pores larger than 100 Å in diameter. Most of the pore volume and specific surface area are maintained after heating to 1073 K. APG remains amorphous up to 1273 K. Since the median particle size is unaltered by irradiation with ultrasound, the APG particles are mechanically stable.

5 References

[1] J. M. Campelo, J. M. Gutierrez, D. Luna, J. M. Marinas, Can. J. Chem. **61**, 2567 (1983)

[2] J. M. Campelo, A. Garcia, D. Luna, J. M. Marinas, M. S. Moreno, Bull. Soc. Chim. **2**, 283 (1988)

[3] A. Blanco, J. M. Campelo, A. Garcia, D. Luna, J. M. Marinas, A. A. Romero , J. Catal. **137**, 51 (1992)

[4] M. A. Aramendia, J. M. Campelo, S. Esteban, C. Jimenez, J. M. Marinas, J. V.Sinisterra, Rev. Inst. Mex. Petrol. **12**, 61 (1980)

[5] J. B. Moffat, Catal. Rev.–Sci. Eng. **18**, 199 (1978)

[6] T. G. Roberie, EP A1 0 496 226 (1992) to W.R. Grace & Co.

[7] J. A. Cabello, J. M. Campelo, A. Garcia, D. Luna, J. M. Marinas, J. Org. Chem. **51**, 1786 (1986)

[8] M. P. McDaniel, M. M. Johnson, J. Catal. **101**, 446 (1986)

[9] M. P. McDaniel, M. M. Johnson, Macromolecules **20**, 773 (1987)

[10] S. T. Wilson, B. M. Lok, C. A. Messina, T. R. Cannan, E. M. Flanigan, J. Am. Chem. Soc. **104**, 1146 (1982)

[11] S. T. Wilson, B. M. Lok, C. A. Messina, E. M. Flanigan, Proc. 6th Int. Zeolite Conf., 97 (1985)

[12] X. Ren, S. Komarneni, D. M. Roy, Zeolites **11**, 142 (1991)

[13] R. Glemza, Y.O. Parent, W. A. Welsh, Div. Pet. Chem., Am. Chem. Soc., **36**, 469 (1991)

[14] S. Brunauer, P. H. Emmett, E. Teller, J. Am. Chem. Soc. **60**, 309 (1938)

[15] E. W. Lard, S. M. Brown, J. Catal. **25**, 451 (1972)

[16] E. P. Barrett, L. G. Joyner, P. P. Halenda, J. Am. Chem. Soc. **73**, 373 (1951)

[17] L. G. Joyner, E. P. Barrett, R. Skold, J. Am. Chem. Soc. **73**, 3155 (1951)'

[18] A. M. L. Hustings, J. J. F. Scholten, Adsorpt. Sci. Technol. **4**, 241 (1987)

[19] B. D. Adkins, B. H. Davis, Adsorpt. Sci. Technol. **5**, 168 (1988)

Key Engineering Materials Vol. 150 (1998) pp. 209-218

Advanced Manufacturing Process for ZnO Surge Arrester Disks

G.H. Wiseman

Raychem Corporation, Surge Arrester Systems,
300 Constitution Drive, Menlo Park, CA 94025-1164, USA

Keywords: Chemical Process, Lightning Protection, Metal Oxide Varistor, Overvoltage Protection, Surge Arrester, ZnO Ceramic

Abstract
In 1968, Dr. Matsuoka and his colleagues at Matsushita Electric Company discovered the devices which are now called metal oxide varistors. These materials, consisting of ZnO mixed with small quantities of bismuth and other metal oxides, can have extremely non-linear voltage-current behavior. Unfortunately, the performance of these devices is often limited by the mechanical powder mixing technology (e.g. ball-milling) typically used in production. Raychem has developed and scaled-up a chemistry-based manufacturing process for ZnO varistor powder. This new process, which eliminates all of the disadvantages of the conventional mixing processes, is described in comparison with the traditional methods. Some electrical performance characteristics of the surge arrester disks made from this powder are also presented.

History of ZnO Varistor and Surge Arrester Development
In 1968, Dr. Matsuoka and his colleagues at Matsushita Electric Company discovered that ceramic devices made from ZnO mixed with small quantities of bismuth and other metal oxides can have extremely non-linear voltage-current behavior.[1] Other researchers had observed this effect in ZnO before Matsuoka, but apparently had not recognized its significance.[2] Surge arresters containing ZnO ceramics are now providing superior overvoltage protection for all types of electrical networks, ranging from 12 volts to over 1 million volts.

A typical current-voltage curve for a Raychem ZnO surge arrester disk and some common terminology are shown in Figure 1. These devices have extremely non-linear current-voltage characteristics - in certain voltage ranges they conduct 10 orders of magnitude more current after only a two-fold increase in voltage. The surge arresters are typically connected in parallel to the power system and earthed. At normal operating voltages, the devices act like insulators. However, if an overvoltage occurs due to a lightning strike for example, the ZnO surge arrester becomes conductive and diverts the excess energy to ground. The voltage on the system is thus limited or "clamped" to a safe level and other equipment on the network is protected.

The main advantage of ZnO-type surge arresters compared to previously used materials, e.g. SiC-type arresters, was that they could be applied directly to the voltage source without isolating gaps. This feature eliminated a major source of complexity and unreliability in these types of devices. The first gapless ZnO arrester design for high voltage surge arresters was developed by the General Electric Corporation in 1976. [3] These ZnO surge arresters have indeed had an excellent overall service record compared to SiC arresters and other forms of overvoltage protection. Raychem improvements to ZnO technology are built upon this fine general record of performance for ZnO-based materials.

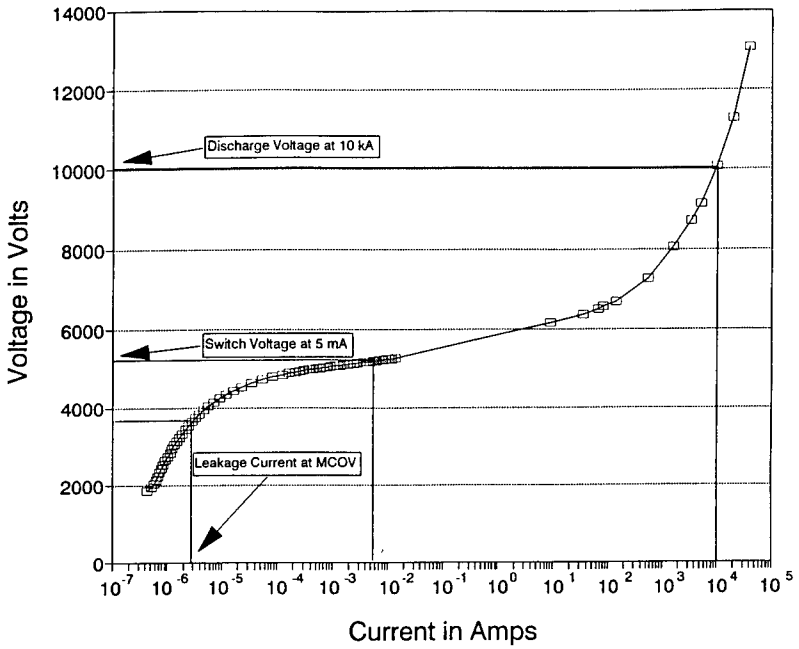

Figure 1 - I-V curve for Raychem ZnO disk

One major problem with some early ZnO materials was that the leakage current or watts loss increased with time. This increase could be accelerated by temperature and followed an Arrhenius relationship, as shown in Figure 2. Thus, it is now common to test ZnO devices for 1000 hours at 115°C because this test represents approximately 100 years life. Raychem and other manufacturers have made substantial improvements to the ZnO arrester performance so that the watts loss no longer increases with time. A typical watts loss versus time plot for a Raychem ZnO disk is shown in Figure 3. However, not all manufacturers have solved this problem. Some manufacturer's arresters still have increasing watts loss when the surrounding atmosphere is depleted of oxygen.[4]

Voltage Non-linearity Mechanism in ZnO Varistors

A schematic of a typical ZnO varistor is shown in Figure 4. The varistor has a composite-type microstructure, with ZnO grains separated from each other by grain boundaries. These grain boundaries consist of bismuth and other metal oxides, and are responsible for the voltage non-linear properties. In order for the varistor to work properly, the dopant metal oxides must be well-distributed within the ZnO ceramic body, and ideally should uniformly coat the ZnO grains.

Each one of the ZnO grain/grain boundary/ZnO grain interfaces has non-linear behavior, with a "switch voltage" (defined as the voltage at 1 mA current) of approximately 3 volts.[5] The switch voltage of any device is equal to the number of grain boundaries in the ceramic times the voltage per grain boundary. A typical surge arrester disk which is 3 cm in height will have approximately 1700 grains in a path from top to bottom, and therefore will have a switch voltage of approximately 5000 volts.

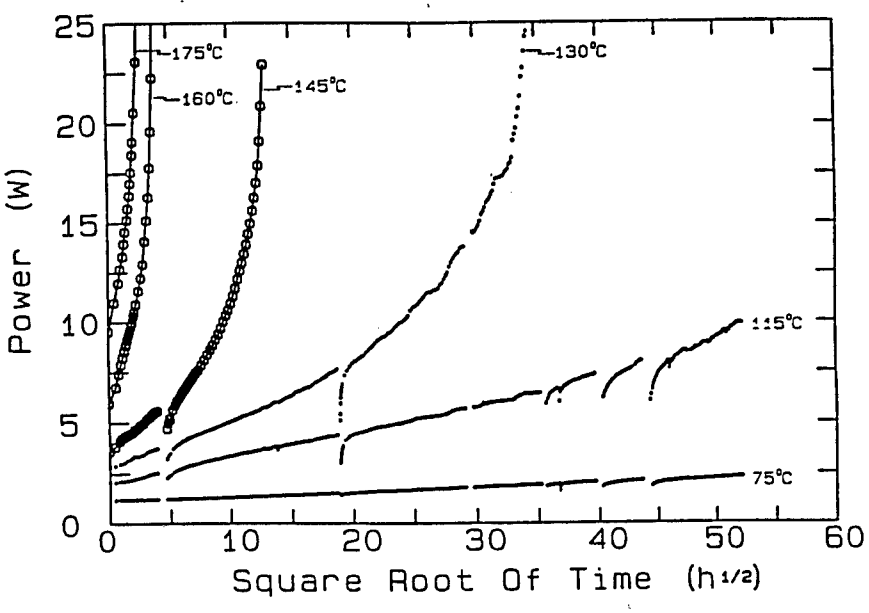

Figure 2 - Watts loss/time curves at various temperatures for early ZnO materials

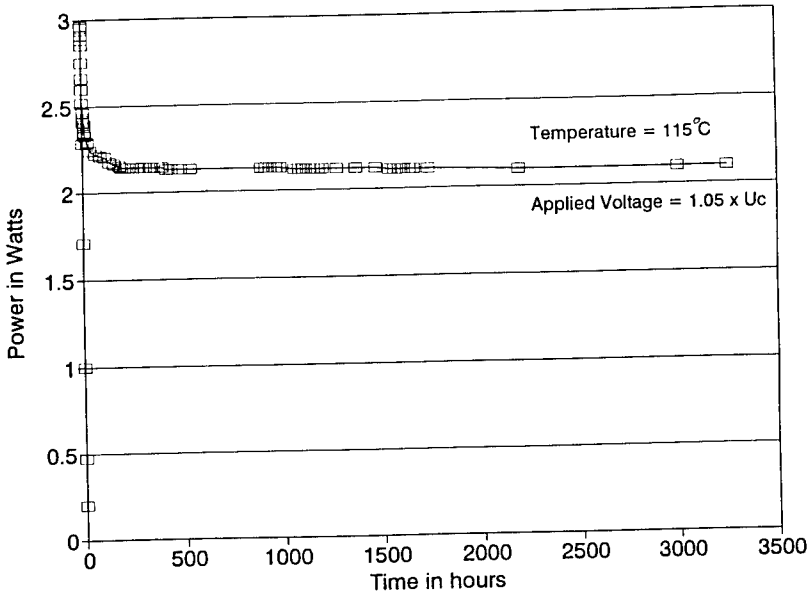

Figure 3 - Watts loss/time for Raychem ZnO disk at 115°C

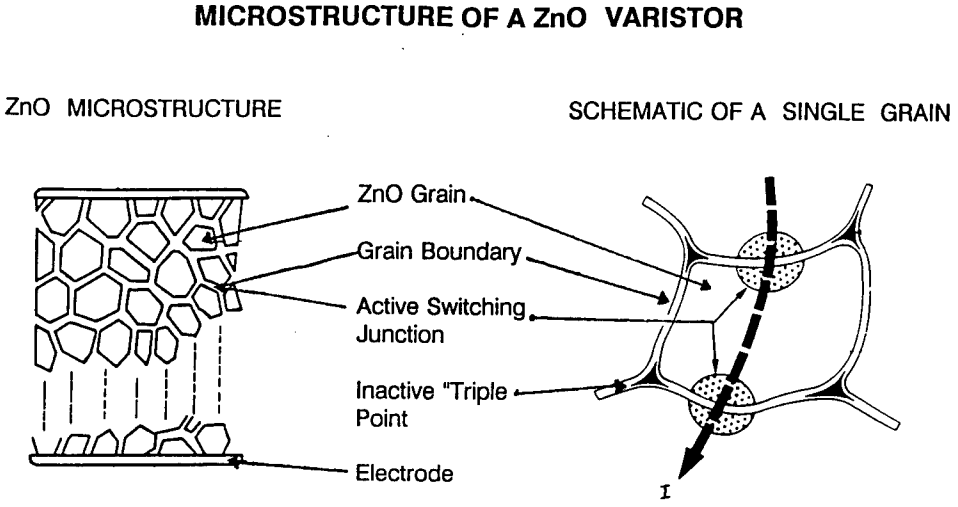

Figure 4 - ZnO grain/grain boundary structure

It is now widely believed that the switching mechanism in ZnO varistors is best described as a "back-to-back" Schottky barrier, as shown in Figure 5. At low voltages, the barrier prevents current from flowing in the device. However, when the voltage across the barrier is high enough, electrons will "tunnel" across the barrier and current will flow. Thus, the devices exhibit non-linear current flow as a function of voltage.

It is extremely important that the current flows uniformly throughout the ZnO varistor. If a large current flows in a small region of the device, punctures and cracks may form there and the surge arrester may fail. Other more subtle problems may also occur in non-uniform devices, such as excessive leakage current at normal voltages, or the deformation of the Schottky barriers during high current impulses. The major focus of Raychem's technical work has been to develop ZnO materials which conduct current in a uniform manner.

A Comparison of Manufacturing Processes for ZnO Surge Arresters

Seven years ago at Raychem, we began to work on advanced processes for making ZnO powder.[6] At the time, we believed that the most important step in the manufacturing process was the mixing of the ZnO and the other metal oxides which make up the grain/grain boundary structure discussed previously. We are now convinced that our hypothesis was correct, and that we can achieve improved performance by concentrating on this mixing step. The differences between our new process and the conventional manufacturing process will now be compared.

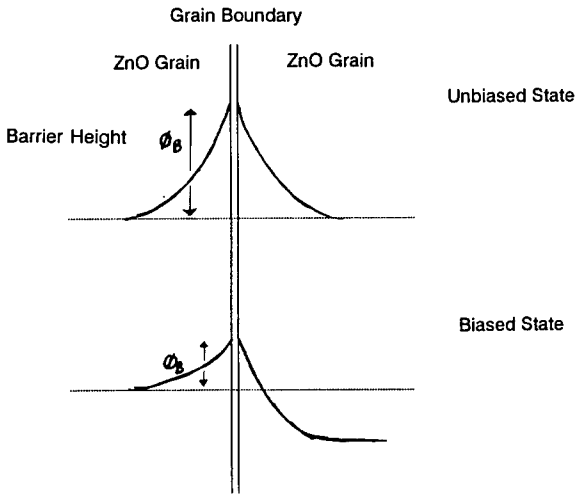

Figure 5 - Back-to-back Schottky barrier model for ZnO varistor

The conventional method for making the ZnO powder formulation is to mix the pure ZnO powder with other metal oxide powders in a ball mill or other mechanical mixing equipment. This type of mixing technology has been used since the earliest recorded era of ceramics processing. A typical manufacturing process diagram is shown in Figure 6. The metal oxide dopants are premixed in ball mill to reduce the particle size of the powders. The dopant mixture is then added to the ZnO powder and the two are mixed in a large ball mill or circulating attrition mill. This mixed powder is then spray-dried and "calcined" (heated to about 900°C) to begin forming the grain boundaries. However, the powders are usually not mixed well enough at this stage, so the manufacturer must grind up the powder again. The mixture is then spray-dried again before it is pressed into disks.

Unfortunately, there are several major problems when this technique is used to make ZnO powder for varistors:

1. At best, a random mixing of the ZnO and dopant metal oxide powders can be produced, as shown in Figure 7. Because the dopant oxides are used in small concentration, very few particles are actually present relative to the number of ZnO particles. In order for a uniform varistor microstructure to be produced, these few dopant particles must somehow diffuse throughout the ceramic.

2. It is usually impossible to grind the dopant powders into particles as small as the ZnO particles. Thus, even the mixing of particles shown in Figure 7 is optimistic.

3. The grinding process can introduce contamination in the powder from the grinding materials and the equipment.

4. Because the materials are poorly mixed, the powder must be sintered or fired at a very high temperature. Unfortunately, bismuth oxide can evaporate at high temperatures, contaminating the oven or the atmosphere,[7] and leading to intrinsic process variability.

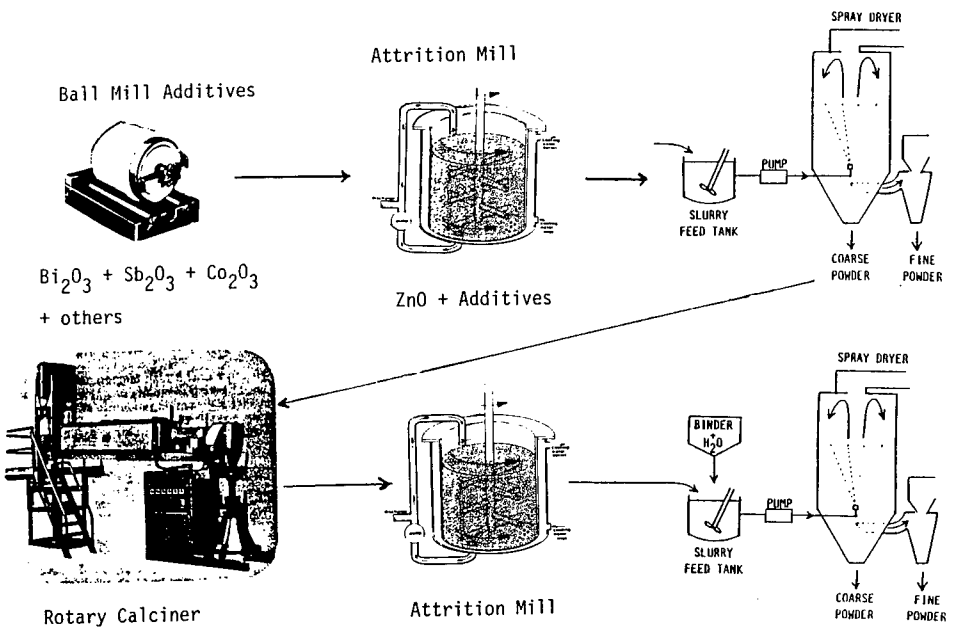

Figure 6 - Conventional ZnO Powder Manufacturing Process

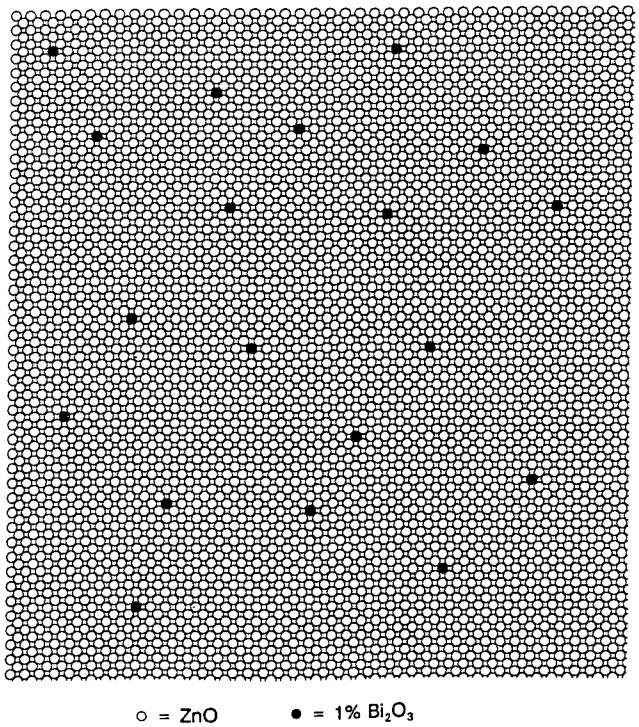

Figure 7 - Random mixing of ZnO and "dopant" powder as in conventional powder manufacturing process

Raychem ZnO Manufacturing Process

Raychem has developed a manufacturing process for ZnO varistor powder which eliminates all of the disadvantages of the conventional mixing process.[8] A schematic of the Raychem process is shown in Figure 8. An aqueous slurry of ZnO powder is combined with a chemical solution of the dopant metals. The two slurries are mixed together in a continuous process. A chemical reaction occurs in the reactor and the ZnO powder is coated with the dopant metals. A scanning electron micrograph showing the coated ZnO powder is shown in Figure 9. This uniformly coated ZnO powder is very much like the fired ceramic varistor in its final form.

The advantages of the Raychem powder-making process are as follows:

1. The ZnO powder is uniformly mixed with the dopant metal oxides, thus improving the uniformity of the fired ZnO varistor. In addition, the particle size of the dopants is substantially smaller than that of the ZnO resulting in a higher intrinsic degree of mixing.

2. There is no need to grind the powders. The continuous chemical process is readily controlled and easy to reproduce.

3. There is almost no possibility for chemical contamination to be introduced.

4. Because of the intimate mixing of the dopants and ZnO, the material may be fired at low temperature, thus eliminating the problem of bismuth oxide evaporation.

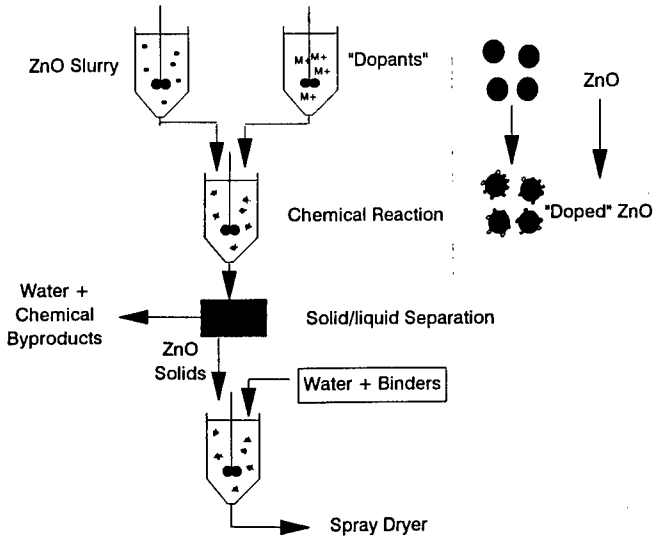

Figure 8 - Raychem Advanced ZnO Manufacturing Process

Once the powder is made, the remaining steps in the Raychem disk manufacturing process are not unusual, and are shown in Figure 10. Thus, the powder is mixed with an organic binder, spray dried, and then pressed into disks. The binder material is carefully burned-out, and the disks are fired in a continuous oven. After firing, the sides of the dense ceramic disks are coated with an epoxy material. The faces of the disks are then ground flat and parallel, and an aluminum electrode is sprayed onto each face. Finally, each disk is tested to a rigorous specification prior to assembly in the surge arrester.

Raychem has now successfully scaled-up this new powder manufacturing process. Although other manufacturers are working on similar improvements in ZnO powder manufacturing, Raychem is the only manufacturer with such a chemical process in commercial production.

Performance Advantages of Raychem ZnO Disks

Because of our unique powder manufacturing process, Raychem ZnO disks exhibit the following improved performance characteristics:

1. Low leakage current/watts loss:
   Low leakage current is produced when the grain boundary barriers are well-formed and the grain size is uniform.

2. Low discharge voltage:
   Low discharge voltages are produced when the ZnO grains are properly "doped" to make them conductive.

3. Impulse Stability:
   Impulse stability is defined as the lack of change of leakage current or watts loss after a high current impulse, e.g. 65 kA or 100 kA lightning strike. High quality ZnO surge arresters show relatively little change in leakage current after repeated impulses, as shown for Raychem disks in Figure 11.

4. Energy Handling Capability:
   Energy handling capability is defined as the ability of the surge arrester to absorb a large energy surge without being damaged, and is expressed as kJ/kV of rating or as J/cc of disk volume. At Raychem, we have found that ZnO surge arresters are most susceptible to damage from impulses of 50 to 100 A/cm^2 of electrode area. Therefore, we may conservatively rate our distribution arrester at 2.7 kJ/kV rating (200 J/cc) based on its ability to withstand 2 msec square wave impulses of 500 amps. (Other manufacturers may use different criteria to rate their energy handling capability). The Raychem HDA arrester with 42 mm diameter disks will also pass the IEC 100 kA high current test.

5. Temporary Overvoltage (TOV) Withstand:
   Excellent TOV performance comes from good energy handling capability and also from the ability of the manufacturer to precisely control the current-voltage characteristics of the surge arrester.

We have also found the chemical manufacturing process can be controlled so that these characteristics are produced on a consistent basis.

Figure 9 - Transmission Electron Micrograph of Raychem ZnO Powder

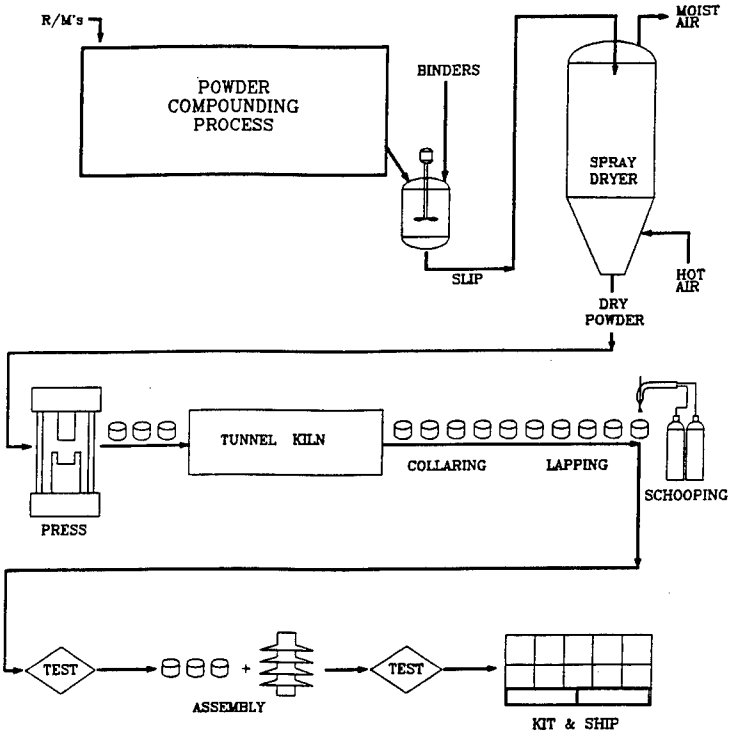

Figure 10 - Raychem ZnO disk manufacturing process

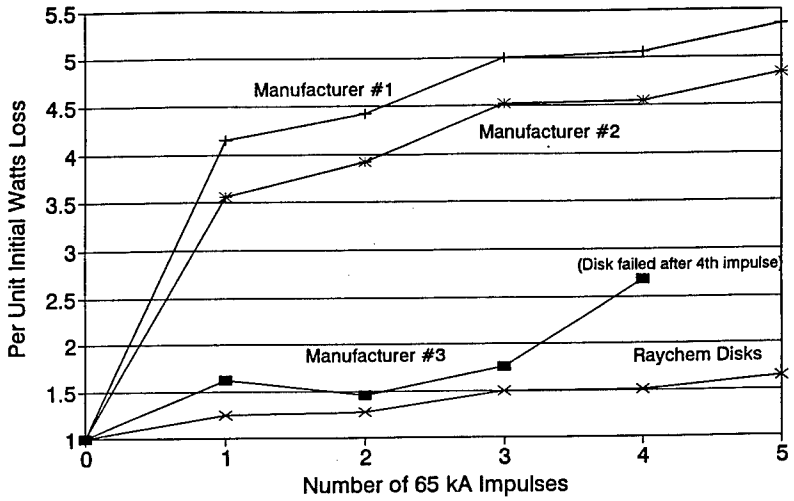

Figure 11 - Impulse stability (watts loss change) of various ZnO disks after 65 kA impulses

Summary and Conclusion

Raychem has developed and commercialized a chemical process for manufacturing ZnO powder. As a result of this unique process, Raychem can produce ZnO disks which have improved electrical performance characteristics. These disks are used in high performance surge arresters which provide increased protection and reliability for electrical networks.

References

[1] M. Matsuoka, pp. 3-9 in Ceramic Transactions Vol. 3 - Advances in Varistor Technology. Edited by L.M. Levinson, The American Ceramic Society, Inc., Westerville, Ohio, 1989.
[2] M.S. Kosman and E.G. Pettsold, Leningrad Gosvdarst Pedagog Inst. **207,** 191 (1961).
[3] E.C. Sakshaug, J.S. Kresge, and S.A. Mischke, Jr., IEEE Trans. on Power App. & Systems **96** [2], 647 (1977).
[4] H. Knobloch, R. Göhler, W. Kühne, K. Reichelt, H.B. Solbach, R. Bruchhaus, and W. Holubarsch, IEEE Trans. on Power Delivery **6** [2], 680 (1991).
[5] J.T.C. van Kemenade and R.K. Eijnthoven, J. Appl. Phys. **50** [2], 938 (1971).
[6] M.S. Thompson and G.H. Wiseman, Ceram. Int. **15** [5], 281 (1989).
[7] N. Russell, Industrial Heating **June**, 42 (1986).
[8] M.S. Thompson, G.H. Wiseman, and E.S. Sherman, US Patent 5,039,452, 13 August 1991.

Acknowledgments

The author wishes to thank Jeff Bennett, Mark Green, Tom Bialek and Derek Leong for valuable assistance in preparing and reviewing this paper.

Key Engineering Materials Vol. 150 (1998) pp. 219-226

Preparation and Properties of Poly(Vinyl Acetate)/Silica-Gel Hybrids Obtained by Sol-Gel Process: Effect of Methyl Groups in Silicon Alkoxide

S. Yano[1], M. Kodomari[2] and T. Furukawa[2]

[1] National Institute of Materials and Chemical Research, 1-1 Higashi, Tsukuba Ibaraki 350, Japan

[2] Shibaura Institute of Technology, 3-9-14 Shibaura, Minato-ku, Tokyo 108, Japan

Keywords: Poly(Vinyl Acetate), Copoly(VAc/VTES), Hybrid, Tetraethoxysilane, Methyltriethoxysilane, Dimethyldiethoxysilane, Sol-Gel Process

Abstract

A copolymer of vinyl acetate (VAc) and vinyl triethoxysilane (VTES) having molar ratio of 9:1 was synthesized and incorporated with silica-gel by the sol-gel process. Tetraethoxysilane (TEOS), methyltriethoxysilane (MTES), and dimethyldiethoxysilane (DMDES) were used as silicon alkoxides. The tensile strength of copoly(VAc/VTES)/silica-gel hybrids was higher than that of PVAc/silica-gel hybrids because of strong bonding between copolymer and silica-network. The strength of the copolymer hybrids prepared from TEOS and MTES increased up to 50 MPa and 43 MPa, respectively. On the other hand, the strength of the hybrid from DMDES decreased with DMDES content. The elongation of the hybrids increased by mixing 20 wt% of MTES and DMDES. The dynamic modulus, G', of the hybrids increased when they were prepared from TEOS and MTES. DMDES having two methyl groups in the alkoxide chain, decreased the G' value of the hybrid. The tan δ peak position of the hybrids from TEOS and MTES shifted to a higher temperature range with increasing amounts of mixed silicon alkoxides, but DMDES lowered the tan δ peak temperature.

Introduction

The sol-gel process involving hydrolysis and polycondensation reactions of metallic alkoxide is a new process to produce ceramics at low temperature. The production of high-performance or high-functional materials has recently been paying close attention to unique hybrids composed of organic polymers and ceramics such as silica[1,2], alumina[3], titania[4], and zirconia[5]. As organic components, various kinds of polymers such as polydimethyl siloxane[2, 6], poly(ethylene-oxide)[7], polyoxazolines[8], and polyimide[9,10] have been used. These hybrids have combined characteristics of organic polymers (low density, toughness, flexibility, formability, etc.) and ceramics (surface hardness, transparency, high modulus, high strength, heat-resistance, etc.). Organic polymers can be easily incorporated in ceramics by the sol-gel process. A solution of organic polymer is mixed with alkoxide, e.g. tetraethoxysilane (TEOS) mixed with a small amount of hydrochloride and water, and the mixture is hydrolyzed and polycondensed between room temperature and 200°C after removal of the solvent. However, an important point for incorporation of organic polymers with ceramics is the bonding between organic polymers and ceramic networks. If the silicon alkoxide group is introduced into the organic polymer chain, it may react covalently with the silica network during polycondensation reaction of TEOS.

In this study, a copolymer of VAc and VTES was synthesized, and then incorporated with silica-gel networks by the sol-gel process using three types of silicon alkoxide, i.e. TEOS ($Si(OC_2H_5)_4$), MTES(, CH_3-$Si(OC_2H_5)_3$), and DMDES ($(CH_3)_2$-$Si(OC_2H_5)_2$). The mechanical properties of the hybrids made of VAc-VTES copolymer and three kinds of silicon alkoxides such as TEOS, MTES, and DMDES were measured, and the effect of methyl group in silica-networks was investigated.

Experimental

Copolymerization and Hybridization

In order to introduce the silicon alkoxide group (-Si(OC_2H_5)$_3$) into the PVAc chain, copolymerization of VAc and VTES was carried out. 31.6 g (98.5 mol%) of VAc and 6.08 g (1.5 mol%) of VTES were dissolved in 80 g of benzene together with 1.0 g of 2,2'-azobis(isobutyronitrile). The mixture was heated at 77 °C for 15 h. The copolymer obtained was purified by eliminating the benzene and VAc monomer by distillation at 90 °C at atmospheric pressure, and then removing the VTES monomer at 90 °C and 30 mmHg. The copolymer yield was 80 % and the number average molecular weight was 5,000, which was measured by using a Hitachi Perkin-Elmer Molecular Weight Apparatus 115 in benzene. This copolymer contains 90 mol% of VAc and 10 mol% of VTES from a composition curve[11] calculated from Q-e values, i.e., Q=0.026 and e=-0.220 for VAc, and Q=0.03 and e=0.100 for VTES[12].

Hybridization of the copolymer and silica-gel was performed as follows: a 20 wt% of acetone solution of the copolymer was mixed with silicon alkoxides such as TEOS, MTES, and DMDES together with HCl and H2O under stirring by using an ultrasonic wave homogenizer. Weight fractions of silicon alkoxide in the mixture were varied at 20, 40, 50, 60, and 80 wt%. The mixture was poured into a petri dish, left for 5 days for drying and precuring at room temperature, and then heated at 60 °C for one week.

Measurements

The tensile properties of the hybrids were measured by using a Tensilon UTM (Orientec Co. LTd.) at 25 °C and 50 % relative humidity. The cross-head speed was 10 mm/min and the gauge length was 10mm. Rectangular test specimens (width 5 mm and thickness about 0.2 mm) were used.

The dynamic viscoelastic properties of the hybrids were measured using a DMS 110 (Seiko Instruments Inc.) at the heating rate of 2°C/min and the frequency of 10 Hz. The dynamic modulus, G', and tan δ were measured as a function of temperature using a shear mode probe.

Results and Discussion

Tensile Properties

PVAc has low tensile strength (ca. 6MPa) and low modulus of elasticity (800 MPa at 25 °C) but large elongation (260 %). PVAc was incorporated with silica-gel by the sol-gel process as a model for improving mechanically-poor polymers. Fig. 1 shows the tensile properties of PVAc/silica-gel and

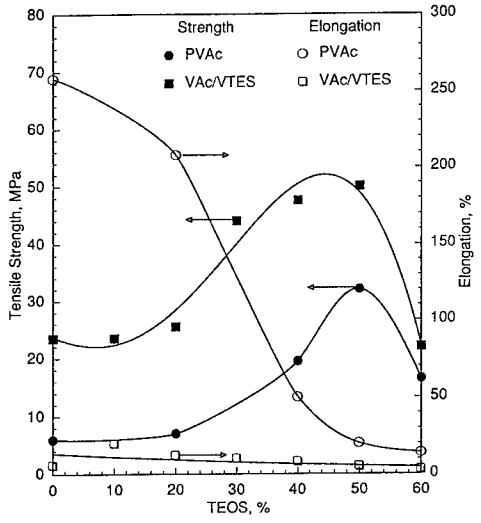

Fig. 1. Tensile properties of PVAc- and copoly (VAc/VTES)-hybrids as a function of TEOS content.

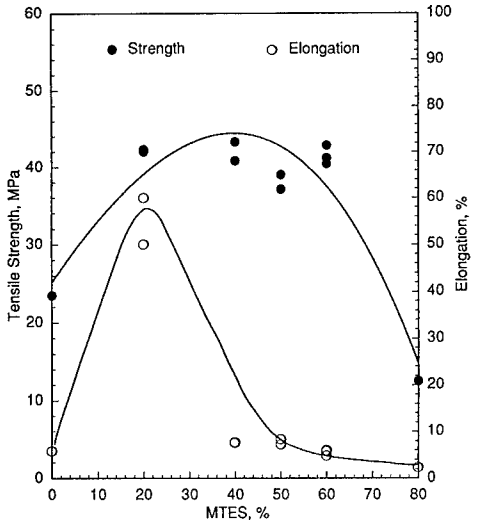

Fig. 2. Tensile properties of copoly(VAc/VTES) hybrid as a function of MTES content.

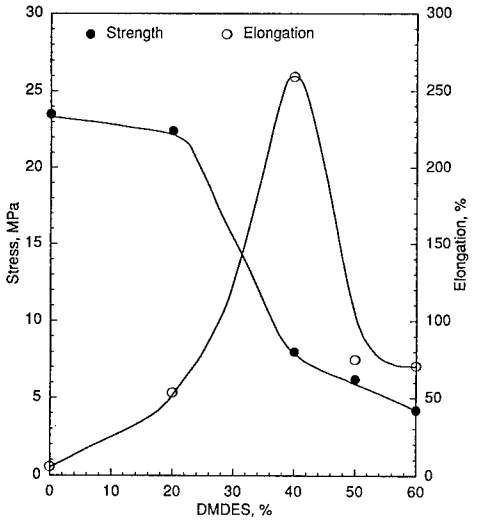

Fig. 3. Tensile properties of copoly(VAc/VTES) hybrid as a function of DMDES content.

copoly(VAc/VTES)/silica-gel hybrids as a function of the amount of mixed TEOS. The tensile strength of PVAc was improved up to 30 MPa by mixing 50 wt% of TEOS from 6 MPa. An important point to improve the mechanical properties of the hybrid is strong bonding between organic polymers and silica-networks. Copoly(VAc/VTES) has silicon alkoxide group in the main chain and this group reacts with mixed TEOS during polycondensation reaction to form covalent bonds between the organic polymer and silica-network. The copoly(VAc/VTES) itself could be polycondensed without TEOS, and the tensile strength of the copolymer was 24 MPa, which was much higher than that of PVAc (6 MPa). The tensile strength of copoly(VAc/VTES)/silica-gel hybrid increased with increasing amounts of mixed TEOS, and reached up to 50 MPa at 50 wt% of TEOS. However, above 60 wt% the strength decreased and the hybrid became very brittle as is typical of ceramics. The strength of the copolymer hybrid was much higher than that of the PVAc hybrid. This was caused by the peculiarity of the structure of the copolymer hybrid. The elongation of both hybrids decreased with increasing TEOS content. The elongation of the copolymer hybrid was lower than that of the PVAc hybrid because the silica content of the copolymer hybrid was higher than that of the PVAc hybrid.

When TEOS was used for hybridization, the strength and modulus of the hybrid increased, and the hybrid became hard but brittle, since the silica-network was composed of only hard linkages of -O-Si-O-. In contrast, silicon alkoxide having organic groups may have softened the inorganic network due to the free volume of the organic group. Fig. 2 shows the tensile properties of a copoly(VAc/VTES) hybrid made of MTES having a methyl group. The tensile strength increased with increasing amounts of mixed TEOS, reaching a maximum value of 45 MPa, and decreased to 12 MPa at 80 wt% of MTES. In the case of MTES free-standing film could be obtained by mixing the silicon alkoxide up to 80 wt%. The elongation of the hybrid increased at first to 60 % by mixing 20 wt% of MTES, and then decreased as the mixed amounts of MTES increased. The methyl group in MTES softened the inorganic networks and increased the elongation, but excess amounts of MTES hardened the hybrid and made it brittle, as was the case with TEOS.

Fig. 3 shows the tensile properties of the hybrid made of copoly(VAc/VTES) and DMDES. DMDES has two methyl groups in the molecular chain and is polymerized not to a three-dimensional network but

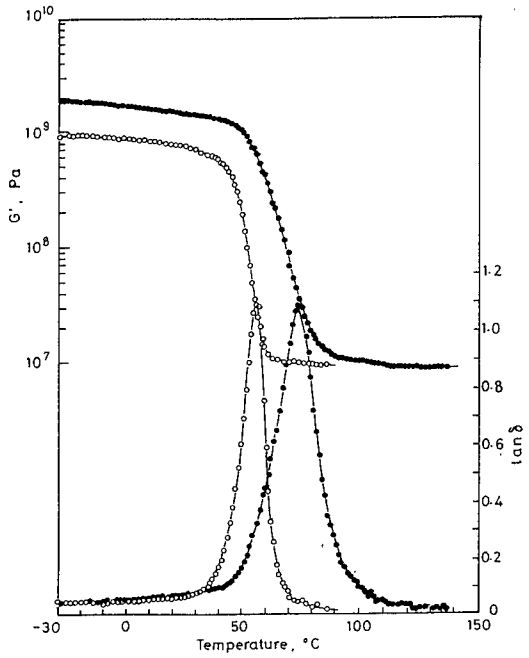

Fig. 4. Temperature dependence of the dynamic viscoelastic properties of PVAc (O) and copoly (VAc/VTES) (●).

to a linear polymer, i.e., polydimethylsiloxane. The behavior of DMDES was much different from other alkoxides. The strength of the hybrid decreased with increasing amounts of mixed DMDES. The elongation increased with the amount of DMDES, reaching a maximum value of 260 % at 40 wt% of DMDES, but decreasing to ca. 70 % at 60 wt% of DMDES. The maximum value of 260 % was almost the same value of PVAc, as can be seen in Fig. 1.

Dynamic Viscoelastic Properties

The temperature dependence of the dynamic viscoelastic properties of polymers gives important information concerning glass transition behavior, relaxation phenomena, and changes in rigidity and mobility. Fig. 4 compares the dynamic viscoelastic properties of PVAc with those of copoly(VAc/VTES). G' of the copolymer was higher than that of PVAc over the wide temperature range between -30 and 150 °C, since the copolymer was cross-linked without TEOS by an alkoxysilane group in the main chain. In the tan δ curve of PVAc, a sharp peak appeared at 50 °C. The tan δ peak of copoly(VAc/VTES) occurred at about 70 °C and was broader than that of PVAc. The broad tan δ peak of the copolymer reflects the complex structure of the copolymer caused by branching and cross-linking.

Fig. 5 shows the dynamic viscoelastic properties of copoly(VAc/VTES)/silica-gel hybrid prepared with TEOS. The level of G' of the hybrid increased with TEOS content over the wide temperature range from -30 to 150 °C. A plateau of G' was observed above 90, 110, and 120 °C for 20, 40, and 50 wt% of TEOS, respectively, and the level of the plateau increased from 10^7 Pa for 20 wt% to 10^8 Pa for 50 wt% of TEOS. The hybrid prepared from TEOS is brittle. In the tan δ curve, a peak caused by glass transition occurred at 75, 85, and 90 °C for the hybrid mixed with 20, 40, and 50 wt% of TEOS, respectively. As the amount of mixed TEOS increased, the location of the peak shifted to the higher temperature, peak height lowered, and peak width broadened.

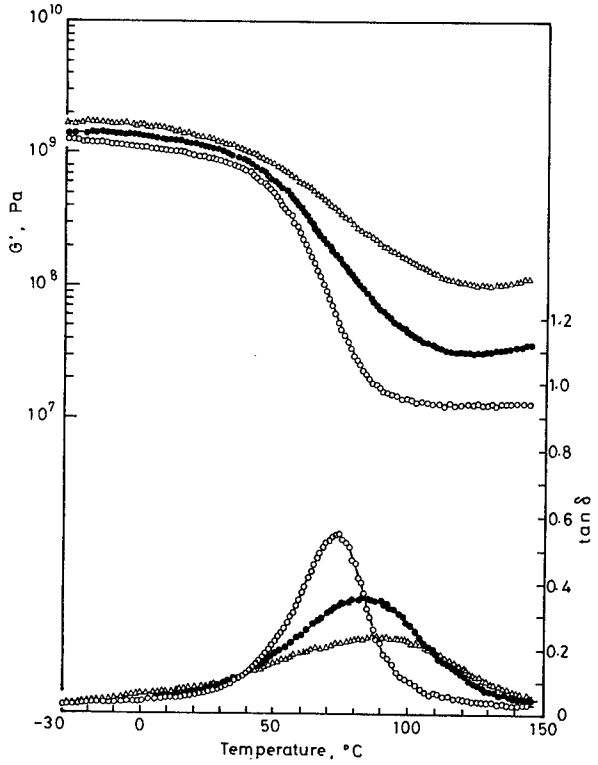

Fig. 5. Temperature dependence of the dynamic viscoelastic properties of copolymer hybrid made of various TEOS content, (O) 20, (●) 40, and (Δ) 50wt% .

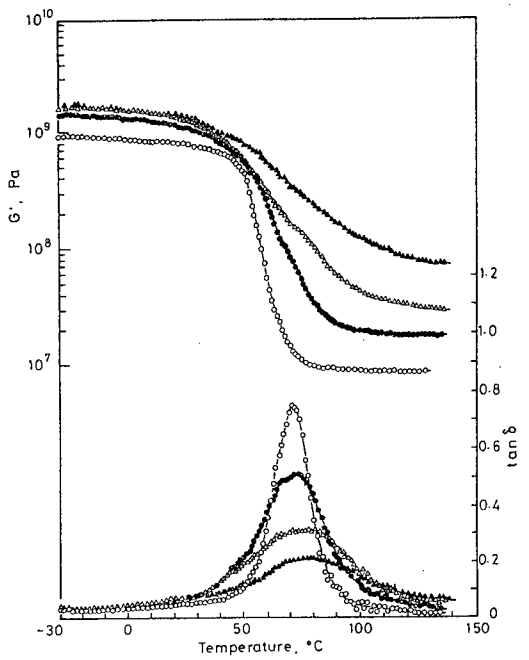

Fig. 6. Temperature dependence of the dynamic viscoelastic properties of copolymer hybrid made of various MTES content, (O) 20, (●) 40, (Δ) 50, and (▲) 60wt%.

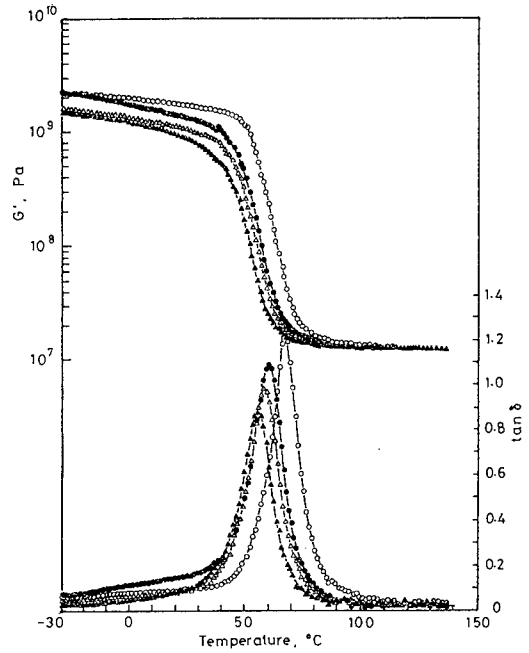

Fig. 7. Temperature dependence of the dynamic viscoelastic properties of copolymer hybrid made of various DMDES content (O) 20, (●) 40, (Δ) 50, and (▲) 60wt%.

The dynamic viscoelastic properties of the hybrid prepared from MTES are given in Fig. 6. The level of G' value increased with mixed MTES content, especially above Tg. The level of the plateau increased with MTES amount. G' of the hybrid with larger loading of silica-gel, such as 60 % of MTES, did not drop sharply at Tg as compared with that of the hybrid mixed with 20 wt% of MTES. In the tan δ curve, a peak appeared at 65, 70, 72, and 79 °C for the hybrid from 20, 40, 50, and 60 wt% of MTES. The height and width of the tan δ peak lowered and broadened with increasing MTES content. The peak position shifted to a higher temperature range, but was not significant if it was compared with TEOS. This may be due to the methyl group in the silica-network.

In the case of DMDES, the dynamic viscoelastic behavior of the hybrid was very different from that of the TEOS- and MTES-hybrids, as can be seen in Fig. 7. G' sharply dropped at around 50 °C at any DMDES content. The level of G' decreased with increasing amounts of DMDES below Tg. This behavior was completely opposite that of TEOS and MTES. Two methyl groups in the silicon alkoxide plasticized the inorganic-network. When DMDES content increased, a sharp tan δ peak which occurred at 55 - 65 °C shifted to a lower temperature, and the peak height lowered. The peak width did not change with DMDES content.

The tan δ peak positions of the hybrids prepared from TEOS, MTES, and DMDES, which correspond to the glass transition temperature, are illustrated in Fig. 8. The peak temperature for the TEOS-hybrid increased with increasing amounts of TEOS. In the case of MTES, the tan δ decreased from 72 °C to 65 °C at 20 wt%, and then increased with MTES content. On the other hand, the tan δ peak of the DMDES-hybrid decreased with silicon alkoxide content. The plasticization effect of the methyl group on the silica-network is clearly seen in this figure.

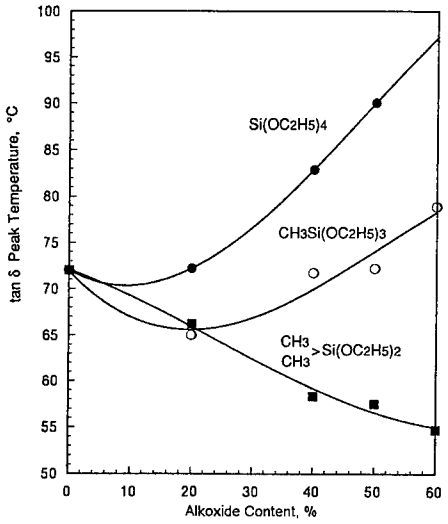

Fig. 8. Relationship between the tan δ peak temperature and alkoxide content.

References

[1] H. Schmidt, J. Non-Cryst. Solid, **112**, 419(1987)
[2] H.H.Huang, B.Orler, and G.L.Wilkes, Polymer Bull., **14**, 557(1985) .
[3] F.Suzuki, K.Onozato, and Y.Kurokawa, J. Appl. Polym. Sci., **39**, 371(1990)
[4] K.A.Mauritz and C.K.Jones, ibid, **40**, 1401(1990) .
[5] R.H.Glaser and G.L.Wilkes, Polymer Bull., **22**, 527 (1989) .
[6] S. Wang, P. Xu, and J. E. Mark, Rubber Chem. Technol., **64**, 746(1991) .
[7] D.Ravanaine, A.Seminel, Y.Charbouillot, and M.Vincens, J. Non-Cryst. Solid, **82**, 210(1986) .
[8] T.Saegusa, J. Macromol. Sci.-Chem., **A28**, 817(1991) .
[9] A.Morikawa, Y.Iyoku, M.Kakimoto, and Y.Imai, Polym. J., **24**, 107(1992) .
[10] M.Nandi, J.A.Conklin, L.Salvati, Jr., and A.Sen, Chem. Mater., **3**, 201(1991).
[11] S.Yano, K.Nakamura, and N.Yamauchi, J. Appl. Polym. Sci., to be published.
[12] "POLYMER HANDBOOK SECOND EDITION", J.Brandrup and E.H.Immergut Eds., Wiley, New York, 1975, pp.II-387 - II-404.

AUTHOR INDEX

Your Direct Access

World Wide Web

Please visit us on the World Wide Web at

http://www.ttp.ch

where detailed information on all published titles is provided as well as:

- Online Shopping
- Site Search
- Full Tables of Contents
- New & Forthcoming Titles
- Periodicals & Book Series
- Preview Service
- Download Area

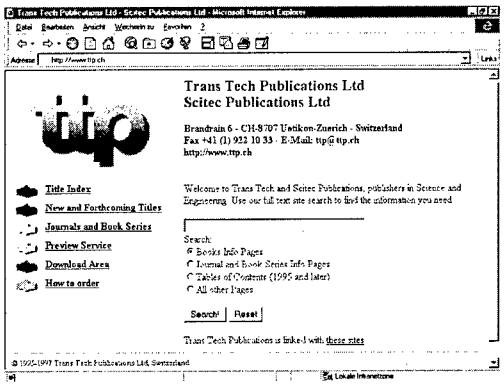

TTP Preview Service

Trans Tech Publications' preview service offers automatic delivery by e-mail of information on new books and periodical issues in *your area of interest*, including tables of contents - several weeks before the actual release of the respective publication.

Included are all titles published including the following periodicals and book series:

- Advanced Manufacturing Forum
- Advanced Materials Research
- Defect and Diffusion Forum
- Environmental Research Forum
- GeoResearch Forum
- Key Engineering Materials
- Materials Science Forum
- Materials Science Foundations
- Molten Salt Forum
- Production and Logistics Forum
- Solid State Phenomena

This service is free of charge. For details please send an e-mail message containing the line
help
to **preview@ttp.ch**
or register your e-mail address and areas of interest online at http://www.ttp.ch

For regular e-mail please use the address **ttp@ttp.ch**

Trans Tech Publications Ltd
Brandrain 6 • CH-8707 Uetikon-Zuerich • Switzerland
Fax +41 (1) 922 10 33 • e-mail: ttp@ttp.ch
http://www.ttp.ch

Nanophase Materials

Eds. E. Bonetti and D. Fiorani

Proc. of the 2nd National Meeting on Nanophase Materials, held in Rome, Italy, May 1995

Materials Science Forum Vol. 195

ISBN 0-87849-709-9
1996, 240 pp, CHF 128.00 / US$ 98.00

The purpose of this book is to present a survey of the latest developments in the field of nanophase materials. The topics included are interdisciplinary in nature, covering theory, materials preparation, structural characterization, thermodynamic aspects and mechanical, optical, electrical and magnetic properties.

Contents Sections:

Some Highlights:

Trans Tech Publications Ltd

Brandrain 6
CH-8707 Uetikon-Zuerich
Switzerland

Fax: +41 (1) 922 10 33
e-mail: ttp@ttp.ch
Web: http://www.ttp.ch